THE EFFECT OF ELEVATED TEMPERATURE ON THE WEAR OF STAINLESS STEEL IN CONTACT WITH TUNGSTEN CARBIDE

by

Stanley John Petraitis BSc MSc

A thesis submitted to the University of Aston in Birmingham for the degree of

Doctor of Philosophy

Department of Physics
April 1982

THE UNIVERSITY OF ASTON IN BIRMINGHAM

The Effect of Elevated Temperature on the Wear of Stainless Steel in Contact with Tungsten Carbide

SUMMARY

The bearings in the air motors of modern jet aircraft engines must operate dry in hostile conditions at temperatures up to 500 °C, where the thrust races in the actuators operate at temperatures up to 300 °C. One of the few metallurgical combinations which can function efficiently under these conditions is martensitic stainless steel on tungsten carbide. The work described was initiated to isolate the wear mechanisms of two such steels in contact with tungsten carbide at temperatures up to 500 °C.

Experiments were carried out on angular contact bearings similar to these used in service, where both rolling and sliding is present and also for pure sliding conditions using a pin-on-disc apparatus. Wear measurements of the bearings were obtained with wear rates, friction and surface temperatures from the pin-on-disc machine for a series of loads and speeds. Extensive X-ray diffraction analysis was carried out on the wear debris, with also S.E.M. analysis and hardness tests on the worn surfaces along with profilometry measurements of the disc. The oxidational parameters of the steel were obtained from measurements of oxide growth rates by ellipsometry.

Three distinct mechanisms of wear were established and the latter two were found to be present in both configurations. These involve an oxidational-abrasive mechanism at loads below 40 N with pin surface temperatures up to about 300 °C, with the mechanism changing to severe wear for higher loads. As the temperature increases a third wear mechanism appears due to transfer of relatively soft oxide films to the steel surface reducing the wear rate. Theoretical K factors were derived and compared with experimental values which were found to be in good agreement for the severe wear mechanism. The pin-on-disc experiments may be useful as a screening test for material selection, without the considerable cost of producing the angular contact bearings.

Stanley John Petraitis, M.Sc., 1982.

Key Words

Bearings/Wear/Surface Analysis/K Factors

ACKNOWLEDGEMENTS

I would like to express my thanks to my supervisor, Mr. J. L. Sullivan for his advice and encouragement throughout this project. I am also grateful to Dr. T. F. J. Quinn for his valuable advice. I would like to thank Lucas Aerospace Limited for provision of equipment and materials and Mr. M. V. Parks of that company for his advice and assistance during the investigation.

I would also like to thank the staff of the Physics workshops, Professor S. E. Hunt in whose department the work was carried out and the Science Research Council for providing financial support.

CONTENTS

FIGURE TITLES

TABLES

CHAPTER 1
INTRODUCTION

1.1 Background to the Research

The thrust reverser and variable nozzle control mechanisms on a typical modern jet aircraft engine are driven by actuators bolted onto the engine where they are expected to function at temperatures of 200 to 300 ^{o}C. They are in turn driven by flexible shafting linked to an air motor driven by hot air up to 500 ^{o}C from the engine. The nozzle control air motor drives four actuators and is used all the time in flight to maintain correct thrust where its speed can be around 14,000 r.p.m. The thrust reverser air motor which is only used on landing drives only two actuators, but its speed approaches 20,000 r.p.m. All the actuators are subject to gas from the engine when the thrust reverse mechanism is applied briefly on landing. Although speeds are very high, it is considered that the high temperatures are the main source of trouble. These high temperatures lead to tribological problems in the bearings of the air motor and the thrust races in the actuators. Conventional lubrication is not possible due to the very high temperatures. When solid lubricants have been utilised, for example MoS_2, they were not effective because they would not remain in contact with the surfaces. To operate in these hostile conditions therefore special materials were required. Material combinations which will function efficiently for any period of time under such conditions are rare. Experimental bearings of Lescalloy BG42 races a martensitic stainless steel and WC-11% Co balls were first used in 1970. They were introduced in 1971 on the RB199 Rolls Royce engine thrust reverser and variable

nozzle actuators. Before 1970 materials such as tool steel were used for balls and races. It was found that the Lescalloy BG42 races with the WC-11% Co balls were the far superior with the balls lasting about ten times longer. As engine performances increase the air temperatures and load increase. They are expected to last for approximately 1000 hours at present.

The work described was to investigate the wear mechanisms for two such steels in contact with tungsten carbide in a temperature range up to 500 ^{o}C. A major aim of the study was to isolate the wear mechanisms at elevated temperatures and to apply the knowledge gained in the selection of new materials, so as to increase the load and temperature limit requirements to levels needed for the next generation of aircraft engines.

The martensitic stainless steels investigated were Lescalloy BC42 of weight composition 1.15% C, 14.5% Cr, 4.0% Mo, 0.5% Mn, 1.2% V, 0.3% Si and A.I.S.I. 440C MOD of composition 1.1% C, 15.0% Cr, 4.0% Mo, 0.7% Mn, 0.15% V, 0.4% Si and 0.75% Ni, the steels being hardened to 8.29×10^{9} and 8.09×10^{9} N m^{-2} respectively. The sintered tungsten carbide grade G contained 11% Co which acts as a binder and of nominal hardness 13.00×10^{9} N m^{-2}.

1.2 Classification of Unlubricated Wear

When materials slide together under unlubricated conditions wear is encountered which results in loss of material from one or both of the interacting surfaces. There are usually several factors involved in the wear process. The surfaces may retain their original character if the process is mainly mechanical, or they can be changed by

a chemical process occurring between the wearing surfaces and the environment. In the majority of engineering situations there is lubrication between the rubbing surfaces, but occasionally there are situations where lubrication is impossible or intolerable.

General classifications of dry wear have been proposed by Burwell and Strang[1] and Archard and Hirst[2] in 1952 and 1956 respectively. The classifications proposed by Burwell and Strang in 1952 were adhesive wear, corrosive wear, surface fatigue wear, fretting, abrasive wear, erosion and cavitation. Adhesive wear is when adhesion between the surfaces causes parts of one surface to be removed by a cold welding mechanism, Bowden and Tabor.[3] These fragments then either break away to become wear particles or they may be transferred. This classification is no different from severe wear as defined by Archard and Hirst.[2] Corrosive wear occurs when sliding takes place in a corrosive environment, the products of corrosion form a film on the surface which slows further corrosion. However, the action of sliding removes the film allowing the corrosive attack to continue. Quinn[4] suggests that the corrosive wear classification is so difficult to assign, that it would be better to use the mild wear classification for the beneficial form of wear and the term severe wear for the deleterious form in which the environment is truly corrosive. Surface fatigue wear occurs after many millions of repeated loading and unloading cycles at a surface asperity, when sub surface cracks eventually reach the surface they form large pits in the surface. Fretting is a form of wear occurring under conditions where small oscillatory tangential motion occurs between two surfaces which are held together in such a way that the oxide wear particles

cannot escape, thereby causing severe stresses. Quinn[4] suggests that this type of wear can be classified as a special form of mild wear. It is also the view of Quinn[4] that abrasive wear, erosion and cavitation are all forms of wear which occur when a rough hard surface or hard particles for erosion, or bubbles of liquid for cavitation, slides or impinges at high velocities upon a softer surface causing a series of grooves or large holes to be formed. They are all forms of abrasion which can occur in different stages of both mild or severe wear.

The Burwell and Strang[1] classifications are special cases of the simpler classifications proposed by Archard and Hirst[2] namely those of mild wear or severe wear. These classifications are sufficient for most purposes, being based only on observable phenomena such as measurements of contact resistance, surface topography and analysis of the size and composition of the wear debris. Archard and Hirst[2] found that for a wide range of mainly metallic materials sliding in unlubricated conditions, each wear test began with a changing wear rate until the surface conditions became stabilised. For most of the materials the relation between wear rate and load was close to direct proportionality. They were able to draw a clear distinction between two types of wear regimes. Adhesive wear, a form of severe wear, is characterised by intermetallic contact with metallic wear particles present in the debris. In mild wear the surfaces are smooth and are usually protected by surface oxide layers generated during rubbing, the wear debris consisting of fine particles of the oxide. This broad classification of wear into mild and severe was further studied by Kerridge and Lancaster,[5] when they rubbed

60/40 brass against hardened steel. The brass pin which was made radioactive was used to follow the history of the material during the rubbing process. It was found that material transfer was taking place and that it was a two stage process. There was severe wear of the soft brass and the wear rate was proportional to the load. Welsh(6) in a comprehensive series of experiments with a range of plain carbon steels described these patterns in detail in terms of 3 main transitions. Quinn(4) proposed that severe wear is what happens when mild wear processes cannot occur. It is suggested that an important form of severe wear mechanism is the delamination mechanism recently proposed by Suh.(7) If one has microscopically non-conforming surfaces or if one has unreactive surfaces, then severe wear must prevail.

Abrasive wear is when damage occurs to one or both of two sliding surfaces, due to the presence of a third abrasive body. This could be an abrasive grit or perhaps an abrasive product of the wearing surface. Also if there is a large difference in hardness of the two sliding surfaces abrasive wear can occur. In any particular instance of wear one may have any of these mechanisms operating separately or in combination. This makes the task of suggesting an all combined wear theory a difficult and perhaps impossible task.

There are a number of wear theories relating to fairly specific circumstances, all of which start from the concept of the real area of contact. The so called Archard(8) wear law is just an attempt to express the wear rate in terms of the real area of contact.

$$w = K\,A \qquad \text{.......................................(1.1)}$$

In much the same way as the friction theories depend on relating the frictional force to the real areas of contact, theories of wear must relate the volume removed per unit sliding distance w ($m^3\ m^{-1}$), to

the real area of contact A (m^2). Archard(9) interprets K as the probability of producing a wear particle at any given asperity encounter.

$$A = W/p \quad \ldots\ldots\ldots\ldots (1.2)$$

Bowden and Tabor(3) gives equation (1.2) and combing this with the Archard wear law produces equation (1.3).

$$w = K\,W\,/\,p \quad \ldots\ldots\ldots\ldots (1.3)$$

W is the load and p is the bulk hardness of the softer of the two materials. The expression indicates that w is proportional to load for circumstances in which K is constant. But its value depends on the materials and on the conditions of sliding, so it is more normally found that this is not true. Archard and Hirst(2) suggested that K is the important factor in determining the wear rate and also that it can vary over 5 orders of magnitude. Therefore since K can vary over so many orders of magnitude 10^{-2} to 10^{-7} the designer can never allow for the wear of the moving parts of a machine. If a method could be found for estimating K from first principles then this would be of great importance. The factors influencing K should be given the highest priority in our research into the fundamentals of wear.

1.3 Severe Wear

Severe wear is recognised according to Archard and Hirst(2) by the wear debris consisting mainly of large approximately 10 μm diameter metallic particles, where also microscopic examination revealed rough deeply torn surfaces. They found that this type of wear also gives rise to low contact resistance measurements. It was assumed that adhesive or welded junctions are formed between solids at the actual contact areas. These junctions are broken with sliding

and at some of the events the junctions would be stronger than the surrounding metal removing a particle out of the surface. In general severe wear processes are very efficient at removing material from the sliding surfaces. K can be interpreted as the probability of producing a wear particle at any given asperity encounter. $1 / K$ is the number of interactions which a given part of the surface can endure before fracture. For example if K is approximately 10^{-3} one encounter in 1000 produces a particle. This implies that the majority of events which will determine the frictional force are contacts between asperities which separate without damage.

Kerridge and Lancaster[5] investigated the severe wear of 60/40 brass on hardened steel using a radioactive tracer technique which demonstrated the occurrence of metal transfer. A transferred film of brass builds up on the steel surface and when the thickness reaches a steady value, wear particles start to appear. From these experiments there was no back transfer, probably due to the brass particles becoming work hardened at the initial transfer. Rabinowicz[10] maintains that severe wear is favoured by factors which encourage adhesion such as clean surfaces, chemical and structural similarities. Wear increases if the material couple are mutually soluble, hence the use of unlike material combinations in engineering situations. A sliding model was proposed by Finkin[11] which includes the influence of asperity interaction distance. In the model the asperities move against each other for a considerable distance l, in comparison to the length at the junction. He expresses the probability of wear particle formation, which is related to K as a function of l.

Suh[7] [12] has proposed a delamination theory for metallic wear based on the formation of dislocations and vacancies in the subsurface layers. This damage occurs only in the subsurface layers because the surface layer receives less cold working enabling it to absorb plastic

deformation. Cracks begin parallel to the surface and occasionally grow to a length far greater than the dimensions of the real contact area. This eventually causes delamination of the surface into thin wear sheets parallel to the surface resulting in the formation of thin sheet-like wear debris. Engel[13] shows how Suh's mechanism leads to the expression:-

$$w = \left[\frac{B_1 \times G_1}{J_1} + \frac{B_2 \times G_2}{J_2} \right] A \quad \ldots\ldots\ldots (1.4)$$

As previously w the wear rate is the volume removed per unit sliding distance and A is the real area of contact. G is the removed layer thickness from each of the surfaces, J the critical plastic displacements where B depends mainly on surface topography.

1.4 Mild Wear

If an environment is hostile the wear is rapid but if the environment is normal it is possible to obtain a mild form of wear known as oxidational wear. So mild wear clearly involves reaction with the environment, in particular with the oxygen in the environment. The formation of an oxide coating on metal surfaces preventing intermetallic contact have been found to be beneficial to their sliding by reducing friction or wear. The wear debris consist of small approximately 1 μm diameter particles which have been produced by reaction with the ambient atmosphere, Archard and Hirst.[2] Also microscopic examination of the surfaces revealed extremely smooth surfaces, often smoother

than the original. Archard[14] showed that the K factor can vary from 10^{-2} to 10^{-5} depending on whether one used mild steel upon mild steel where $K = 10^{-2}$, or stellite upon tool steel $K = 10^{-5}$, all other operating parameters being maintained constant. It is this wide variation of K factors, which sometimes even occurs merely by changing the load by a few percent above or below a transition load, Welsh[6], which makes wear results more difficult to analyse than friction results.

In oxidational wear temperature is important because an increase in temperature can produce an initial softening and rupture at the film producing severe wear. A further increase in temperature could increase the oxidation rate and cause the transition back to mild wear. Welsh[6] showed that for a 0.63% C steel as the hardness tended to fall oxidation was essential to preserve mild wear. Since oxidation rates are temperature dependent, the factors involved in their breakdown and removal are also temperature dependent. There are a number of theories which have been proposed, some differ by approach others by interpretations of various parameters. There are two main processes taking place oxide growth and oxide removal.

Oxidation growth rates obey various rate laws, the most commonly adopted are the parabolic and logarithmic laws. Since the sliding surfaces are at unknown temperatures, pressures and environment it makes prediction of oxidation difficult. Since the whole of the apparent area of contact will be activated to some extent, the question of whether the majority of oxide is grown on the wearing asperities during actual contact or at some other period arises. A careful appraisal of the conditions used in several wear experiments with steel

by Quinn[15] in 1962, together with static oxidation tests, led to the hypothesis that the mild wear of unlubricated steel specimens principally involves the oxidation of newly exposed bulk metal at the hot-spot or contact temperature between contacting asperities. The oxide formed during the unlubricated sliding of steel is a variable composition of the three oxides of iron. The actual compositions of the oxide depends on the temperature of sliding. The variation of the proportions of iron, rhombohedral oxide and spinel oxide with measured bulk pin temperature was used by Quinn[16] in an attempt to give an estimate of the contact temperature. Since it has now been established that oxidation takes place during the contact period, Quinn et.al.[17]

Two idealised models have been demonstrated by Tao[18] which could represent oxidational wear. The first model assumes gradual growth of an oxide layer, which is removed instantaneously by the rubbing action when a certain thickness is reached. The second model which Tao favoured assumes the time for oxide growth is negligibly small in comparison with the time for removing the oxide layer. Quinn[19] suggests that the oxide thickness is built up over a number of traversals until a critical thickness is reached, it is then removed producing oxide flakes. The critical oxide thickness may be such that the substrate is no longer able to support it. The electron micrographs of Quinn[20] show signs of cracking and detachment possibly by thermal or contact microfatigue. Earles and Powell[21] found experimentally for En1A steel that the oxide layer generated by sliding, builds up gradually to a critical thickness before becoming detached from the substrate to form a wear particle.

The oxidational wear mechanism which has gradually evolved over the past 19 years by Quinn[15] [16] [19] [20] [22] [23], Quinn et. al.,[17] Quinn and Sullivan[24] gives a suitable expression for the K factors found in mild wear. After the initial severe wear stages, the surfaces will have achieved a measure of conformity, so that large areas of both surfaces come into contact during sliding. At any given instant one of these areas will bear most of the load. The area then expands so that one has a plateau of contact which will tend to remain in contact until it is removed by wear. There will occur a certain amount of oxidation of the surface of the particular plateau in contact, this oxidation mainly occurring at the temperature of the interface between the areas of contact on the plateau and similar areas on the opposing surface. These plateau have been observed by Quinn[20] and Quinn and Wooley.[25] They are extremely smooth with fine wear tracks parallel to the direction of sliding and they are about 2 μm in height. The surface surrounding the plateau is rough and packed with wear debris and contains no wear tracks. There are several sub-areas of contact on each plateau and that these are the regions of actual contact at which oxidation occurs. The oxide film builds up until it reaches a critical thickness, at which time the film becomes unstable and is removed. When all the sub-areas of contact have been removed from the plateau, then another plateau elsewhere on the surface becomes the operative one. The untouched surface beneath the original plateau can only oxidize at the general temperature of the surface which is relatively low compared to the contact temperature when no external heating is applied. Therefore the original plateau sub-surface region will not oxidize significantly until it becomes the dominant area of

contact once more.

During the time for 1 / K contacts to occur a critical oxide film of thickness h_c, builds up on each of the contacts before they become detached. This is based on Archards(9) interpretation of the K factor namely that 1 / K encounters arc needed on average for a wear particle to be produced. It was assumed that the oxidation rate is parabolically dependent on total time t_c, which is the time required to form this critical oxide film thickness h_c, Quinn.(22)

$$K = d / U t_c \qquad \ldots\ldots\ldots\ldots\ldots\ldots\ldots\ldots\ldots\ldots\ldots\ldots (1.5)$$

U is the linear sliding speed, d is the distance at a wearing asperity contact during which oxidation occurs at the contact temperature given by T_o. Therefore for mild wear the oxidational wear theory Quinn and Sullivan(24), leads to the following expression for the wear rate w, the volume removed per unit sliding distance.

$$w = \left[\frac{d \; A_p \; e^{-(Q_p / R \; T_o)}}{U \; f^2 \; h_c^2 \; \rho^2} \right] A \qquad \ldots\ldots\ldots (1.6)$$

This expression was first obtained by Quinn(19) for metals exhibiting mild wear under unlubricated conditions of sliding. R is the gas constant, A is the real area of contact, A_p the Arrhenius constant for parabolic oxidation during wear, Q_p the activation energy for parabolic oxidation where f is the mass fraction of oxide which is oxygen and ρ is the average density of the oxide. The only term in this equation to be affected by the number of asperity contacts N is d. Quinn(23) supposes that on the operative plateau there will be N areas of contact, each of area πa^2, where a is the radius of the area of contact which for convenience is assumed to be circular, so

equation (1.2) can be written as follows:

$$N \pi a^2 = W / p \quad \ldots\ldots\ldots\ldots\ldots\ldots\ldots\ldots\ldots\ldots (1.7)$$

We can express d as being equal to 2 a which gives the following equation, Quinn.[23]

$$d = 2 (W / \pi N p)^{1/2} \quad \ldots\ldots\ldots\ldots\ldots\ldots\ldots\ldots (1.8)$$

Before one can use this theory to predict wear rates one must know the oxidation characteristics of the metal, the temperature of oxidation T_o which is the contact temperature, h_c the critical oxide film thickness and the number of asperity contacts N. Quinn[23] following Archards[26] approach in deducing the flash temperature, obtained the following expression for the temperature of oxidation T_o.

$$T_o = (\alpha(\text{theory}) \; T_p) + T_s \quad \ldots\ldots\ldots\ldots\ldots\ldots (1.9)$$

T_p is the fictitious flash temperature at the interface assuming all the heat is supplied to the pin, T_s is the surface temperature and $\alpha(\text{theory})$ is the theoretical division of heat at the sliding interface. The presence of this oxide film and the assumption that there are N areas of contact will of course affect $\alpha(\text{theory})$. Since T_o depends on $\alpha(\text{theory})$ equation (1.9), this means that T_o also depends on N and h_c. Quinn[23] used a computer search technique to deduce the appropriate values of T_o, h_c and N which will satisfy equation (1.6) the oxidational wear equation. Values of h_c and N were found which gave $\alpha(\text{theory})$ equal to the experimentally division of heat, equations (14) and (8) of reference (23) respectively. The appropriate values of T_o were then found based on equation (1.9).

A simplified theory for the oxidation wear of steels was proposed by Tenwick and Earles[27] in 1971. A theory of oxidation wear which

could be used to predict wear accurately under a wide range of conditions is unlikely to be possible because of the complex nature of the sliding process which involves surface geometry, temperature distributions, the conditions necessary for the formation of a wear particle and the work hardening of the surfaces. To reduce the complexity they proposed a simple steady state model such that contact between the sliding surfaces occurs at only one asperity above the surrounding surface, N = 1. This is assumed to remain in contact until an oxide wear particle is formed and the process is then repeated with another asperity. The real sliding process consists of a series of collisions between asperities of the other surface. Since consecutive collisions for a given asperity may be infrequent the time spent with the asperity at T_s the surface temperature, is greater than at the contact temperature. Therefore they suggested that T_s was representative of the effective temperature controlling the wear mechanism. Their values of the activation energies for En1A mild steel pins sliding on a N75 80% Ni, 20% Cr - Ti track and a En1A track, were much smaller than values reported for static oxidation tests. This showed the effect of both the track and pin substrate properties on the oxidation of the pin. Tenwick and Earles[27] then modified the theory by changing the rate law from linear to parabolic, incorporating h_c the critical oxide film thickness into the wear equation which is important in determining wear. They proposed that before a generalised wear theory can be found the effects of speed, surface strength and temperature on h_c must be found.

Unless one has all the measurements of surface temperatures, division of heat at the sliding interface, wear rates, friction coefficients and the analysis of the wear debris, one cannot hope to understand any wear processes.

1.5 Abrasive Wear

Abrasive wear usually a form of severe wear, is the removal of solid material from a surface by it being ploughed or gouged out by a much harder surface or body. There are two general situations for this type of wear. In the first case or cutting wear the ploughing or abrasive removal of material is produced by one of the two rubbing surfaces. It occurs according to Burwell[28], when there is great dissimilarity in hardness between the surfaces and in addition that the harder of the two possess a certain amount of roughness. The asperities under the applied normal load dig into the softer surface and literally plough up furrows that break loose as wear particles.

In the second case a third body, generally a small hard particle of grit or abrasive caught between the two surfaces abrades either one or both of the surfaces, Burwell.[28] These hard particles can come from the external environment or they can be corrosive wear products which are generally metal oxides and are generally harder than the parent metal. Burwell[28] stated that it is also possible that the small particles of metal produced by adhesive wear will have been sufficiently work-hardened that they can abrade one or the other of the surfaces. He also suggested that abrasive wear occurs most readily when the abrasive particles are coarse rather than fine and when the abrasive material is significantly harder than the abraded material. In addition, its hardness relative to that of each of the two rubbing surfaces, will distinguish whether it will exist as loose rolling particles moving around between the two surfaces or whether it will become embedded in the softer of the two surfaces and act like a lap on the other surface. Haworth[29] found that angular particles of a soft material produced more wear than rounded harder ones.

Oberle[30] points out that probably a truer measure of abrasive wear resistance is the amount of elastic deformation that the surface can sustain. In other words, in the presence of a harder abrasive particle the surface deforms elastically to get out of the way, but after the particle has passed on, it returns to its original configuration with no plastic deformation or permanent damage. Burwell[28] gave the following expression for the elastic limit of stain E_{lim}.

$$E_{lim} \sim H_d / E \quad \text{.....(1.10)}$$

E_{lim} is equal to the elastic limit of stress divided by the elastic modulus E. The elastic limit of stress has been found empirically to be proportional for a wide range of materials to the indentation hardness H_d. The larger the elastic limit of strain the better should the surface be able to resist damage by an abrasive or other hard surfaces. A means for increasing H_d includes surface hardening by carburizing and nitriding of steels, plating with a hard metal such as chromium, hard facing with materials such as tungsten or chromium carbide, flame or induction hardening of steels, etc. A means for combining a low elastic modulus with a high hardness in the same material is by introducing interruptions or voids in the structure. Oberle[30] introduced slots or holes into a steel specimen and reduced its elastic modulus reducing the wear rate.

In the process by which metal is removed during abrasion, attempts have been made to relate the amount of material removed with the actions of individual abrasive particles. Sedriks and Mulhearn[31] used pyramidal tungsten carbide tools to simulate abrasive particles, in which their cutting and rubbing characteristics at various orientations were studied by optical microscopy. The information obtained was used

to derive equations which relate the cross-sectional area of the groove ploughed during sliding, with the orientation and geometry of the tools and the mechanical properties of the material being abraded. Lead was used as the abraded material because it is essentially a non work-hardening material. The mechanics of abrasive cutting, derived from a force analysis at the interface for lead work pieces, has been extended by Sedriks and Mulhearn[32] to include fully work-hardened metals and alloys such as copper, aluminium and brass. The fully worked state was considered as the state of deformation, imparted to the annealed bulk material by compression at which no increase in hardness takes place on further deformation. The increase in force opposing the motion of an abrasive particle is primarily due to work-hardening of the abraded material.

Archard and Hirst[33] made a detailed study of the wear of hardened high speed tool steel sliding on itself at a speed of 0.66 m s^{-1} under loads up to about 20 N. Under mild wear conditions they found that for well run-in surfaces the wear particles may be as small as a 10 nm. Therefore the surfaces were very smooth and the height of the surface features were generally less than those of the aggregrates of loose wear particles which were present on the surfaces. Most of the load must therefore be borne by this loose material and since there was an increase in the wear rate Archard and Hirst concluded that the final wear mechanism between run-in surfaces is one of abrasion by loose oxide wear particles.

1.6 Summary of Previous Research

In 1958 Golden and Rowe[34] investigated the transfer of tungsten carbide to soft metals during sliding. A small radioactive hemisphere of WC - 6% Co was slid slowly over copper and steel blocks under a

load of 14.7 N. The material transferred was assessed by taking autoradiographs which were obtained by exposing the wear tracks to a photographic film. They showed that tungsten carbide was firmly embedded in copper even after several traversals in each direction over the track. Single traversals on mild and stainless steels also produced steady embedded wear. Figure 3a of reference (34) shows this smooth wear produced by traversing a tungsten carbide slider once over each track on a stainless steel block. The amount of wear was comparable with that found on mild steel and only about 1/5 of that on copper. Almost the whole of the transferred carbide was strongly bonded to the block. When reciprocating traversals were made on mild and stainless steels a considerable proportion of the transferred carbide was scattered loosely on the surface. The autoradiograph figure 3b of reference (34) shows this effect on a stainless steel block when the tungsten carbide slider had traversed ten times in each direction over each track. The total wear of tungsten carbide on steel was very much less than that on copper. Golden and Rowe[34] suggested that the difference between the first and subsequent traversals on steels is due to the embedded particles acting as an abrasive. With copper which is much softer than steel, a greater number of abrasive particles are pushed down well into the material causing damage to the tungsten carbide slider.

Golden and Rowe[35] produced short straight tracks on copper blocks using a radioactive slider of tungsten carbide containing 6% Co and 2% TaC under a load of 19.6 N. On smooth surfaces uniform autoradiographic density was observed. Spots were observed on the autoradiographs if the copper surface was not sufficiently well prepared, showing first the short lived ^{187}W activity and finally the long-lived

^{60}Co activity. They stated that the composition of the wear deposit corresponds closely to the initial composition. Examination by optical and electron microscopy revealed no wear fragments as large as the original grains 1 to 2 μm across. When a large single crystal of tungsten carbide was used, the wear was steady on well prepared copper plates and they reported that it is false to assume that hard tungsten carbide is unable to wear uniformly on a soft material. Therefore Golden and Rowe[35] concluded that for cobalt bonded tungsten carbide, both the soft matrix and the hard grains wear steadily away together during dry sliding.

Miller[36] investigated the friction and wear of hard solids such as sintered TiC, diamond and single crystals of SiC, TiC and sapphire which in sliding contact with steel. A steel ball-bearing was supported and caused to rotate in a vacuum at speeds up to 500 m s^{-1} by means of a rotating magnetic field. The ball was gripped under a load of approximately 2 N by four flat specimens so that the friction causes it to slow down. The variation of the coefficient of friction with sliding speed was calculated from a speed-time curve. Figure 11 of reference (36) shows the coefficient of friction against speed, for steel sliding on sintered TiC and a single crystal of TiC. For sintered TiC the coefficient of friction decreases slowly from about 0.23 at 100 m s^{-1} to about 0.08 at 300 and 500 m s^{-1}. With the single crystal the shape of the curve was similar but the coefficient of friction was slightly lower. Miller[36] showed that all these hard solids can undergo extensive wear when rubbed against steel or metals of much lower hardness. This effect is due partly to the abrading effect of small particles of the harder material which becomes dis-

lodged and dragged across the surface. The sights from which particles are removed may be inclusions, defects or perhaps asperities which are subject to thermal shock or fatigue type failures. When adhesions are formed at higher initial sliding speedssliding occurs on a metal to metal interface. High temperatures were produced at the interface due to the presence of droplets of metal in the wear debris and by the nature of the wear marks on the balls. Miller[36] suggested that at high sliding speed it is the nature of the sliding metal rather than the hard solid which determines the frictional behaviour because marked changes were observed when the steel balls were replaced by balls plated with copper nickel and chrome. With all these hard solids the coefficient of friction for high speed sliding of steel were almost the same and were similar to those determined by Bowden and Persson[37] for steel sliding on steel at comparable speeds.

Trent[38] [39] investigated the wear processes on cemented carbide tools used for cutting steel. According to Trent[39] when cemented carbide tools containing only tungsten carbide and cobalt are used there is a strong tendency for the steel to be welded to the tool at the cutting edge. Whether this occurs or not there is generally very little wear at this part of the top surface. Farther away from the cutting edge on the rake face a crater is worn in the top surface so rapidly that the tool soon fails when cutting at high speeds. Trent[38] [39] showed that when tungsten carbide containing cobalt was heated on steel in a vacuum little reaction occurred until approximately 1300 ^{o}C. At 1325 ^{o}C the reaction was extremely rapid and the tungsten carbide reacted with the steel to form a molton phase. These experiments suggested an explanation of the extremely rapid cratering of the top

surface of cemented carbide tools when used for cutting steels at high speeds. Cratering is caused by the formation of an extremely thin fused layer between the chip and tool surface, consisting of an alloy of tungsten carbide with the steel. The molten alloy formed at temperatures of the order of 1300 ^{o}C generated by friction is carried away by the chip. James[40] shows a S.E.M. micrograph figure 4 of reference (40) of the floor of a wear crater on a WC - 6% Co tool after cutting EN24 steel. The wear pattern shows a smooth surface as a result of diffusion wear. Figure 2 of reference (38) shows a polished section through the seized surfaces of a bearing consisting of an outer sleeve of cemented tungsten carbide containing TiC and Co running against a steel inner part. The fused zone was a fine unresolvable structure, the steel has fused with the tungsten carbide grains while the titanium - tungsten carbide grains have remained intact attached to the steel. Trent[38] stated the length at the worn surface on the flank face of the tool is generally much too short for the cratering temperature to be reached. Hard particles in the steel and small particles of carbide which may be broken away from the edge may score the flank of the tool.

Trent[41] showed there was oxidation of the carbide tool especially on the flank face, with only slight oxidation on the rake face away from the wear scar when cutting steel at high speed. He reported that the main wear processes on carbide tools seem to be based on diffusion and attrition with little evidence of abrasion as an important wear process under most cutting conditions. Trent[41] stated that the rate of diffusion wear which predominates at high cutting speeds is controlled mainly by temperature and the flow rate of the work material very close to the tool surface. The rate of attrition wear, the tearing of small

fragments from the tool surface is dependent mainly on irregularity in the flow of metal over the tool surface and is therefore greater at low cutting speed. Trent[41] assumed that the cause of low wear rates at high cutting speeds was due to the presence of some lubricating or protective constituent in the steel or in the interaction between the carbide tool and the steel.

Shimura and Tsuya[42] studied the effects of atmosphere and temperature on the wear rates of ceramics and cermets. A pin terminating in a hemisphere was worn against a cylindrical disc under a load of 19.6 N. The linear sliding velocity varied from 0.073 to 0.12 m s^{-1}. Shimura and Tsuya[42] showed that the coefficient of friction for WC - 9.2% Co sliding on itself at a pressure of 10^{-6} torr remains substantially constant, rising from 0.4 at room temperature to 0.5 at 600 ^{o}C. The coefficient of friction for ceramics are sensitive to atmospheric pressure with characteristics similar to graphite according to Shimura and Tsuya[42]. They found that the coefficient of friction remains constant at 0.4 from 10^{-8} to 10^{-2} torr. It reaches a maximum at 1 torr and then falls rapidly to less than 0.3 at atmospheric pressure. The volume wear rate which was calculated from the weight loss after sliding gave a maximum at a pressure of 10^{-2} torr. The wear rates and the coefficient of friction are higher at reduced pressure than in air. From these effects and from observations of tested surfaces, Shimura and Tsuya[42] postulated that the ceramics are lubricated with a thin soft surface layer which is naturally formed by an effect of absorbed moisture present in the air.

Mordike[43] studied the frictional properties of carbides over a temperature range from room temperature to 2000 ^{o}C at a pressure of

10^{-4} torr. After outgassing the specimens by heating above 1400 ^{o}C they were heated to the required temperature and the friction values were taken at intervals on cooling. The linear rate of sliding was quite low and the normal load was varied between 0.245 and 29.4 N. For tungsten carbide sliding on itself the coefficient of friction showed an initial decrease from 0.6 at room temperature to a minimum of about 0.3 at 830 ^{o}C, followed by a sharp increase as the temperature was increased. He showed that at room temperature the coefficient of friction was low approximately 0.2, but the effect of outgassing shows that this was due to the lubricating properties of the surface film. Mordike[43] concluded that the coefficient of friction of carbides on carbides first decreased with increasing temperature and then at a definite and reproducible temperature between 800 to 1400 ^{o}C increased rapidly. Over this temperature range a change occurred which resulted in increased adhesion between sliders and crystallites.

Parks[44] investigated the unlubricated track wear of angular contact bearings made from Lescalloy BG42 martensitic stainless steel at temperatures up to 350 ^{o}C. Each angular contact bearing contained twenty 3 mm WC - 11% Co balls. There was a one second run up to 33 revs s^{-1} with a 30 second dwell period between cycles. Track wear measurements were obtained by shadowgraph recording at a magnification of 100. He stated that track profile geometry was not too important as the initial form was short lived and tended to circular arc-close conformity in all cases. Therefore the track wear was linear with increasing number of cycles as shown in figure 1.1. The effect of temperature on the track wear is shown in figure 1.2. There is a progressive increase in wear with increasing temperature up to a peak in the 300 to 350 ^{o}C region. The balls showed virtually no measurable

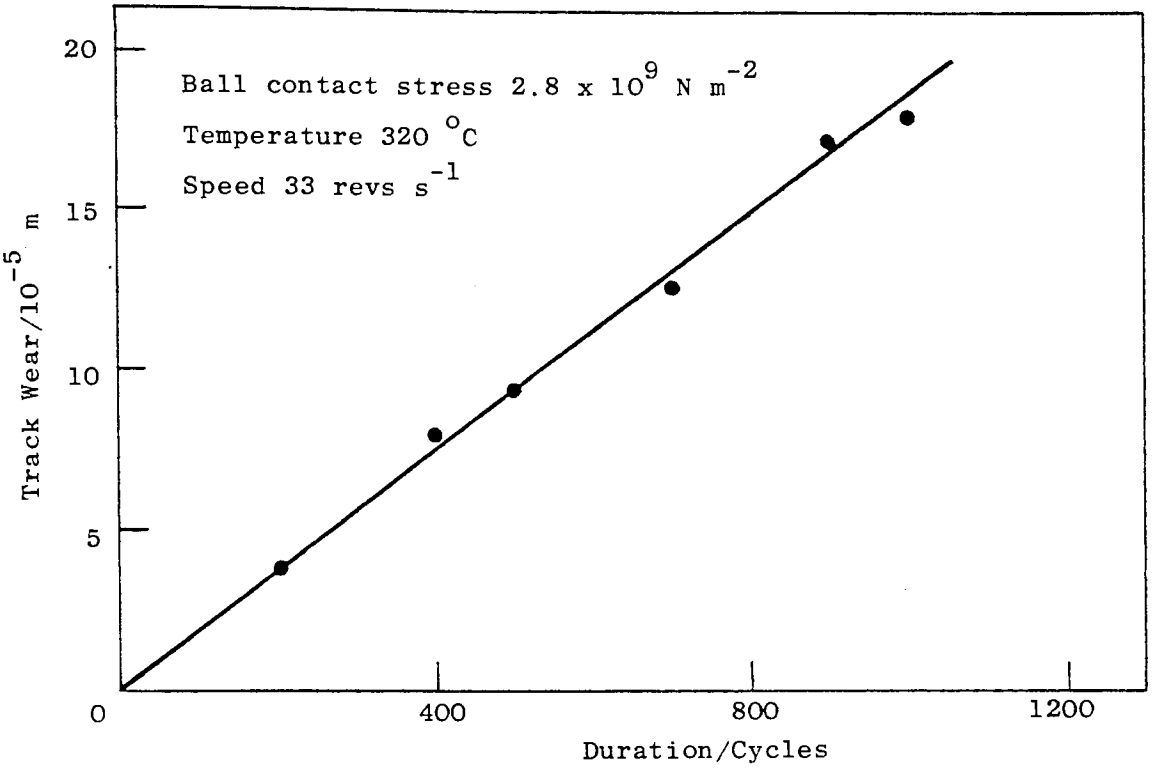

Fig. 1.1. Lescalloy BG42 steel bearing track wear, Parks (44).

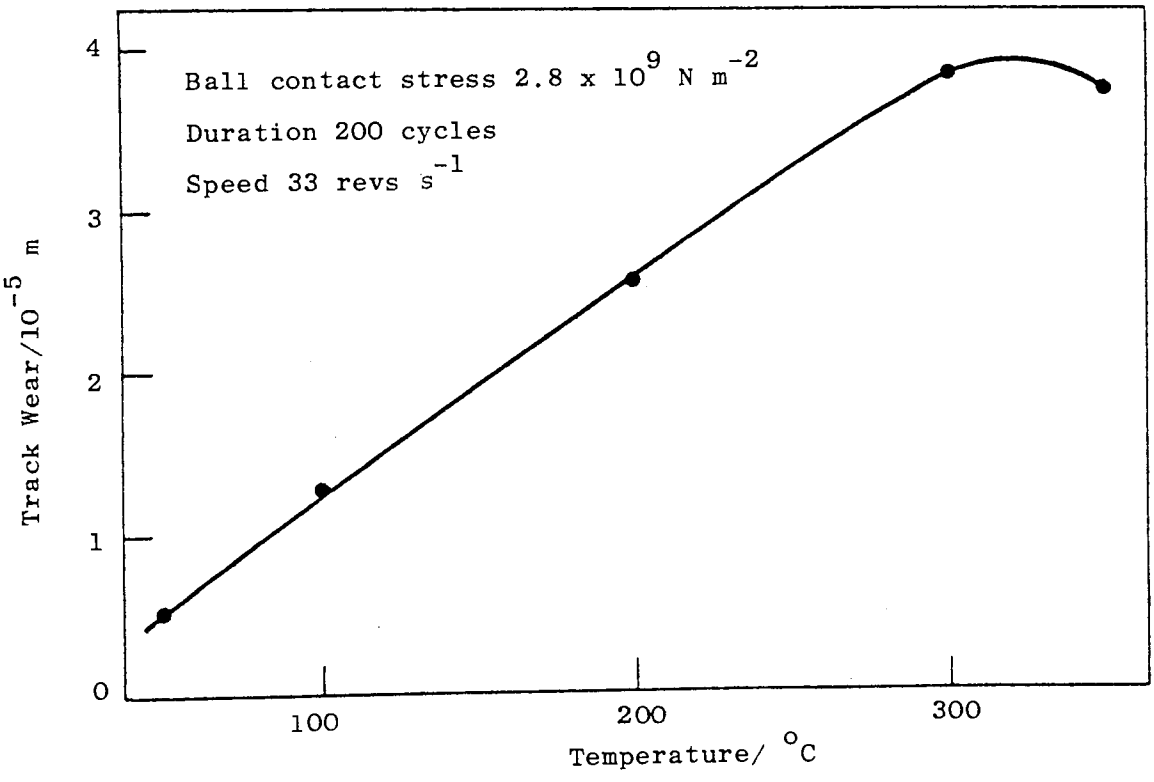

Fig. 1.2. The effect of temperature on the wear of Lescalloy BG42 steel bearings, Parks (44).

wear. According to Parks[44] the effect of temperature on the wear process was two fold. Firstly the material softened off as the temperature rose and more evidently there was the formation of various types of oxides occurring at different temperatures.

1.7 The Metallurgy and Oxidation of Stainless Steel

The role of carbon in steel is described, for example, by Alexander and Street.[45] When pure iron is heated to 906 ^{o}C the iron atoms spontaneously rearrange from the body-centred cubic form into the face-centred cubic lattice pattern. At room temperature less than 0.01% carbon can exist in solid solution in slowly cooled iron of body-centred cubic form called ferrite. At high temperatures up to 1.7% carbon can be taken into solid solution in face-centred cubic iron or austenite. When carbon is present, the atomic reshuffling on heating commences at about 723 ^{o}C and concludes at that or some higher temperature depending on the amount of carbon as shown by the iron-carbon phase diagram, Hansen.[46] The striking variation of properties of steel is associated primarily with its carbon content and secondly with the rate of cooling from the austenite state. When slowly cooled (annealing) the carbon forms a hard iron carbide Fe_3C called cementite. This is deposited in layers arranged alternately with layers of the surplus ferrite and is called pearlite. The presence of pearlite gives hardness and strength to steel. With cementite alone the steel would be brittle, with ferrite alone it would be soft. If steels are quenched in water from the austenite state, the steel cools so rapidly that the carbon atoms have no time in which to come out of solid solution to form cementite. Because of the enforced presence of these carbon atoms the iron atoms can revert only to a distorted form of the body-centred cubic arrangement called martensite. This severe

distortion is responsible for the great hardness and brittleness produced. Tempering of a martensitic steel makes it tough and springy but does not restore the pearlitic structure.

Stainless steels can be divided into three categories, they are martensitic, ferritic and austenitic. The martensitic group which can be hardened by quenching contains approximately 13% chrome and no other major alloying element. The ferritic group contains 17 to 30% chrome with also no other major alloying element present. The austenitic group contains about 18 to 20% chrome with 8 to 15% nickel. The iron-carbon phase diagram at 13% chrome is given by Bungardt et. al.[47]

The metallurgy of martensitic stainless steels is described by Colombier and Hochmann.[48] These steels are used when high hardness is essential irrespective of ductility. Hardness is the prime consideration even at some cost to corrosion resistance. The structure of the steel is in fact determined by the balance between those elements that form ferrite such as Mo, W, V, Cr, Ti, Nb, Si and Al with those that stabilize austenite such as C, Mn and Ni. Chrome, for example, extends the ferrite phase field and narrows down or suppresses the austenite phase field which disappears completely at 25% chrome. In alloys with up to 10% chrome the carbide formed is a cementite $(Fe, Cr)_3C$. Beyond this level the complex carbides $(Cr, Fe)_{23}C_6$ and $(Cr, Fe)_7C_3$ are formed. Chrome also has a significant influence on the as - quenched hardness. For steels quenched from 1000 ^{o}C, the hardness falls off substantially as the chrome content is increased from 13 to 17%. Since a high chrome content is unavoidable to ensure good corrosion resistance a compromise must be

made between the two properties. Hardness can only be increased at the expense of corrosion resistance. Maximum hardness for a 0.6 to 1.0% carbon martensitic stainless steel is reached when quenched from about 1070 °C, with rapid reduction in hardness at higher temperatures. Figure 2.11 of reference (48) shows the hardness as a function of quenching temperature for a 0.7 and 1.0% carbon martensitic stainless steel. Large amounts of residual austenite are obtained on quenching to room temperature which cannot be all broken down even by cooling to -80 °C. The characteristic microstructure after heat treating for maximum hardness consists of a uniform dispersion of fine alloy carbides in a martensitic matrix.

When tempering a 1% carbon martensitic stainless steel the hardness falls off appreciably between 150 and 250 °C. Above 300 °C the hardness tends to increase slowly corresponding to the break down of residual austenite and the precipitation of carbides. The high hardness of Lescalloy BG42 a martensitic stainless steel, can be maintained upon exposure to elevated temperatures because peak hardnesses develop on tempering in the 510 to 538 °C range. Subsequent exposure to temperatures approaching this level does not lower the room temperature hardness.

Alloying elements such as molybdenum in martensitic stainless steel reduces the hardenability and necessitates the use of higher austenitizing temperatures. Nickel is used to maintain hardenability at high chrome contents. The presence of vanadium produces hard alloy carbides which give wear resistant properties.

According to Colombier and Hochmann[48] the corrosion resistance of a stainless steel is a result of their chrome content. The chrome undergoes preferential oxidation since its affinity for oxygen is

higher than that of the iron. It forms a thin surface film on the metal comprising of oxides impermeable to and insoluble in corrosive media. This protective film can only form in the presence of oxidizing agents. Figure 6.13 of reference (48) shows oxidation as a function of time for stainless steels at 1000 ^{o}C. Martensitic stainless steels with 13% chrome have good scaling resistance up to 800 ^{o}C. Due to the preferential oxidation of chrome amounts greater than 12% below 1000 ^{o}C increase the oxidation resistance of iron almost a hundred fold as measured by film thickness, Kubaschewski and Hopkins.[49] As soon as a layer consisting of Cr_2O_3 or rather $(Cr, Fe)_2O_3$ or the spinel type oxide $FeO \cdot Cr_2O_3$ is formed a protective effect is accomplished. Stoddart and Hondros[50] using Auger electron spectroscopy on a 1 μm film oxidized on 18% chrome, 8% nickel steel at 900 ^{o}C found enrichment of chrome in the outer layers of oxide. With long exposures to oxidation, iron ions obviously diffuse through the spinel film and build up an outer layer consisting mainly of iron oxides, Kubaschewski and Hopkins.[49] Isherwood and Quinn[51] using X-ray glancing angle on thin oxide films formed on iron chrome alloys containing up to 40% chrome, showed that temperature was more important than chrome content in determining which type of oxide was present. They concluded that the transition temperatures of 270 ^{o}C characterised by the formation of rhombohedral oxide and γ-Fe_2O_3, 350 ^{o}C by the appearance of the spinel phases and finally at 550 ^{o}C when the wustite phases appear were almost unaffected by chrome content. The rhombohedral oxide is a solid solution consisting of a mixture of α-Fe_2O_3 and Cr_2O_3, the spinel oxide is a solid solution of Fe_3O_4 and $FeCr_2O_4$. The wustite phases consist of

FeO and CrO where γ-Fe_2O_3 is simple cubic. Isherwood and Quinn[51] showed that the relative proportions of wustite to other oxide phases for temperatures greater than 600 °C decreased with increasing chrome content for amounts greater than 10%. They suggested the presence of γ-Fe_2O_3 found in the high temperature patterns could possibly be due to its formation during cooling and storage.

Colombier and Hochmann[48] shows that the addition of nickel to stainless steel improves the corrosion resistance. Also additions of molybdenum improves the corrosion resistance in moist surroundings. The silicon content needed to bring about a significant improvement is about 2%.

1.8 The Tungsten-Carbon-Cobalt System

The phase diagram of the tungsten carbon system has been shown by Hansen[46] which formed the consensus of work until 1958, Orton[52] in 1964 and Sara[53] in 1965. They show that two carbides WC and W_2C can exist in two forms. According to Hansen[46] tungsten carbide of hexangonal structure which occurs at 6.12% carbon remains stable up to 2600 °C. Orton[52] shows that tungsten carbide exists up to 1760 °C with α-W_2C + carbon appearing. At 2525 °C there is liquid and carbon with the carbon disappearing completely at 2750 °C. Sara[53] shows that tungsten carbide at a temperature of 2755 °C decomposes into the face-centred cubic phase and carbon, this exists over a narrow range of temperature going to liquid and carbon at 2785 °C. Tungsten carbide itself is brittle, but in combination with cobalt the properties of this binding or cementing metal decrease the brittleness, Rieck.[54]

The effect of cobalt on tungsten carbide has been described by Young.[55] Cobalt was introduced as the metal matrix to contain and

bind the hard carbide particles. The tungsten carbide should have a total carbon content of 6.05 to 6.2% and a free carbon content not above 0.1%. In cemented carbide production the grain size and the ratio of cobalt to tungsten carbide may vary widely. Increasing the cobalt content decreases the hardness and increases the toughness of the cemented carbide. The grain size of the tungsten carbide in the final hard metal is determined largely by the grain size of the tungsten metal powder originally used. Cobalt is usually added in the form of metal powder but cobalt oxide may be employed. The sintering temperature is quite critical and differs for the various grades of carbide, this is about 1300 ^{o}C for 20% cobalt. During the sintering process which causes a 20% shrinkage, the cobalt melts and dissolves about 14% of tungsten carbide, all but 1% of which is reprecipitated on cooling. According to Dawihl and Frisch[56] the alloy after sintering is subject to internal stresses due to different expansion behaviours of tungsten carbide and the cobalt phase. They suggested that the relief of internal stresses at elevated temperatures increased the mechanical resistance and reduced the wear. They also showed that cemented tungsten carbide has excellent hot hardness and hot strength. Gurland and Norton[57] showed that the effectiveness of cobalt as a binder is due to the relatively low melting temperature of the cobalt - tungsten carbide solid solution, the solubility of tungsten carbide in cobalt and the wetting of solid carbide particles by the liquid binder. Densification occurs as the result of a re-arrangement of the carbide particles, which achieve a denser packing under the influence of the surface tension forces of the binder.

Rautala and Norton[58] published part of the tungsten-carbon-cobalt ternary system. They assumed that the cobalt-tungsten carbide

system which is shown in figure 1.3 behaves like a simple binary. The specimens were subjected to fast cooling rates and they believed that the high temperature structures were satisfactorily retained. Gurland[59] studied the effect of carbon content on the structure and properties of tungsten carbide containing cobalt. A vertical section through the tungsten-carbon-cobalt ternary diagram at 16% cobalt is shown in figure 1.4. Gurland[59] identified the phases by metallographic and X-ray diffraction techniques after being water quenched from the temperature of investigation. The temperatures of the invariant planes at 1298 and 1357 ^{o}C were established by Rautala and Norton[58]. Gurland[59] showed that tungsten carbide and a cobalt rich solid solution are present in the sintered structure if the carbon composition corresponds very closely to the theoretical carbon content of tungsten carbide which is 6.12%. Small deviations from the ideal carbon content result in the appearance of either graphite (C) or the double carbide W_3Co_3C, the n-phase. A deficiency of carbon will have more detrimental effect than an excess, since the former produces the n carbide which reduces the strength by displacing the binder from the sintered structure, Gurland.[59] Figure 1.4 shows the n-phase will form during sintering and will be present at room temperature if the tungsten carbide contains less than approximately 6% carbon. If the carbon content is about 6.05% the n-phase can only be maintained at room temperature by rapid cooling.

X-ray photographs of cobalt powder taken by Edwards and Lipson[60] show that above a temperature of 500 ^{o}C the face-centred cubic phase β-Co is stable. At room temperature about equal amounts of hexagonal and face-centred cubic forms were found to be present. They found

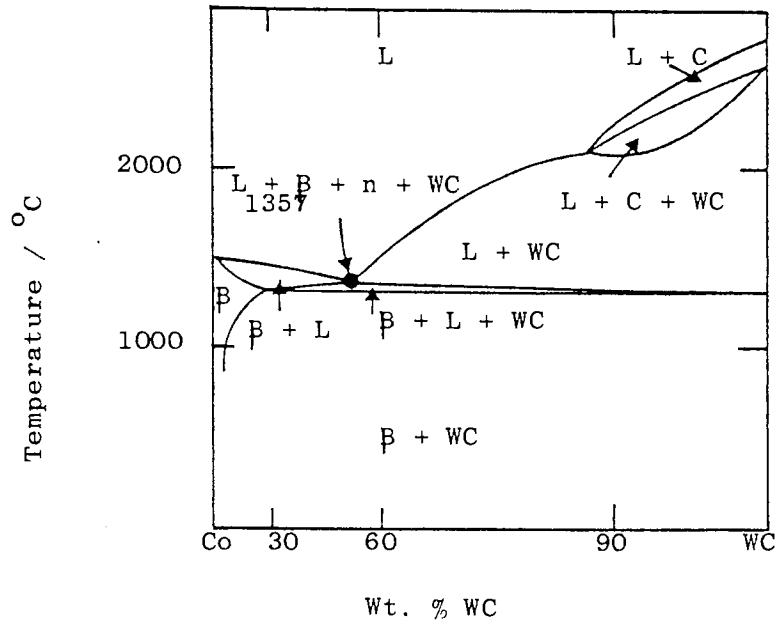

Fig. 1.3. Vertical section of Co - WC, Rautala and Norton (58).

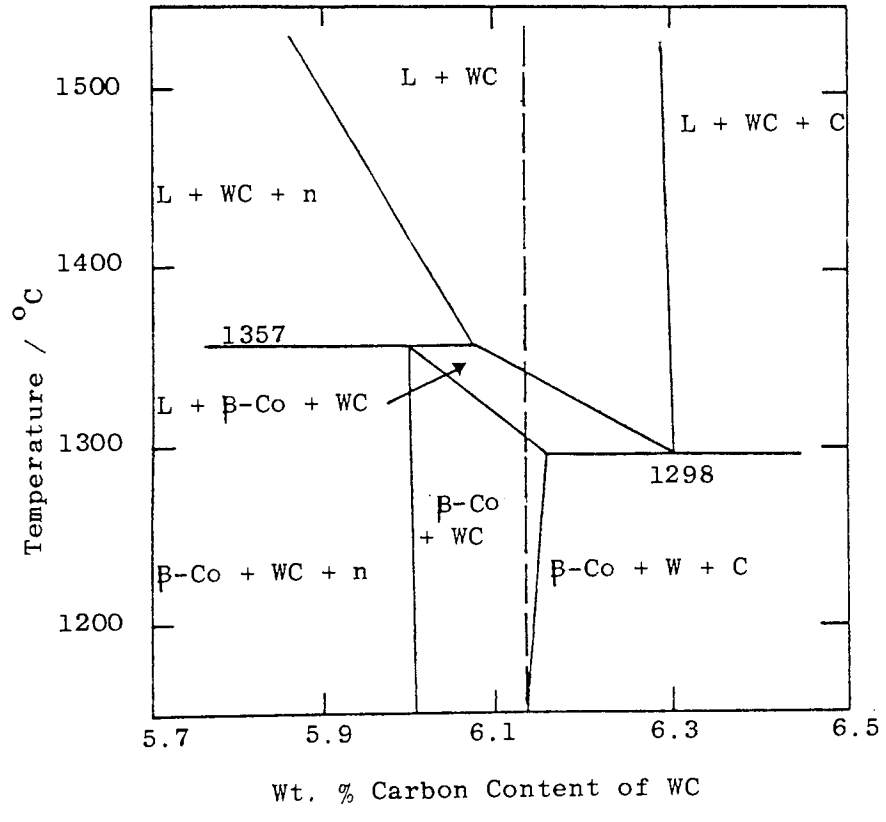

Fig. 1.4. Vertical section through the ternary diagram at 16 wt. % Co, Gurland (59).

with rod specimens the transformation on cooling begins at about 400 ^{o}C and is almost complete at about 300 ^{o}C. On heating, the transformation back to the cubic form takes place for both specimens at about 500 ^{o}C. Troiano and Tokich[61] using X-ray analysis, showed that the allotropic transformation from cubic to hexangonal occurred at 388 ^{o}C in coarse grained cobalt. This type of reaction could not be detected in fine grained cobalt. They showed that the time required for the isothermal transformation from hexangonal cobalt to cubic decreased as the temperature was raised. Owen and Madoc-Jones[62] in 1954 showed that the stable structure of cobalt was found to depend on the grain size between room temperature and about 450 ^{o}C. When the grain size is very small as in cobalt sponge the stable structure is face-centred cubic. When the grain size is large as in a solid rod the stable structure is close-packed hexangonal. They showed at temperatures above 450 ^{o}C the rod changed to a face-centred cubic structure. Owen and Madoc-Jones[62] stated that all specimens of cobalt whatever the grain size annealed at about 1000 ^{o}C and quenched show a mixture.

Webb et. al.[63] showed that two oxides form during the oxidation of tungsten between temperatures of 700 and 1000 ^{o}C in oxygen. They found the outer layer was yellow tungstic oxide WO_3 and the inner layer was a dense thin dark blue adherent oxide of uncertain composition. The oxidation reaction followed initially the parabolic rate law, but eventually there was a transition to the linear rate law. Webb et. al.[64] invested the oxidation of tungsten and tungsten carbide at temperatures of 700 and 1000 ^{o}C in oxygen. They suggested the higher rate of oxidation of tungsten carbide compared to tungsten was due to rupture of the oxide film due to formation of CO and CO_2.

They found that tungsten carbide oxidized according to a linear rate law. An examination of the oxide film formed on tungsten carbide at 700°C revealed only the presence of yellow tungstic oxide WO_3. There was no lower blue oxide layer found like that on tungsten. According to Newkirk[65] fine tungsten carbide powder containing approximately 6.2% carbon reacts relatively slowly with air below a temperature of 500 °C. Above this temperature it begins to oxidize rapidly which at 529 °C leads to complete burning. He showed that the onset of rapid oxidation occurred at about 565 °C for macro-crystalline tungsten carbide also containing 6.2% carbon.

The oxidation of cobalt has been described by Young.[55] Like iron, cobalt has three well known oxides, the monoxide or cobaltous oxide CoO, cobaltic oxide Co_2O_3 and cobaltosic oxide Co_3O_4. Above a temperature of approximately 850 °C the cobaltous oxide CoO is the stable oxide. Co_2O_3 is formed when cobalt compounds are heated at a low temperature in the presence of an excess of air. Co_2O_3 is completely converted into Co_3O_4 at temperatures above 265 °C. Below 700 °C the rate is controlled by the diffusion rate of cobalt cations through the Co_3O_4 layer, above 700 °C the rate is determined by diffusion through the CoO layer. Gulbransen and Andrew[66] studied the oxidation of cobalt over the temperature range of 200 to 750 °C. They showed the oxidation of cobalt was parabolic over the temperature range 350 to 550 °C in oxygen at 1 atmosphere. The rate of oxidation was found to increase abruptly between 600 and 700 °C. In this temperature range of 600 to 700 °C the oxide films cracked on cooling while at temperatures less than 600 °C the oxide appeared coherent.

1.9 Brief Description of Research

Experiments were conducted at temperatures up to 500 °C on angular

contact bearings similar to those used in service in the air motor. The balls were constructed from tungsten carbide containing 11% cobalt and the inner and outer races from martensitic stainless steels, Lesc-alloy BG42 and A.I.S.I. 440C MOD. Since both rolling and sliding occurs and because of the geometry it was difficult to do a complete physical analysis of wear, heat flow and worn surfaces for this configuration. Therefore experiments were carried out under pure sliding conditions using a pin-on-disc apparatus for disc temperatures up to 500 ^{o}C. The disc was made of WC - 11% Co and the pins of the martensitic stainless steel. This particular configuration was chosen because most of the wear was expected to occur on the steel which made measurement of wear far easier. The frictional force was measured and so was the heat flow along the pin from which the surface temperature was computed.

Compounds in the wear debris and present on the surfaces were identified using X-ray diffraction. The surfaces of selected worn pins and the worn tracks of the angular contact bearings were investigated using the scanning electron microscope. This was also used in conjunction with an energy dispersive analyser, which identified the surface elements present. Hardness tests were taken of these pins and surface profiles were taken of the disc for tracks of interest. The thickness of oxide films under static conditions on the martensitic stainless steels were measured using a technique known as ellipsometry.

CHAPTER 2

EXPERIMENTAL DETAILS

2.1 Introduction

Experiments were conducted on a Lucas angular contact bearing test rig and on a conventional pin-on-disc test machine at temperatures up to 500 ^{o}C. The angular contact bearings outer and inner races were made of Lescalloy BG42 and A.I.S.I. 440C MOD martensitic stainless steel and the balls of tungsten carbide containing 11% cobalt. On the elevated temperature sliding wear pin-on-disc test machine, the pins were made of the steel and the disc of the WC - 11% Co. Track and ball wear measurements were obtained from the angular contact bearing tests with also friction and wear measurements from the pin-on-disc machine. The heat flow along the pin was also measured from which the surface temperature was computed. Samples for analysis were produced by both test machines with the majority coming from the pin-on-disc experiments.

Surface profiles were taken of the disc using the talylin to show certain wear tracks of interest. The compounds in the wear debris were identified using powder X-ray diffraction with $Co_{K\alpha}$ radiation. Glancing angle X-ray diffraction was used to identify the compounds present on the surfaces of the balls and on selected steel pins. The scanning electron microscope was used to observe and photograph the surfaces of slected worn pins taken from the elevated temperature sliding wear pin-on-disc test rig and also the worn tracks of the angular contact bearings. The scanning electron microscope was also used in conjunction with an energy dispersive analyser to identify the surface elements present. Hardness tests were taken of these pins using a

Vickers hardness tester and a miniload system for measuring the surface hardness.

For both types of martensitic stainless steel, the thickness of an oxide film produced by placing the samples in a furnace at temperatures up to 600 ^{o}C were measured using a technique known as ellipsometry. From the oxidation rates the rate constants were obtained, this enabled the activation energy and the Arrhenius constant to be calculated from measurements of oxidational growth rates.

2.2 The Lucas Angular Contact Bearing Test Rig

The 35 mm diameter angular contact bearings were made from Lescalloy BG42 and A.I.S.I. 440C MOD martensitic stainless steels having a track surface finish of 0.15 to 0.2 μm c.l.a. Each bearing contained twenty 3 mm diameter WC - 11% Co Wimet grade G balls with a surface finish less than 0.2 μm c.l.a. A typical bearing is shown in figure 2.1 with part of its outer race removed exposing the balls and wear track on the inner race. Figure 2.2 shows a section of the bearings and loading arrangement which was placed inside a furnace. Two angular contact bearings were used, the test bearing and a second bearing just for alignment. They were loaded using a spring, the calibration curve for which is shown in figure 2.3. An axial load of 776 N was applied through a sleeve onto the inner race of the housing alignment bearing. The load was then transmitted through the bearing housing, which was prevented from rotational movement, to the test bearing. The shaft was driven by an hydraulic motor, where the speed was measured with an inductive tachometer capable of measuring speeds up to 10,000 r.p.m. The speed of the shaft reached 33.3 revs s^{-1} over a one second period, with a delay time of 27 seconds so as to prevent rapid temperature rise. This was achieved using a variable timer controlling a

Fig. 2.1. An angular contact bearing. Part of the outer race has been removed exposing the WC - 11% Co balls and wear track on the inner race.

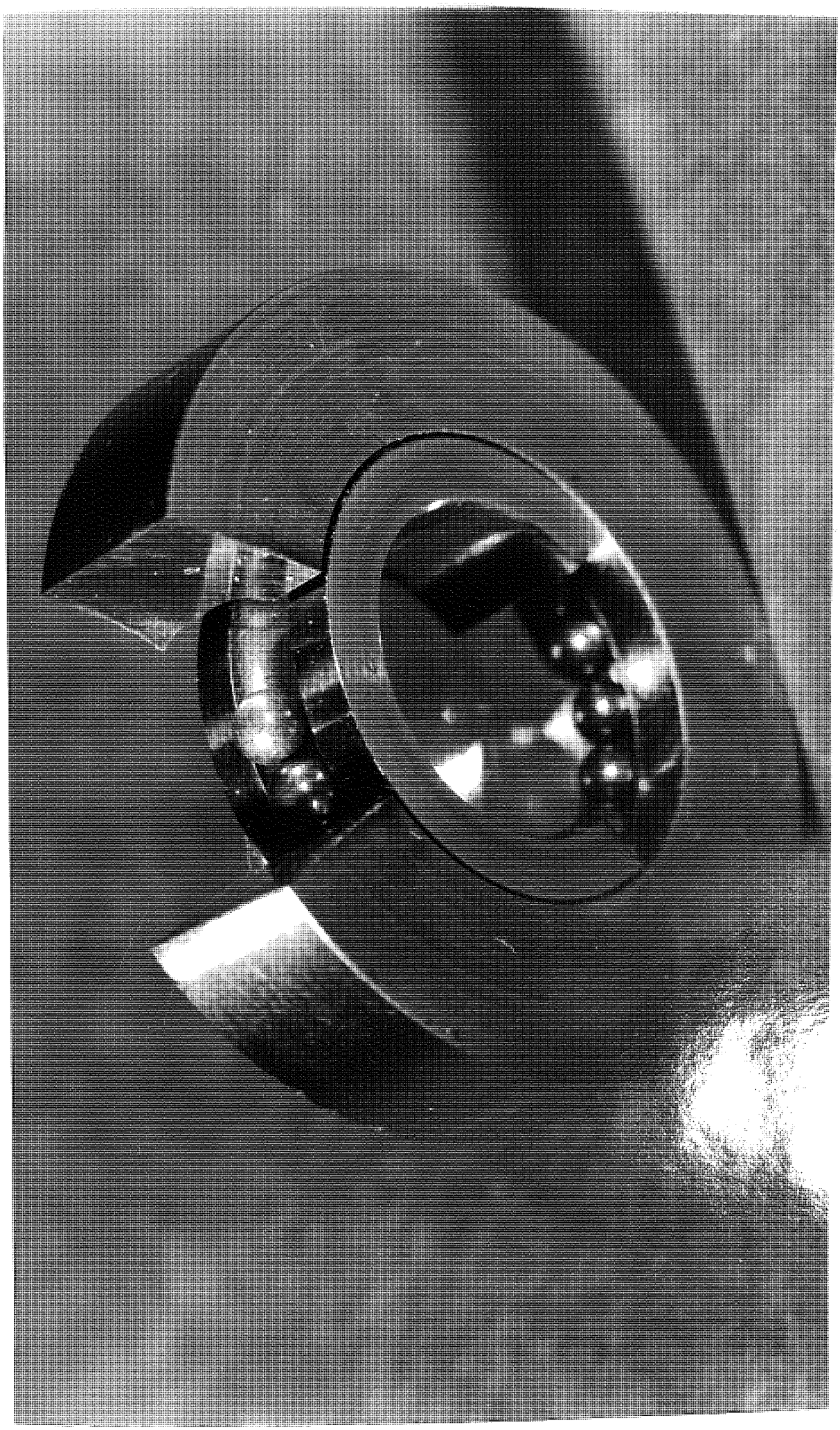

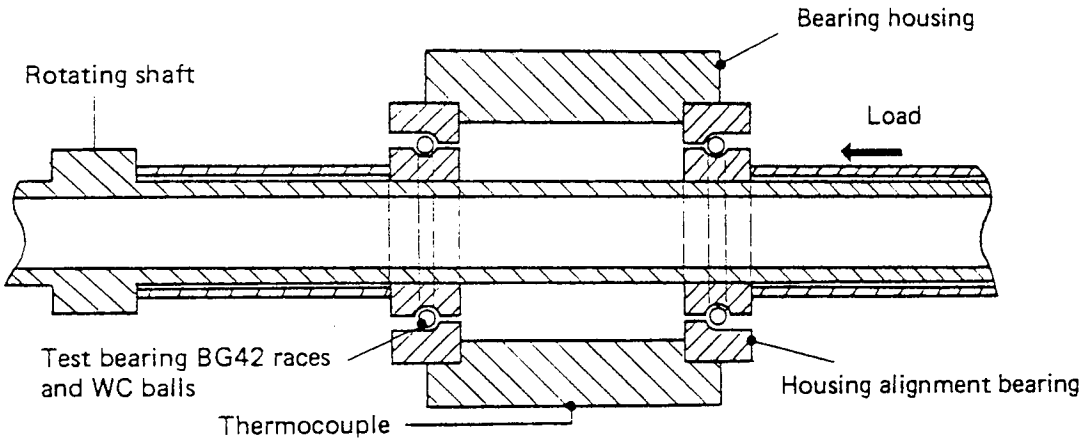

Fig.2.2. Schematic of the angular contact bearing test machine showing a section through the bearings and loading arrangement. The whole of this part of the machine was enclosed in a furnace.

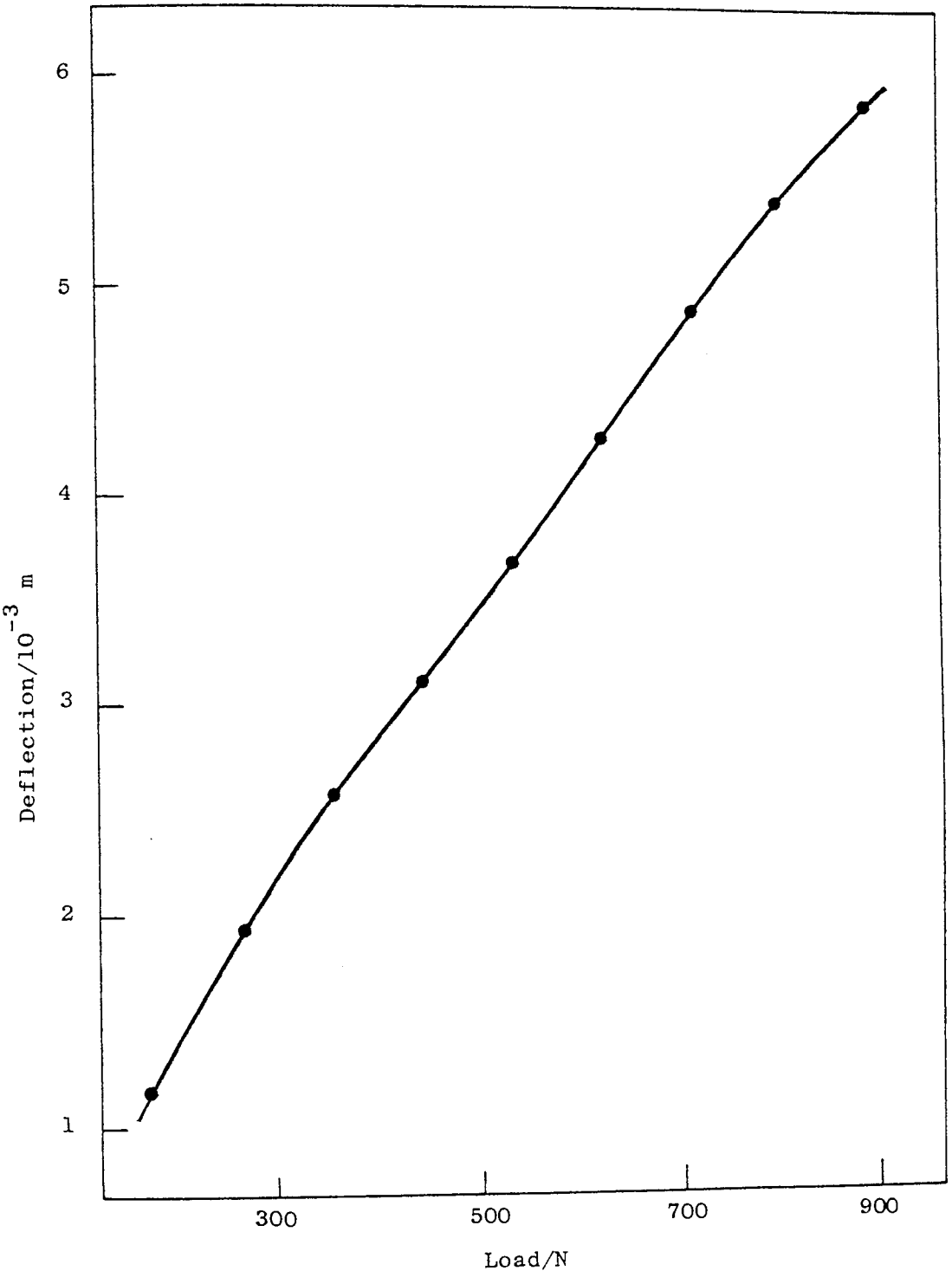

Fig. 2.3. Spring deflection as a function of load.

solenoid value situated in the inlet line to the motor as shown in figure 2.4. The number of cycles were recorded using a mechanical counter triggered by the variable timer unit. Chromel-alumel thermo-couples were used for furnace regulation and angular contact bearing temperature measurement.

The bearings were investigated over the temperature range 100 to 500 ^{o}C. All the bearings were run for 400 cycles at the required temperature to obtain a 50% track conformity before starting the wear tests. This was to obtain a track radius equal to the radius of the ball, so producing a constant area of contact.

$$\text{Track conformity} = \frac{\text{track radius}}{\text{ball diameter}} \times 100 \qquad \ldots\ldots\ldots\ldots\ldots\ldots (2.1)$$

The classical Hertz formulae for contact stress assumes the contacting surfaces to be non-conforming, for example see Timoshenko and Goodier[67] and Levit.[68] This is not true for a circular arc track in which the ball and track wear to a matching conformity of 50%. In this case the calculated Hertz stress becomes zero, since theoretically the conforming contact of the infinite bodies implies infinite contact area.

$$W_b = Q / z \sin \gamma \qquad \ldots\ldots\ldots\ldots\ldots\ldots\ldots\ldots (2.2)$$

W_b is the load on the ball, Q is the axial load, z the number of balls and γ the contact angle. The ball contact stress is given by equation (2.3).

$$\sigma = \left[\frac{W_b \, E^2 \, (1.1804 + 0.0987 \, d_b / D)^6}{156 \, . \, 249 \, d_b^2} \right]^{1/3} \qquad \ldots\ldots (2.3)$$

Where E is the average elastic modulus of the materials (3.89×10^{11} $N m^{-2}$), d_b the ball diameter and D the inner diameter of the outer race (2×10^{-2} m, see figure 2.5). Equations (2.2) and (2.3) were used by

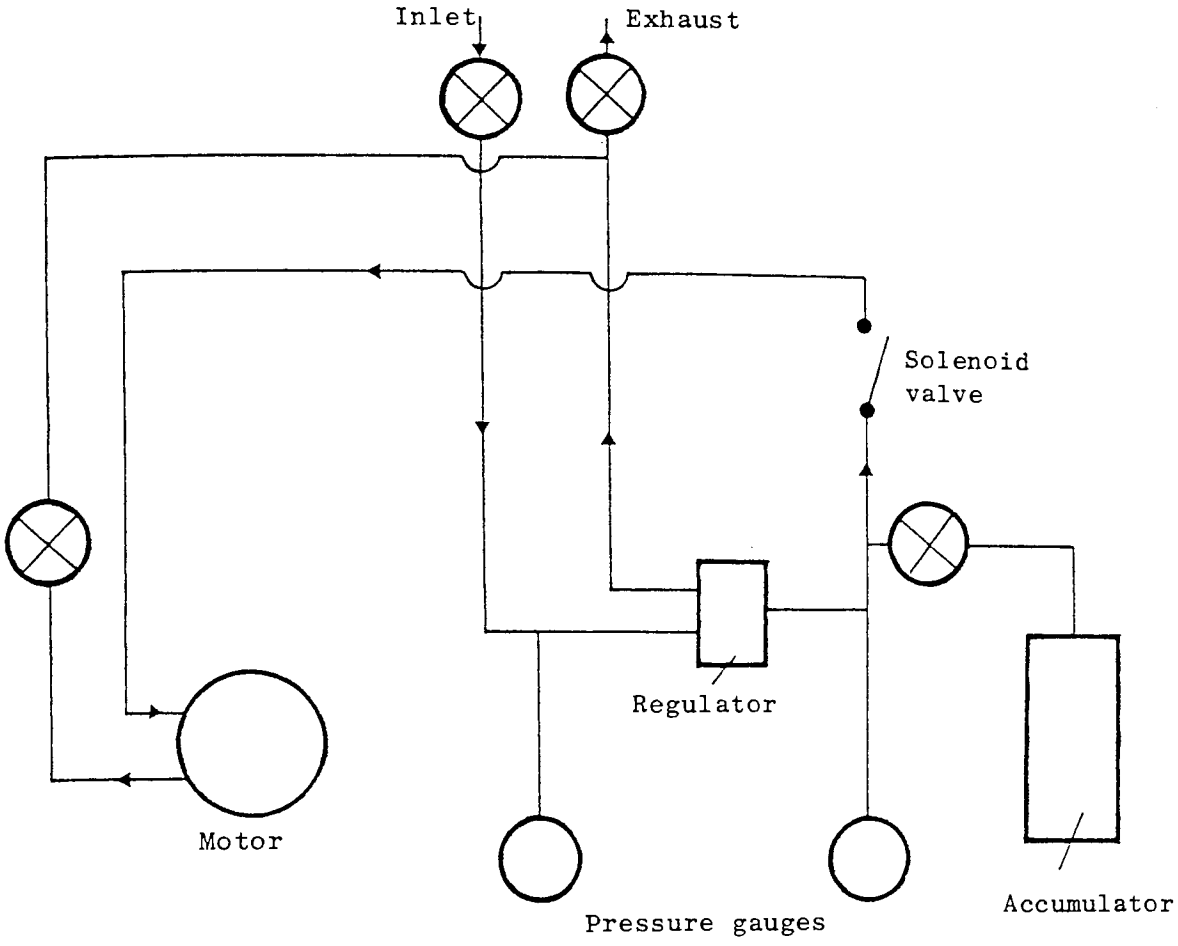

Fig. 2.4. The hydraulic system.

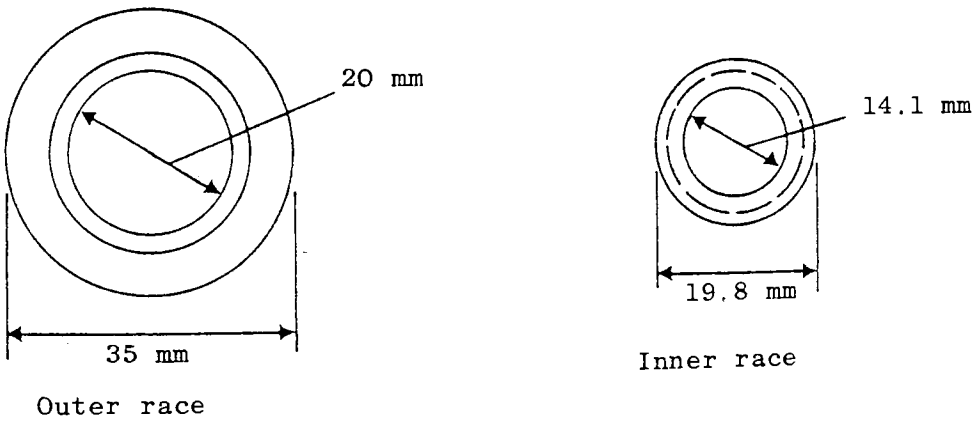

Fig. 2.5. An angular contact bearing.

Parks[44] and are valid for 56% to 50% track conformity, the range over which the area of the contacting ellipse has been allowed for. For a 52% track conformity γ = 35 degrees, using equation (2.2) the load on the ball W_b = 67.6 N and from equation (2.3) the ball contact stress σ = 2.8 x 10^9 N m^{-2}. For a 50% track conformity γ = 45 degrees, therefore W_b = 54.9 N and σ = 2.6 x 10^9 N m^{-2}.

For a new set of balls the bearings were run for 1000 cycles at the appropriate temperature. The depth of the wear track on the bearings inner race was measured from shadowgraph recordings of the track profile. The shadowgraph was an optical instrument which magnified a test specimen up to a hundred times by projecting its image onto a screen. The outer race was not considered because of possible error due to bearing alignment, and also replicas taken of the wear tracks produced refraction effects when observed with the shadowgraph. At the end of the experiments eight balls were taken from each bearing and measured using a micrometer where an average was then taken.

2.3 The Elevated Temperature Sliding Wear Test Machine

The sliding wear test rig was a conventional pin-on-disc machine which was originally described by Dunckley[69] in 1977. A general view of the test rig showing all the instrumentation is shown in figure 2.6. On the test rig the pins were of 6.52 mm diameter flat faced Lescalloy BG42 and A.I.S.I. 440C MOD martensitic stainless steel of length 31.8 mm, sliding against a 127 mm diameter WC - 11% Co disc. The surface finish of both the pin and disc was 0.2 μm c.l.a. which was approximately the same as the materials used in the angular contact bearing experiments. Prior to each experiment they were cleaned and degreased first with a detergent and then with propanol. Due to insufficient material the A.I.S.I. 440C MOD pins were brazed onto A.I.S.I. 440C shafts.

The disc was mounted onto the water cooled rotating shaft via a sindanyo block preventing heat loss by conduction due to its low thermal conductivity. The loading arm was modified which allowed tests to be carried out at two separate track radii, 50 and 58 mm, allowing the disc to be used four times before repolishing for the experiments which required no external heating. The disc was polished using fine grade alumina powder. The load on the pin was applied by an air piston mounted along the axis of the shaft for loads of 19.6 N and higher. Loads less than 19.6 N were applied by weights. This was necessary due to the friction in the air piston which would have possibly caused error. The air piston was calibrated using a strain gauge dynamometer which measured the force for a given air pressure supplied by a cylinder. The load exerted by the piston as a function of air pressure is shown in figure 2.7,where loads of up to 170 N were obtained. The frictional force, the wear rate of the pin and temperatures were obtained directly from the test machine. The frictional force was measured using a strain guage dynamometer and the wear rate was continuously monitored using a linear voltage displacement transducer, see section 2.5. Both the frictional force and the wear rate were displayed on a chart recorder. The linear sliding speed of the disc at the pin U is given by equation (2.4).

$$U = 2 \pi R_w f_s \quad \ldots\ldots\ldots\ldots\ldots\ldots\ldots\ldots\ldots\ldots\ldots\ldots\ldots\ldots\ldots\ldots (2.4)$$

R_w is the radius of the wear track on the disc and f_s the speed of the rotating shaft. The speed of the shaft driven by a 5 H.P. motor was measured using a handheld mechanical tachometer.

The heater was a 2 kW domestic cooker ring which was fixed to the face of the disc opposite to the wearing surface as shown in figure 2.8. Its power was supplied by carbon brushes running on slip rings.

Fig. 2.6. A general view of the elevated temperature sliding wear test machine showing all the instrumentation.

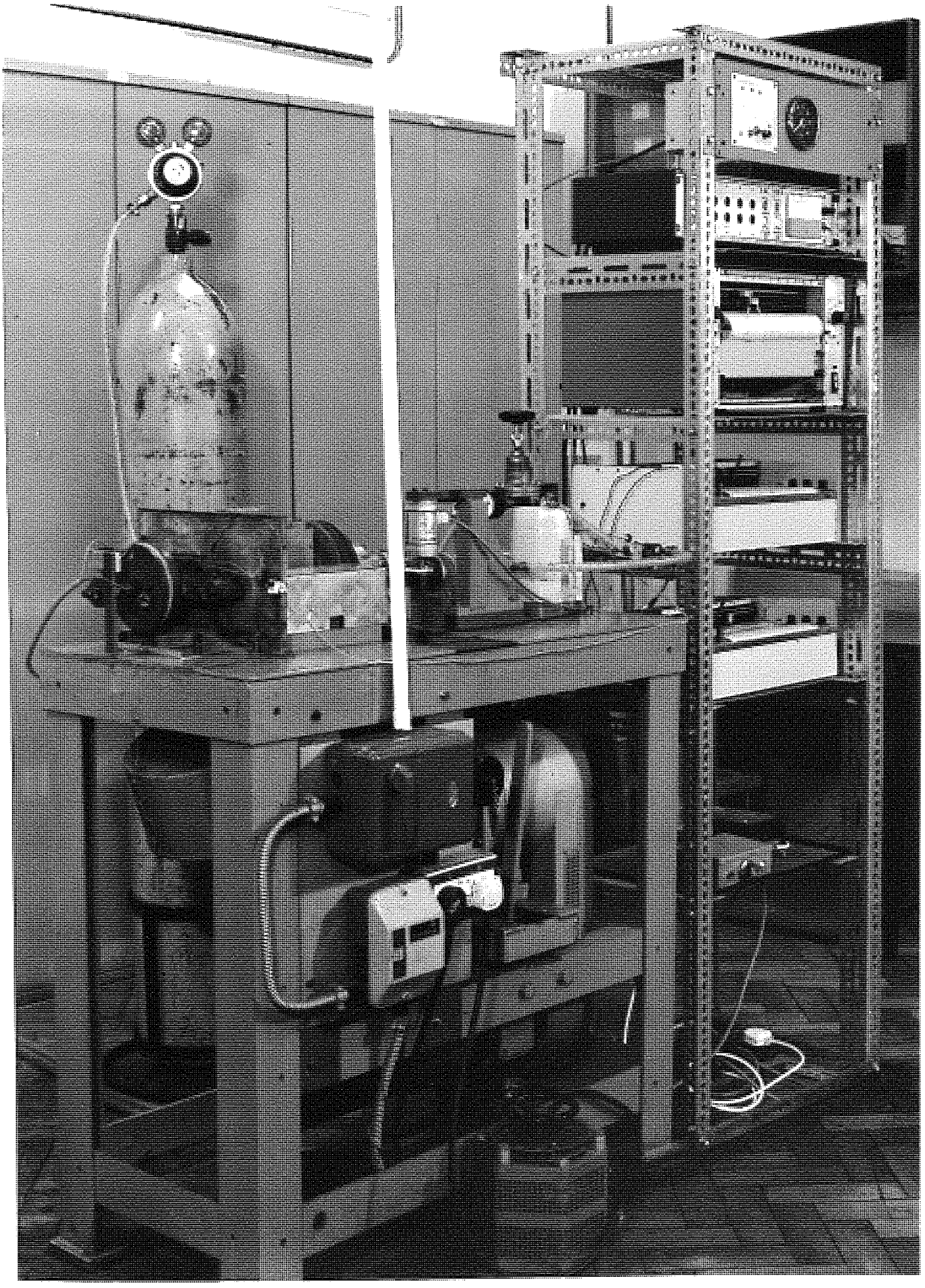

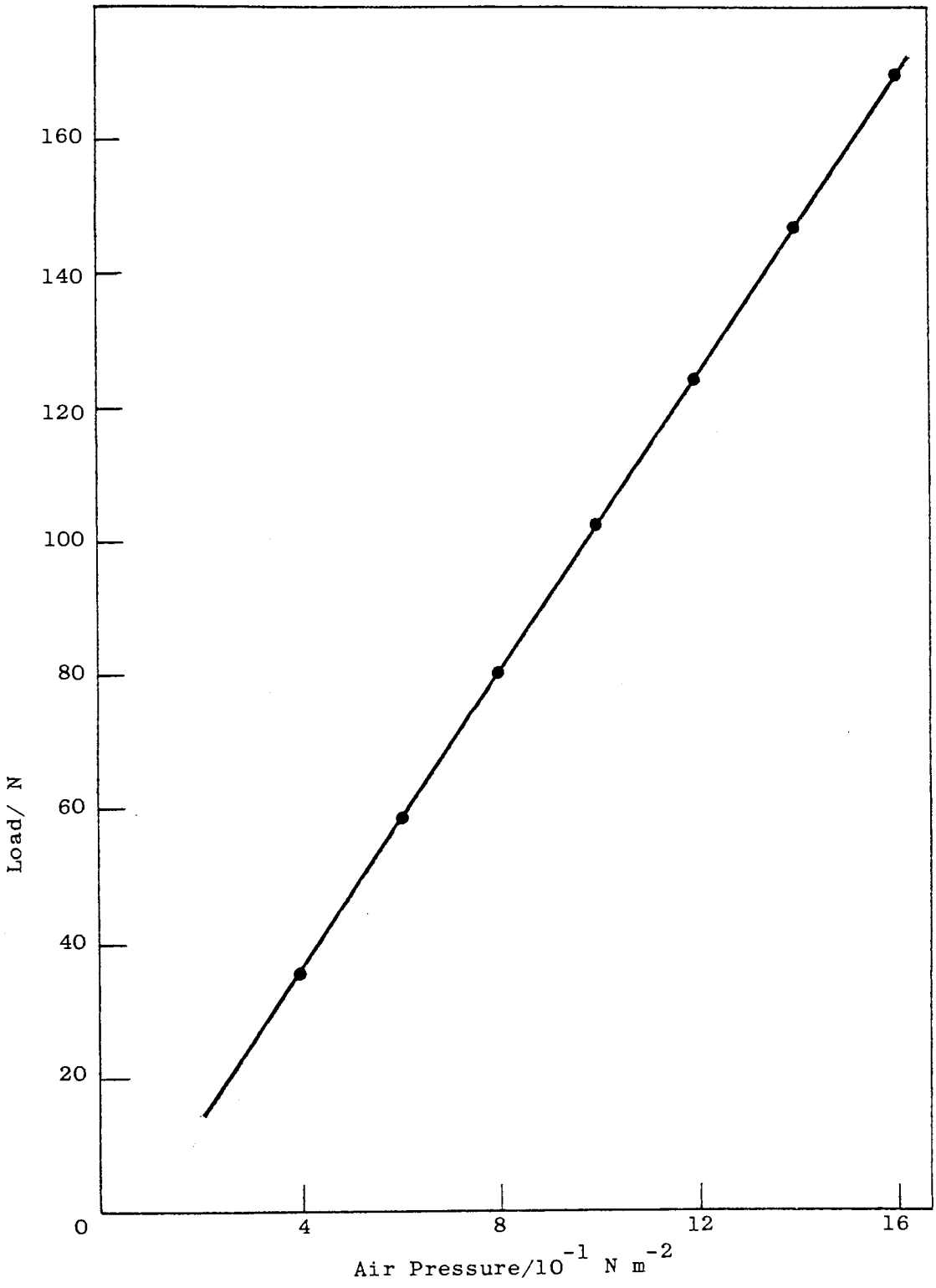

Fig. 2.7. Load exerted by the piston as a function of air pressure.

Fig. 2.8. Detail of the elevated temperature wear rig showing loading arm and steel pin against the WC - 11% Co disc, with the heater element clamped to the rear of the disc. The slip rings on the front (pin) side of the disc are for the thermocouple, those at the rear feed the heater.

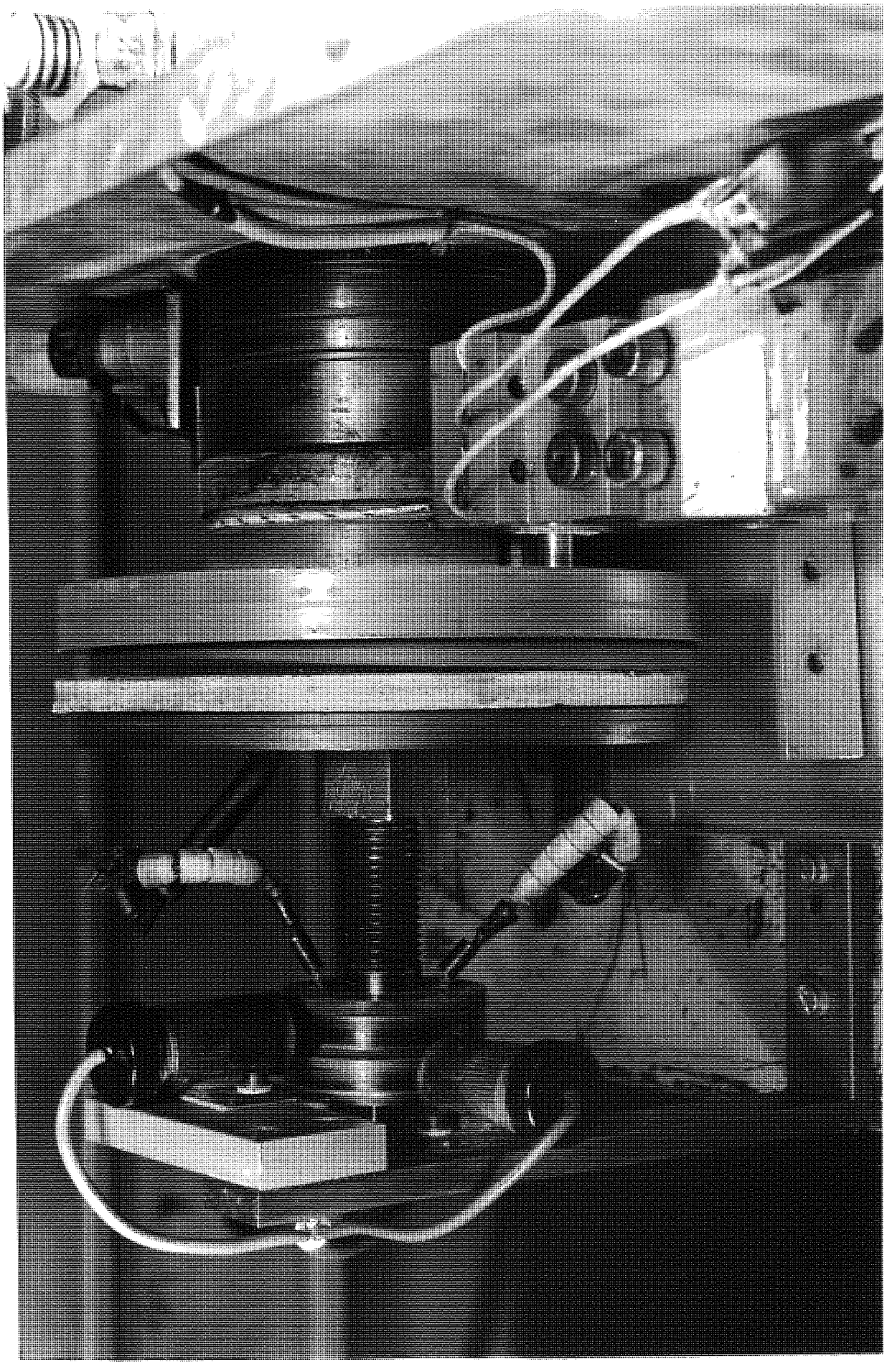

The temperature of the disc was measured using a chromel-alumel thermocouple in contact with the disc at a radius of 30 mm, where again slip rings were used for connection. This was used in conjunction with a self designed temperature controller described in section 2.4, which stabilized the temperature of the disc by controlling the power to the heater. This prevented any further increase in temperature caused by frictional heating. A variable auto-transformer was used in series with the heater to reduce the heater current. This prevented temperature overshoot each time power was supplied to the heater by the controller. The pin was held in a calorimeter arrangement where the temperature at two points along the pin and also the calorimeter were measured using chromel-alumel thermocouples. This enabled the heat flow along the pin to be measured continuously from which the surface temperature was computed, see section 2.6. All the temperatures were displayed on chart recorders.

The wear rates and the frictional force were measured over a range of loads in the region of 4.9 to 166.8 N, for linear sliding speeds of 0.6, 2.0 and 3.0 m s^{-1} for no external heating, and then at disc temperatures of 200, 300, 400 and 500 ^{o}C at 2.0 m s^{-1}.

2.4 The Temperature Controller

The instrument was designed to stabilize the temperature of the tungsten carbide disc over the temperature range 200 to 500 ^{o}C to within ± 5 ^{o}C. A photograph of the complete unit is shown in figure 2.9. The temperature of the disc was measured using a chromel-alumel thermocouple, with both its reference junctions at 0 ^{o}C. The small e.m.f. produced by the thermocouple was amplified using a d.c. amplifier which enabled it to switch a transistor controlling the current to the heater.

Fig. 2.9. The temperature controller unit.

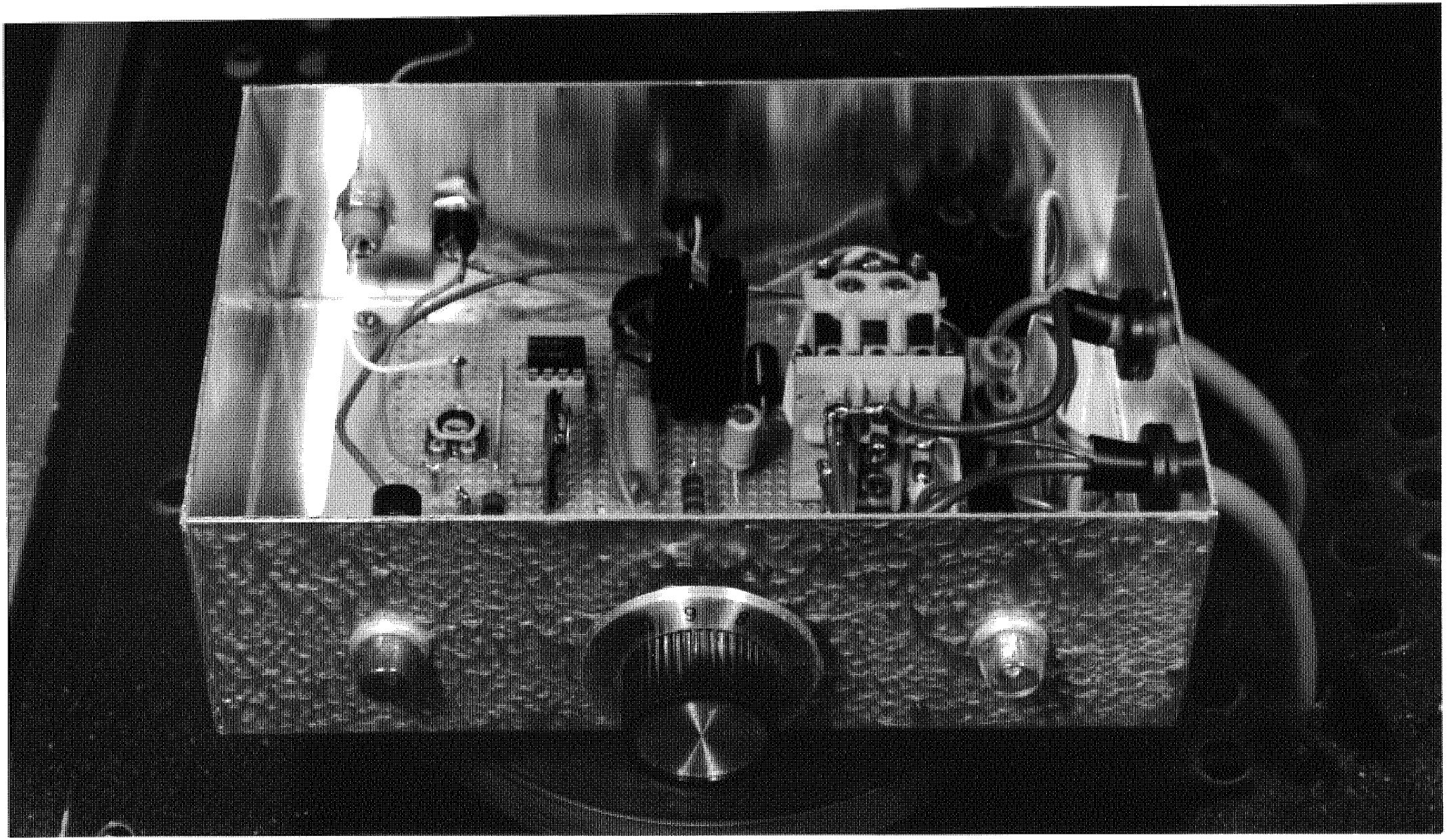

A circuit diagram of the temperature controller is shown in figure 2.10. The unit had a high input impedance of approximately 2 MΩ which did not disturb the e.m.f. produced by the thermocouple. The d.c. amplifier used was a 741 operational amplifier in a 8-pin D.I.L. package connected in the non-inverting configuration. For zero input voltage the output at the operational amplifier was set to zero using RVI. The non-inverting closed loop gain is given by equation (2.5).

$$A(d.c.) = 1 + RV2 / R1 \qquad \ldots\ldots\ldots\ldots\ldots\ldots\ldots\ldots (2.5)$$

The voltage gain of the operational amplifier was set to about 300 using RV2. This value was chosen to keep the output between approximately 2 and 7 volts over the temperature range 200 to 500 ^{o}C. Since the output from the thermocouple was taken through slip rings a small alternating voltage was produced when the disc was rotating. This was undesirable so the a.c. gain was kept to a minimum by CI which produced a large amount of negative feedback. Considering the circuit the a.c. voltage gain is given by equation (2.6).

$$A(a.c.) = 1 + \frac{1}{R1}\left[\frac{(RV2)^2}{1 + (RV2)^2 w^2 C1^2}\right]^{1/2} \qquad \ldots\ldots (2.6)$$

Using the value of RV2 from equation (2.5) the gain ranges from 1.16 at 100 Hz to 4.18 at 5 Hz, which is small compared to the d.c. voltage gain.

The disc temperature was controlled by potentiometer RV3 which applied a selected positive voltage onto the base of transistor Tr1. As the voltage increased due to the increase in disc temperature, the collector current of Tr1 increased closing the relay and cutting the power to the heater. The two pole changeover relay had a 12 V d.c.

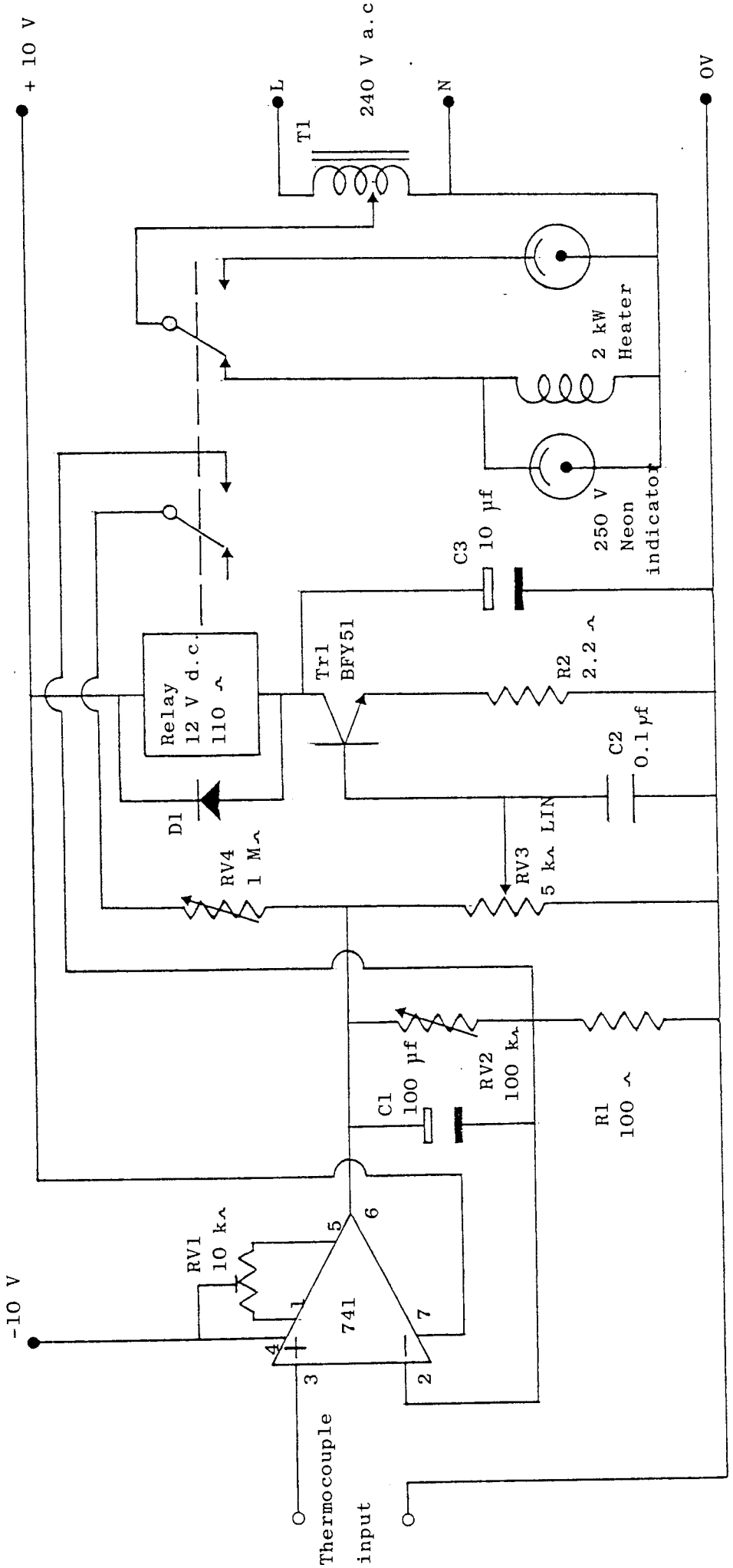

Fig. 2.10. Circuit diagram of the temperature controller.

110 Ω coil with gold-flashed silver contacts rated at 10 A at 250 V a.c. Because the collector current can be quite high the transistor Tr1 required a heatsink of thermal resistance 50 $^{o}C\ W^{-1}$. In order for the relay to open, the collector current would have to decrease by a large amount which would require a large temperature decrease at the disc. To prevent the thermal cycling of the disc, the collector current of Tr1 was decreased automatically once the relay had closed by switching RV4 in parallel with RV2. This reduces the gain of the 741 operational amplifier and thus the voltage on the base of Tr1, leaving just enough collector current to hold the relay closed. Therefore only a small temperature decrease was necessary to cause the relay to open and therefore supply power to the heater. Also a variable auto-transformer T1 was used to reduce the heater current which prevented temperature overshoot each time power was supplied to the heater.

The diode D1 protects the transistor from the voltage pulses caused by the switching of an inductor. Because the emitter-collector current can increase with transistor temperature negative feedback was applied by R2. Therefore when the emitter-collector current rises it produces an increase in voltage on the emitter reducing the base-emitter voltage and thus stabilizing the collector current. The variable resistors RV1, RV2 and RV4 are all open skeleton presets.

After switching on the heater the temperature of the disc was allowed to increase until the required temperature was reached as indicated on the chart recorder. The potentiometer RV3 which is located on the front of the controller was rotated from zero on the dial until the green neon lamp was illuminated. The disc temperature was now stabilized and fine adjustment was made using RV3 where it was found necessary.

2.5 Friction and Wear Measurements

The frictional force was measured by a strain gauge dynamometer capable of measuring loads up to 890 N. Its output was amplified using a d.c. amplifier which was then recorded on a chart recorder. For a fixed voltage gain, the output voltage of the strain gauge varying with compressive load is shown in figure 2.11. The frictional force F (N) is given by equation (2.7).

$$F = x_o \, q \, / \, G \, (b - R_w) \qquad \ldots\ldots\ldots\ldots\ldots\ldots\ldots\ldots\ldots\ldots (2.7)$$

G is the slope from figure 2.11 (2.548×10^{-3} V N^{-1}), q the distance of the strain gauge to the load axis (6.1×10^{-2} m), b the distance of the load axis to the rotating shaft (10.7×10^{-2} m), R_w is the radius of the wear track on the disc (5×10^{-2} m, 5.8×10^{-2} m) and x_o is the displacement taken from the chart recorder (V). The coefficient of friction was obtained by dividing the frictional force by the applied load.

The wear rate was continuously measured using a linear voltage displacement transducer. Since it contained an internal amplifier its output was displayed directly onto the chart recorder. Its output voltage as a function of displacement is shown in figure 2.12. The wear rate which is the volume of material removed per unit sliding distance w (m^3 m^{-1}) is given by equation (2.8).

$$w = \pi \, x_o \, R_t^{\,2} \, / \, G \, t \, U \qquad \ldots\ldots\ldots\ldots\ldots\ldots\ldots\ldots\ldots\ldots (2.8)$$

G is the slope from figure 2.12 (825 V m^{-1}), R_t the radius of the pin (3.26×10^{-3} m), U the linear sliding speed of the disc at the pin (m s^{-1}), x_o the displacement taken from the chart recorder (V) and t the time for this displacement (s).

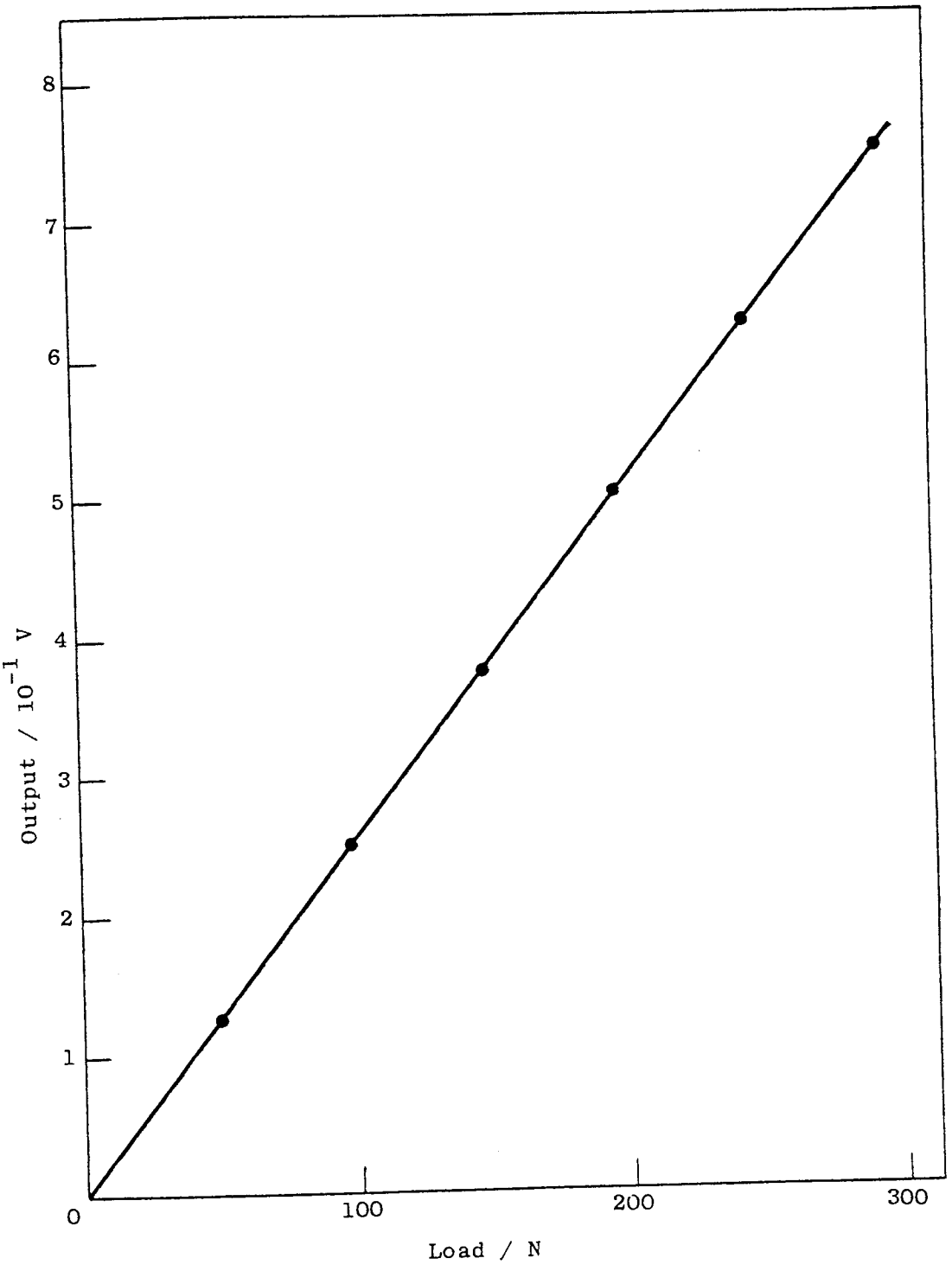

Fig. 2.11. Strain gauge dynamometer calibration.

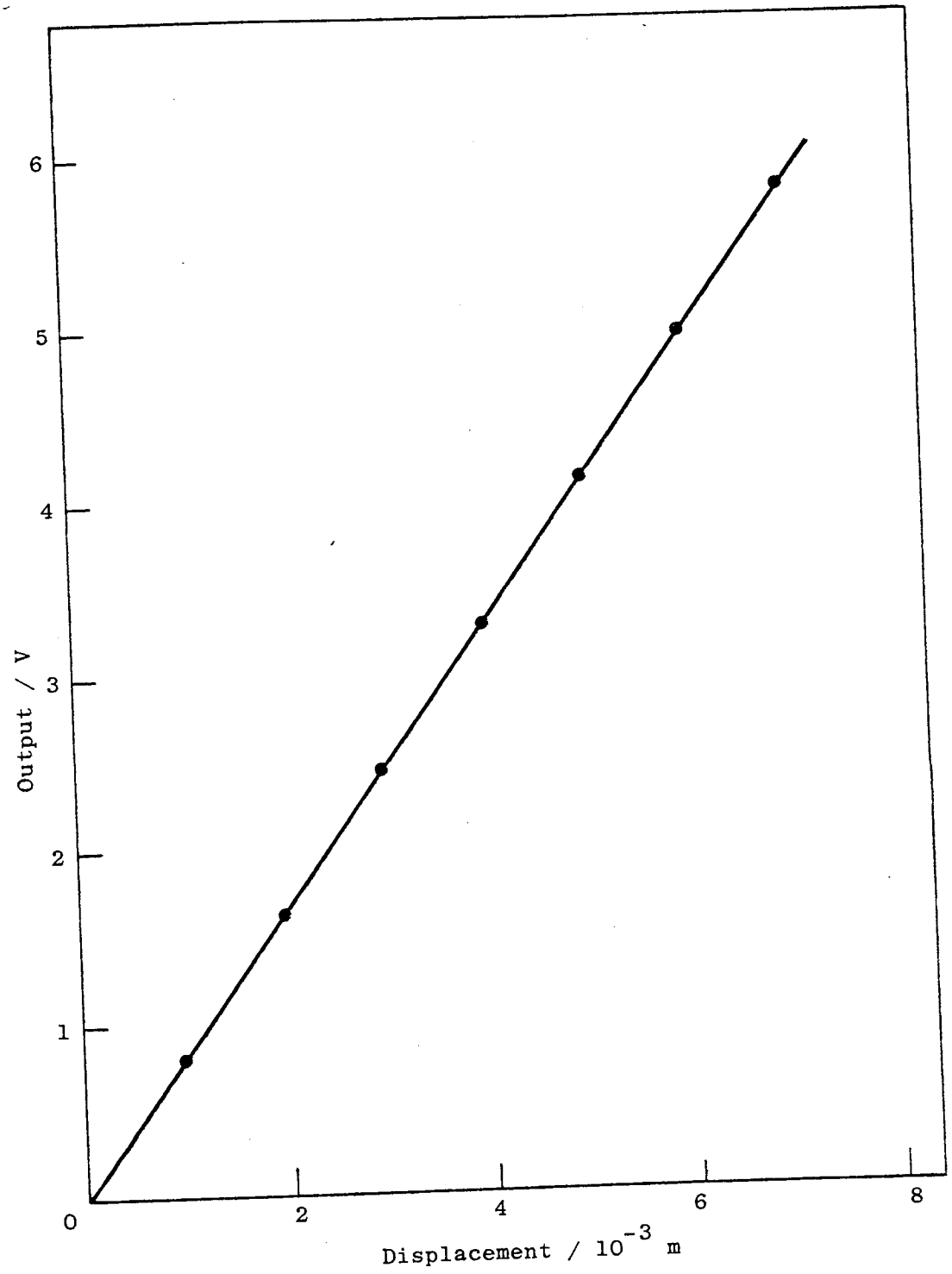

Fig. 2.12. Wear transducer calibration.

Vibrations and noise were eliminated by placing a 100 μf capacitor across both pairs of input terminals on the chart recorder producing a low impedance path to earth for changing voltages. Therefore smooth traces were obtained for both the frictional force and the wear rate, enabling wear rates of less than 10^{-14} m^3 m^{-1} to be measured at a linear sliding speed of 2 m s^{-1}.

2.6 Heat Flow and Pin Surface Temperature Measurements

The pin was held in a copper calorimeter where the temperature at two points along the pin and also the calorimeter were measured using chromel-alumel thermocouples. A diagram of the pin and its calorimeter arrangement is shown in figure 2.13 which enabled the heat flow along the pin to be measured continuously. The thermocouples were operated with their reference junctions at 0 ^{o}C and their outputs displayed on chart recorders. Calibration tables were used to convert the thermocouple e.m.f. to temperature. Because of the relatively low input impedance of the chart recorder, especially on the 10 mV range, the voltage recorded was not the true e.m.f. of the thermocouple. Figure 2.14 shows the temperature as indicated on the chart recorder varying with temperature measured using a high input impedance digital voltmeter. Therefore the correct temperatures were obtained by mulitplying the temperatures as indicated on the chart recorders by a correction factor of 1.04.

The heat flow theory for no external heating was originally developed by Coy[70] where equations (2.9) to (2.12) were obtained. The temperature of the surface of the pin outside the real area of contact T_s (^{o}C) is given by equation (2.9).

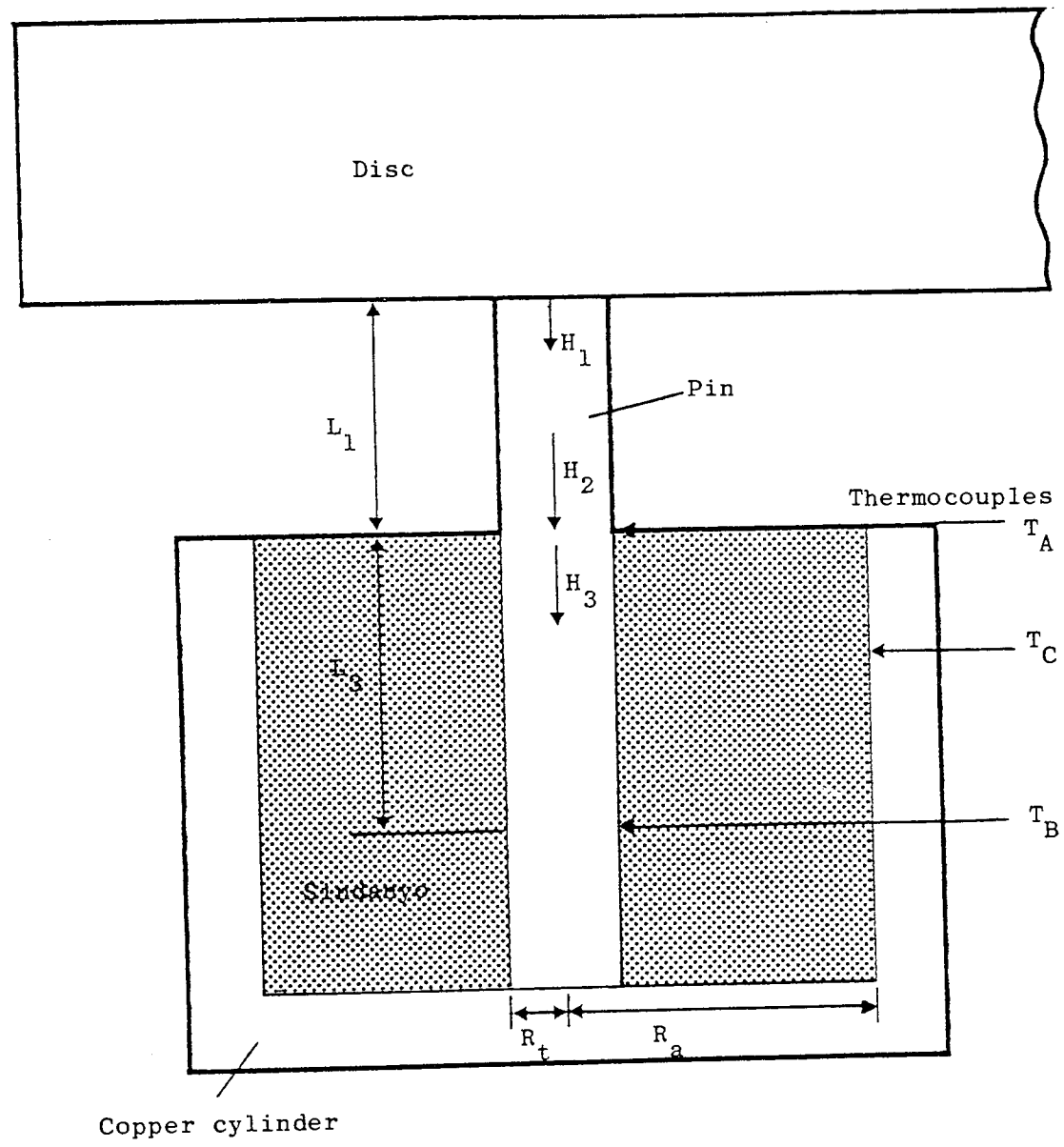

Fig. 2.13. Cross-sectional diagram of the heat flow calorimeter.

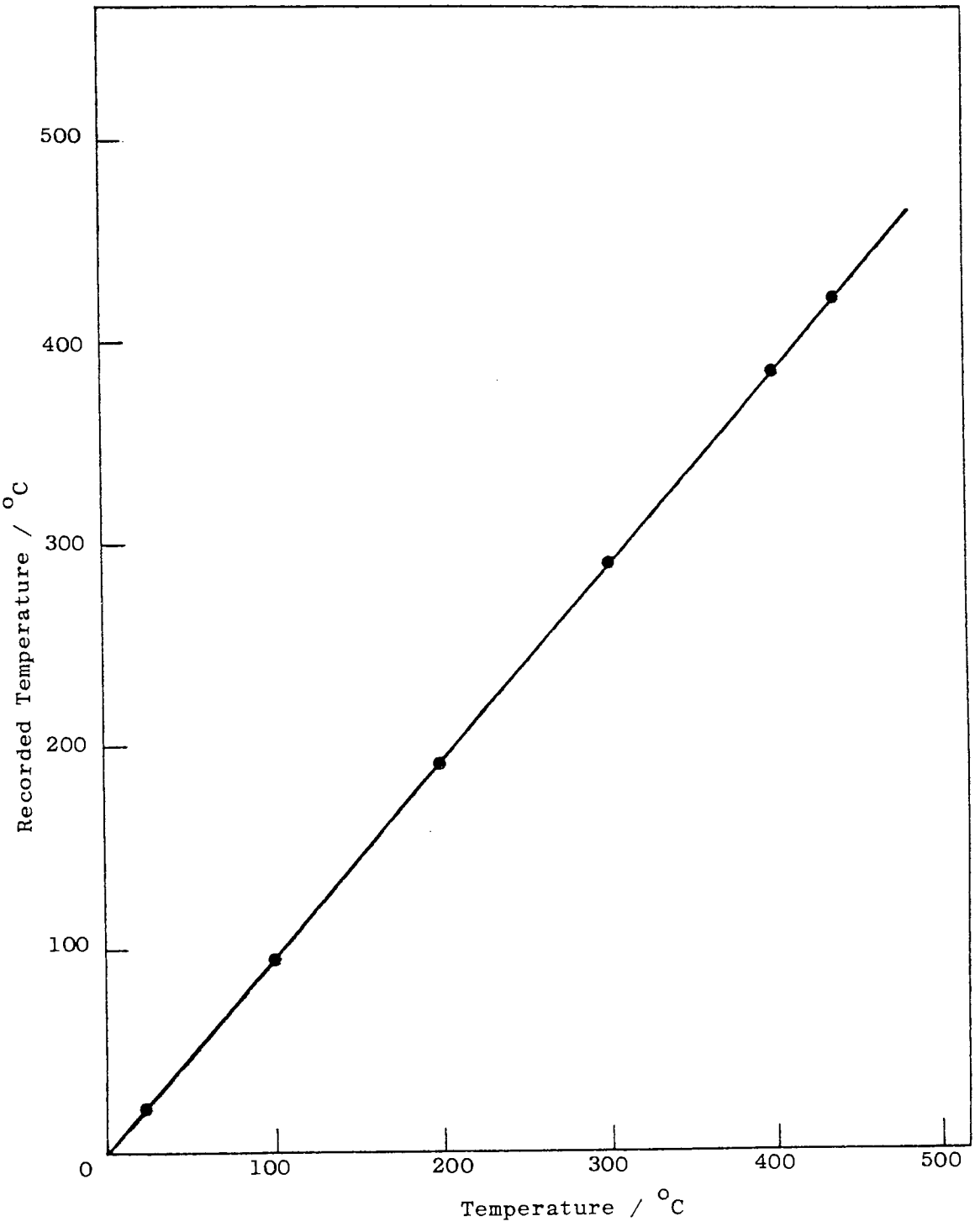

Fig. 2.14. Chart recorder temperature correction.

$$T_s = (T_A - T_E) \cosh (L_1/Z R_t) + \frac{Z H_2}{K_s \pi R_t} \sinh (L_1/Z R_t) + T_E \quad \ldots\ldots\ldots(2.9)$$

T_A is the temperature recorded by a thermocouple at the pin surface just as it emerges from the pin holder (^oC) and T_E is the temperature of air flowing past the pin, well away from the boundary layer on the cylindrical surface of the pin (^oC). It was assumed that the air which flows past the pin has a temperature T_C, the temperature of the copper calorimeter (^oC). R_t is the radius of the pin (0.00326 m), K_s the thermal conductivity of the steel pin (23.86 J s^{-1} m^{-1} $^oC^{-1}$), L_1 the final length of pin exposed to the air between the holder and the disc (m) and H_2 the heat flow per second entering the section of the pin where the thermocouple measuring T_A is conducting heat away (J s^{-1}), see appendix 1.

$$Z = (K_s / 2 R_t h)^{1/2} \quad \ldots\ldots\ldots(2.10)$$

The heat transfer coefficient h (J s^{-1} m^{-2} $^oC^{-1}$) from the cylindrical exposed surface of the pin to the air was derived experimentally, see appendix 1. This over came the necessity for analysing the complex heat flow situation, in which the surface layer of air around a solid transfers heat by conduction whilst the bulk of the air transfers heat by convection.

The experimentally measured division of heat at the pin-disc interface $\hat{d}$(expt) is given by equation (2.11).

$$\hat{d}(\text{expt}) = H_1 / H(\text{total}) \quad \ldots\ldots\ldots(2.11)$$

H_1 is the heat flow per second along the pin at the interface between the pin and disc (J s^{-1}), see appendix 1.

$$H(total) = F\ U \qquad \ldots\ldots\ldots\ldots\ldots\ldots\ldots\ldots\ldots\ldots\ldots\ldots (2.12)$$

H(total) is the total heat per second evolved at the pin-disc interface for no external heating ($J\ s^{-1}$), U the linear sliding speed of the disc at the pin ($m\ s^{-1}$) and F the frictional force (N). The computer programme which was used to calculate H_1, T_s, $d_{(expt)}$ and H(total) is shown in appendix 1.

Under mild wear conditions the temperatures T_A, T_B and T_C were quite steady, but for greater wear rates their final values were taken as equilibrium conditions could not be obtained. When the wear rate was rapid the temperature T_A would give a fairly linear temperature rise with time. From this an approximate surface temperature T_s (^oC) was obtained given by equation (2.13).

$$T_s \sim \frac{\Delta T_A \ L_1}{t \ w_r} + T_A \qquad \ldots\ldots\ldots\ldots\ldots\ldots (2.13)$$

T_A is the final temperature recorded by a thermocouple at the pin surface just as it emerges from the pin holder (^oC), L_1 the final length of pin exposed to the air between the holder and the disc (m), w_r the linear wear rate of the pin ($m\ s^{-1}$) and t the time (s) for the temperature rise ΔT_A (^oC).

2.7 Surface Profiles of the Disc

Surface profiles of selected wear tracks present on the WC - 11% Co disc were obtained using the talylin. The talylin consisted of a stylus which moved horizontally across a surface. This followed the surface topography where the small vertical deflections were amplified and displayed on a chart recorder. It has a much greater distance of horizontal travel than the talysurf which is mainly used for obtaining the surface finish. The maximum horizontal magnification of the talylin was x10 which was used to expand out the wear track as

much as possible. It had six ranges of vertical magnification x200, x400, x1 k, x2 k and x10 k. So a suitable magnification was chosen where the full scale deflection (m) on the chart recorder is given by equation (2.14).

$$\text{f.s.d.} = 0.05 / \text{Mag.} \quad \ldots\ldots\ldots\ldots\ldots\ldots\ldots\ldots\ldots\ldots (2.14)$$

It ranged from 250 μm f.s.d. at x200 magnification to 5 μm f.s.d. at x10 k.

2.8 X-Ray Analysis of Surfaces and Debris

The compounds in the wear debris collected from the angular contact bearing tests and selected pin-on-disc experiments were identified using powder X-ray diffraction. The Debye powder diffraction camera consisted of a collimator to admit and define the incident beam, a beam stop to confine and stop the beam, a means for holding the film against the inside circumference of the camera and a specimen holder which could be rotated. The wear debris were packed into 0.5 mm diameter glass capillary tubes which were fixed to the specimen holder. The diameter of the camera used was 114.6 mm which gave a circumference of 360 mm. This enabled values of 2θ where θ is the Bragg angle to be measured directly from the fi1m since 1 mm was equal to 1 degree.

The wear debris were exposed to $Co_{K\alpha}$ X-ray radiation at 40 kV, 30 mA for 1 to 2 hours. An iron filter was used which absorbed the unwanted $K\beta$ component which has a shorter wavelength, due to the abrupt change in its absorption coefficient. Since the low orders of reflection are usually produced by transmission the absorption by the specimen was kept to a minimum, preventing also unwanted fluorescent radiation. Table 2.1 shows the mass absorption coefficient values μ_m ($m^2\ kg^{-1}$) for the major elements present. $Co_{K\alpha}$ radiation was used because its wavelength was longer than the K absorption edge of iron,

Table 2.1. The mass absorption coefficients (m^2 kg^{-1}) for the various available X-ray wavelengths, Peiser et. al. (7i)

Element	$Mo_{K\alpha}$ 0.711 Å	$Zn_{K\alpha}$ 1.436 Å	$Cu_{K\alpha}$ 1.542 Å	$Ni_{K\alpha}$ 1.659 Å	$Co_{K\alpha}$ 1.790 Å	$Fe_{K\alpha}$ 1.937 Å	$Mn_{K\alpha}$ 2.103 Å	$Cr_{K\alpha}$ 2.291 Å
C	0.07	0.443	0.55	0.676	0.85	1.07	1.38	1.79
O	0.15	1.14	1.27	1.62	2.02	2.52	3.22	4.01
Cr	3.04	21.3	25.9	31.6	39.2	49.0	7.05	8.99
Fe	3.83	27.0	32.4	39.7	5.95	7.28	9.09	11.5
Co	4.16	29.2	35.4	5.44	6.59	8.06	10.2	12.6
W	10.5	14.3	17.1	20.9	25.8	32.0	38.0	45.6

therefore the mass absorption coefficient of the iron was relatively low as shown in table 2.1. Since there were 5 major elements present it was difficult or impossible to satisty this condition for every element. Therefore there was a large amount of absorption by the chrome and tungsten producing also K characteristic fluorescent radiation of longer wavelength than the exciting radiation. This fluorescent radiation emitted exposed the film giving diffraction patterns of low contrast. It was also quite possible the film was exposed by the short wavelength components of the continuous spectrum which excited K radiation, diffraction of the continuous spectrum, diffuse scattering from the specimen and scattering from other objects in the camera.

For mixtures of elements and for compounds the overall mass absorption coefficient μ_m ($m^2\ kg^{-1}$) is given by equations (2.15) and (2.16) respectively, Henry et. al.[72]

$$\mu_m = \sum f\ \mu_m \qquad \text{.....(2.15)}$$

$$\mu_m = \frac{\sum n\ \mu_m\ A_w}{\sum n\ A_w} \qquad \text{.....(2.16)}$$

A_w is the atomic weight, f the weight fraction of component elements and n the relative numbers of the atoms present. The average mass absorption coefficients were calculated for the Lescalloy BG42 martensitic stainless steel using equation (2.15) and for WC-11% Co using equations (2.15) and (2.16). The values obtained for the various possible X-ray wavelengths are shown in table 2.2. Considering equal mixtures in the wear debris the lowest overall mass absorption coefficient occurs when using $Co_{K\alpha}$ radiation with the exception of $Mo_{K\alpha}$. This radiation was not used because Braggs law shows that the shorter the wavelength the smaller the Bragg angle θ for planes of a given spacing, therefore seriously reducing the resolution of the diffraction

Table 2.2. Mass absorption coefficients ($m^2\ kg^{-1}$) for the various available X-ray wavelengths.

Sample	$Mo_{K\alpha}$ 0.711 Å	$Zn_{K\alpha}$ 1.436 Å	$Cu_{K\alpha}$ 1.542 Å	$Ni_{K\alpha}$ 1.659 Å	$Co_{K\alpha}$ 1.790 Å	$Fe_{K\alpha}$ 1.937 Å	$Mn_{K\alpha}$ 2.103 Å	$Cr_{K\alpha}$ 2.291 Å
Lescalloy BG42 steel	3.57	25.13	30.21	37.00	11.97	14.58	10.32	12.29
WC - 11% Co	9.23	15.18	18.21	18.09	22.32	27.68	32.94	39.58

lines on the film.

Glancing angle X-ray diffraction was used to identify the compounds present on the surfaces of the steel pins and on the WC - 11% Co balls. The samples were fixed firmly in the centre of the powder diffraction camera and irradiated at a glancing angle of about 30 degrees with $Co_{K\alpha}$ radiation for 1 to 2 hours. Values of 2θ were measured directly from the film, where the interplanar spacings d_{hkl} were obtained using tables. The compounds were identified by comparing the d_{hkl} values with compounds listed in the powder diffraction data file.

The X-ray intensity does not suddenly become zero at any one depth but decreases exponentially with distance below the surface. By assuming that on a diffraction pattern 95% of the information refers to the layer of depth X_p and not to the material below it. The effective depth of penetration X_p (m) is given by equation (2.17), Cullity.[73]

$$X_p = \frac{\ln \left[1 / (1 - G_x) \right]}{\mu \left[1 / \sin \alpha + 1 / \sin \beta \right]} \quad \ldots\ldots\ldots\ldots\ldots\ldots (2.17)$$

G_x is the intensity diffracted by a layer considered as a fraction of the total integrated intensity by a specimen of infinite thickness (0.95), α is the angle between the incident beam and sample (30 degrees), β is the angle between the diffracted beam and sample ($2\theta - \alpha$). μ is the linear absorption coefficient which is the product of the mass absorption coefficient multiplied by the density, (9.30×10^4 m^{-1} for Lescalloy BG42 steel and 3.24×10^5 m^{-1} for WC - 11% Co). Since the effective depth of penetration X_p varies with Bragg angle θ, maximum depth of penetration occurred when 2θ was equal to 120 degrees. Therefore from equation (2.17) the maximum effective depth of penetration of the X-rays for the glancing angle of 30 degrees was found to be

10.8 μm for Lescalloy BG42 steel and 3.1 μm for WC - 11% Co. Thus this technique is not particularly surface sensitive and one would expect the results of the surface analysis to contain a considerable contribution from the bulk material, particularly in the case of the steel where the Fe(Cr) lines should predominate. One would expect the surface films, whether transfer or oxide, to be of the order 1 to 4 μm thick.

2.9 Surface Examination Using the Scanning Electron Microscope

The surface examination was carried out using the Stereoscan 150 scanning electron microscope. The basic function of the instrument was to produce on a C.R.T. an image of 3-dimensional appearance, derived from the action of an electron beam scanning the surface of a specimen. The electron beam was scanned across the specimen, similar to the way in which a T.V. picture is scanned. Low energy secondary electrons generated in the specimen and high energy primary electrons reflected from the specimen surface travelled towards a collector system. The collector had a grid, which was made positive so that both the low and high energy electrons were detected. Behind the grid was a positively biased scintillator optically coupled to a photomultiplier. When electrons impinged on this scintillator photons were emitted which travelled along a light guide to the photocathode of the photomultiplier. The signals then passed through an amplifier so as to modulate the brightness of the C.R.T.

The magnification can be varied continuously between x20 and x100 k without any refocusing being necessary. This represents a scanned area on the specimen of 6 mm x 5 mm to 1.2 μm x 1 μm at a 10 mm working distance. The true magnification at all working distances was indicated by a scale on the display. The highest resolution achievable

with this instrument is about 7 nm. The S.E.M. has a large depth of field compared to the optical microscope, which is approximately 5 mm at a magnification of x20. Thus there will be a range over which different parts of the object are effectively all in focus at the same time, Southworth.[74]

The Stereoscan 150 S.E.M. was used to observe and photograph the surfaces of selected worn pins taken from the elevated temperature sliding wear pin-on-disc test rig and the worn tracks of the angular contact bearings. The S.E.M. was also used in conjunction with an X-ray energy dispersive analyser, which identified the surface elements with atomic numbers greater than 9 present on the surfaces. Prior to analysis all specimens were subject to ultrasonic cleaning in petroleum spirit. The X-rays emitted by a particular element have certain characteristic energies. The energy of the X-ray was measured by the number of ionizations it produced in the detector. The detector was a solid state lithium drifted silicon semiconductor positioned along side the electron detector. The output was then fed into a multi-channel analyser (computer memory) which displayed the number of counts for a particular X-ray energy. A magnification of x20 was selected so that the 20 kV electron beam would scan all the pins surface. A permanent record of the number of counts versus X-ray energy was obtained by the use of a graph plotter. The tungsten X-ray image of those pins having material transfer were displayed on the C.R.T. of the S.E.M. These X-ray images were examined over a range of magnification and were photographed when found desirable.

The electron spread or penetration R (m) is given by equation (2.18) which was determined experimentally by Andersen[75] in 1966.

$$R = 6.4 \times 10^{-5} E_o^{1.68} / \rho \quad \ldots\ldots\ldots\ldots\ldots\ldots\ldots\ldots\ldots\ldots (2.18)$$

E_o is the accelerating potential (20 kV) and ρ is the density (7.77×10^3 kg m^{-3} for Lescalloy BG42 steel and 14.5×10^3 kg m^{-3} for WC - 11% Co.) Therefore from equation (2.18) the electron penetration was found to be 1.26 μm for Lescalloy BG42 steel and 0.68 μm for WC - 11% Co.

2.10 Hardness Tests

Both micro-hardness tests using a miniload system and Vickers hardness tests were carried out on selected worn steel pins. The micro-hardness tests were carried out with a 2.943 N load and the Vickers hardness tests carried out using a 294.3 N load applied to the diamond pyramid indentor. A total of six indentations were made for each specimen and an average obtained. The hardness values p (N m^{-2}) were obtained from the Vickers formula equation (2.19), which was available in table form.

$$p = 1.854 W / l_d^2 \quad \ldots\ldots\ldots\ldots\ldots\ldots\ldots\ldots\ldots\ldots (2.19)$$

W is the load applied to the diamond pyramid indentor (N) and l_d is the length of the indentation diagonal (m).

The angularity of the diamond pyramid indentor was 136 degrees, so the depth of penetration X_p is related to the length of the indentation diagonal by 0.202 l_d. Substituting for l_d in equation (2.19) the depth of penetration X_p (m) is given by equation (2.20).

$$X_p = (7.565 \times 10^{-2} W / p)^{1/2} \quad \ldots\ldots\ldots\ldots\ldots\ldots\ldots\ldots\ldots\ldots (2.20)$$

The depth of penetration of the diamond pyramid indentor for the micro-hardness tests was 5.0 to 7.5 μm for a hardness range of 9×10^9 to 4×10^9 N m^{-2} respectively. For the Vickers hardness tests or bulk hardness tests the penetration depth was 50 to 75 μm for the same hardness range.

2.11 Oxide Film Thickness Measurement by Ellipsometry

Ellipsometry is a technique that allows the determination of the thickness of a thin film on a flat substrate. Films a few Å thick on a metallic substrate can be detected by measuring the ellipticity of light after reflection. If plane polarized light makes an angle other than 0 or 90 degrees with respect to the plane of incidence the reflected light is elliptically polarized. Elliptically polarized light is defined as two perpendicular vibrations of different amplitudes out of phase. The ellipse depends on the angle of incidence and on the optical constants of the metal n and k. The basic equation of ellipsometry is given by equation (2.21), see appendix 2.

$$r_p/r_s = \tan \Psi \, e^{i\Delta} \quad \ldots\ldots\ldots\ldots\ldots\ldots\ldots\ldots\ldots\ldots (2.21)$$

r_p and r_s are the Fresnel reflection coefficients parallel and perpendicular to the plane of incidence. Ψ is the relative amplitude reduction ratio and Δ is the relative phase difference between the p and s components, where both these parameters can be obtained from the instrument.

The basic layout of the ellipsometer is shown in figure 2.15. The white light source was a tungsten filament lamp where monochromatic light at a wavelength of 549 nm was produced using an interference filter. The light was rendered plane polarized by passing through a sheet of polariod known as the polarizer before falling on the sample at an angle of incidence of 61.5 degrees. After reflection in general from the specimen the light was elliptically polarized. It was analysed by passing through a compensator or quarter wave plate which introduced a phase difference of 90 degrees for light with electric vectors parallel and perpendicular to the plane of incidence. The

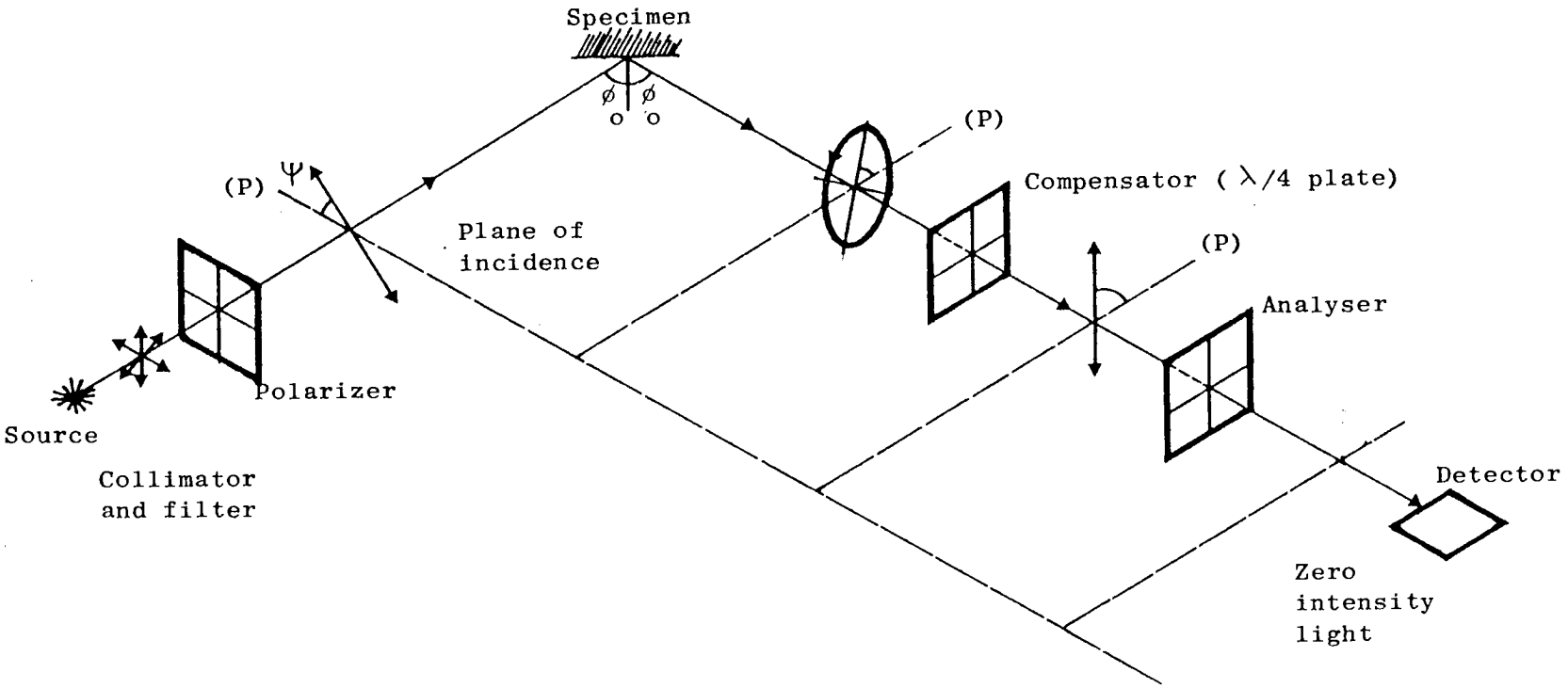

Fig 2.15. The arrangement of components for a basic ellipsometer.

light was then intercepted by a sheet of polariod the analyser, before reaching the detector. The light sensitive detector was a photomultiplier where the output signal was displayed on a digital voltmeter. The polarizer, analyser and compensator were mounted on divided circular scales calibrated 0 to 360 degrees.

Before measurements could be undertaken the reference positions of the polarizer, analyser and compensator were first determined, See Neal.[76] To find Ψ and Δ the optical parameters, the compensator was set at 45 degrees from a reference position. The polarizer and analyser were rotated until minimum light was observed as measured by the photomultiplier. This was repeated to find all four positions for the polarizer and the analyser. Ψ was obtained from the polarizer and is the angle between the polarizer setting and the horizontal aximuth at extinction. If x is the angle between the analyser setting and the horizontal aximuth at extinction then Δ the phase difference is given by $2x - 90$.

The 10 mm by 20 mm samples of Lescalloy BG42 and A.I.S.I. 440C MOD martensitic stainless steel were polished to a surface finish of approximately 1 μm c.l.a. They were cleaned initially with detergent and then they were subject to ultrasonic cleaning in warm propanol. The equilibrium oxide film thickness at room temperature was assumed to be 3.5 nm. Latham and Brah[77] reported a stable oxide film of (3.8 ± 0.5) nm on stainless steel. Fane et. al.[78] reported the equilibrium thickness to be about 3.0 nm on a stainless steel sample as polished and cleaned. The samples were placed in a heated furnace for a set time, after which they were removed and their optical parameters Ψ and Δ measured using the ellipsometer. The samples were then returned to the furnace for a further time and the procedure

repeated. The oxide growth rates were investigated over the temperature range 200 to 600 ^{o}C.

Providing the optical constants of the clean surface are known, then any changes in Ψ and Δ can be used to determine the thickness of an oxide film, Neal and Fane,[79] see appendix 2. Values for the optical constants of an atomically clean stainless steel surface free of oxide were given by Fane et. al.[78] in 1973, where n = 2.28 and k = 3.77 at a wavelength of 547.8 nm. Since there is preferential oxidation of the chrome, Kubaschewski and Hopkins,[49] the oxide film was assumed to consist mainly of chromium oxide. The optical constants used were n = 2.42 and k = 0, which were obtained by Hill and Weaver[80] for a film on a polished bulk sample of chrome measured at a wavelength of 546.1 nm. Depending on which type of oxide is assumed present, the computed thickness up to approximately 30 nm would only be changed by less than 10%, Fane et.al.[78] The chromium oxide film thickness was computed and is shown in figure 2.16 as a function of $\dot{\Delta}$, see appendix 2.

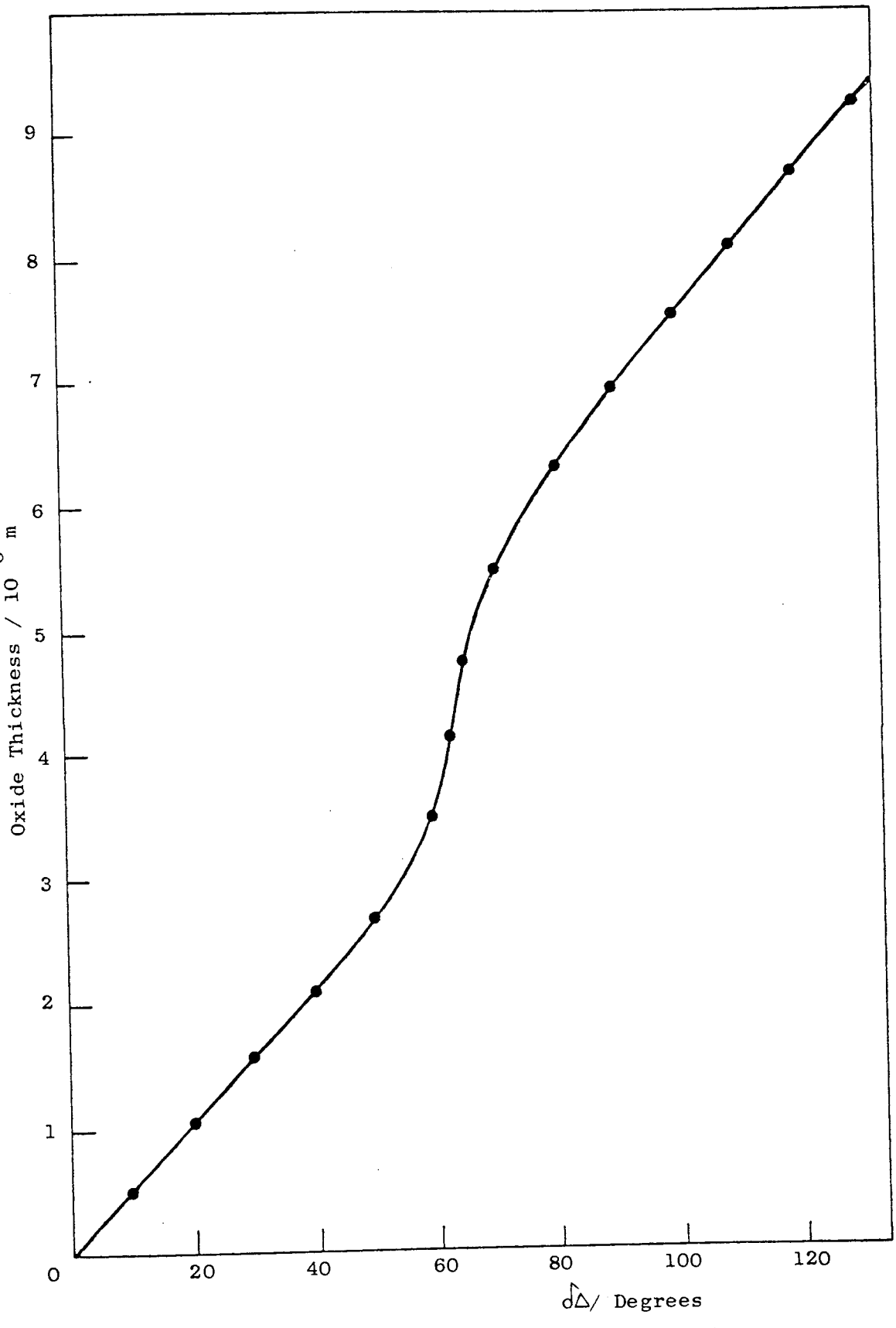

Fig. 2.16. Computed oxide thickness as a function of $\delta\Delta$ for stainless steel.

CHAPTER 3

RESULTS

3.1 Angular Contact Bearing Track Wear and Ball Measurements

Figure 3.1 shows the track wear depth of the angular contact bearings inner race, as a function of bearing temperature for a 1000 cycle duration with a ball contact stress of 2.6×10^{9} N m^{-2}. For the Lescalloy BG42 martensitic stainless steel angular contact bearings, the track wear showed a maximum around a temperature of 260 ^{o}C. In this region assuming pure sliding, the track wear rate corresponds to $(1.3 \pm 0.3) \times 10^{-11}$ m^{3} m^{-1}. Since rolling is also present the wear rate due to sliding can be greater than this value. For both types of steel the trends are similar with maximum track wear at a temperature of about 200 ^{o}C for the A.I.S.I. 440C MOD steel bearings, figure 3.1(b).

The wear debris identified from the Lescalloy BG42 steel bearings by X-ray diffraction consisted of tungsten carbide WC and α-Fe(Cr) before the maximum track wear, α-Fe(Cr) indicates the original bulk steel structure. At a temperature of 300 and 350 ^{o}C the wear debris consisted of rhombohedral oxide, tungsten carbide WC and α-Fe(Cr) with tungstic oxide WO_3 and cobalt tungsten oxide $CoWO_4$ being first detected at 400 ^{o}C. The rhombohedral oxide is a solid solution consisting of a mixture of α-Fe_2O_3 and Cr_2O_3 as described by Isherwood and Quinn.(51) At a temperature of 500 ^{o}C iron tungsten oxide Fe_2WO_6 and chromium tungsten oxide Cr_2WO_6 was detected in the wear debris, see table 3.8. The wear debris identified from the A.I.S.I. 440C MOD steel bearings was similar to the other type of steel, but with WO_3 being first detected at a temperature of 350 ^{o}C. The complete X-ray diffraction analysis is described in section 3.4.

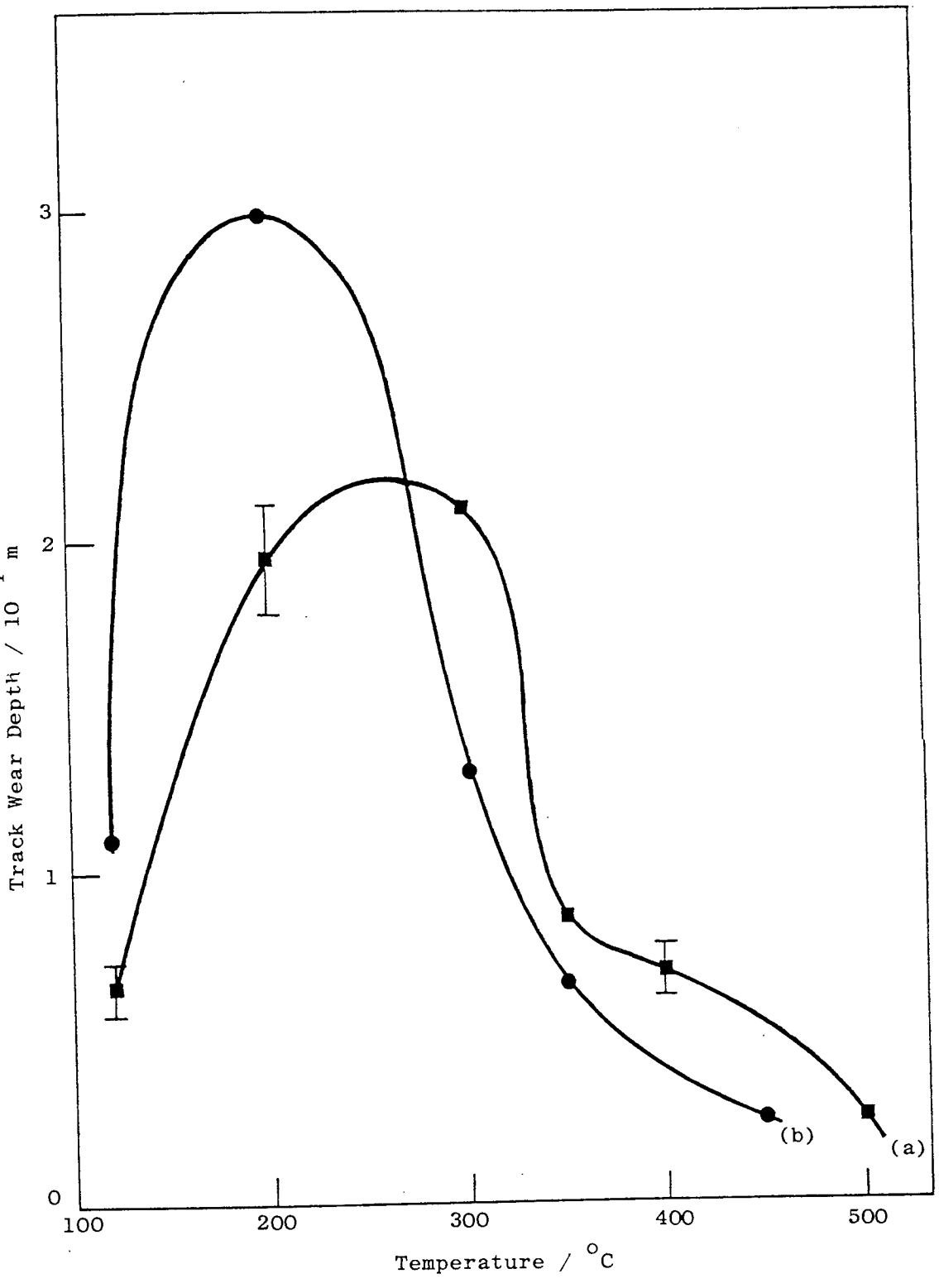

Fig. 3.1. Track wear depth of the bearing inner race versus bearing temperature for a 1000 cycle duration with a ball contact stress of 2.6×10^{9} N m^{-2}; (a) Lescalloy BG42 steel; (b) A.I.S.I. 440C MOD steel.

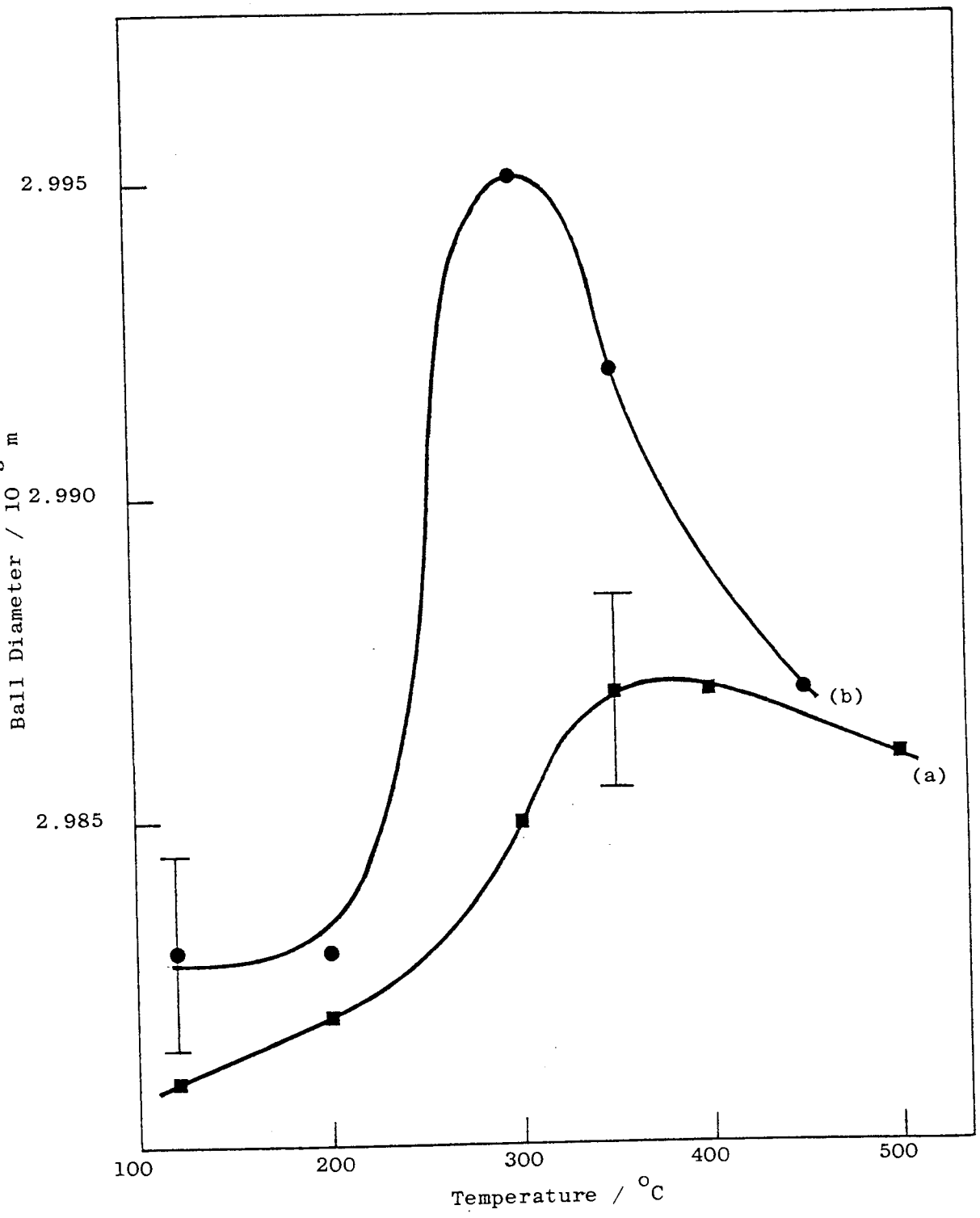

Fig. 3.2. Ball diameter versus bearing temperature for a 1000 cycle duration with a contact stress of 2.6×10^{9} N m^{-2}; (a) balls taken from Lescalloy BG42 steel races; (b) balls taken from A.I.S.I. 440C MOD steel races.

For temperatures greater than maximum track wear S.E.M. analysis has shown that there is an increase in the amount of tungsten transfer to the wear track, see section 3.5.

The WC - 11% Co ball diameter versus bearing temperature is shown in figure 3.2. For balls taken from Lescalloy BG42 steel races figure 3.2(a), there is minimum wear in the temperature region 360 to 390 ^{o}C. Balls taken from A.I.S.I. 440C MOD steel races figure 3.2(b), show minimum wear at a temperature of about 300 ^{o}C. For both types of steel bearings minimum ball wear was at approximately 100 ^{o}C higher than the temperature at which maximum track wear occurred. The balls taken from the Lescalloy BG42 and A.I.S.I. 440C MOD steel races appeared grey at temperatures below 350 and 300 ^{o}C respectively. This was due to metal transfer from the bearing race, which was identified by glancing angle X-ray diffraction.

3.2 Wear, Friction, Heat Flow and Pin Surface Temperature Measurements

Figure 3.3 shows the wear rate as given by equation (2.8), of Lescalloy BG42 martensitic stainless steel pins as a function of load, at sliding speeds of 2 and 3 m s^{-1} for pin-on-disc experiments with no external heating. The results for both speeds are very similar with the wear rate at 3 m s^{-1} figure 3.3(b), being greater as expected. From X-ray diffraction of the wear debris for loads below about 40 N the debris contained α-Fe(Cr), rhombohedral oxide (a mixture of α-Fe_2O_3 and Cr_2O_3 as described by Isherwood and Quinn,[51]), tungsten carbide WC and γ-Fe with sometimes γ-Fe_2O_3 being detected. α-Fe(Cr) indicates the original bulk steel sturcture, where γ-Fe indicates austenite which is of lower hardness. The wear particles were small and on the whole non-metallic in appearance. Glancing angle X-ray diffraction on the surface of a worn pin at a load of 19.6 N and a

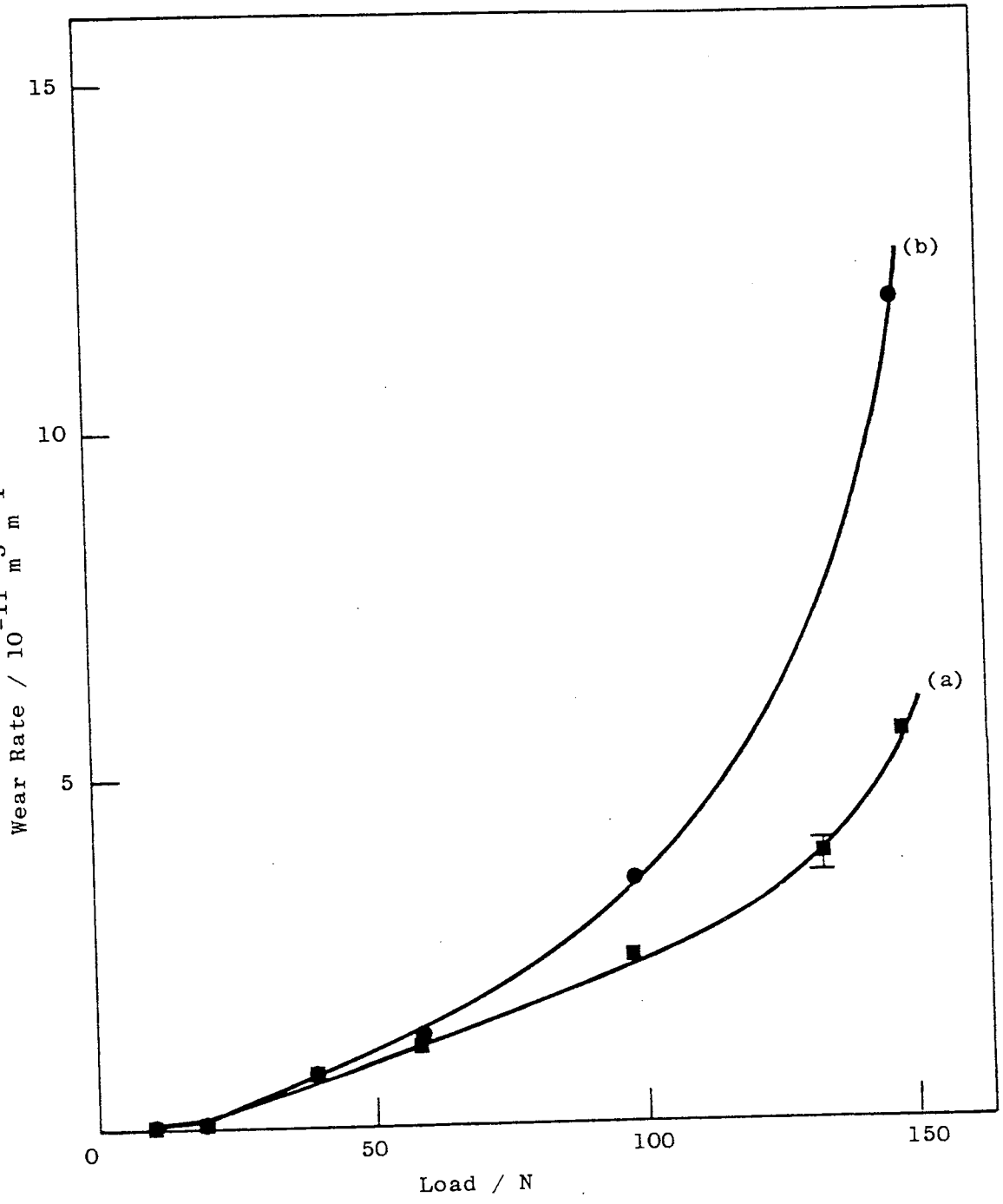

Fig. 3.3. Wear rate of Lescalloy BG42 martensitic stainless steel versus load for pin-on-disc experiments with no external heating; (a) 2 m s^{-1} sliding speed; (b) 3 m s^{-1} sliding speed.

sliding speed of 2 m s^{-1} showed in decreasing order α-Fe(Cr), (WC, γ-Fe) and rhombohedral oxide. The compounds enclosed in brackets gave diffraction lines of about the same intensity. For loads greater than about 40 N the debris consisted of large metallic particles free from oxide which when analysed proved to be a mixture of α-Fe(Cr), γ-Fe and WC. No oxides were present either in the debris or on the surface of the pins. The wear rate starts to increase rapidly at the high loads as the material softens with the γ-Fe becoming more predominant in the wear debris, see table 3.10.

Figure 3.4 shows the wear rate for both Lescalloy BG42 and A.I.S.I. 440C MOD steel pins versus load, for a sliding speed of 2 m s^{-1} with no external heating applied to the disc. The softer material figure 3.4(b), behaves very similar to Lescalloy BG42 steel which has already been explained, figure 3.4(a). The oxide to metallic wear transition occurs at a slightly higher load due to the presence of the rhombohedral oxide. The wear rate in the severe metallic wear region is greater for the softer material as expected, figure 3.4(b). From X-ray diffraction of the wear debris from an A.I.S.I. 440C MOD steel pin at a 98.1 N load, the debris contained in decreasing order according to the strength of the diffraction lines (α-Fe(Cr), γ-Fe) and WC. Unlike the Lescalloy BG42 steel at this load the γ-Fe gives diffraction lines equal in strength to the α-Fe(Cr).

Figure 3.5 shows the wear rate of the two types of steel pins versus load for a sliding speed of 2 m s^{-1} and a disc temperature of 200 ^{o}C. For both types of steel the wear rate increases with load as expected. The shape of the curves are similar with A.I.S.I. 440C MOD steel pins figure 3.5(b), having the greater wear rate for a given load. The wear debris at loads less than 40 N from both steels

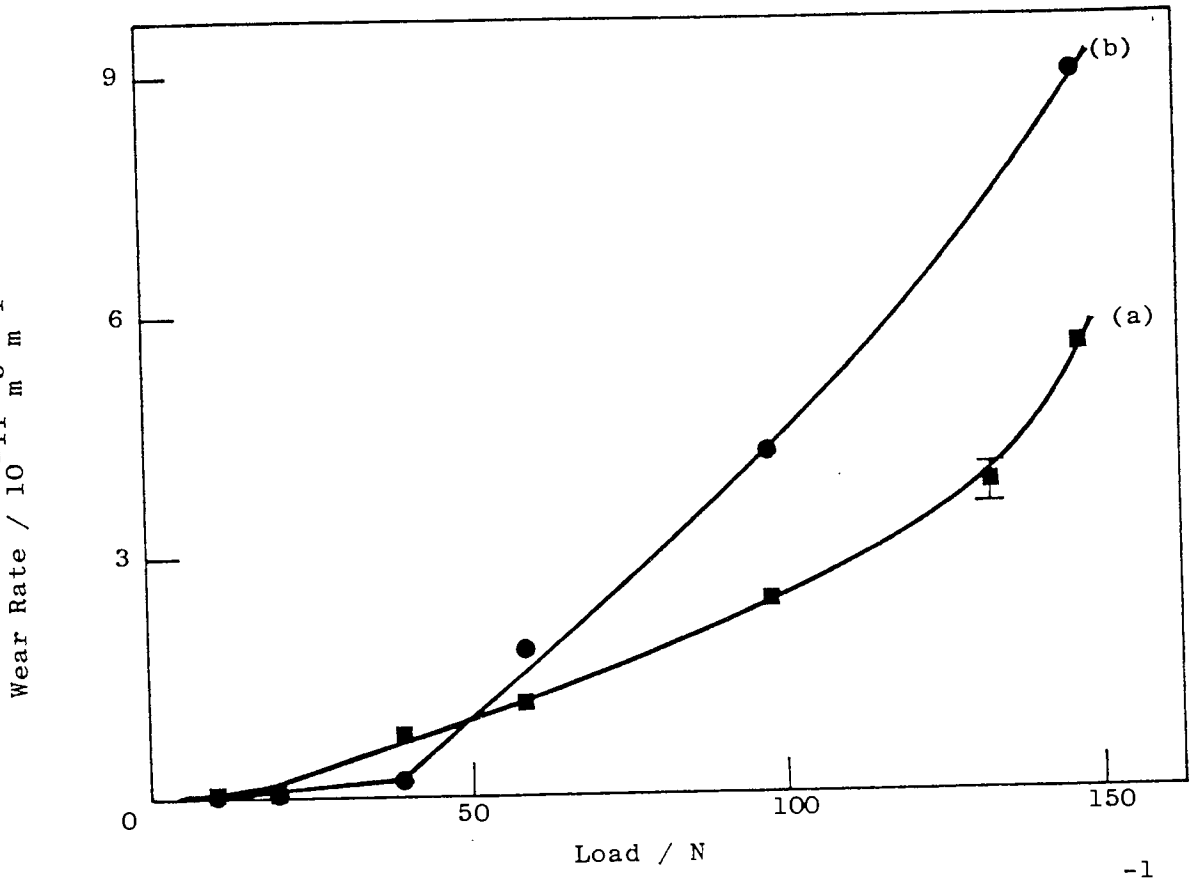

Fig. 3.4. Wear rate versus load for a sliding speed of 2 m s^{-1} with no external heating applied to the disc; (a) Lescalloy BG42; (b) A.I.S.I. 440C MOD steel.

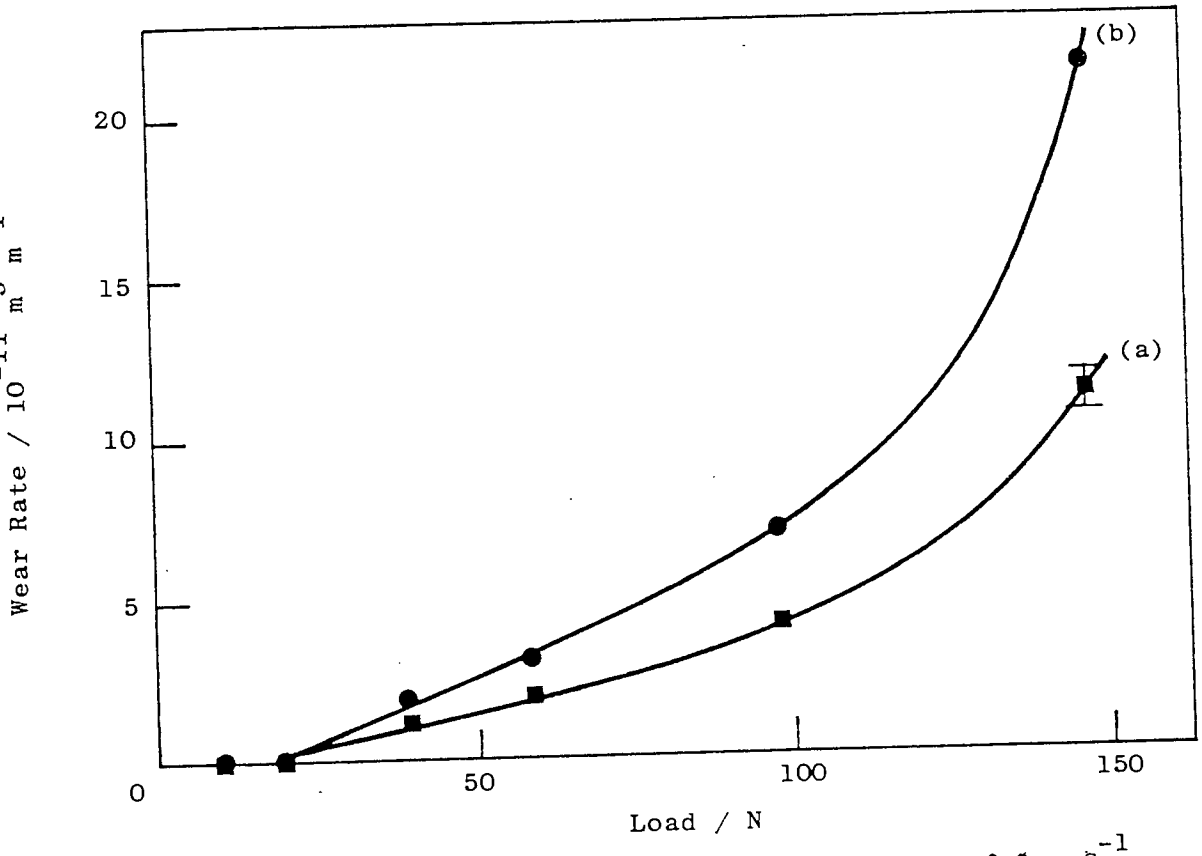

Fig. 3.5. Wear rate versus load for a sliding speed of 2 m s^{-1} and a disc temperature of 200 ^{o}C; (a) Lescalloy BG42; (b) A.I.S.I. 440C MOD steel.

contained α-Fe(Cr), rhombohedral oxide, γ-Fe, γ-Fe_2O_3 and WC which were identified by X-ray diffraction. For loads greater than about 40 N the wear debris contained γ-Fe, α-Fe(Cr) and WC.

The wear rate of Lescalloy BG42 steel pins versus load for a sliding speed of 2 m s^{-1} and a disc temperature of 400 ^{o}C is shown in figure 3.6. Again the wear rate increases with load as expected. For loads less than about 30 N S.E.M. analysis and X-ray data show transfer of material from the disc to the pin in the form of cobalt tungsten oxide $CoWO_4$, tungstic oxide WO_3 and tungsten carbide WC. Between loads of about 30 and 122 N no major transfer of material is occurring except for a little tungsten carbide WC, see sections 3.4 and 3.5. At loads greater than 122 N no oxides are present in the debris indicating severe metallic wear.

For both types of steel pins figure 3.7 shows the wear rate versus load for a sliding speed of 2 m s^{-1} and a disc temperature of 500 ^{o}C. Quite a different mechanism is apparent at a temperature of 500 ^{o}C since there is a considerable fall in the wear rate of the steel. Both X-ray data and S.E.M. analysis show that transfer of material is occurring from the disc to the pin. For Lescalloy BG42 steel pins figure 3.7(a), there are two wear mechanisms operating. It was not possible to identify where the transition occurs hence the two regions at about 80 N load. The A.I.S.I. 440C MOD steel pins figure 3.7(b), show a linear increase in wear rate with load. At all loads cobalt tungsten oxide $CoWO_4$ and tungstic oxide WO_3 give rise to strong X-ray diffraction lines in the debris. For Lescalloy BG42 steel pins figure 3.7(a), for loads less than about 80 N the debris and surfaces are like those of the A.I.S.I. 440C MOD steel pins. Above about 80 N load iron tungsten oxide Fe_2WO_6

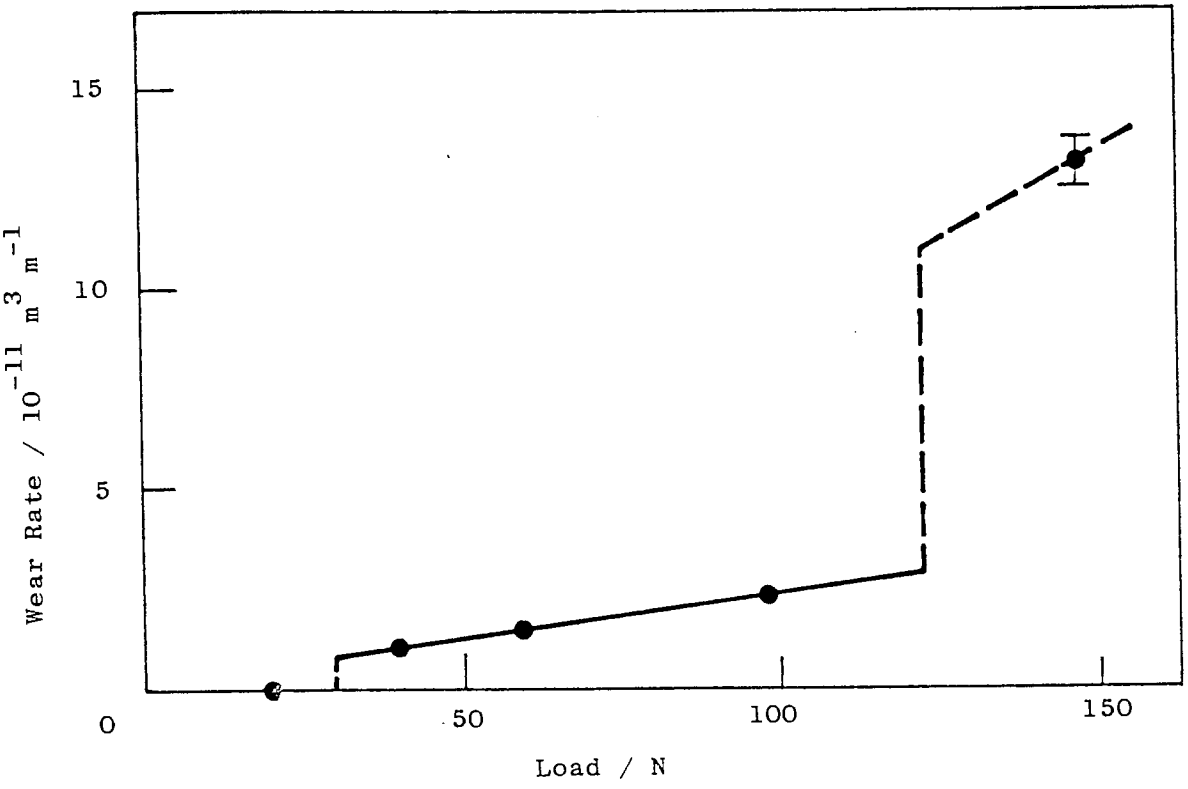

Fig. 3.6. Wear rate of Lescalloy BG42 martensitic stainless steel versus load for a sliding speed of 2 m s^{-1} and a disc temperature of 400 ^{o}C.

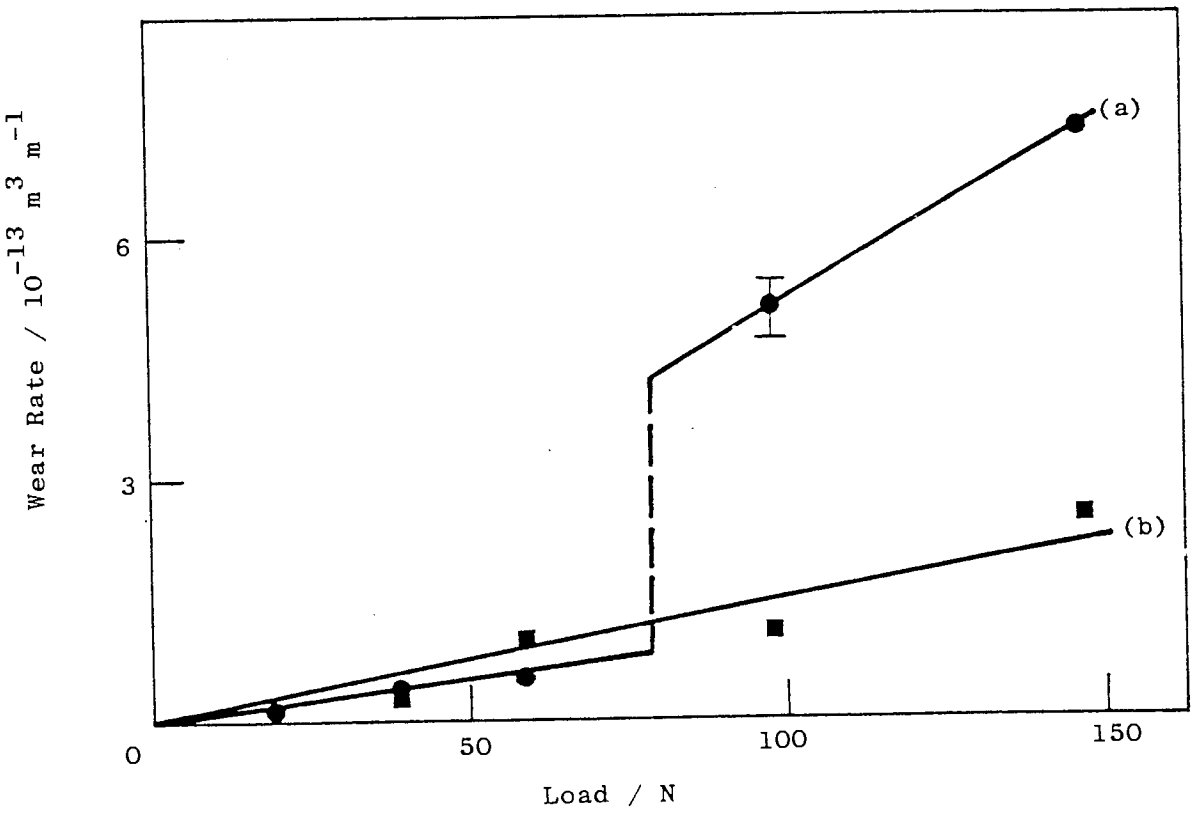

Fig. 3.7. Wear rate versus load for a sliding speed of 2 m s^{-1} and a disc temperature of 500 ^{o}C; (a) Lescalloy BG42; (b) A.I.S.I. 440C MOD steel.

and chromium tungsten oxide Cr_2WO_6 are formed on the surface of the pins and is also present in the wear debris, see table 3.12.

For the pin-on-disc sliding experiments, the wear rate of Lescalloy BG42 steel pins plotted against load is shown in figure 3.8 for sliding speeds of 0.6, 2.0 and 3.0 m s^{-1} for no external heating. In order to show the wear rate at all three sliding speeds a logarithmic scale was used. Form X-ray diffraction of the wear debris, a mixture of WC, α-Fe(Cr) and γ-Fe was found for all loads at a sliding speed of 0.6 m s^{-1}, figure 3.8(a). The results for sliding speeds of 2.0 and 3.0 m s^{-1} are shown in figures 3.8(b) and 3.8(c) respectively. For loads below about 40 N the wear particles were small and on the whole non-metallic in apperance, an oxidational-metallic type of wear. For loads greater than 40 N the wear was severe, the debris consisted of large metallic particles free from oxide. The corresponding coefficient of friction values calculated by equation (2.7) are shown in figure 3.9. For all sliding speeds the coefficient of friction decreased with increasing load, especially at a sliding speed of 2.0 m s^{-1}, figure 3.9(b).

The wear rate of Lescalloy BG42 and A.I.S.I. 440C MOD steel pins versus load, for a sliding speed of 2 m s^{-1} with no external heating applied to the disc is shown in figure 3.10. A logarithmic scale was chosen due to the large range of wear rate. Both types of steel behave very similar with the softer A.I.S.I. 440C MOD steel having the highest wear rate for loads greater than about 50 N, figure 3.10(b). The corresponding coefficient of friction values are shown in figure 3.11. For both types of steel the coefficient of friction decreases with increasing load.

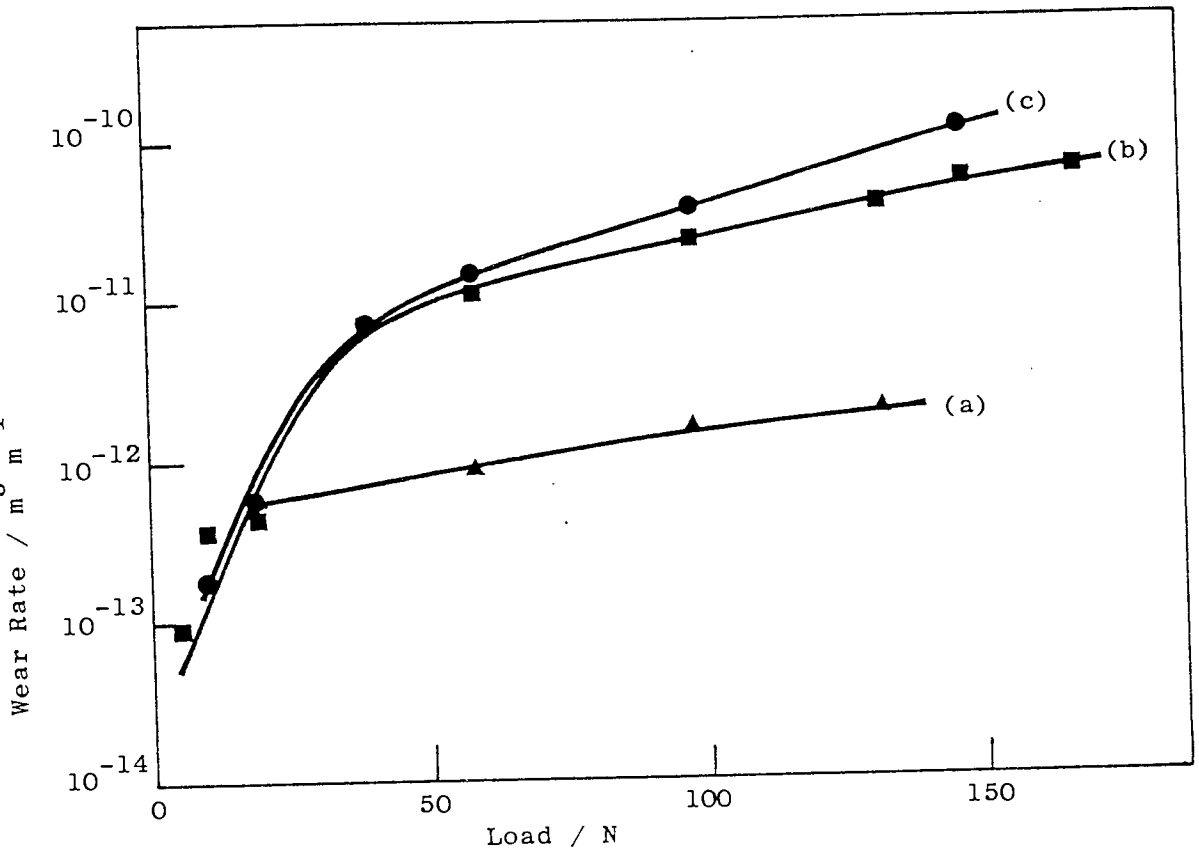

Fig. 3.8. Wear rate of Lescalloy BG42 martensitic stainless steel versus load for pin-on-disc experiments with no external heating; (a) 0.6 m s^{-1} sliding speed; (b) 2.0 m s^{-1} sliding speed; (c) 3.0 m s^{-1} sliding speed.

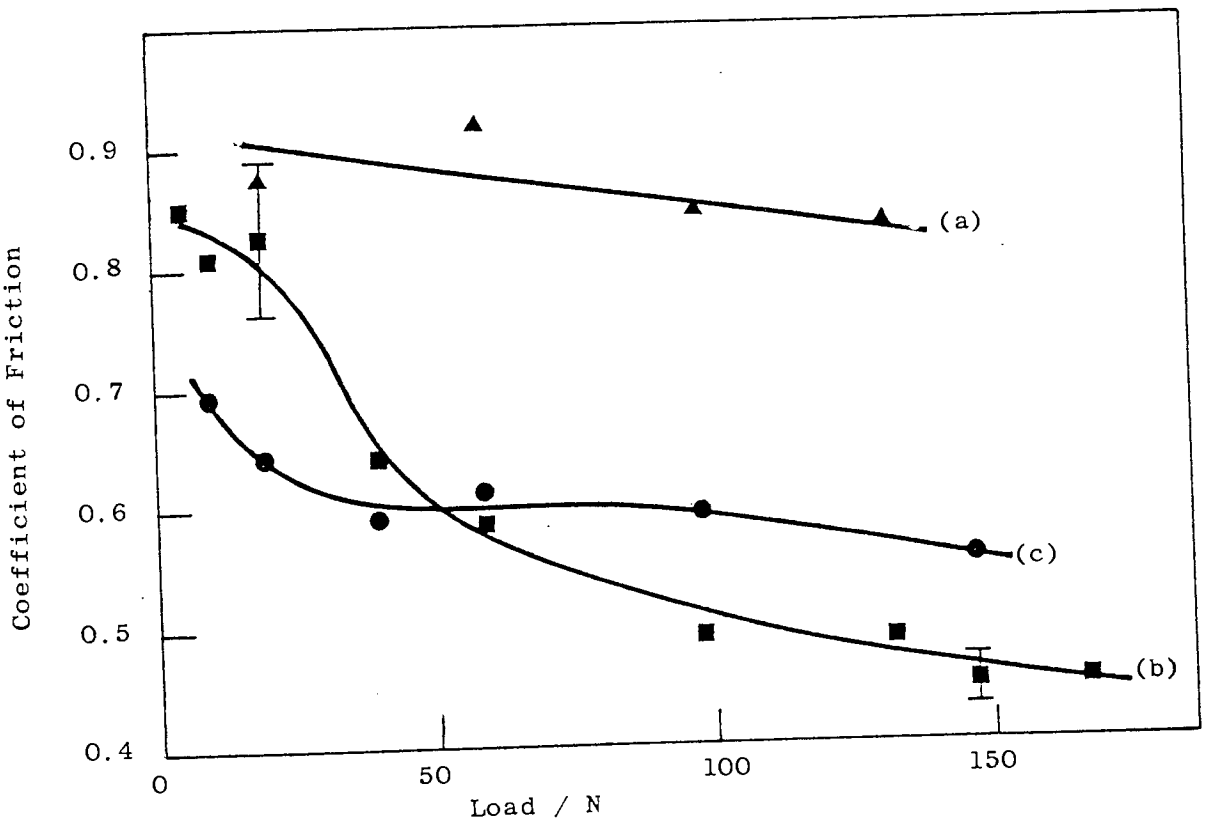

Fig. 3.9. Coefficient of friction of Lescalloy BG42 steel versus load for pin-on-disc experiments with no external heating; (a) 0.6 m s^{-1} sliding speed; (b) 2.0 m s^{-1} sliding speed; (c) 3.0 m s^{-1} sliding speed.

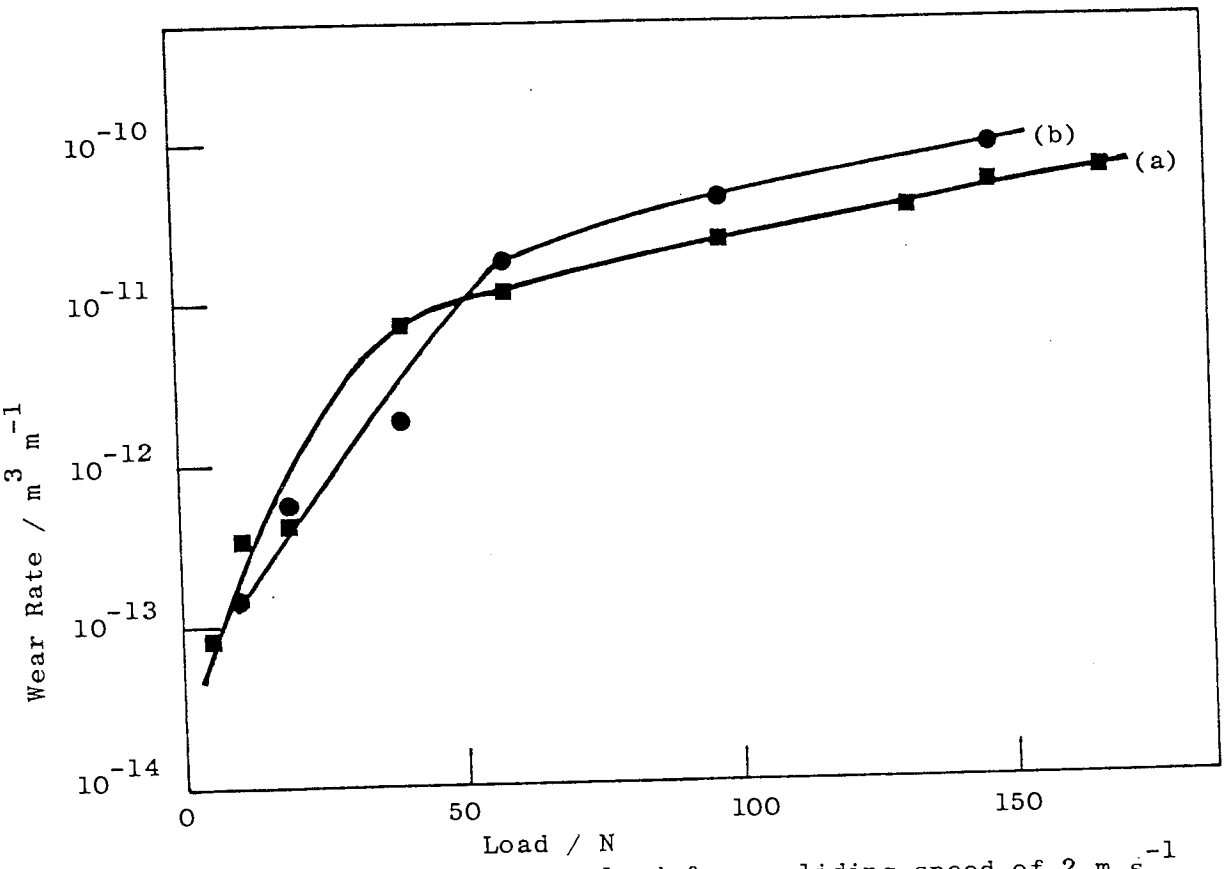

Fig. 3.10. Wear rate versus load for a sliding speed of 2 m s^{-1} with no external heating applied to the disc; (a) Lescalloy BG42; (b) A.I.S.I. 440C MOD steel.

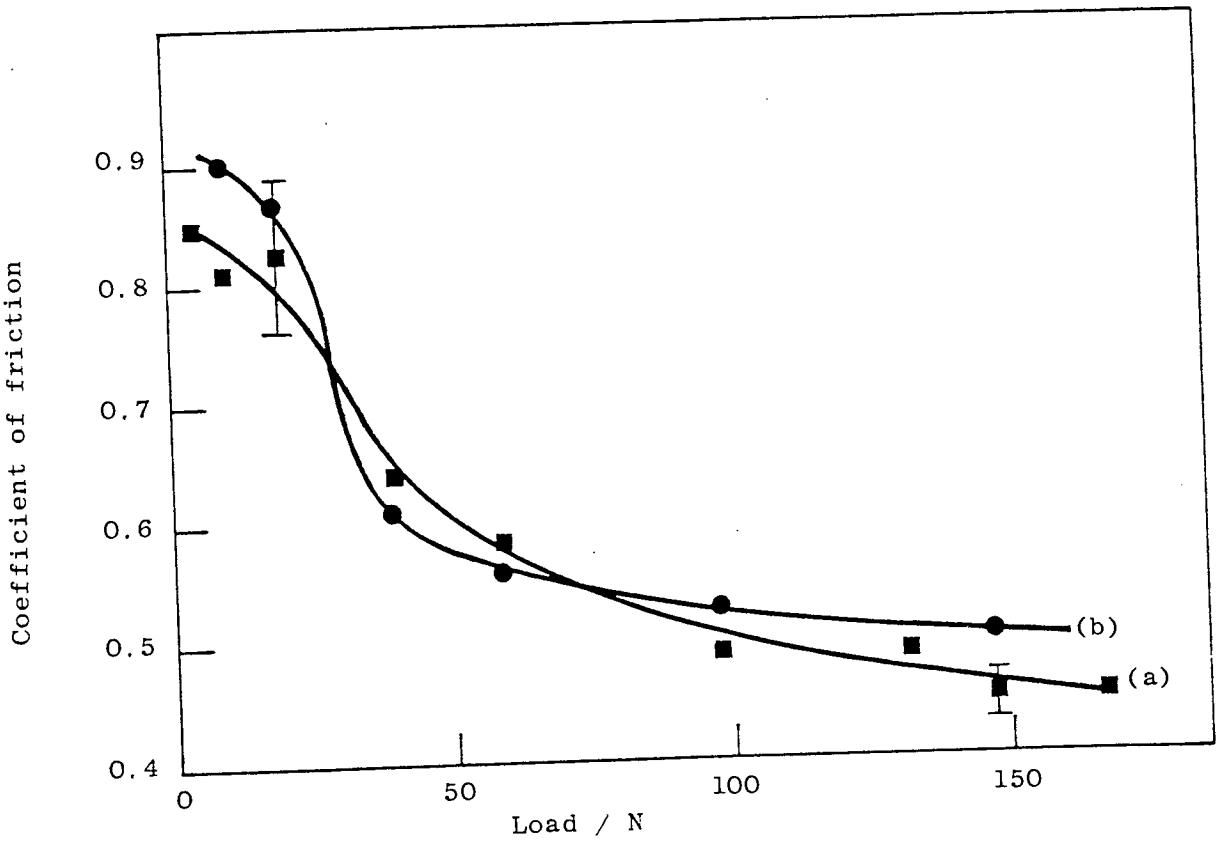

Fig. 3.11. Coefficient of friction versus load for a sliding speed of 2 m s^{-1} with no external heating applied to the disc; (a) Lescalloy BG42; (b) A.I.S.I. 440C MOD steel.

Figure 3.12 shows the complete elevated temperature results for the wear rate of Lescalloy BG42 steel pins versus load for various disc temperatures at a sliding speed of 2 m s^{-1}. Again a logarithmic scale was used due to the large range in wear rate. The two distinct regions of wear may be seen for the pin-on-disc experiments with no external heating and with disc temperatures of 200 and 300 ^{o}C. Below about 40 N load the debris analysis and magnitude of wear rates suggest a mixed oxidational-metallic type of wear. When the load exceeds this value the wear is severe with large metallic wear particles and high wear rates. At a disc temperature of 400 ^{o}C the wear rate cannot be simply divided into these two types of wear as shown in figure 3.6. Quite a different mechanism is apparent at a disc temperature of 500 ^{o}C figure 3.12(e), where there is a considerable fall in the wear rate of the steel. Both X-ray data and S.E.M. analysis show that transfer of material in the form of oxides is occurring from disc to pin, see sections 3.4 and 3.5. The corresponding coefficient of friction values are shown in figure 3.13. There is the usual decrease with increasing load except at disc temperatures of 400 and 500 ^{o}C figures 3.13(d) and 3.13(e) respectively. At a disc temperature of 400 ^{o}C the coefficient of friction increases rapidly from about 0.43 at 98.1 N load to 0.58 at 147.1 N load. At this load of 147.1 N X-ray data shows there is no longer any oxides present in the wear debris, see table 3.13.

Figure 3.14 shows the elevated temperature results for the wear rate of A.I.S.I. 440C MOD steel pins, as a function of load for various disc temperatures at a sliding speed of 2 m s^{-1}. The corresponding coefficient of friction values are shown in figure 3.15. As with the Lescalloy BG42 steel they show the three distinct types of wear. For

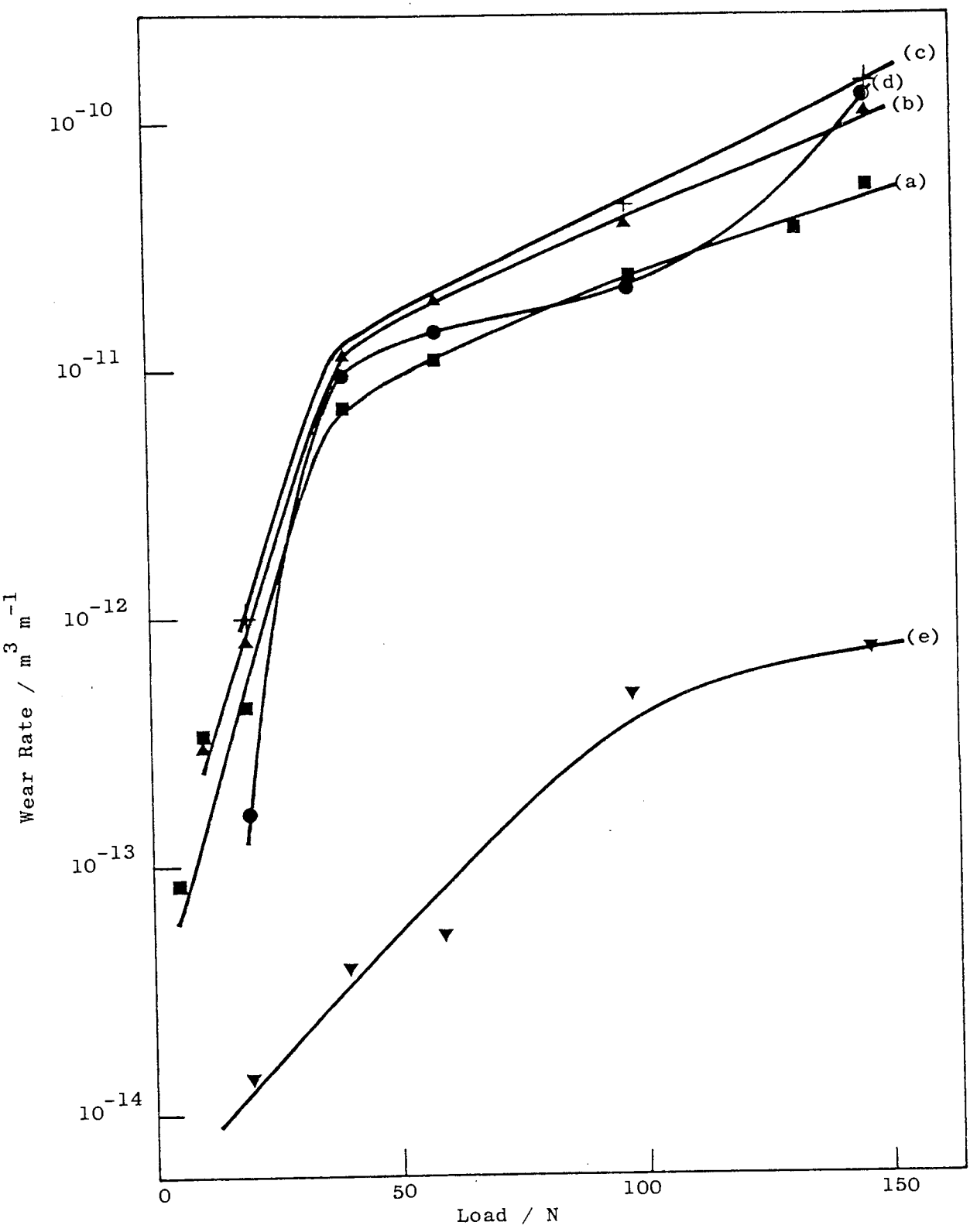

Fig. 3.12. Wear rate of Lescalloy BG42 martensitic stainless steel versus load for a sliding speed of 2 m s^{-1}; (a) no external heating applied to the disc; (b), (c), (d) and (e) for disc temperatures of 200, 300, 400 and 500 ^{o}C respectively.

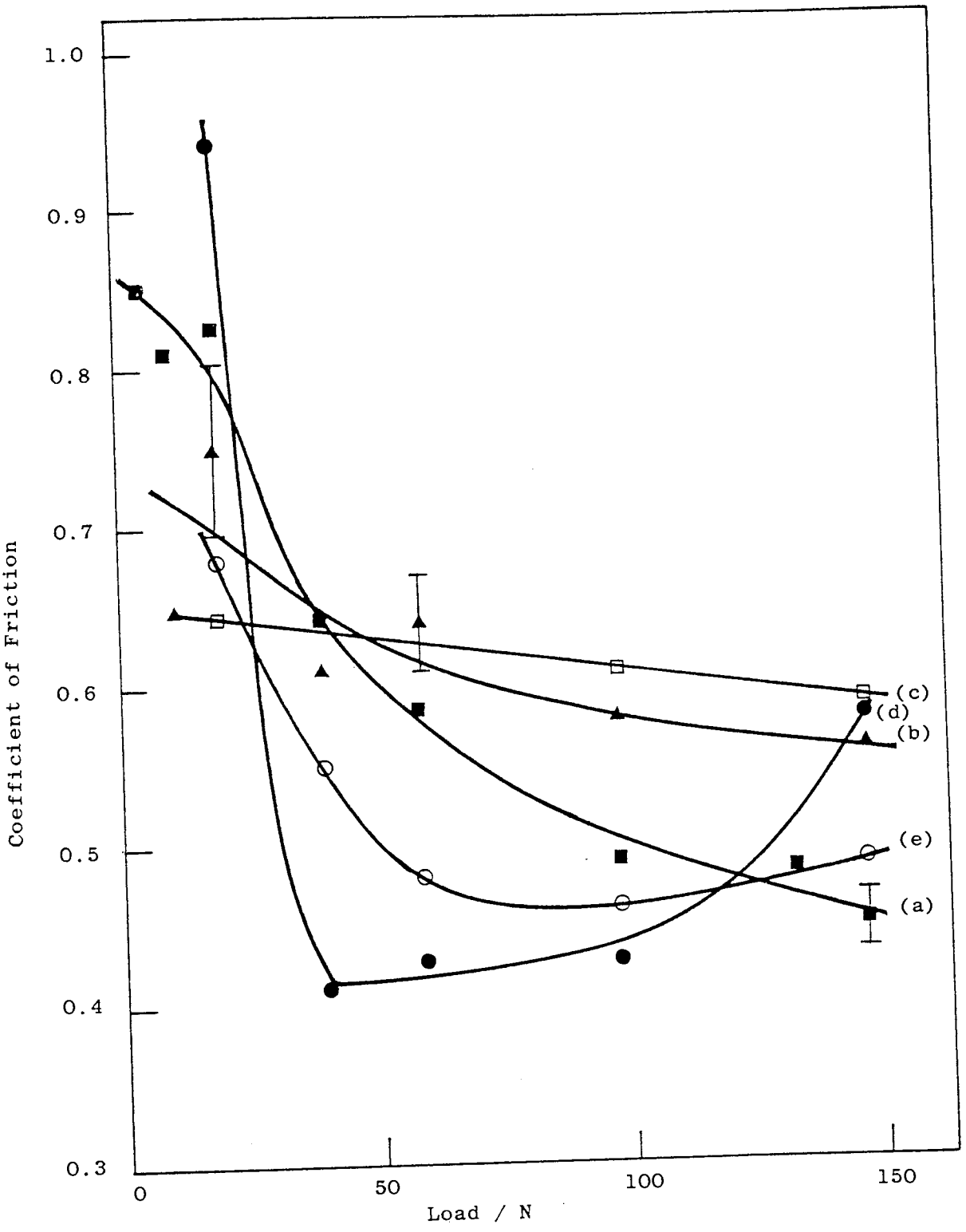

Fig. 3.13. Coefficient of friction of Lescalloy BG42 steel versus load for a sliding speed of 2 m s^{-1}; (a) no external heating applied to the disc; (b), (c), (d) and (e) for disc temperatures of 200, 300, 400 and 500 ^{o}C respectively.

pin-on-disc experiments with no external heating and a disc temperature of 200 ^{o}C figures 3.14(a) and 3.14(b), there is a mixed oxidational-metallic type of wear below about 40 N load. Above this load the wear is severe indicated by large metallic wear particles and high wear rates. At a disc temperature of 500 ^{o}C figure 3.14(c), there is a considerable fall in the wear rate of the steel, where X-ray data and S.E.M. analysis show that material is transferring in the form of oxides from the disc to the pin. The coefficient of friction as usual decreases with increasing load at all disc temperatures.

Figure 3.16 shows the wear rate of Lescalloy BG42 steel pins versus disc temperature for a series of loads at a sliding speed of 2 m s^{-1}. Again a logarithmic scale was used because of the large range in the wear rate. All the curves show the same general trends with initial increase in wear rate followed by a sharp decrease at temperatures above 300 to 350 ^{o}C depending on load. There is the expected wear rate increase with load with maximum wear rate occurring at slightly higher disc temperatures. For loads less than about 40 N X-ray data and S.E.M. analysis show oxidational-metallic wear approaching the maximum wear rate temperature, above which there is transfer of material in the form of oxides from the disc to the pin. For loads above 40 N the wear is severe up to the maximum wear rate temperature, above which the wear rate decreases due to possibly first an oxide film before there is transfer of material in the form of oxides from the disc to the pin, see section 3.4. The corresponding coefficient of friction values are shown in figure 3.17.

The heat flow per second along the pin at the interface between the pin and disc H_1 (J s^{-1}) for Lescalloy BG42 steel pins versus load is shown in figure 3.18, for experiments with sliding speeds of 0.6,

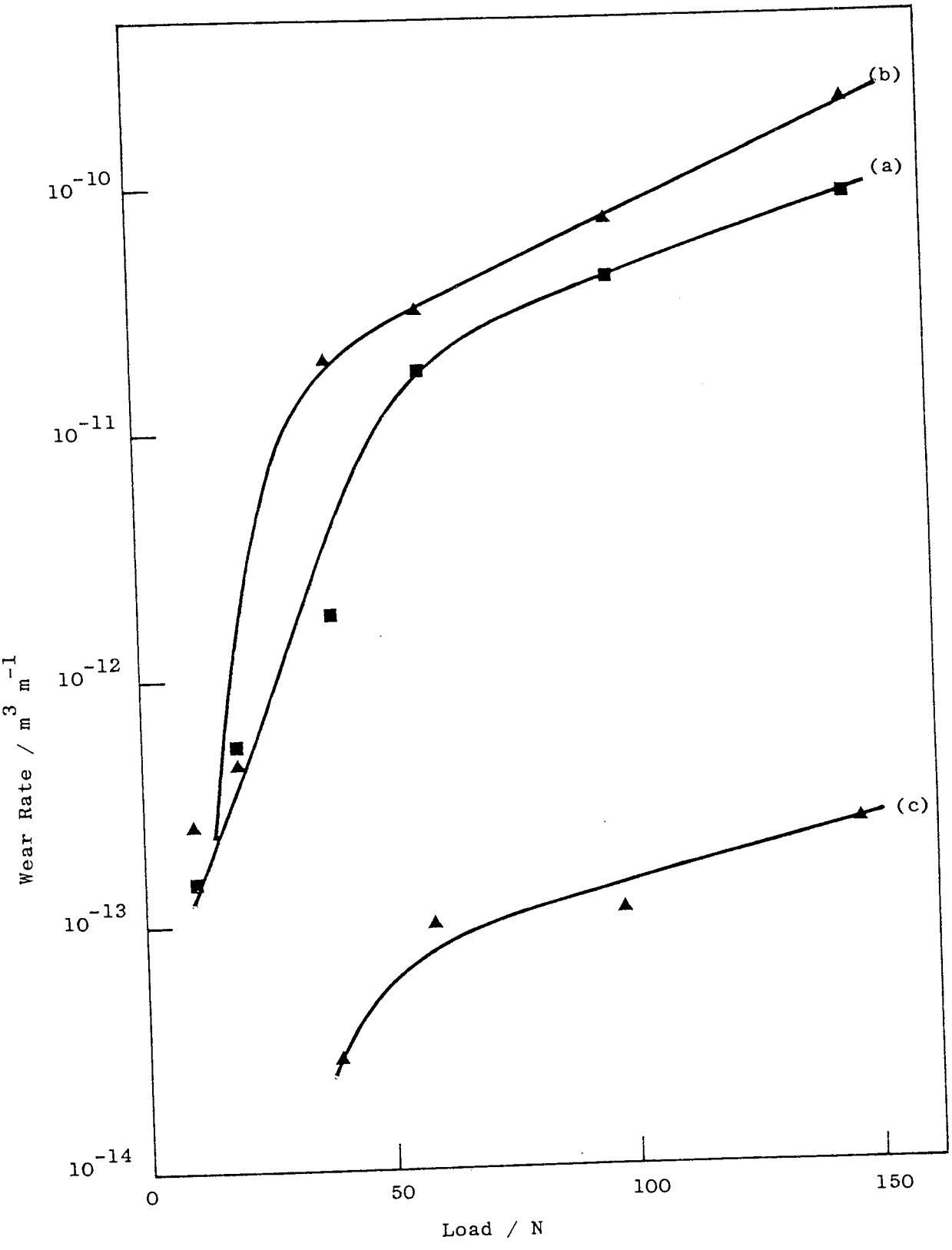

Fig. 3.14. Wear rate of A.I.S.I. 440C MOD martensitic stainless steel versus load for a sliding speed of 2 m s^{-1}; (a) no external heating; (b) disc temperature 200 ^{o}C; (c) disc temperature 500 ^{o}C.

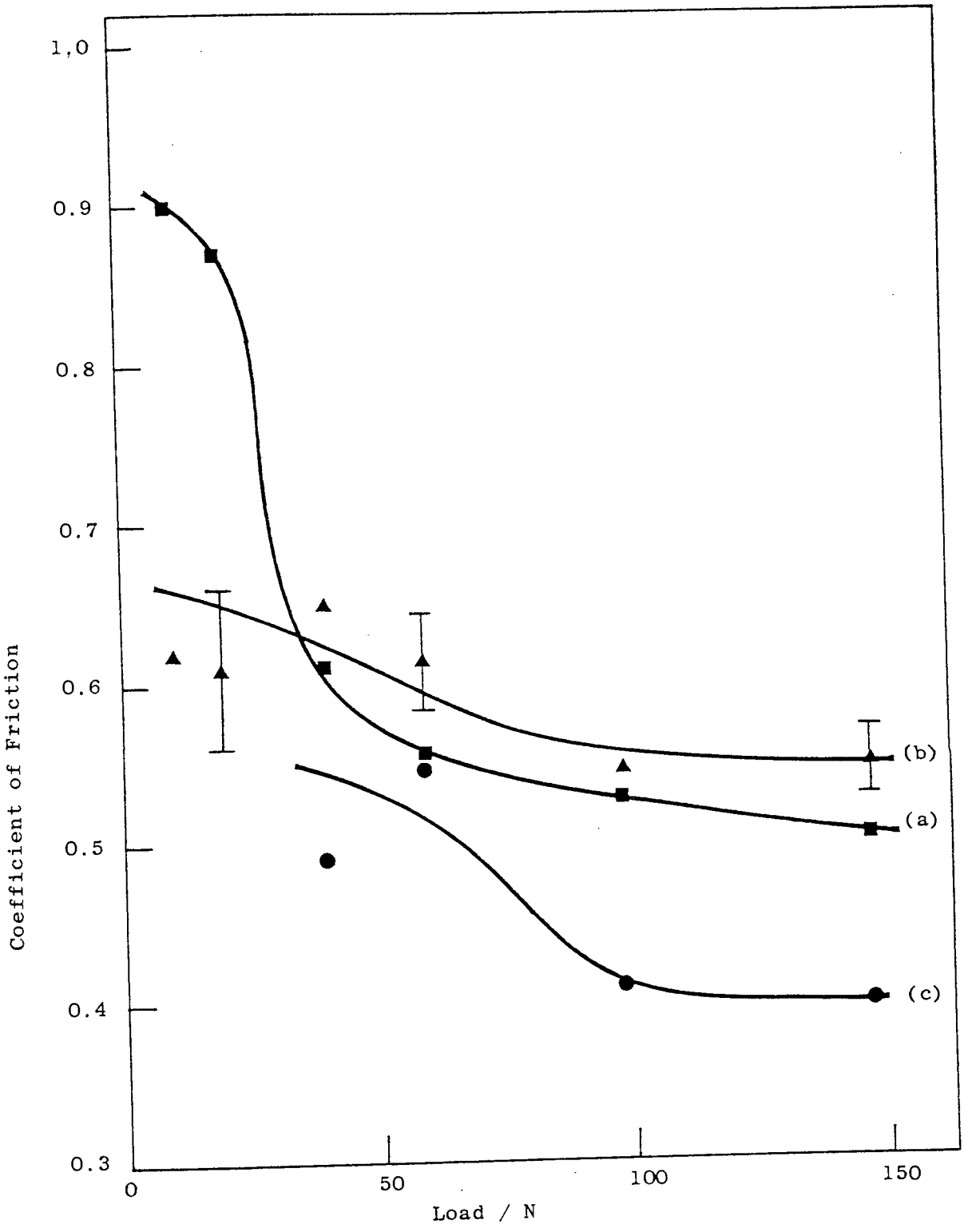

Fig. 3.15. Coefficient of friction of A.I.S.I. 440C MOD steel versus load for a sliding speed of 2 m s^{-1}; (a) no external heating; (b) disc temperature 200 ^{o}C; (c) disc temperature 500 ^{o}C.

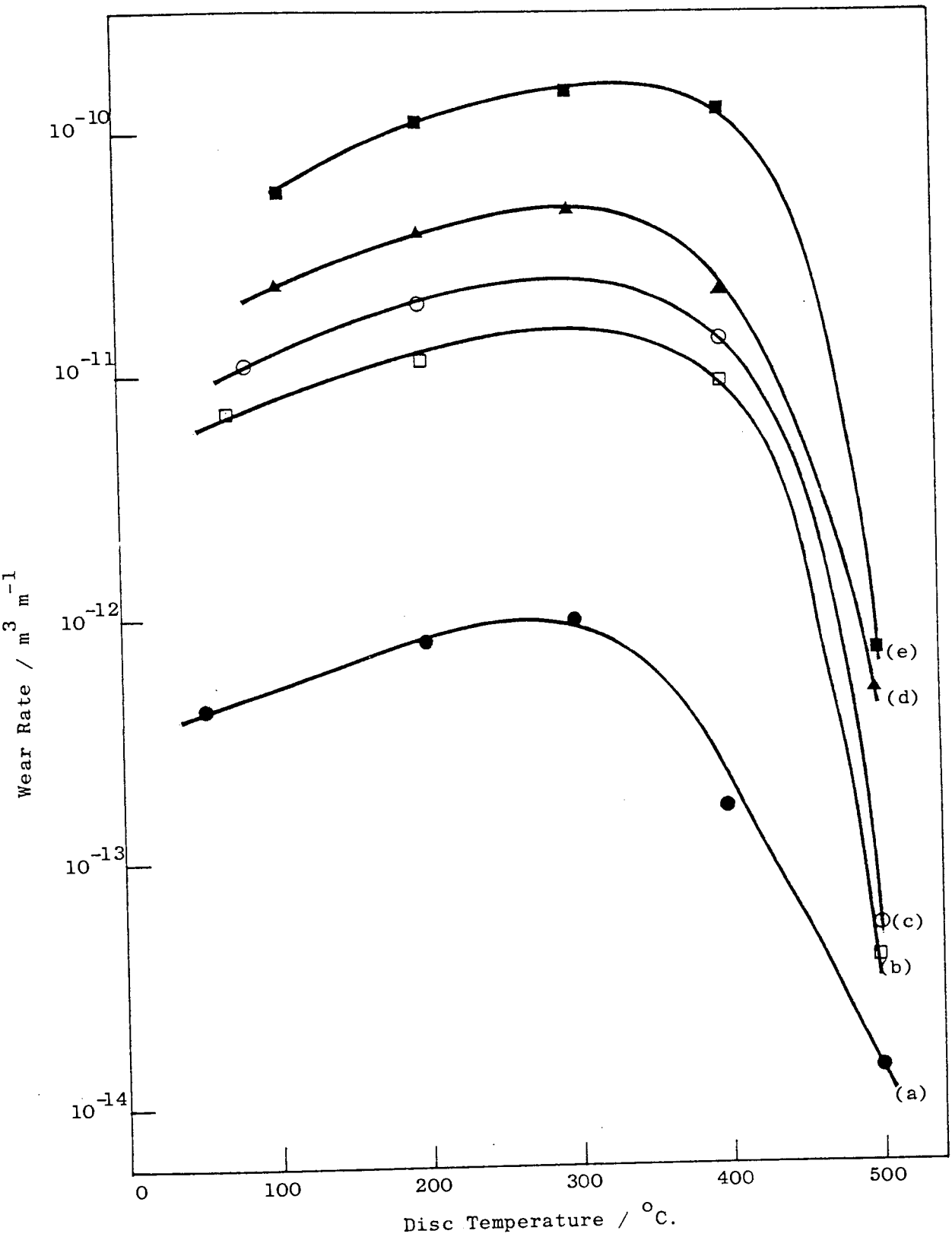

Fig. 3.16. Wear rate of Lescalloy BG42 martensitic stainless steel versus disc temperature at a sliding speed of 2 m s^{-1}; (a) 19.6 N load; (b) 39.2 N load; (c) 58.9 N load; (d) 98.1 N load; (e) 147.1 N load.

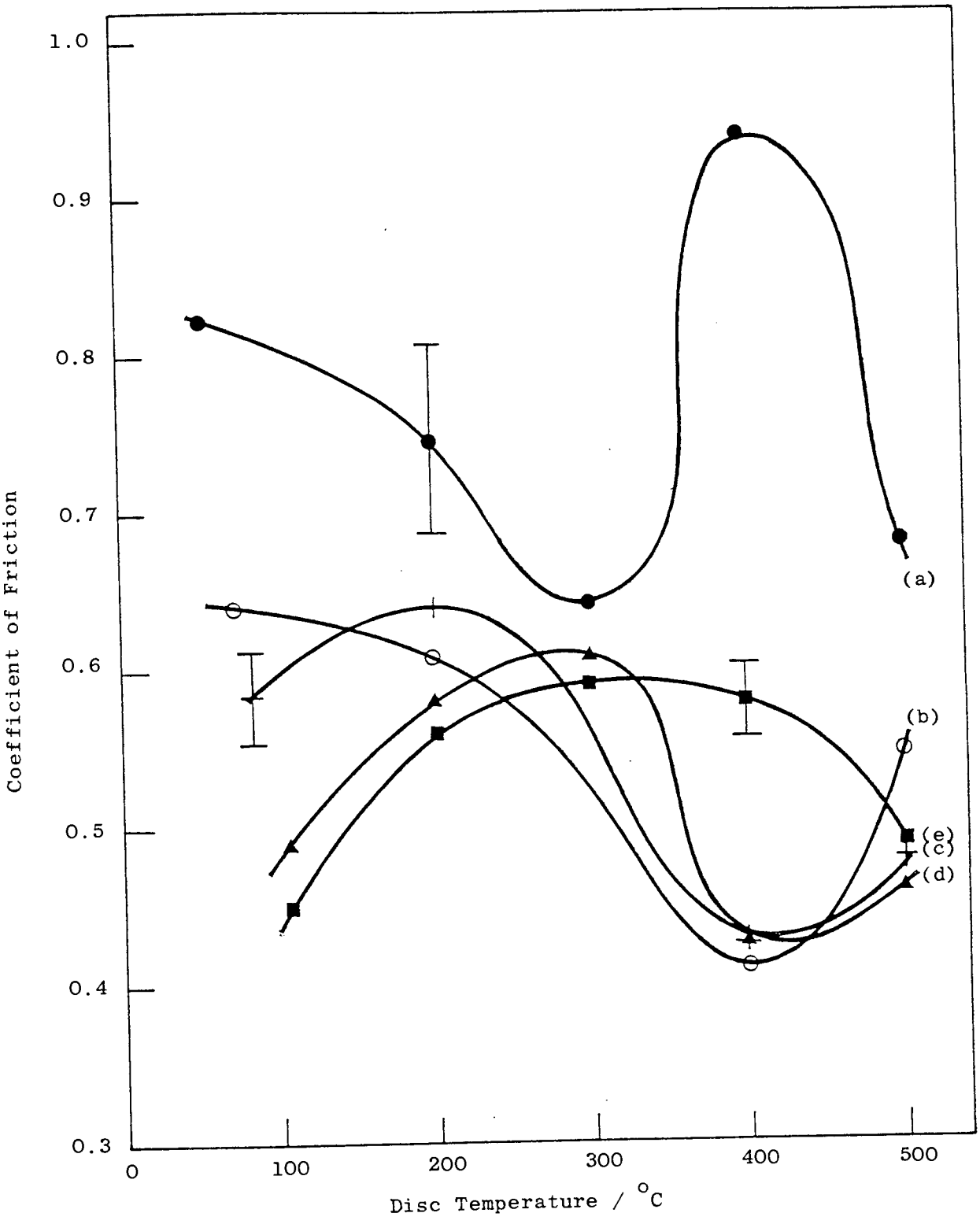

Fig. 3.17. Coefficient of friction of Lescalloy BG42 steel versus disc temperature at a sliding speed of 2 m s^{-1}; (a) 19.6 N load; (b) 39.2 N load; (c) 58.9 N load; (d) 98.1 N load; (e) 147.1 N load.

2.0 and 3.0 m s^{-1} with no external heating. For the computation of the H_1 values see appendix 1. H_1 increases at all sliding speeds with increasing load. For sliding speeds of 2.0 and 3.0 m s^{-1} figures 3.18(b) and 3.18(c), H_1 starts to increase more rapidly with load. This is due to the decreasing hardness of the pin substrate as shown by X-ray data increasing the number of asperities in contact beneath the pin.

Figure 3.19 shows H_1 for A.I.S.I. 440C MOD steel pins versus load for various disc temperatures at a sliding speed of 2 m s^{-1}. With no external heating applied to the disc figure 3.19(a), H_1 starts to increase more rapidly for loads above about 40 N, due to softening of the pins surface as shown by X-ray data increasing the number of asperities in contact beneath the pin. At a disc temperature of 200 ^{o}C figure 3.19(b), there is a linear increase in H_1 with increasing load. At a disc temperature of 500 ^{o}C figure 3.19(c), H_1 remains fairly constant where its magnitude at about 140 N load is less than the H_1 value at a disc temperature of 200 ^{o}C. This is due to material transfer in the form of oxides from the disc to the pin as shown by X-ray data and S.E.M. analysis, which acts like an insulator reducing the heat flow rate along the pin.

H_1 for Lescalloy BG42 steel pins versus load for various disc temperatures at a sliding speed of 2 m s^{-1} is shown in figure 3.20. At disc temperatures of 200, 300 and 400 ^{o}C H_1 increases linearly with increasing load. For the unheated disc see the explanation given for figure 3.18(b). At a disc temperature of 500 ^{o}C figure 3.20(e), the rate of increase in H_1 with load is fairly low and its magnitude at about 100 N load is less than for a disc temperature of 300 ^{o}C. This is because of material transfer in the form of oxide from the disc to

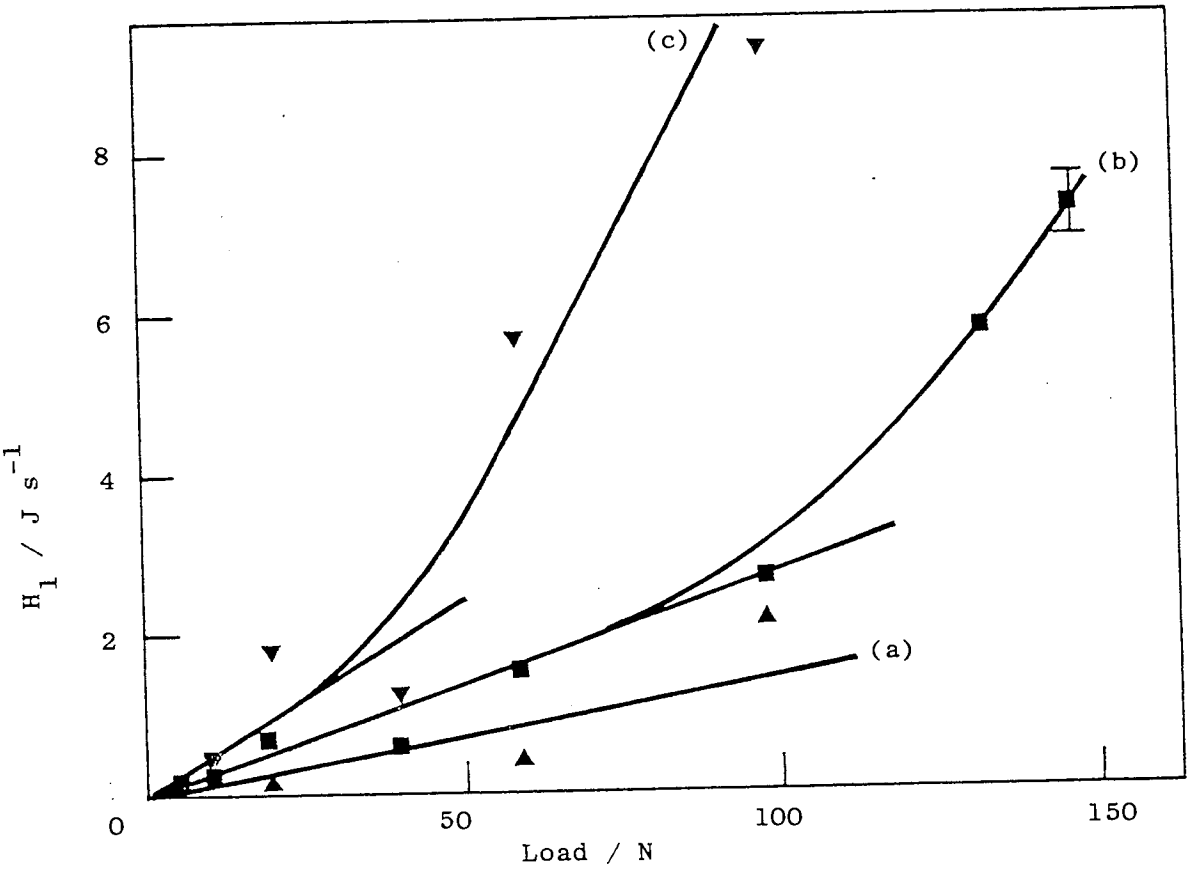

Fig. 3.18. The heat flow rate along Lescalloy BG42 steel pins at the pin-disc interface versus load for experiments with no external heating; (a) 0.6 m s^{-1} sliding speed; (b) 2.0 m s^{-1} sliding speed; (c) 3.0 m s^{-1} sliding speed.

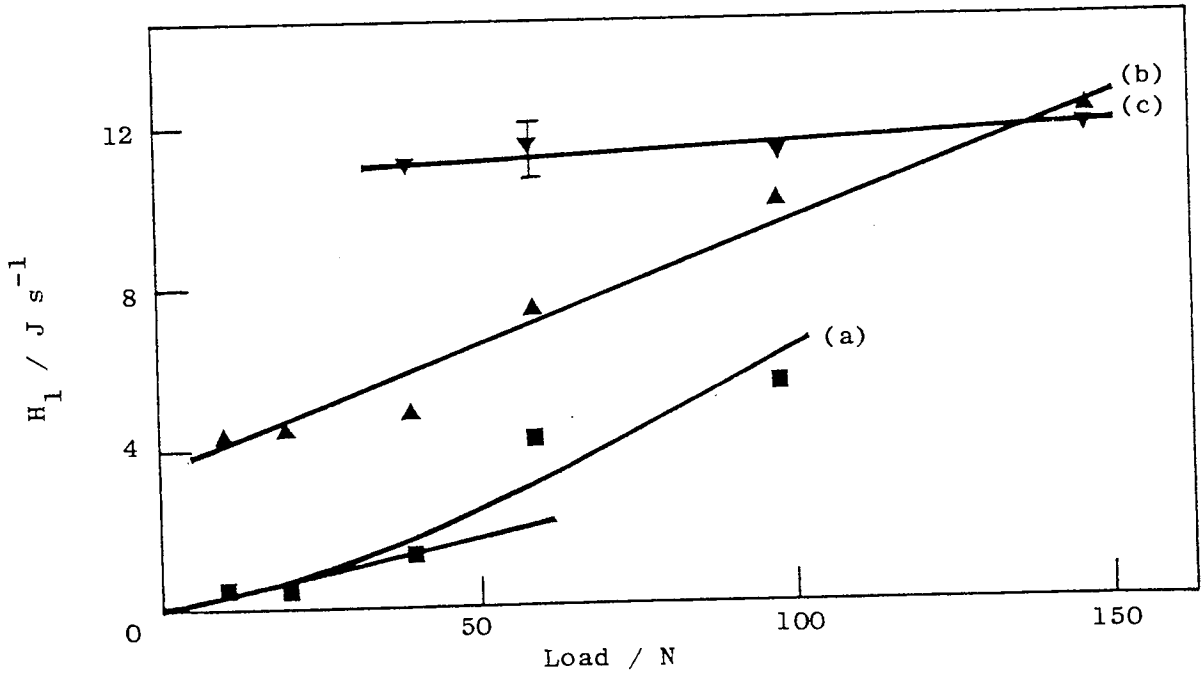

Fig. 3.19. The heat flow rate along A.I.S.I. 440C MOD steel pins at the pin-disc interface versus load for a sliding speed of 2 m s^{-1}; (a) no external heating; (b) disc temperature 200 ^{o}C; (c) disc temperature 500 ^{o}C.

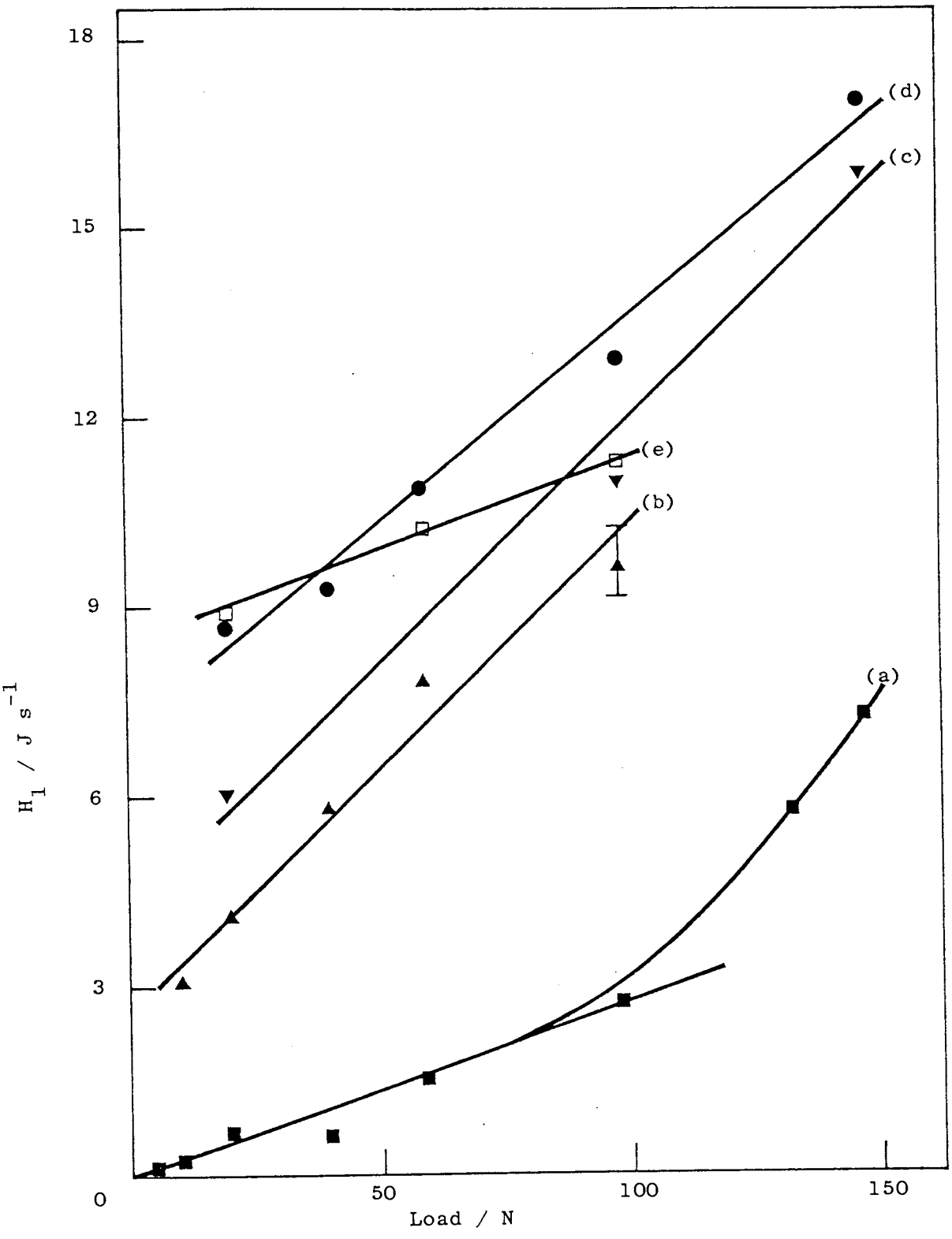

Fig. 3.20. The heat flow rate along Lescalloy BG42 steel pins at the pin-disc interface versus load for a sliding speed of 2 m s^{-1}; (a) no external heating applied to the disc; (b), (c), (d) and (e) for disc temperatures of 200, 300, 400 and 500 ^{o}C respectively.

the pin as shown by X-ray data and S.E.M. analysis which acts like an insulator.

The total heat per second evolved at the pin-disc interface for no external heating H(total) (J s^{-1}) was calculated using equation (2.12). H(total) for Lescalloy BG42 steel pins versus load is shown in figure 3.21, for experiments with sliding speeds of 0.6, 2.0 and 3.0 m s^{-1} with no external heating applied to the disc. There is a linear increase in H(total) with increasing load at all sliding speeds. For the heated disc experiments H(total) could not be determined, because the amount of energy supplied by the heater in conjunction with the temperature controller could not be measured. The exprimentally measured division of heat at the pin-disc interface, δ(expt) was obtained from equation (2.11). Figure 3.22 shows δ(expt) for Lescalloy BG42 steel pins as a function of load at a sliding speed of 2 m s^{-1} with no external heating applied to the disc. After remaining constant with increasing load within the limits of experimental error δ(expt) starts to increase above a load of 60 N. This is due to the decreasing hardness of the pin substrate as shown by X-ray data increasing the number of asperities in contact beneath the pin.

The temperature of the surface of the pin outside the real area of contact T_s (^{o}C) was computed from the heat flow theory using equation (2.9), see section 2.6 and also appendix 1. The computed surface temperature of Lescalloy BG42 steel pins versus load is shown in figure 3.23, for experiments with sliding speeds of 0.6, 2.0 and 3.0 m s^{-1} with no external heating. Figure 3.24 shows the computed surface temperature of A.I.S.I. 440C MOD steel pins versus load, for

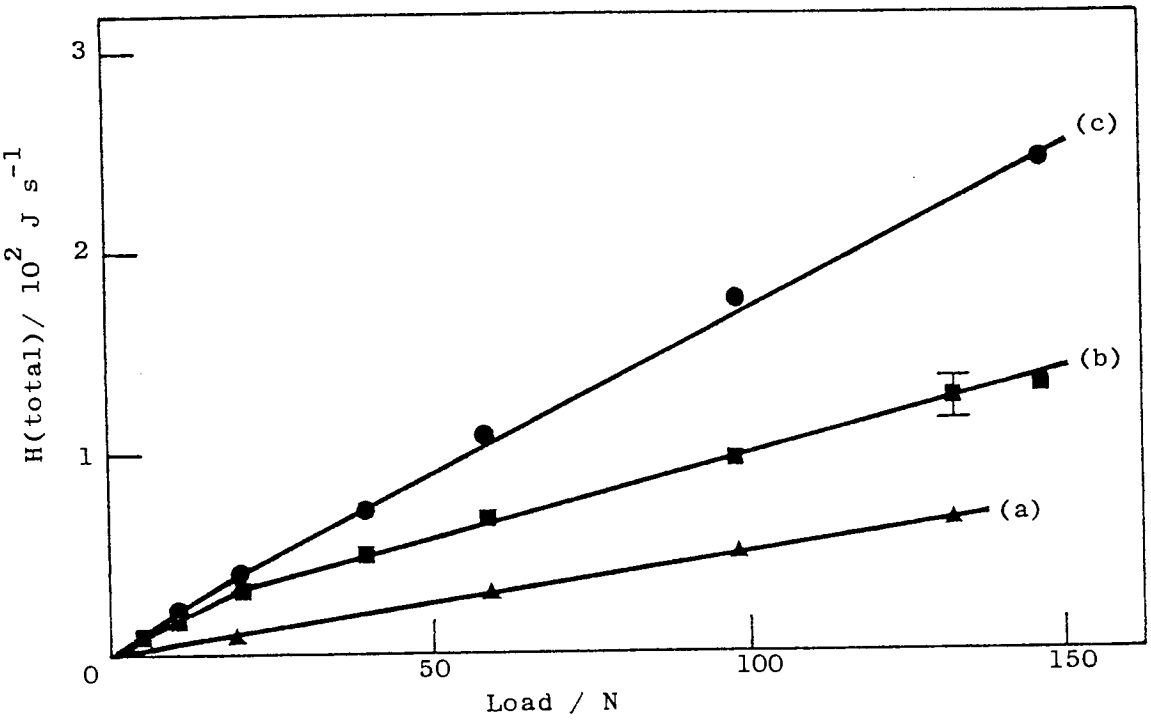

Fig. 3.21. The total heat per second evolved at the pin-disc interface for Lescalloy BG42 steel pins versus load for experiments with no external heating; (a) 0.6 m s^{-1} sliding speed; (b) 2.0 m s^{-1} sliding speed; (c) 3.0 m s^{-1} sliding speed.

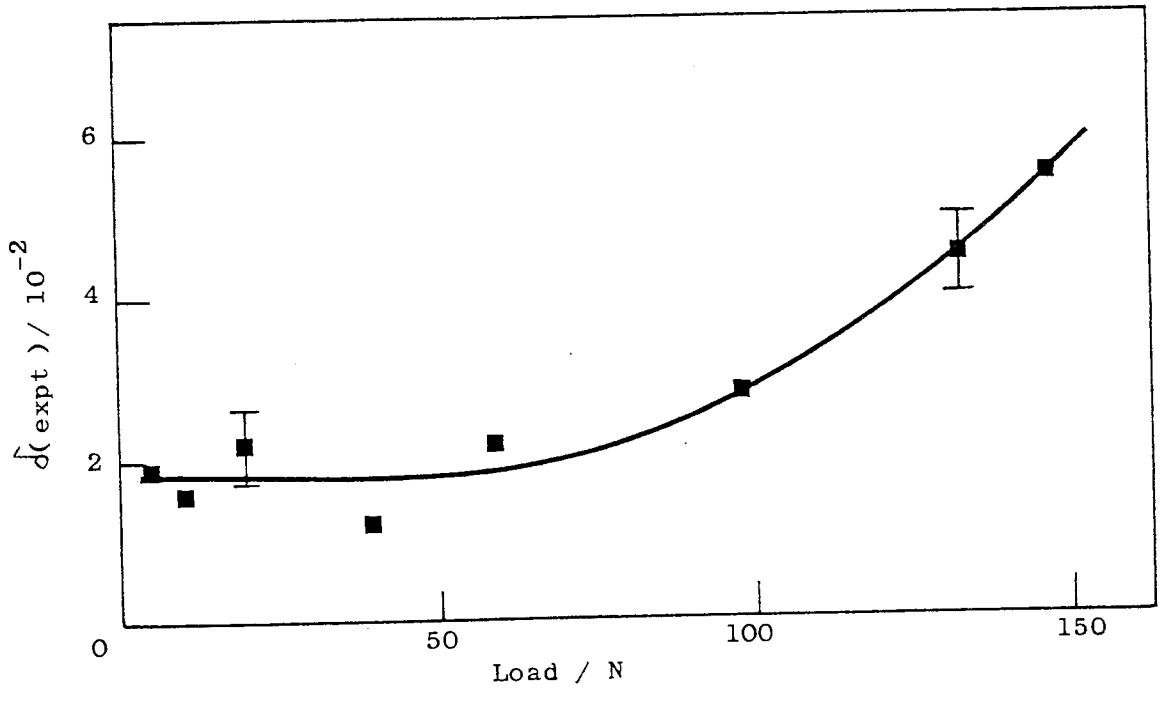

Fig. 3.22. The experimentally measured division of heat at the pin-disc interface for Lescalloy BG42 steel pins versus load, for a sliding speed of 2 m s^{-1} with no external heating applied to the disc.

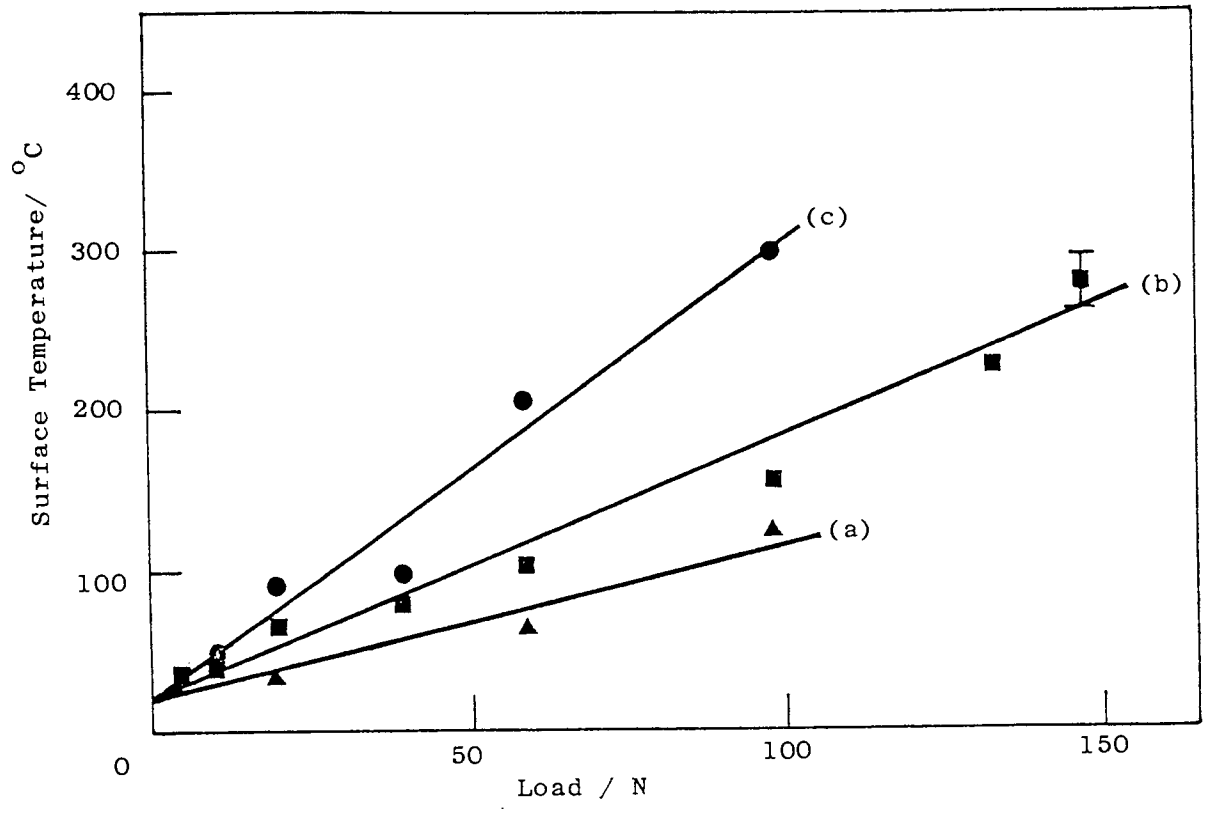

Fig. 3.23. Computed pin surface temperature of Lescalloy BG42 martensitic stainless steel versus load for experiments with no external heating; (a) o.6 m s^{-1} sliding speed; (b) 2.0 m s^{-1} sliding speed; (c) 3.0 m s^{-1} sliding speed.

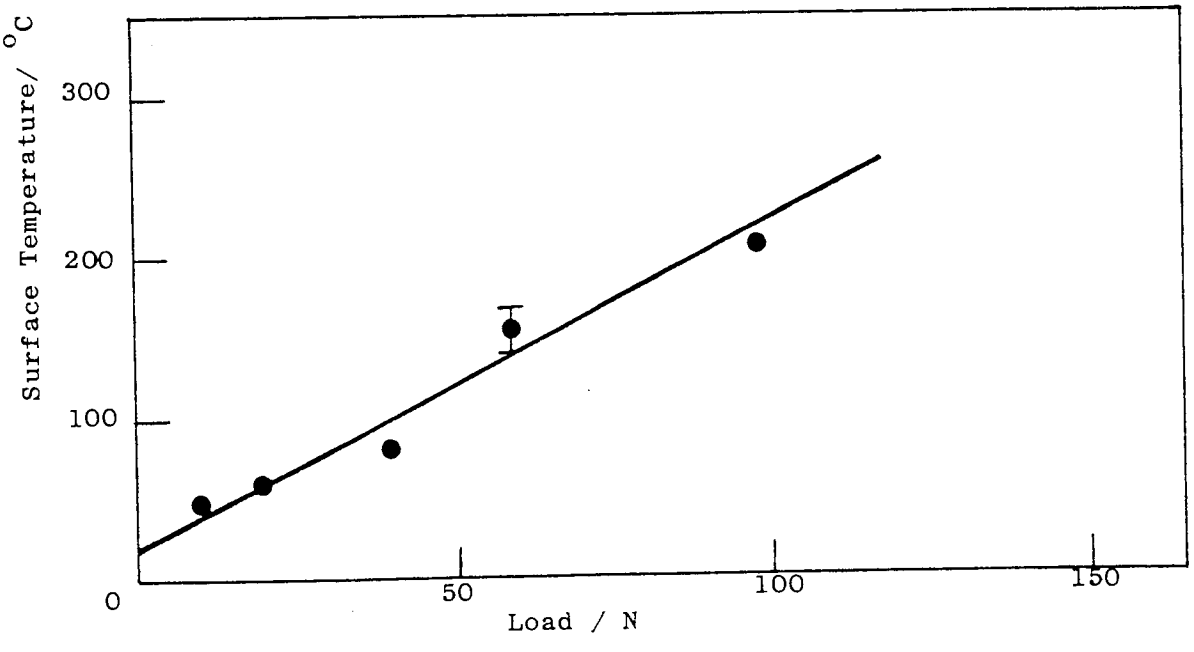

Fig. 3.24. Computed pin surface temperature of A.I.S.I. 440C MOD steel versus load, for a sliding speed of 2 m s^{-1} with no external heating applied to the disc.

a sliding speed of 2 m s^{-1} with no external heating applied to the disc. For both types of steel the surface temperature increases linearly with increasing load within the limits of experimental error. There is of course the expected temperature increase with increasing speed. Figure 3.25 shows the computed surface temperature of Lescalloy BG42 steel pins as a function of load for various disc temperatures at a sliding speed of 2 m s^{-1}. The surface temperature of A.I.S.I. 440C MOD steel pins versus load for the same conditions is shown in figure 3.26. For both types of steel pins the surface temperature is proportional to load within the limits of experimental error at all disc temperatures. For a disc temperature of 500 ^{o}C figure 3.25(e) and 3.26(c) the rate of increase in surface temperature with load is fairly low. Also for small loads the surface temperature can be lower than the disc temperature, because of the formation of oxides on the pin as shown by X-ray data and S.E.M. analysis which acts like an insulator.

Figure 3.27 shows the wear rate of Lescalloy BG42 steel pins versus the computed surface temperature for a series of loads at a sliding speed of 2 m s^{-1}. The only real difference from figure 3.16 is a shift of the curves to higher temperatures. Maximum wear rate occurs at surface temperatures of about 310, 335, 370, 430 and 540 ^{o}C for loads of 19.6, 39.2, 58.9, 98.1 and 147.1 N respectively. As before there is the expected wear rate increase with load.

Figure 3.28 shows the computed surface temperature of Lescalloy BG42 steel pins versus an extrapolated surface temperature, for disc temperatures up to 400 ^{o}C at a sliding speed of 2 m s^{-1} and a 98.1 N load. The extrapolated or approximate surface temperatures were obtained from equation (2.13) section 2.6. This shows that the computed surface temperatures are quite valid at elevated disc temperatures, since

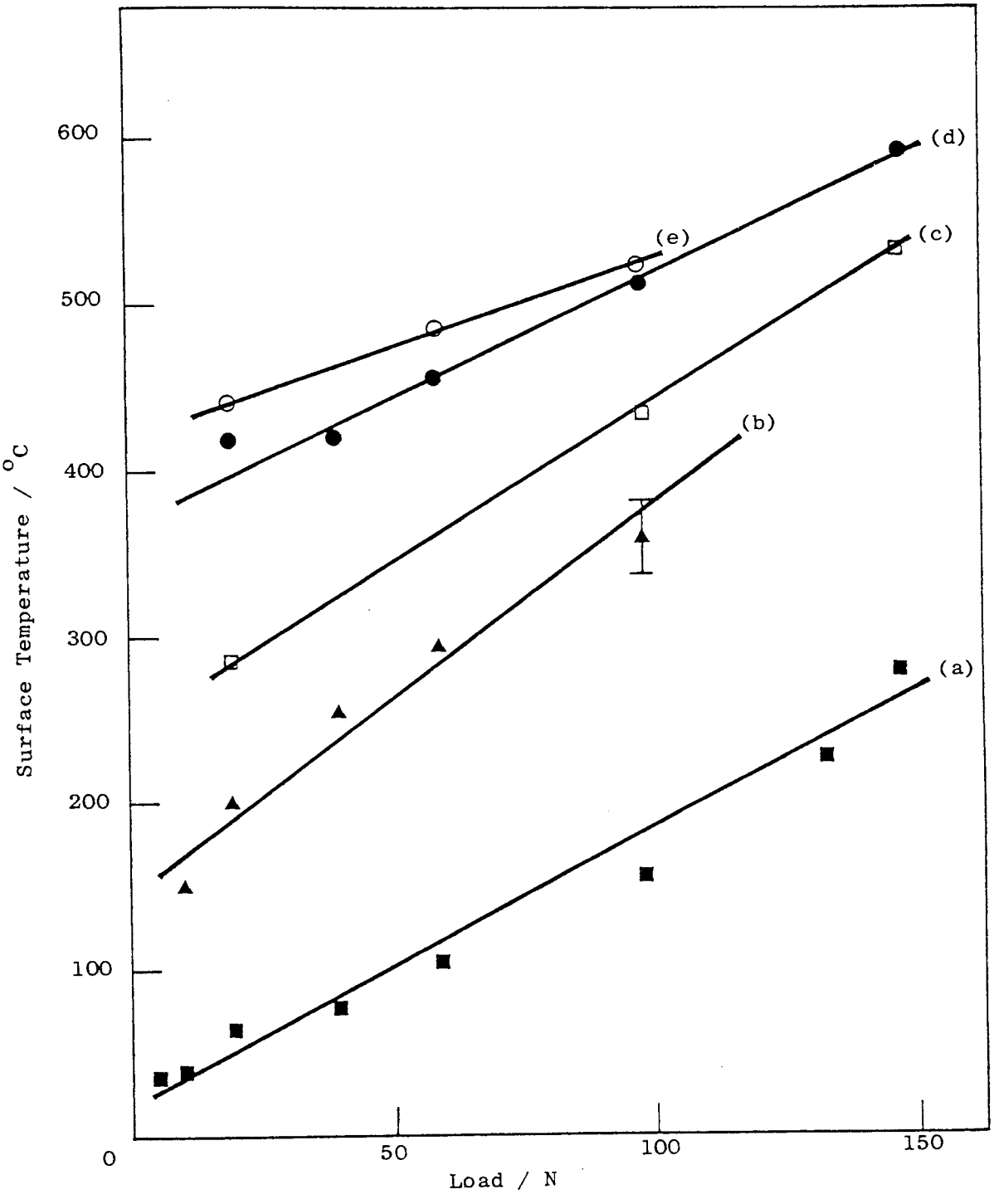

Fig. 3.25. Computed pin surface temperature of Lescalloy BG42 martensitic stainless steel versus load for a sliding speed of 2 m s^{-1}; (a) no external heating applied to the disc; (b), (c), (d) and (e) for disc temperatures of 200, 300, 400 and 500 °C respectively.

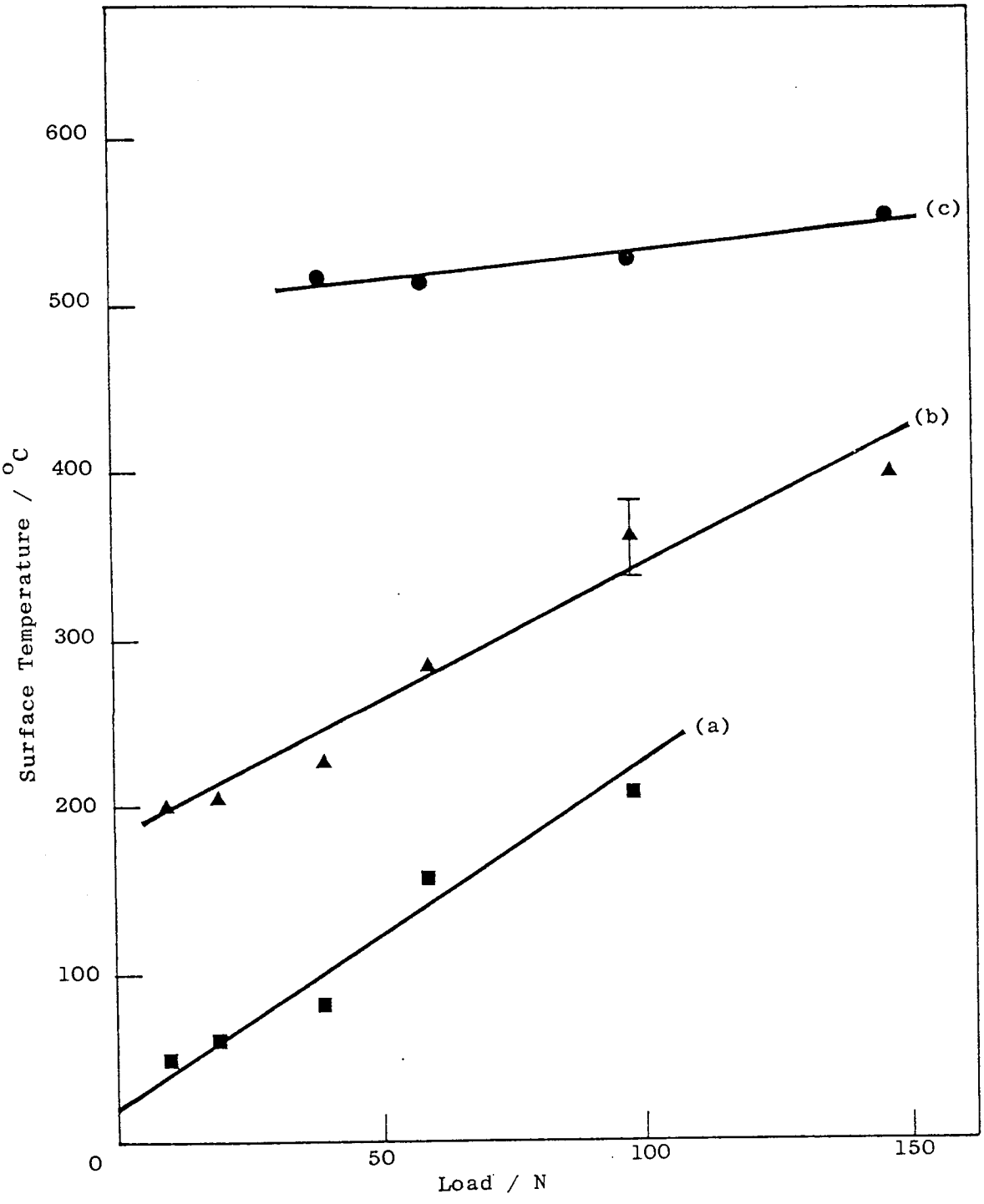

Fig. 3.26. Computed pin surface temperature of A.I.S.I. 440C MOD martensitic stainless steel versus load for a sliding speed of 2 m s^{-1}; (a) no external heating; (b) disc temperature 200 °C; (c) disc temperature 500 °C.

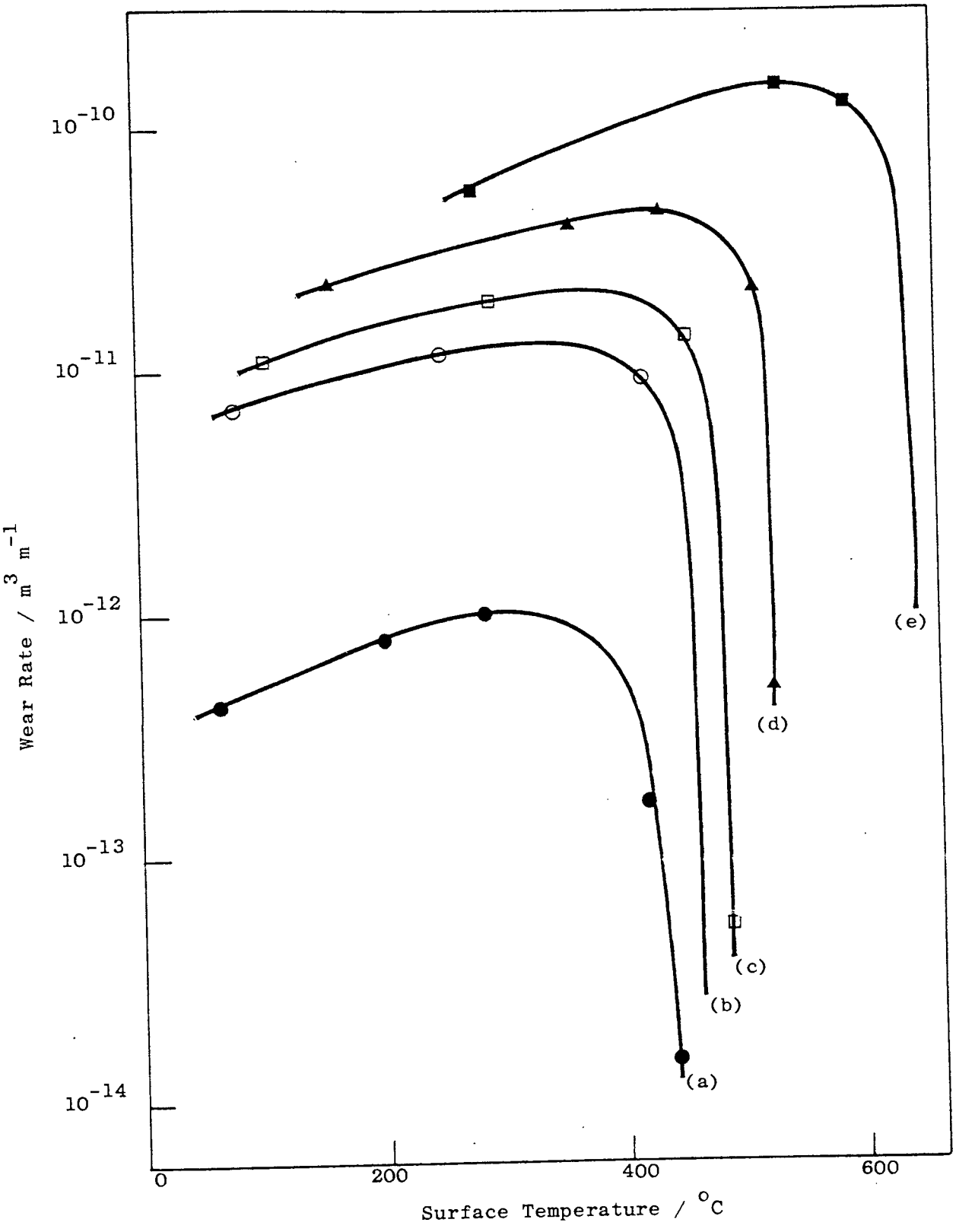

Fig. 3.27. Wear rate of Lescalloy BG42 martensitic stainless steel versus computed pin surface temperature for a sliding speed of 2 m s^{-1}; (a) 19.6 N load; (b) 39.2 N load; (c) 58.9 N load; (d) 98.1 N load; (e) 147.1 N load.

the points are on a straight line within the limits of experimental error. From the graph the extrapolated surface temperatures were found to be about 1.16 times the computed surface temperatures.

The temperature of the real area of contact between the pin and the disc T_c (^oC) is given by equation (3.1), Rowson and Quinn.(81)

$$T_c = T_s + (H_1 / N \pi K_s a) + (H_1 h_f / N \pi K_o a^2) \quad \ldots\ldots\ldots(3.1)$$

T_s is the temperature of the surface of the pin outside the real area of contact, H_1 is the heat flow per second along the pin at the interface between the pin and disc and K_s is the thermal conductivity of the steel pin (23.86 $J\ s^{-1}\ m^{-1}\ ^oC^{-1}$). N is the number of asperities in contact beneath the pin, a is the radius of each of the N circular areas of contact making up the real area of contact, h_f is the thickness of an oxide film at the real areas of contact and K_o is the thermal conductivity of the oxide layer. It is assumed that the total real area of contact A (m^2) is given by equation (3.2), Bowden and Tabor.(3)

$$A = W / p \quad \ldots\ldots\ldots(3.2)$$

W is the normal applied load at the pin and p is the bulk hardness of the steel ($(8.29 \pm 0.05) \times 10^9\ N\ m^{-2}$).

$$A = N \pi a^2 \quad \ldots\ldots\ldots(3.3)$$

From equations (3.1), (3.2) and (3.3) we have:-

$$T_c = T_s + (H_1 p^{1/2} / N^{1/2} \pi^{1/2} W^{1/2} K_s) + (H_1 h_f p / W K_o) \quad \ldots(3.4)$$

For the severe type of wear $h_f = 0$ since there is no oxide film present on the surface. By assuming N = 1 the maximum attainable temperature of the real area of contact T_c can be estimated. In practice N is found to increase with increasing load. Therefore using equation (3.4) the maximum attainable temperatures of the real area of contact T_c for Lescalloy BG42 steel pins are shown in table 3.1. Disc temperatures less than 200 ^oC were generated by frictional heating alone.

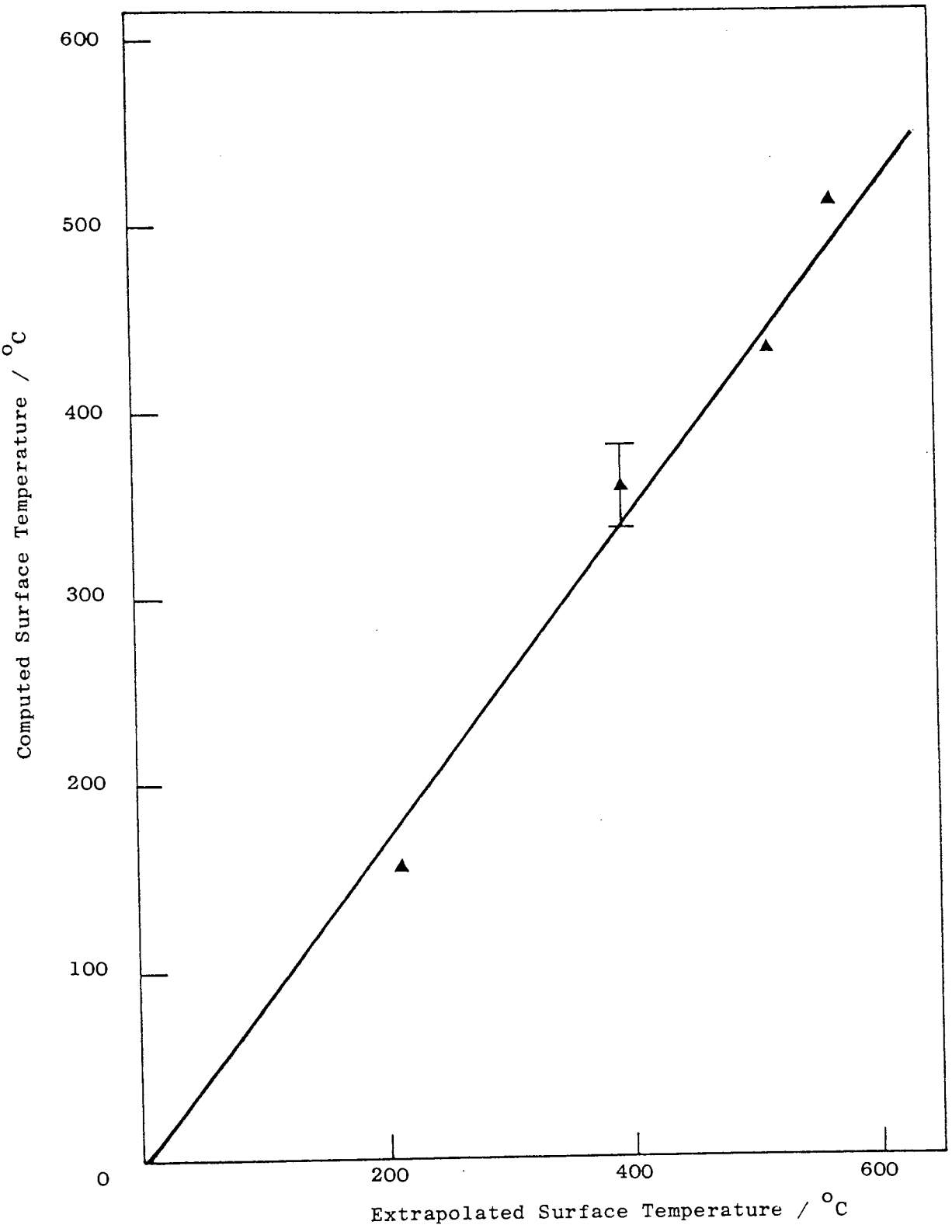

Fig. 3.28. Computed pin surface temperature of Lescalloy BG42 martensitic stainless steel, versus an extrapolated surface temperature up to a disc temperature of 400 °C at a sliding speed of 2 m s^{-1} and a 98.1 N load.

Table 3.1. The maximum attainable temperatures of the real area of contact for Lescalloy BG42 steel pins.

Disc Temperature / ^{o}C $\pm$ 5 ^{o}C	Sliding Speed / m s^{-1} $\pm$ 0.05 m s^{-1}	Load / N $\pm$ 0.9 N	H_1 / J s^{-1} $\pm$ 5%	Surface Temperature / ^{o}C $\pm$ 5%	Contact Temperature / ^{o}C $\pm$ 5%
37	0.60	19.6	0.12	35	93
64	0.60	58.9	0.38	66	172
86	0.60	98.1	2.16	126	595
72	2.00	39.2	0.62	77	290
83	2.00	58.9	1.53	103	532
105	2.00	98.1	2.72	157	748
106	2.00	132.4	5.76	227	1304
106	2.00	147.1	7.28	279	1571
76	3.00	39.2	1.27	98	534
100	3.00	58.9	5.71	208	1809
119	3.00	98.1	9.29	300	2318
200	2.00	39.2	5.82	253	2253
200	2.00	58.9	7.83	295	2490
200	2.00	98.1	9.66	360	2459
300	2.00	98.1	11.01	434	2826
300	2.00	147.1	15.87	535	3351

For the pins which had oxide layers on the surfaces, no estimates could be made of the temperatures at the real area of contact because of the unknown oxide film thickness.

3.3 Surface Profiles of the Disc

The surface profiles of selected wear tracks present on the WC-11% Co disc obtained using the talylin are shown in figures 3.29, 3.30 and 3.31. Figure 3.29(a) shows the wear track on the disc produced by a

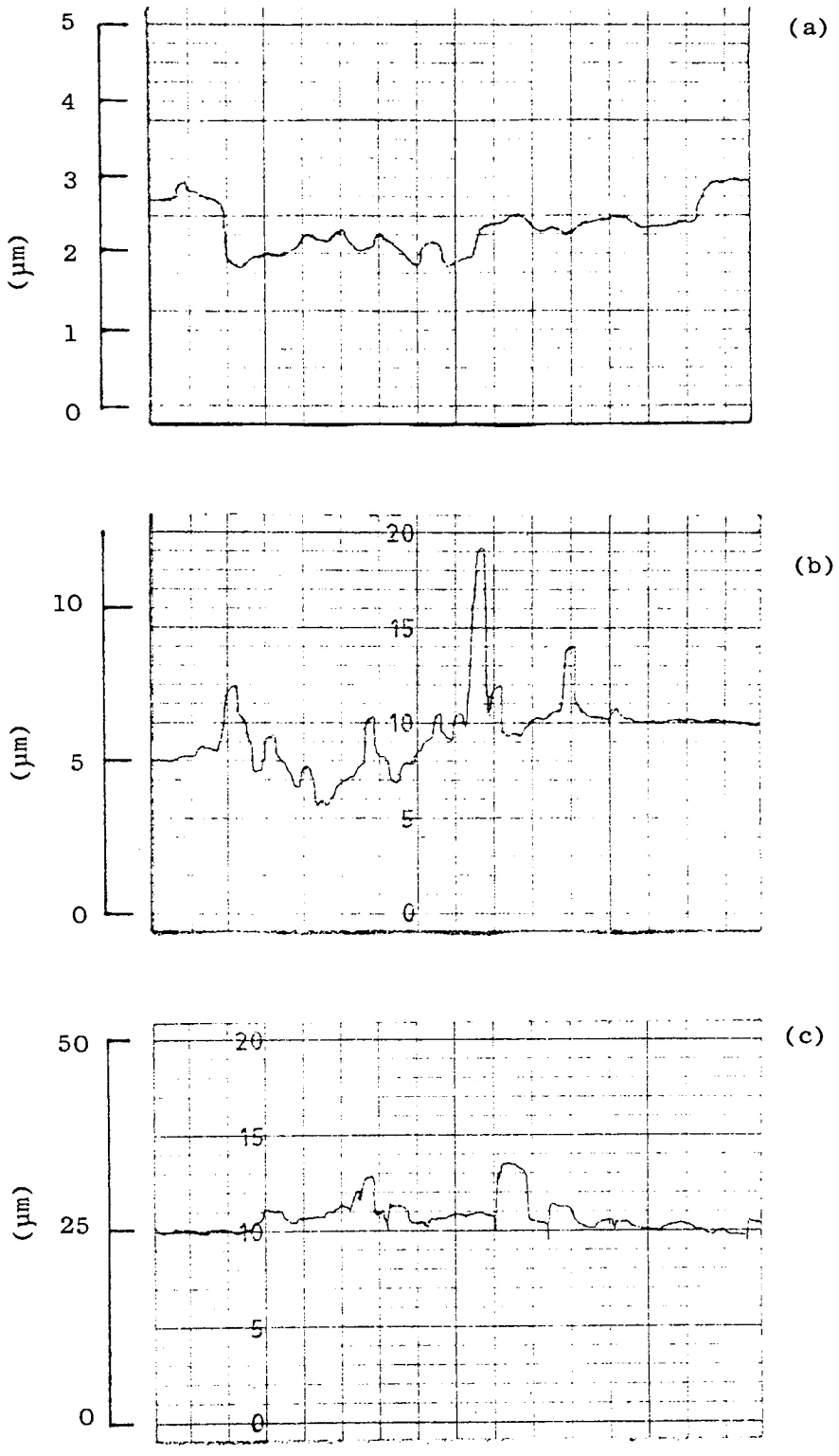

Fig 3.29. Surface profiles of selected wear tracks using a horizontal magnification of x10 present on the disc. The wear tracks were produced by Lescalloy BG42 steel pins at a sliding speed of 2 m s^{-1}; (a) vertical mag. x10,000, 19.6 N load and disc temperature 300 ^{o}C; (b) vertical mag. x4000, 147.1 N load with no external heating applied to the disc; (c) vertical mag. x1000, 147.1 N load and disc temperature 400 ^{o}C.

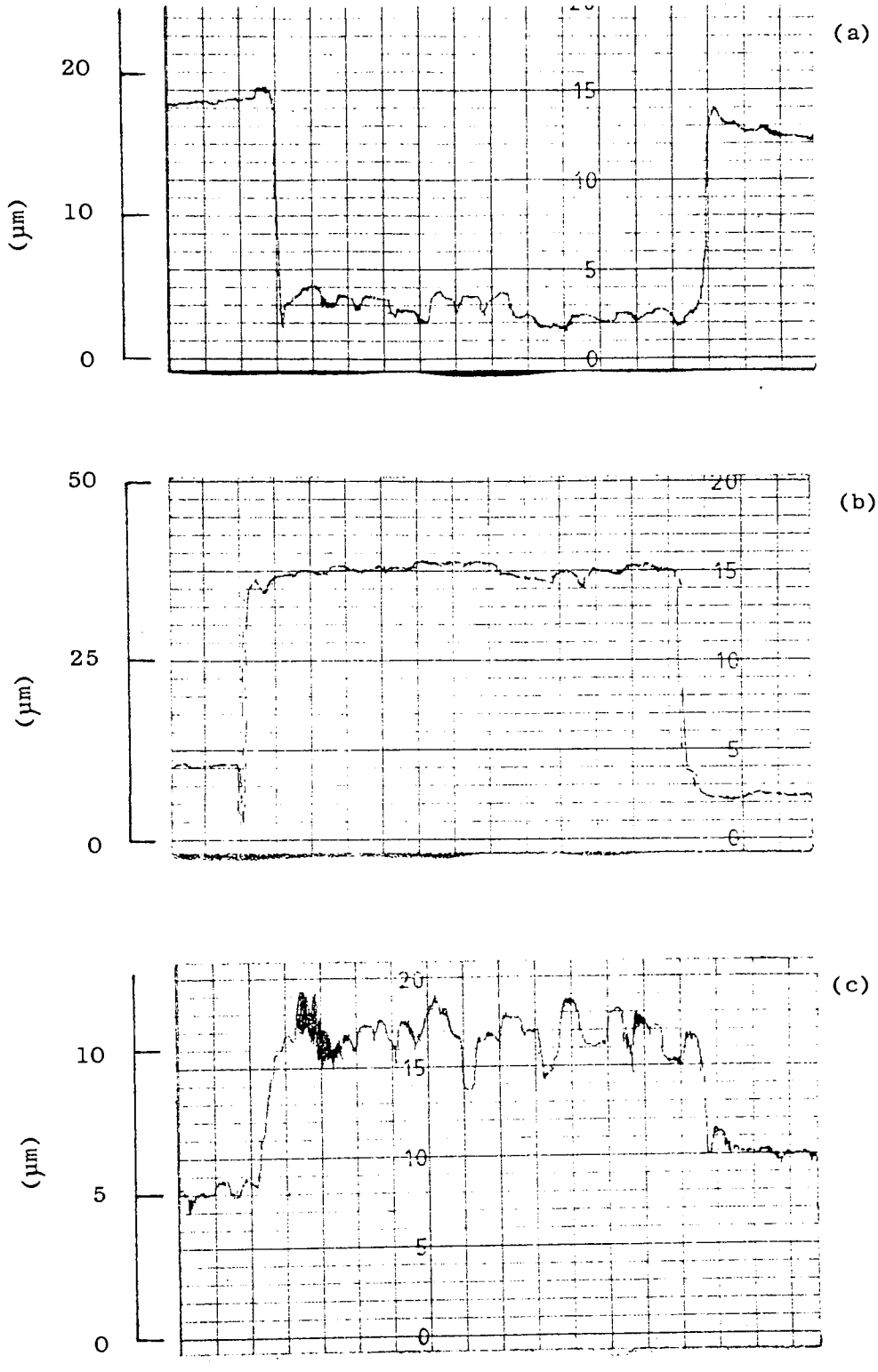

Fig. 3.30. Surface profiles of the worn track using a horizontal magnification of x10 present on the disc. The worn track was produced by a A.I.S.I. 440C MOD steel pin with a sliding speed of 2 m s^{-1} at a load of 39.2 N and a disc temperature of 500 ^{o}C; (a) vertical mag. x2000; (b) vertical mag. x1000, oxide removed from the disc; (c) vertical mag. x4000, oxide removed from the disc and worn track.

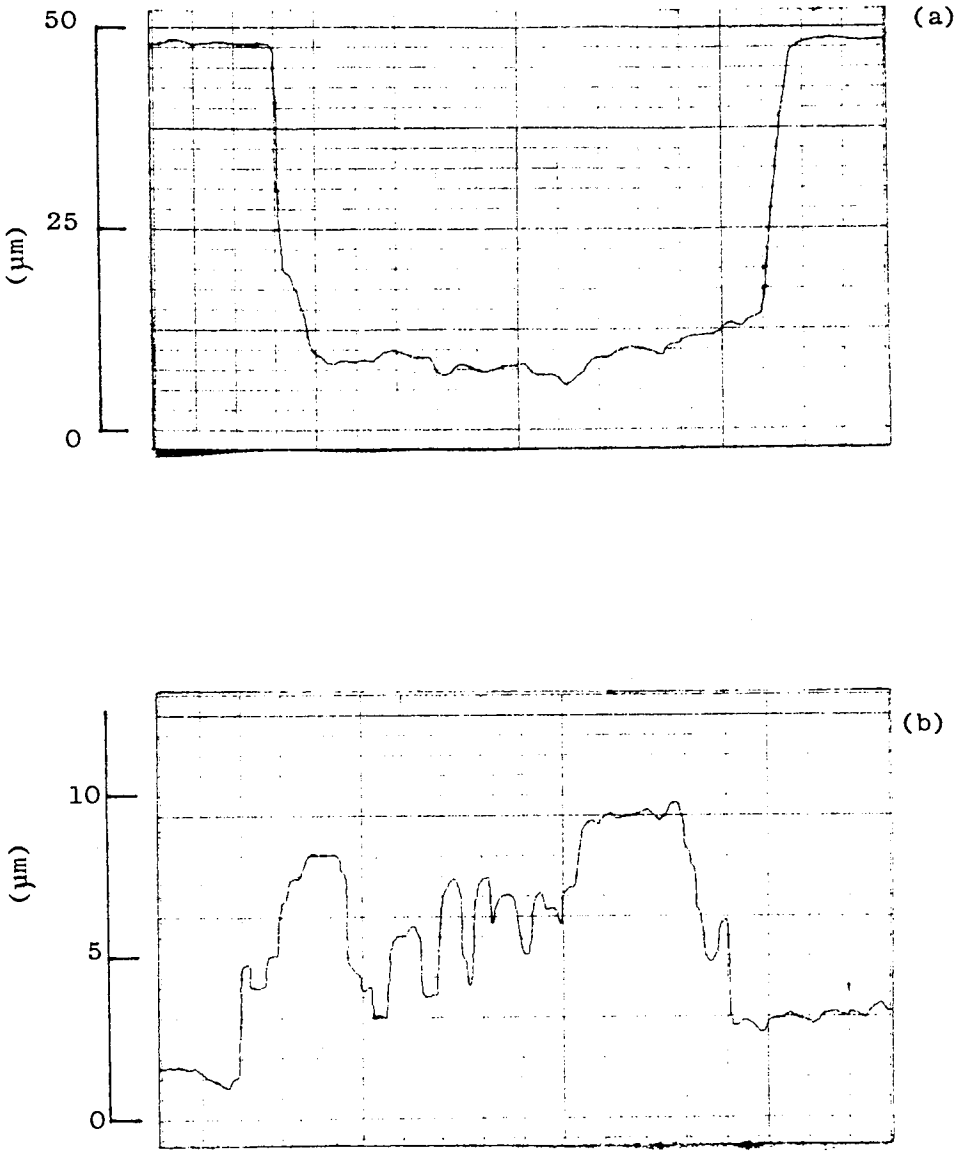

Fig. 3.31. Surface profiles of the worn track using a horizontal magnification of x10 present on the disc. The worn track was produced by a A.I.S.I. 440C MOD steel pin with a sliding speed of 2 m s^{-1} at a load of 98.1 N and a disc temperature of 500 ^{o}C; (a) vertical mag. x1000; (b) vertical mag. x4000, oxide removed from the disc and worn track.

Lescalloy BG42 steel pin with a 19.6 N load at a sliding speed of 2 m s^{-1} and a disc temperature of 300 ^{o}C. This is a typical wear track produced by the oxidational-metallic type of wear, which occurs for loads less than about 40 N and disc temperatures less than 400 ^{o}C. From the profile the wear rate of the disc was found to be (5.0 $\pm$ 0.4) x 10^{-14} m^3 m^{-1}. This is small compared to the wear rate of the pin which was 20 times greater.

Typical wear tracks produced by the severe type of wear are shown in figures 3.29(b) and 3.29(c). Figure 3.29(b) shows the wear track produced by a Lescalloy BG42 steel pin with a 147.1 N load at a sliding speed of 2 m s^{-1} with no external heating applied to the disc. For the same conditions the wear track produced at a disc temperature of 400 ^{o}C is shown in figure 3.29(c). Besides the initial wear of the disc figure 3.29(b), X-ray data shows that steel has also been bonded to the disc, see table 3.15.

Figures 3.30 and 3.31 are typical of the type of wear which occurs when material in the form of oxides is transferring from disc to pin as shown by X-ray data and S.E.M. analysis. Figure 3.30 shows the wear track produced by a A.I.S.I. 440C MOD steel pin with a 39.2 N load at a sliding speed of 2 m s^{-1} and a disc temperature of 500 ^{o}C. For the same conditions the wear track produced at a load of 98.1 N is shown in figure 3.31. It can be seen from figures 3.30(c) and 3.31(b) that a greater amount of disc material has been removed by oxidation than due to wear. For the 39.2 N load figure 3.30, the amount of material removed by the pin was (4.0 $\pm$ 0.1) x 10^{-5} m. Therefore the wear rate was (2.3 $\pm$ 0.2) x 10^{-12} m^3 m^{-1} which was about 80 times greater than the wear rate of the pin.

3.4 Compounds Identified by X-ray Analysis

Typical X-ray diffraction observations are shown in tables 3.2 to

3.7 together with identity of the compounds present. Such tables were

Table 3.2. Powder X-ray diffraction observations of debris taken from an experiment using a A.I.S.I. 440C MOD steel bearing at a temperature of 300 °C with a ball contact stress of 2.6×10^9 N m^{-2}.

* - Indicates the most intense diffraction lines.

Experimental Values		Identity	Diffraction Data File	
2θ/ Deg. ± 0.2 Deg.	d / Å		d / Å	Relative Intensity
28.4	3.65	Rhombohedral oxide	3.66, 3.63	25, 75
36.8	2.83	WC	2.84	45
39.0	2.68*	Rhombohedral oxide	2.69, 2.67	100, 100
41.8	2.51*	WC	2.52	100
		Rhombohedral oxide	2.51, 2.48	50, 95
48.0	2.20	Rhombohedral oxide	2.20, 2.18	30, 40
52.3	2.03	α-Fe(Cr)	2.03, 2.04	100, 100
56.9	1.88	WC	1.88	100
58.0	1.84	Rhombohedral oxide	1.84, 1.82	40, 40
63.7	1.69*	Rhombohedral oxide	1.69, 1.67	60, 90
74.2	1.48	Rhombohedral oxide	1.48, 1.46	35, 25
76.2	1.45	WC	1.45	20
		Rhombohedral oxide	1.45, 1.43	35, 40

constructed for both surface and debris X-ray diffraction data for each combination of load, speed and temperature used in the investigation. It is known from Isherwood and Quinn[51] that for steels of the type under investigation the rhombohedral oxide a mixture of α-Fe_2O_3 + Cr_2O_3 is formed in preference to the isolated individual components. Hence they are identified as such in the tables where d values are given for

Table 3.3. Powder X-ray diffraction observations of debris taken from an experiment using a A.I.S.I. 440C MOD steel pin at a disc temperature of 200 °C with a load of 39.2 N and a sliding speed of 2 m s^{-1}.

* Indicates the most intense diffraction line.

Experimental Values		Identity	Diffraction Data File	
2θ / Deg. ± 0.2 Deg.	d / Å		d / Å	Relative Intensity
36.8	2.83	WC	2.84	45
39.0	2.68	Rhombohedral oxide	2.69, 2.67	100, 100
41.8	2.51	WC	2.52	100
		Rhombohedral oxide	2.51, 2.48	50, 95
51.0	2.08*	γ-Fe	2.08	100
52.2	2.03	α-Fe(Cr)	2.03, 2.04	100, 100
56.8	1.88	WC	1.88	100
59.5	1.80	γ-Fe	1.80	80
64.5	1.68	Rhombohedral oxide	1.69, 1.67	60, 90
76.5	1.44	α-Fe(Cr)	1.43, 1.44	20, 16
		WC	1.45	20
87.8	1.29	WC	1.29	25
89.5	1.27	γ-Fe, WC	1.27, 1.26	50, 14
92.7	1.24	WC	1.24	30
99.3	1.17	α-Fe(Cr)	1.17, 1.18	30, 30
111.0	1.08	γ-Fe	1.08	80
118.7	1.04	γ-Fe	1.037	50
123.5	1.015	α-Fe(Cr)	1.01, 1.02	10, 18

Table 3.4. Powder X-ray diffraction observations of debris taken from an experiment using a Lescalloy BG42 steel pin at a disc temperature of 300 °C with a load of 19.6 N and a sliding speed of 2 m s^{-1}.

* - Indicates the most intense diffraction lines.

Experimental Values		Identity	Diffraction Data File	
2θ / Deg. ± 0.2 Deg.	d / Å		d / Å	Relative Intensity
28.2	3.67	Rhombohedral oxide	3.66, 3.63	25, 75
35.3	2.95	γ-Fe_2O_3	2.95	34
39.0	2.68	Rhombohedral oxide	2.69, 2.67	100, 100
41.7	2.51*	γ-Fe_2O_3	2.52	100
		Rhombohedral oxide	2.51, 2.48	50, 95
48.0	2.20	Rhombohedral oxide	2.20, 2.18	30, 40
51.0	2.08	γ-Fe, γ-Fe_2O_3	2.08, 2.08	100, 24
52.6	2.02*	α-Fe(Cr)	2.03, 2.04	100, 100
58.0	1.84	Rhombohedral oxide	1.84, 1.82	40, 40
63.8	1.69	Rhombohedral oxide	1.69, 1.67	60, 90
67.2	1.62	γ-Fe_2O_3	1.61	33
73.8	1.49	γ-Fe_2O_3	1.48	53
		Rhombohedral oxide	1.48, 1.46	35, 25
75.9	1.45	Rhombohedral oxide	1.45, 1.43	35, 40
		α-Fe(Cr)	1.43, 1.44	20, 16
99.4	1.17	α-Fe(Cr)	1.17, 1.18	30, 30
111.0	1.085	γ-Fe, γ-Fe_2O_3	1.08, 1.09	80, 19

Table 3.5. Powder X-ray diffraction observations of debris taken from an experiment using a Lescalloy BG42 steel pin at a disc temperature of 500 °C with a load of 58.9 N and a sliding speed of 2 m s^{-1}.

* - Indicates the most intense diffraction lines.

Experimental Values		Identity	Diffraction Data File	
2θ / Deg. ± 0.2 Deg.	d / Å		d / Å	Relative Intensity
22.2	4.65	$CoWO_4$	4.67	30
27.0	3.83*	WO_3	3.84	100
27.7	3.74	WO_3, $CoWO_4$	3.76, 3.73	93, 30
28.5	3.63*	WO_3, $CoWO_4$	3.64, 3.61	100, 30
31.0	3.35	WO_3	3.34	50
33.6	3.09	WO_3, WO_3	3.11, 3.08	50, 50
35.8	2.91	$CoWO_4$	2.92	100
39.0	2.68	Rhombohedral oxide	2.69, 2.67	100, 100
		WO_3, WO_3	2.68, 2.66	75, 60
40.0	2.62*	WO_3	2.62	90
41.8	2.51	WO_3	2.51	40
		Rhombohedral oxide	2.51, 2.48	50, 95
42.9	2.45	$CoWO_4$, $CoWO_4$	2.47, 2.46	20, 20
		Co_3O_4	2.44	100
45.2	2.33	$CoWO_4$	2.33	10
49.0	2.16	$CoWO_4$, $CoWO_4$	2.18, 2.18	14, 14
		WO_3, WO_3	2.17, 2.15	50, 60
51.0	2.08	γ-Fe	2.08	100
52.6	2.02	WO_3, WO_3	2.04, 2.02	40, 30
		α-Fe(Cr)	2.03, 204	100, 100
53.8	1.98	WO_3, WO_3	1.99, 1.97	35, 30
55.7	1.91	WO_3, WO_3	1.92, 1.88	50, 50
59.5	1.80	WO_3, WO_3	1.82, 1.81	75, 40

Table 3.5. continued....

Experimental Values		Identity	Diffraction Data File	
2θ / Deg. ± 0.2 Deg.	d / Å		d / Å	Relative Intensity
		γ-Fe, WO_3	1.80, 1.79	80, 50
63.8	1.69	WO_3, $CoWO_4$	1.71, 1.70	60, 25
		$CoWO_4$, WO_3	1.69, 1.69	25, 55
		Rhombohedral oxide	1.69, 1.67	60, 90
		WO_3	1.67	50
66.0	1.64	WO_3, WO_3	1.65, 1.64	40, 65
73.5	1.49	WO_3, WO_3	1.51, 1.50	45, 35
		$CoWO_4$, WO_3	1.50, 1.49	14, 60
		Rhombohedral oxide	1.48, 1.46	35, 25
77.0	1.44	Rhombohedral oxide	1.45, 1.43	35, 40
		$CoWO_4$, $CoWO_4$	1.44, 1.43	10, 14
		α-Fe(Cr)	1.43, 1.44	20, 16
		Co_3O_4	1.43	45
86.0	1.31	WO_3	1.31	45
89.5	1.27	γ-Fe	1.27	50
92.0	1.24	WO_3, WO_3	1.25, 1.24	30, 40
99.5	1.17	α-Fe(Cr)	1.17, 1.18	30, 30

Table 3.6. Powder X-ray diffraction observations of debris taken from an experiment using a Lescalloy BG42 steel pin at a disc temperature of 500 °C with a load of 98.1 N and a sliding speed of 2 m s^{-1}.

* - Indicates the most intense diffraction lines.

Experimental Values		Identity	Diffraction Data File	
2θ / Deg. ± 0.2 Deg.	d / Å		d / Å	Relative Intensity
29.3	3.54	Fe_2WO_6	3.53	80
32.1	3.23*	Cr_2WO_6	3.22	100
36.0	2.89*	$CoWO_4$, Fe_2WO_6	2.92, 2.87	100, 100
		Co_3O_4	2.86	40
42.0	2.50*	γ-Fe_2O_3, Fe_2WO_6	2.52, 2.48	100, 60
		Cr_2WO_6	2.48	90
42.8	2.45	Co_3O_4, Fe_2WO_6	2.44, 2.43	100, 60
46.0	2.29	Fe_2WO_6	2.28	30
52.2	2.03	Fe_2WO_6	2.03	50
57.5	1.86	Fe_2WO_6	1.85	40
62.7	1.72	Fe_2WO_6	1.72	60
64.0	1.69*	$CoWO_4$, $CoWO_4$	1.70, 1.69	25, 25
		Cr_2WO_6, Fe_2WO_6	1.68, 1.68	60, 60
65.0	1.66	Fe_2WO_6	1.66	80
73.0	1.50	Fe_2WO_6	1.50	60
74.3	1.48	γ-Fe_2O_3	1.48	53
77.6	1.43	Co_3O_4	1.43	45

Table 3.7. Glancing angle X-ray diffraction observation of the surface of a Lescalloy BG42 steel pin run at a sliding speed of 2 m s^{-1} with a load of 98.1 N for no external heating applied to the disc.

* - Indicates the most intense diffraction line.

Experimental Values		Identity	Diffraction Data File	
2θ / Deg. ± 0.2 Deg.	d / Å		d / Å	Relative Intensity
51.0	2.08	γ-Fe	2.08	100
52.4	2.03*	α-Fe(Cr)	2.03, 2.04	100, 100
59.7	1.80	γ-Fe	1.80	80
77.0	1.44	α-Fe(Cr)	1.43, 1.44	20, 16
89.4	1.27	γ-Fe	1.27	50
99.4	1.17	α-Fe(Cr)	1.17, 1.18	30, 30
111.0	1.085	γ-Fe	1.08	80
118.8	1.039	γ-Fe	1.037	50
123.5	1.015	α-Fe(Cr)	1.01, 1.02	10, 18

α-Fe_2O_3 and Cr_2O_3 respectively. α-Fe(Cr) indicates the original martensitic steel structure (body-centred tetragonal). Changes to ferrite (body-centred cubic) were not detected because the slight change in d spacing could not be measured. The austenitic steel structure (face-centred cubic) is indicated by γ-Fe which is of lower hardness than α-Fe. The following compounds identified are Co_3O_4 cobaltosic oxide, WC tungsten carbide (hexagonal phase), WO_3 tungstic oxide, $CoWO_4$ cobalt tungsten oxide, Fe_2WO_6 iron tungsten oxide and Cr_2WO_6 chromium tungsten oxide.

The compounds in the wear debris from the angular contact bearing experiments are presented in tables 3.8 and 3.9. From glancing angle

Table 3.8. Compounds identified in the wear debris from worn Lescalloy BG42 steel races by X-ray diffraction using $Co_{K\alpha}$ radiation. All experiments were carried out for a 1000_9 cycle$_2$ duration with a ball contact stress of 2.6×10^9 N m^{-2}.

Bearing Temperature / °C ± 5 °C	Compounds Identified
120	WC, α-Fe(Cr)
200	WC, (α-Fe(Cr), Rhombohedral oxide)
300	Rhombohedral oxide, (WC, α-Fe(Cr))
350	Rhombohedral oxide, (WC, α-Fe(Cr))
400	Rhombohedral oxide, WO_3, $CoWO_4$
500	Fe_2WO_6, Cr_2WO_6, (Rhombohedral oxide, $CoWO_4$).

Table 3.9. Compounds identified in the wear debris from worn A.I.S.I 440C MOD steel races by X-ray diffraction using $Co_{K\alpha}$ radiation. All experiments were carried out for a 1000 cycle duration with a ball contact stress of 2.6×10^9 N m^{-2}.

Bearing Temperature / °C ± 5 °C	Compounds Identified
200	(WC, Rhombohedral oxide), α-Fe(Cr)
300	Rhombohedral oxide, (WC, α-Fe(Cr))
350	Rhombohedral oxide, WO_3
450	($CoWO_4$, Fe_2WO_6, Cr_2WO_6), (Rhombohedral oxide, WO_3).

X-ray diffraction, α-Fe(Cr) was detected on the WC-11% Co balls taken from Lescalloy BG42 steel races at bearing temperatures less than 350 °C. For A.I.S.I. 440C MOD steel races α-Fe(Cr) was detected on the balls

at bearing temperatures less than 300 ^{o}C.

Selected results from the pin-on-disc experiments using Lescalloy BG42 steel pins with no external heating are shown in table 3.10. Compounds on the surface of Lescalloy BG42 steel pins and in the wear debris for elevated temperature experiments, are presented in tables 3.11 and 3.12 for loads of 19.6 and 98.1 N respectively. Disc temperatures less than 200 ^{o}C were generated by frictional heating alone. Table 3.11 was found to be typical of analyses carried out for loads less than 40 N and table 3.12 for loads greater than 40 N. Table 3.13 presents the compounds identified in the wear debris from selected worn Lescalloy BG42 steel pins at disc temperatures of 400 and 500 ^{o}C. Results for disc temperatures less than 300 ^{o}C were not included, since only oxidational-metallic wear and severe wear are exhibited with no transfer of material in the form of oxides from disc to pin occurring. Table 3.14 shows the compounds present in the wear debris from selected worn A.I.S.I. 440C MOD steel pins for a range of loads and disc temperatures. Disc temperatures less than 200 ^{o}C were generated by frictional heating alone. The compounds identified from the wear tracks present on the disc for both types of steel pins are shown in table 3.15. The first temperature was generated by frictional heating alone.

All the pin-on-disc experiments presented in tables 3.11 to 3.15 were carried out at a sliding speed of 2 m s^{-1}. In all the tables 3.8 to 3.15 the compounds are listed in decreasing order according to the intensity of the diffraction lines. The compounds enclosed in brackets give diffraction lines of about equal intensity. The limit of detection of a compound is about 2% by volume.

Table 3.10. Compounds identified in the wear debris from worn Lescalloy BG42 steel pins by X-ray diffraction using $Co_{K\alpha}$ radiation. All experiments were carried out with no external heating applied to the disc.

Speed/m s^{-1} ± 0.05 m s^{-1}	Load/N ± 0.9 N	Surface Temperature/°C ± 5%	Compounds Identified
0.60	98.1	126	(α-Fe(Cr), WC), γ-Fe
2.00	9.8	40	(α-Fe(Cr), Rhombohedral oxide), γ-Fe, WC
2.00	19.6	64	α-Fe(Cr), (Rhombohedral oxide, WC), γ-Fe_2O_3, γ-Fe.
2.00	39.2	77	α-Fe(Cr), (WC, γ-Fe), Rhombohedral oxide
2.00	98.1	157	α-Fe(Cr), (γ-Fe, WC)
2.00	147.1	279	(α-Fe(Cr), γ-Fe), WC
3.00	9.8	50	(α-Fe(Cr), WC, Rhombohedral oxide), γ-Fe.
3.00	58.9	208	γ-Fe, (α-Fe(Cr), WC)
3.00	147.1	-	γ-Fe, (α-Fe(Cr), WC).

Table 3.11. Compounds identified by X-ray diffraction from worn Lescalloy BG42 steel pins using $Co_{K\alpha}$ radiation. All the experiments were carried out at a sliding speed of 2 m s^{-1} and a load of 19.6 N.

Temperature/ °C		Debris	Steel Surface
Disc ± 5 °C	Surface ± 5%		
53	64	α-Fe(Cr), (Rhombohedral oxide, WC), γ-Fe_2O_3, γ-Fe.	α-Fe(Cr), (γ-Fe, WC), Rhombohedral oxide
200	201	α-Fe(Cr), Rhombohedral oxide, (γ-Fe, γ-Fe_2O_3), WC	α-Fe(Cr), γ-Fe, Rhombohedral oxide
300	286	α-Fe(Cr), γ-Fe_2O_3, Rhombohedral oxide, γ-Fe.	α-Fe(Cr), γ-Fe, γ-Fe_2O_3, Rhombohedral oxide, WC.
400	420	α-Fe(Cr), WO_3, (Rhombohedral oxide, $CoWO_4$, Fe_2WO_6, Cr_2WO_6, γ-Fe_2O_3), γ-Fe	α-Fe(Cr), $CoWO_4$ (γ-Fe_2O_3, WO_3, WC, Rhombohedral oxide)
500	441	WO_3, $CoWO_4$, (Co_3O_4, Rhombohedral oxide).	(WO_3, $CoWO_4$), α-Fe(Cr), Rhombohedral oxide.

Table 3.12. Compounds identified by X-ray diffraction from worn Lescalloy BG42 steel pins using $Co_{K\alpha}$ radiation. All the experiments were carried out at a sliding speed of 2 m s^{-1} and a load of 98.1 N.

Temperature/ °C		Debris	Steel Surface
Disc ± 5 °C	Surface ± 5%		
105	157	α-Fe(Cr), (γ-Fe, WC)	α-Fe(Cr), γ-Fe
200	360	γ-Fe, (α-Fe(Cr), WC)	γ-Fe, α-Fe(Cr)
300	434	γ-Fe, WC, α-Fe(Cr), Rhombohedral oxide	γ-Fe, α-Fe(Cr), Rhombohedral oxide
400	513	γ-Fe, γ-Fe_2O_3, (WC, α-Fe(Cr))	γ-Fe, (α-Fe(Cr), γ-Fe_2O_3), Rhombohedral oxide, WC.
500	524	(Fe_2WO_6, Cr_2WO_6), (γ-Fe_2O_3, $CoWO_4$, Co_3O_4).	α-Fe(Cr), $CoWO_4$, Cr_2WO_6, (Fe_2WO_6, Rhombohedral oxide, WC, γ-Fe_2O_3, γ-Fe, Co_3O_4, WO_3).

Table 3.13. Compounds identified in the wear debris from worn Lescalloy BG42 steel pins by X-ray diffraction using $Co_{K\alpha}$ radiation. All the experiments were carried out at a sliding speed of 2 m s^{-1}.

Temperature / °C		Load / N	Compounds Identified
Disc ± 5 °C	Surface ± 5%	± 0.9 N	
400	420	19.6	α-Fe(Cr), WO_3, (γ-Fe_2O_3, Rhombohedral oxide, $CoWO_4$, Fe_2WO_6, Cr_2WO_6), γ-Fe
400	419	39.2	γ-Fe, (α-Fe(Cr), γ-Fe_2O_3), (WC, Rhombohedral oxide)
400	513	98.1	γ-Fe, γ-Fe_2O_3, (WC, α-Fe(Cr))
400	593	147.1	γ-Fe, WC, α-Fe(Cr)
500	441	19.6	WO_3, $CoWO_4$, (Co_3O_4, Rhombohedral oxide)
500	487	58.9	WO_3, $CoWO_4$, (Co_3O_4, α-Fe(Cr), Rhombohedral oxide, γ-Fe)
500	524	98.1	(Fe_2WO_6, Cr_2WO_6), ($CoWO_4$, Co_3O_4, γ-Fe_2O_3)
500	-	147.1	(Fe_2WO_6, Cr_2WO_6, $CoWO_4$), WO_3, (Co_3O_4, Rhombohedral oxide, α-Fe(Cr)).

Table 3.14. Compounds identified in the wear debris from worn A.I.S.I. 440C MOD steel pins by X-ray diffraction using $Co_{K\alpha}$ radiation. All the experiments were carried out at a sliding speed of 2 m s $^{-1}$.

Temperature / ^{o}C		Load / N	Compounds Identified
Disc $\pm$ 5 ^{o}C	Surface $\pm$ 5%	$\pm$ 0.9 N	
49	61	19.6	(α-Fe(Cr), Rhombohedral oxide, γ-Fe_2O_3, γ-Fe), WC
68	82	39.2	α-Fe(Cr), (γ-Fe, WC), Rhombohedral oxide
95	208	98.1	(α-Fe(Cr), γ-Fe), WC
200	206	19.6	α-Fe(Cr), Rhombohedral oxide, (γ-Fe, γ-Fe_2O_3), WC
200	227	39.2	γ-Fe, α-Fe(Cr), WC, Rhombohedral oxide
200	363	98.1	γ-Fe, (α-Fe(Cr), WC)
500	517	39.2	($CoWO_4$, WO_3), α-Fe(Cr), Rhombohedral oxide
500	529	98.1	$CoWO_4$, WO_3, (Co_3O_4, α-Fe(Cr), Rhombohedral oxide)
500	554	147.1	$CoWO_4$, WO_3, (α-Fe(Cr), Co_3O_4, Rhombohedral oxide).

Table 3.15. Compounds identified from the wear tracks by X-ray diffraction using $Co_{K\alpha}$ radiation. All the experiments were carried out at a sliding speed of 2 m s^{-1}.

Steel Pin	Disc Temperature / ^{o}C $\pm$ 5 ^{o}C	Load / N $\pm$ 0.9 N	Compounds Identified
BG42	106	147.1	α-Fe(Cr), WC, γ-Fe
BG42	400	98.1	(γ-Fe, α-Fe(Cr)), γ-Fe_2O_3, WC, Rhombohedral oxide, WO_3
440C MOD	500	39.2	WO_3, $CoWO_4$, (Co_3O_4, Rhombohedral oxide)
440C MOD	500	98.1	WO_3, $CoWO_4$, (Co_3O_4, α-Fe(Cr), Rhombohedral oxide, WC).

3.5 Surface Examination Using the Scanning Electron Microscope

Typical displays of the number of counts versus X-ray energy as obtained by the energy dispersive analyser are shown in figures 3.32 to 3.35. Figure 3.36 shows the relative intensity of $W_{M\alpha}$ X-rays at constant $Fe_{K\alpha}$ from the worn tracks of Lescalloy BG42 steel bearings, as a function of bearing temperature for a 1000 cycle duration with a ball contact stress of 2.6×10^{9} N m^{-2}. The tungsten concentration was normalized to the amount of tungsten transfer at a temperature of 500 ^{o}C, that is the maximum value measured. There is a decrease in the amount of tungsten transfer up to a temperature of about 220 ^{o}C, but as the temperature rises the amount of tungsten transfer rapidly increases.

The relative intensity of $W_{M\alpha}$ X-rays at constant $Fe_{K\alpha}$ from worn

Lescalloy BG42 steel pins, as a function of experimental disc temperature for loads of 19.6 N and 98.1 N at a sliding speed of 2 m s^{-1} is shown in figure 3.37. Figure 3.38 shows the relative intensity of $W_{M\alpha}$ X-rays versus computed surface temperature for the same conditions. For figures 3.37 and 3.38 the tungsten concentration was normalized to the amount of tungsten transfer at a disc temperature of 500 ^{o}C for a load of 19.6 N, that is the maximum value measured. The shape of the curves in figure 3.38 are similar to those of figure 3.37. For the 19.6 N load tungsten transfer to the steel pin increases rapidly for surface temperatures greater than about 286 ^{o}C, figure 3.38(a). For a 98.1 N load figure 3.38(b), there is no tungsten transfer until the surface temperature exceeds about 513 ^{o}C. Figure 3.38(a) was found to be typical of analysis carried out for loads less than 40 N and figure 3.38(b) for loads greater than 40 N. Table 3.16 shows the relative intensity of $W_{M\alpha}$ X-rays from selected A.I.S.I. 440C MOD steel pins for the same conditions as in figures 3.37 and 3.38.

Table 3.16. The relative intensity of $W_{M\alpha}$ X-rays at constant $Fe_{K\alpha}$ from worn A.I.S.I. 440C MOD steel pins. All the experiments were carried out at a sliding speed of 2 m s^{-1}.

Load / N $\pm$ 0.9 N	Disc Temperature / ^{o}C $\pm$ 5 ^{o}C	Surface Temperature / ^{o}C $\pm$ 5%	Relative Intensity of $W_{M\alpha}$ X-rays. $\pm$ 0.02
19.6	49	61	0.01
19.6	200	206	0.03
98.1	95	208	0.00
98.1	200	363	0.00
98.1	500	529	0.92

Disc temperatures less than 200 ^{o}C were generated by frictional heating

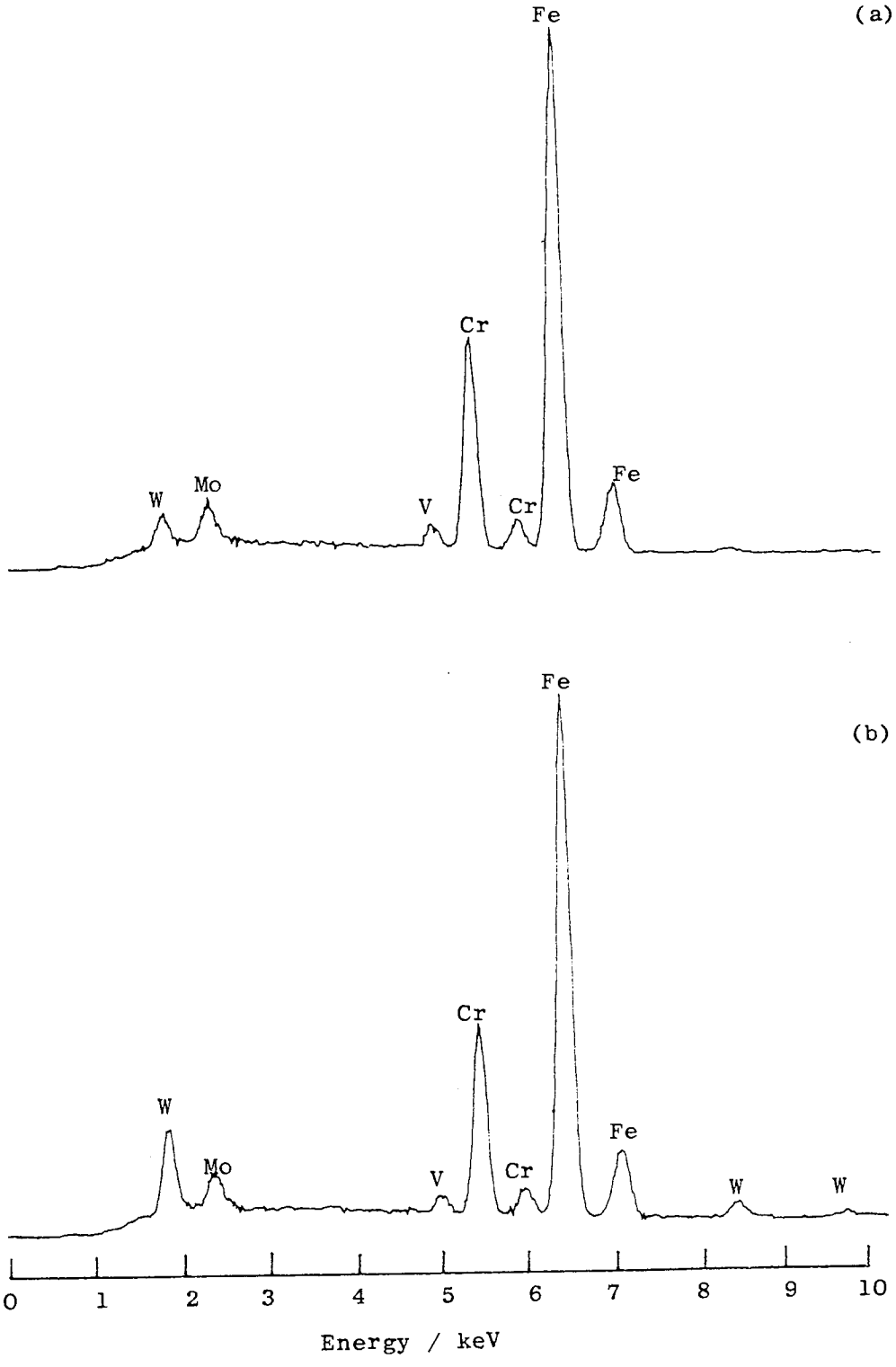

Fig. 3.32. The number of counts versus X-ray energy, as obtained by the energy dispersive analyser from the worn tracks present on Lescalloy BG42 steel angular contact bearings. Each experiment was conducted for a 1000 cycle duration with a ball contact stress of 2.6×10^{9} N m^{-2}; (a) bearing temperature 200 ^{o}C; (b) bearing temperature 400 ^{o}C.

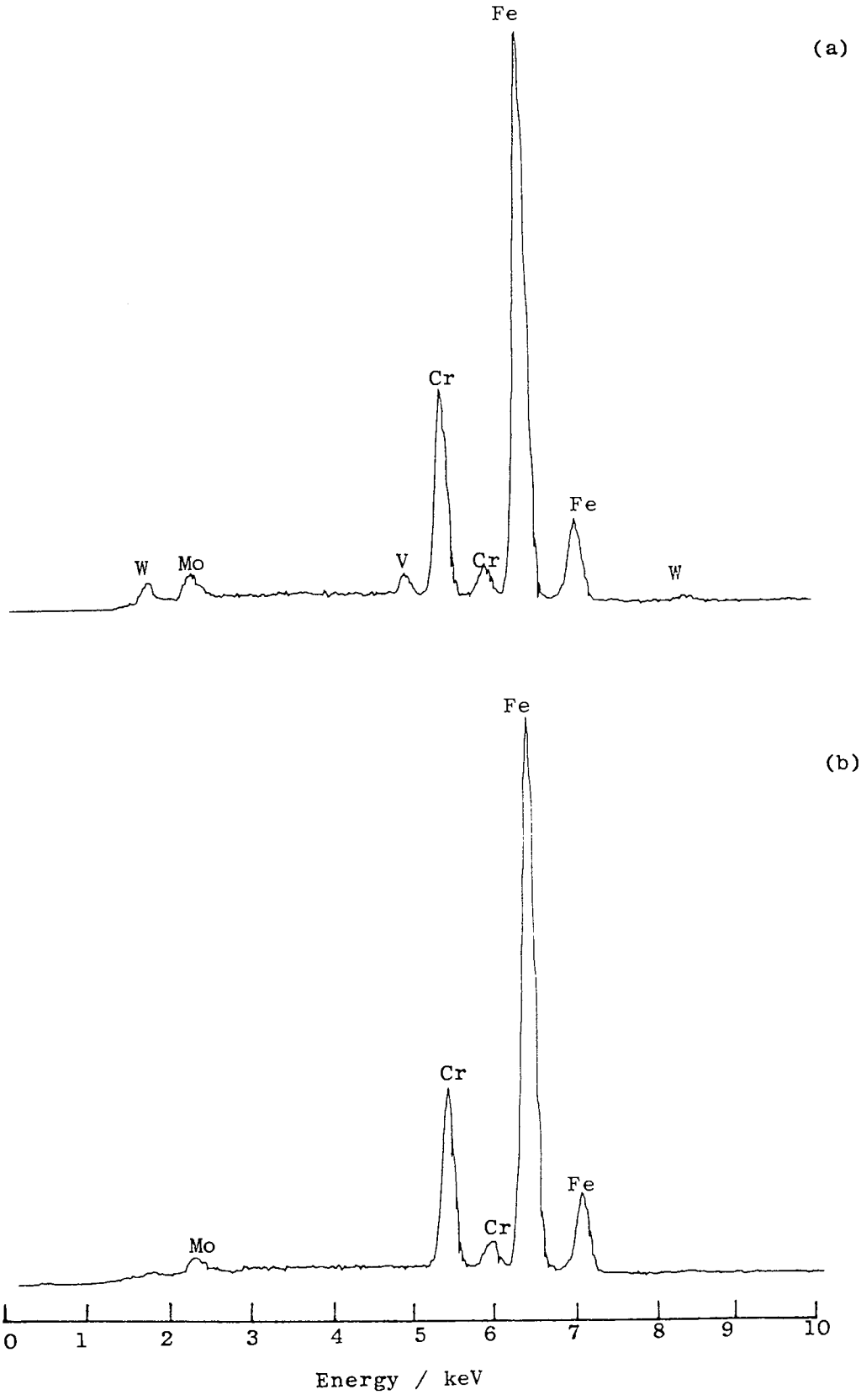

Fig. 3.33. The number of counts versus X-ray energy, as obtained by the energy dispersive analyser from the worn surfaces for experiments with no external heating;

(a) Lescalloy BG42 steel pin, 98.1 N load, 0.6 m s^{-1} sliding speed;

(b) A.I.S.I. 440C MOD steel pin, 19.6 N load, 2.0 m s^{-1} sliding speed.

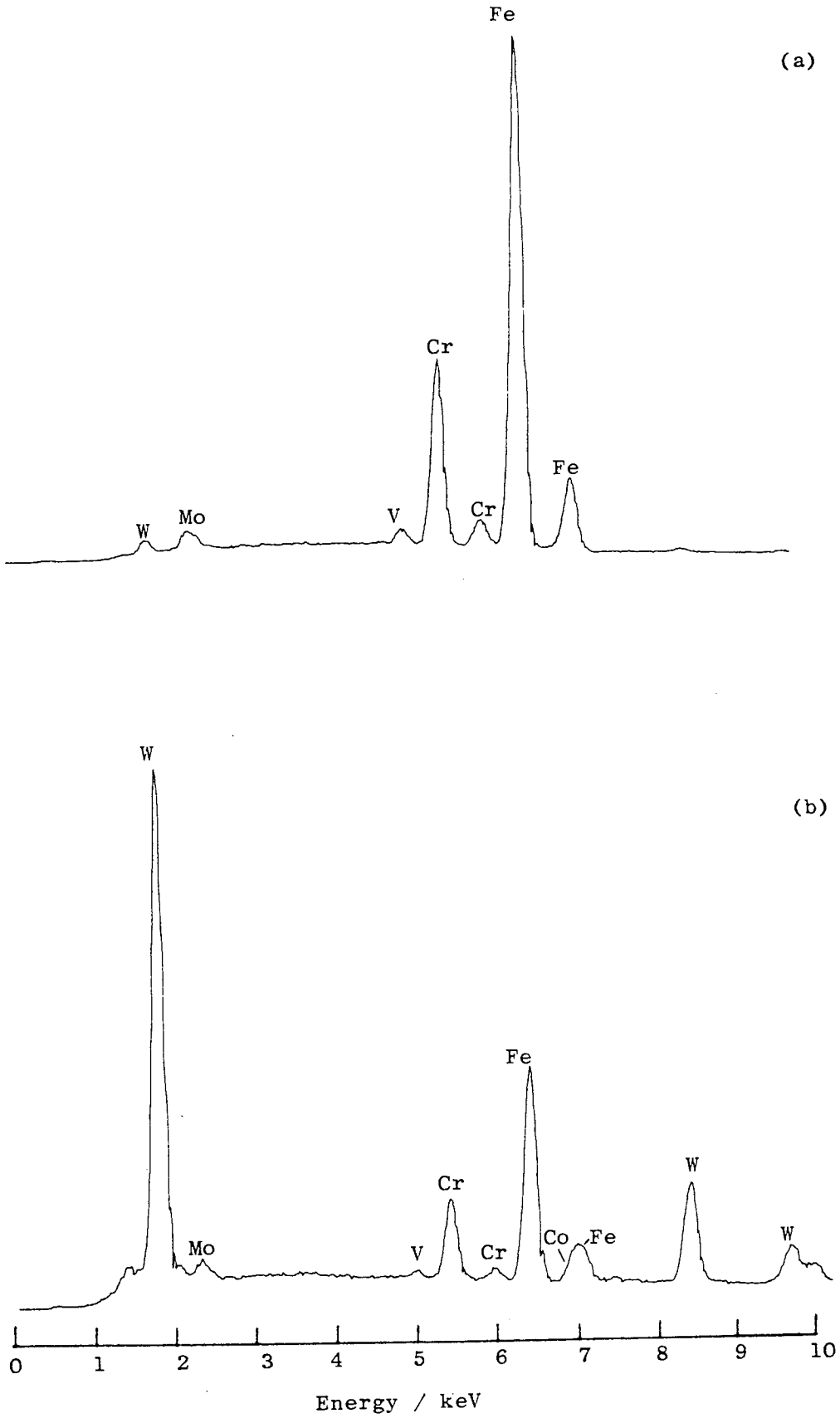

Fig. 3.34. The number of counts versus X-ray energy, as obtained by the energy dispersive analyser from the worn surfaces of Lescalloy BG42 steel pins for a load of 19.6 N and a sliding speed of 2 m s^{-1}; (a) no external heating applied to the disc; (b) disc temperature 500 ^{o}C.

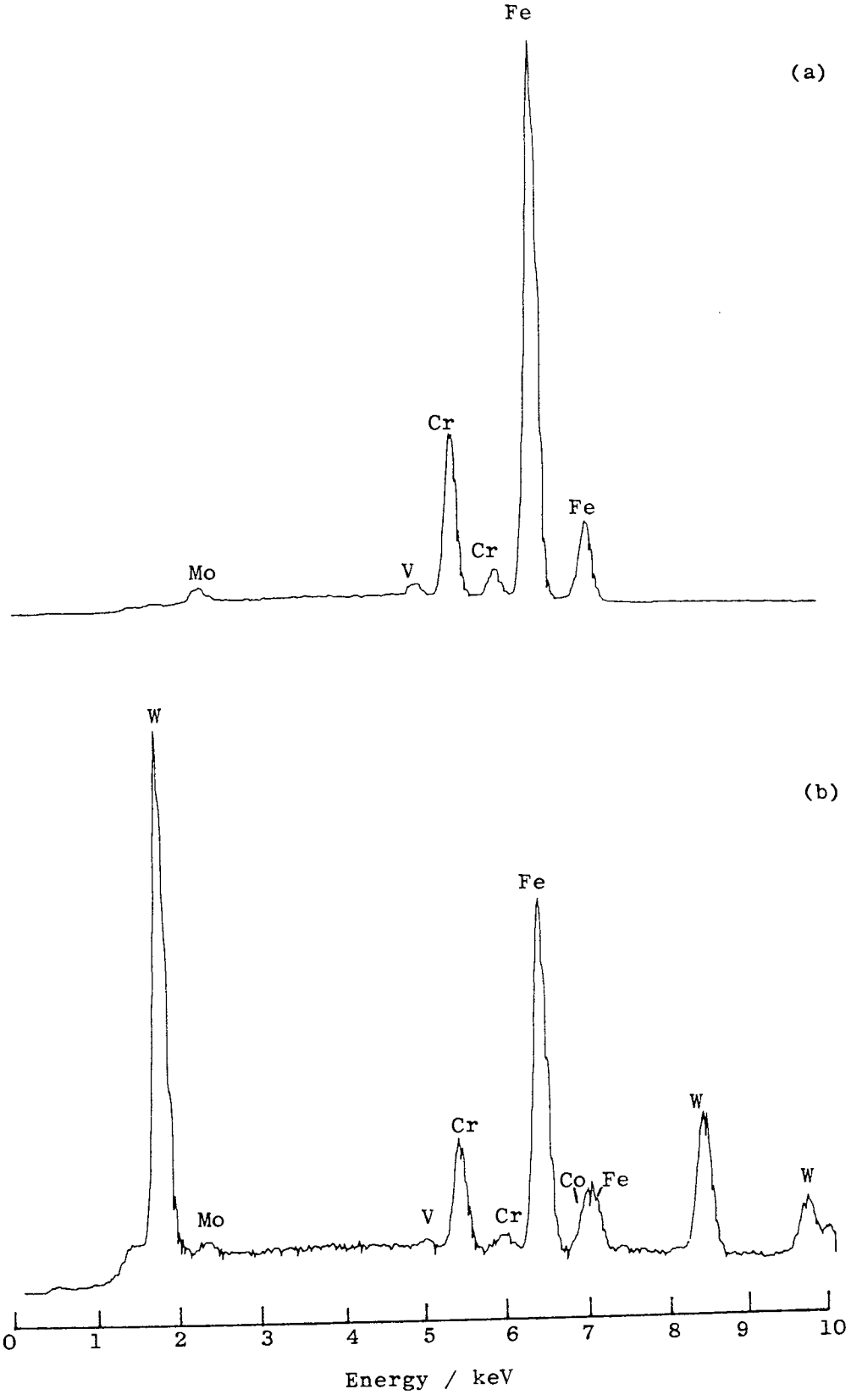

Fig. 3.35. The number of counts versus X-ray energy, as obtained by the energy dispersive analyser from the worn surfaces of Lescalloy BG42 steel pins for a load of 98.1 N and a sliding speed of 2 m s^{-1}; (a) disc temperature 300 ^{o}C; (b) disc temperature 500 ^{o}C.

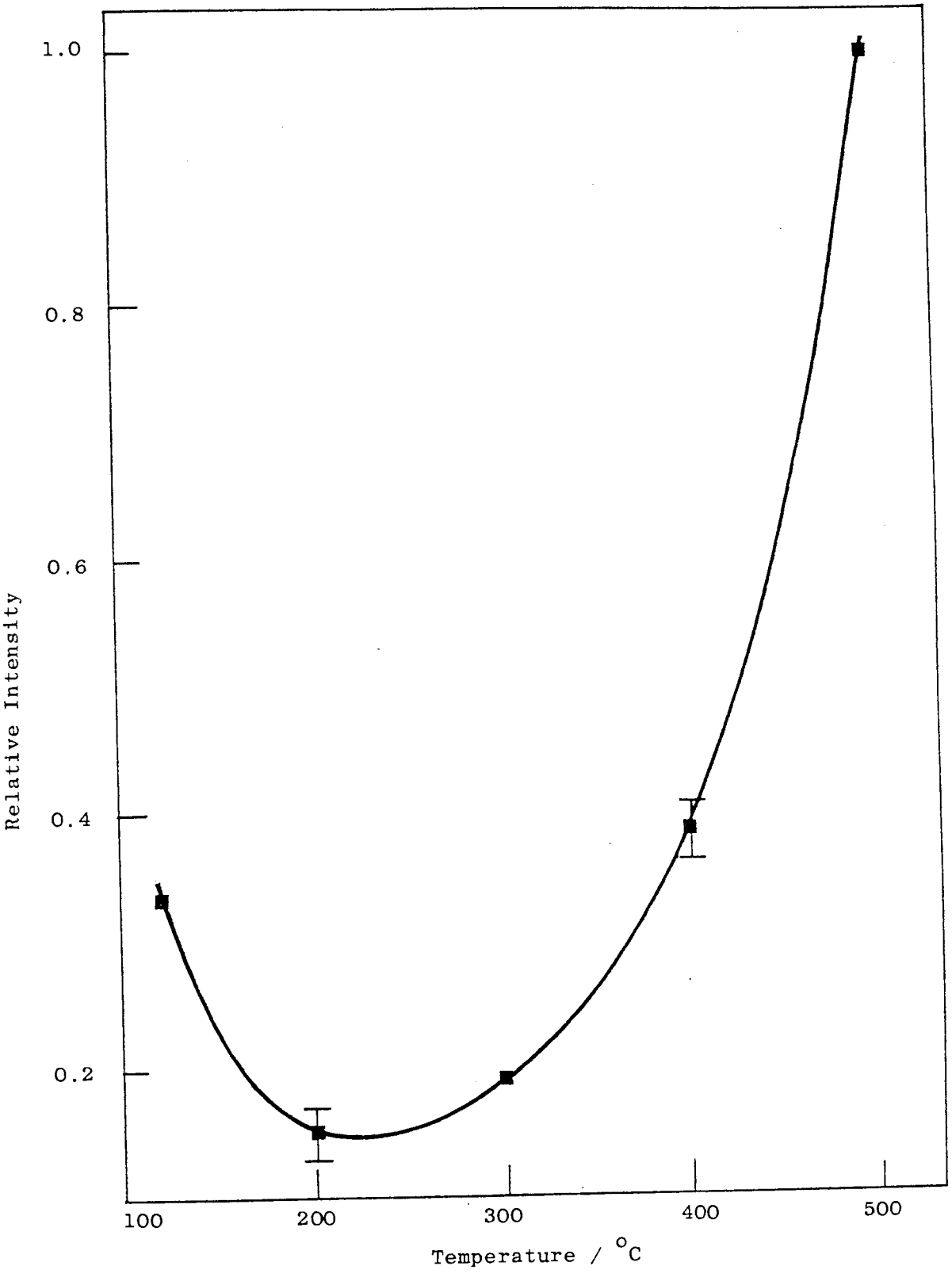

Fig. 3.36. The relative intensity of $W_{M\alpha}$ X-rays at constant $Fe_{K\alpha}$ from worn Lescalloy BG42 steel bearing tracks, as a function of experimental bearing temperature for a 1000 cycle duration with a ball contact stress of 2.6×10^{9} N m^{-2}.

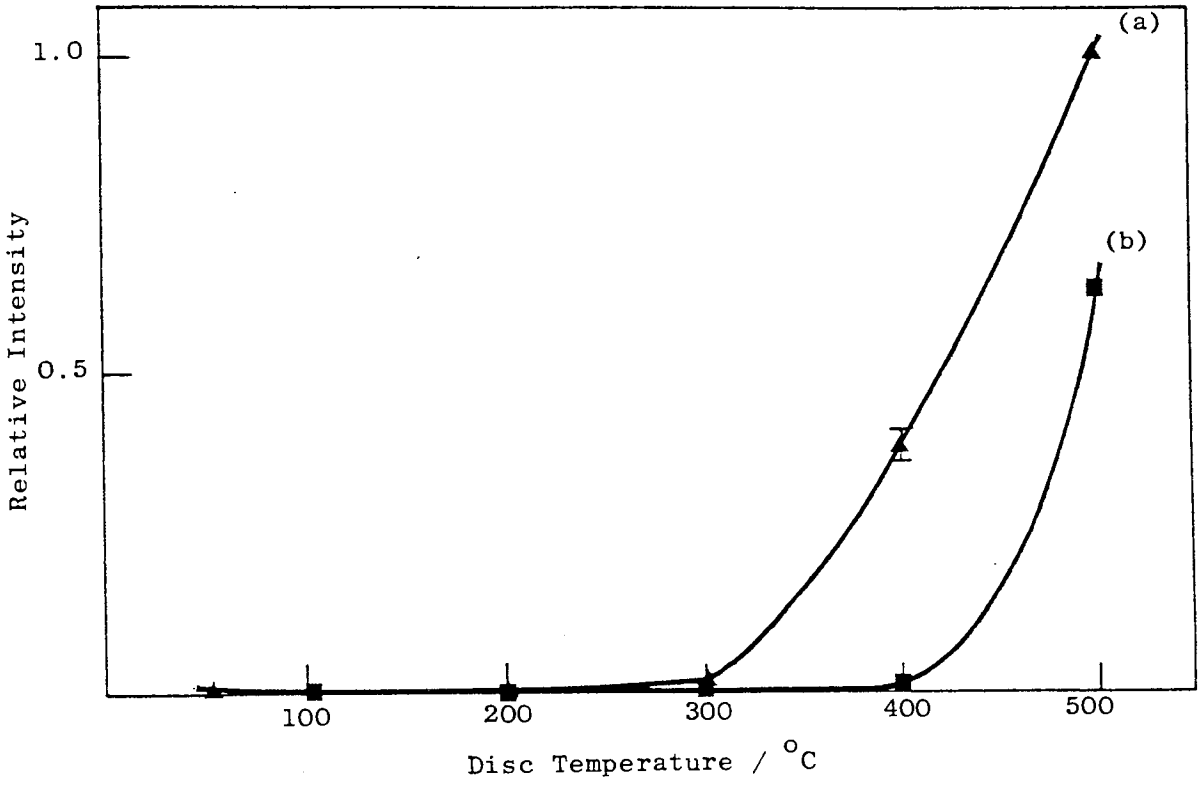

Fig. 3.37. The relative intensity of $W_{M\alpha}$ X-rays at constant $Fe_{K\alpha}$ from worn Lescalloy BG42 steel pins, as a function of experimental disc temperature for a sliding speed of 2 m s^{-1}; (a) 19.6 N load; (b) 98.1 N load.

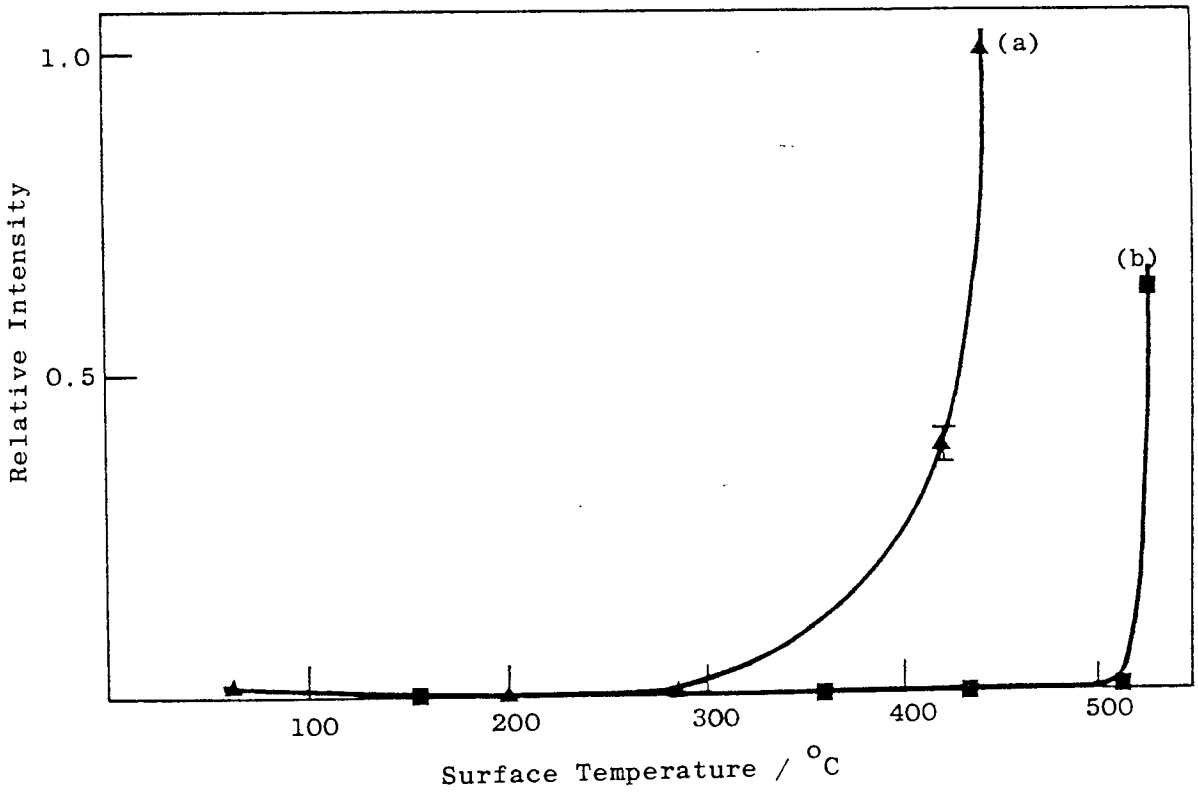

Fig. 3.38. The relative intensity of $W_{M\alpha}$ X-rays at constant $Fe_{K\alpha}$ from worn Lescalloy BG42 steel pins, as a function of computed surface temperature for a sliding speed of 2 m s^{-1}; (a) 19.6 N load; (b) 98.1 N load.

alone. They also show the same trends as the Lescalloy BG42 steel pins.

In order to give some visual appreciation of the mechanisms involved, scanning electron photomicrographs were taken of the worn surfaces of the angular contact bearings and steel pins. Figure 3.39 shows S.E.M. photomicrographs at x1000 magnification of the worn tracks present on the angular contact bearings inner race for various temperatures. All surfaces shown were taken from experiments conducted for a 1000 cycle duration with a ball contact stress of 2.6 x 10^9 N m^{-2}. For a Lescalloy BG42 steel race at a temperature of 350 ^oC figure 3.39(b), the surface is coated with an oxide. Figure 3.39(d) shows small areas of transferred ball material on an A.I.S.I. 440C MOD steel race at a temperature of 350 ^oC.

Figure 3.40 shows S.E.M. photomicrographs at x1000 magnification of the worn surfaces of steel pins for both types of steel at loads of 19.6 and 98.1 N. All surfaces shown were taken from experiments conducted at a sliding speed of 2 m s^{-1} with no external heating applied to the disc. Both types of steel at a load of 19.6 N figures 3.40(a) and 3.40(c), show relatively smooth surfaces typical of those associated with oxidational wear. At a load of 98.1 figures 3.40(b) and 3.40(d), the surfaces show evidence of both plastic flow of the steel and deep grooves formed by abrasive action which are typical of those associated with severe wear.

S.E.M. photomicrographs at x1000 magnification of the worn surfaces of Lescalloy BG42 steel pins for various disc temperatures and loads are presented in figure 3.41. All surfaces shown were taken from experiments conducted at a sliding speed of 2 m s^{-1}. Figure 3.41(a) shows an area of steel surface where an oxide plateau is beginning to

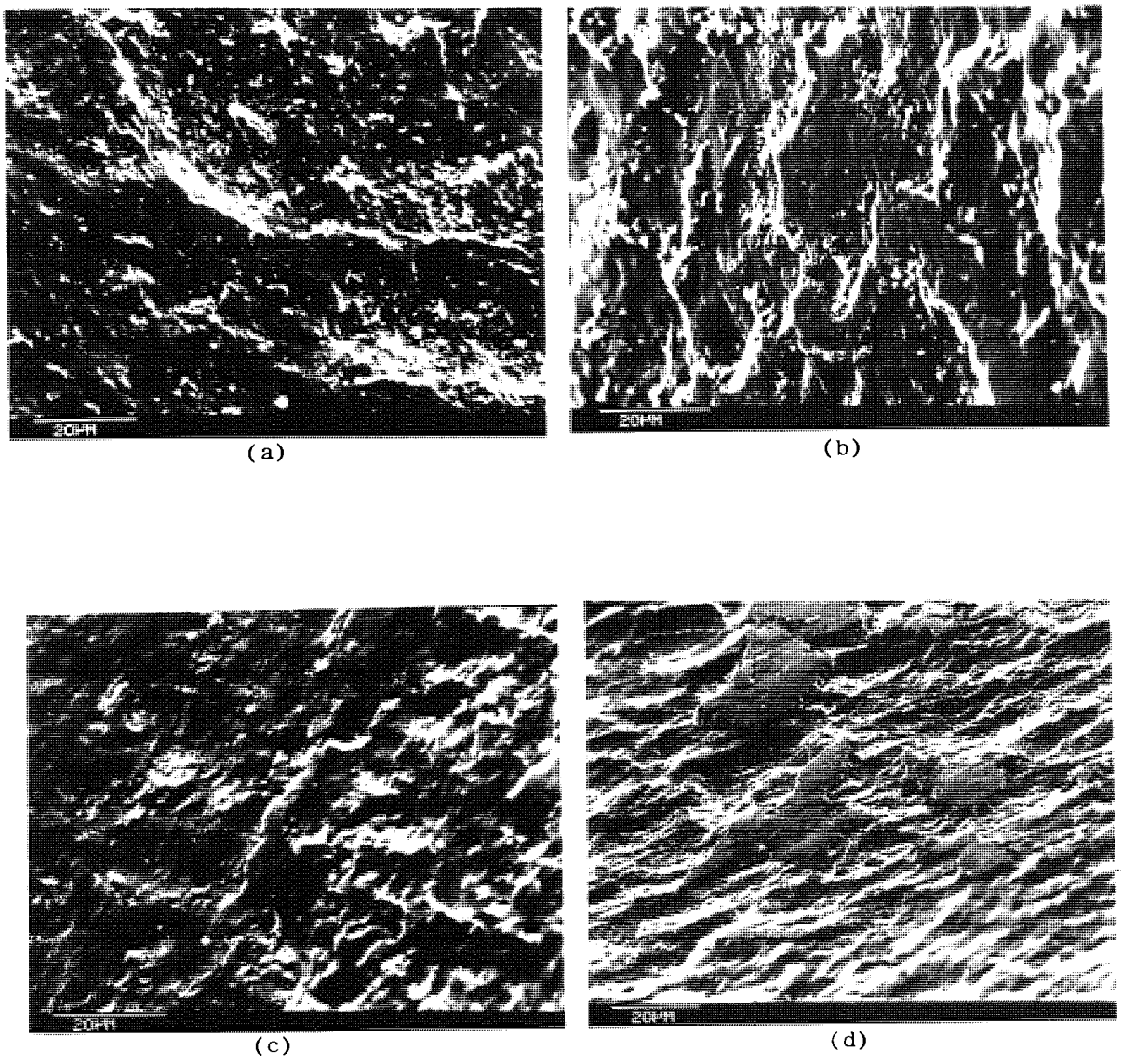

Fig. 3.39. S.E.M. photomicrographs of the worn tracks present on the angular contact bearings inner race at x1000 magnification. All surfaces shown were taken from experiments conducted for a 1000 cycle duration with a ball contact stress of 2.6×10^{9} N m^{-2}.

(a) Lescalloy BG42 steel, bearing temperature 120 ^{o}C.
(b) Lescalloy BG42 steel, bearing temperature 350 ^{o}C.
(c) Lescalloy BG42 steel, bearing temperature 500 ^{o}C.
(d) A.I.S.I. 440C MOD steel, bearing temperature 350 ^{o}C.

break up to form debris. The surface shown was taken from an experiment conducted at a load of 19.6 N and a disc temperature of 200 ^{o}C. For the same conditions but at a disc temperature of 300 ^{o}C figure 3.41(b), oxide is also present on the surface. For a load of 98.1 N and a disc temperature of 300 ^{o}C, the surface shows evidence of both plastic flow of the steel and grooves formed by the abrasive action of the much harder WC-11% Co disc, figure 3.41(c).

Figure 3.42 shows S.E.M. photomicrographs of the worn surface of a Lescalloy BG42 steel pin at a magnification of x1000 and x5000. All photomicrographs shown were taken from an experiment conducted at a sliding speed of 2 m s^{-1} with a load of 19.6 N and a disc temperature of 400 ^{o}C. Figure 3.42(a) shows at a magnification of x1000 smooth areas which are transferred material from the disc identified by X-ray data and the energy dispersive analyser. The same area is shown at a magnification of x5000 in figure 3.42(b). Figure 3.42(c) shows a tungsten elemental map of the same area as in figure 3.42(b). Figure 3.43 shows S.E.M. photomicrographs of the worn surface of a Lescalloy BG42 steel pin at a magnification of x200 and x1000. All photomicrographs shown were taken from an experiment conducted at a sliding speed of 2 m s^{-1} with a load of 98.1 N and a disc temperature of 500 ^{o}C. Figure 3.43(a) shows at a magnification of x200 a smooth film. Figure 3.43(b) also shows a smooth film at x1000 magnification as does figure 3.43(c) a tungsten elemental map of the same area. The obvious feature where removal of a piece of the film has taken place is visible on both.

Figure 3.44 shows S.E.M. photomicrographs of the worn surfaces of A.I.S.I. 440C MOD steel pins at loads of 39.2 and 98.1 N. All surfaces shown were taken from experiments conducted at a sliding speed of 2 m s^{-1} with a disc temperature of 500 ^{o}C. For a load of 39.2 N figure

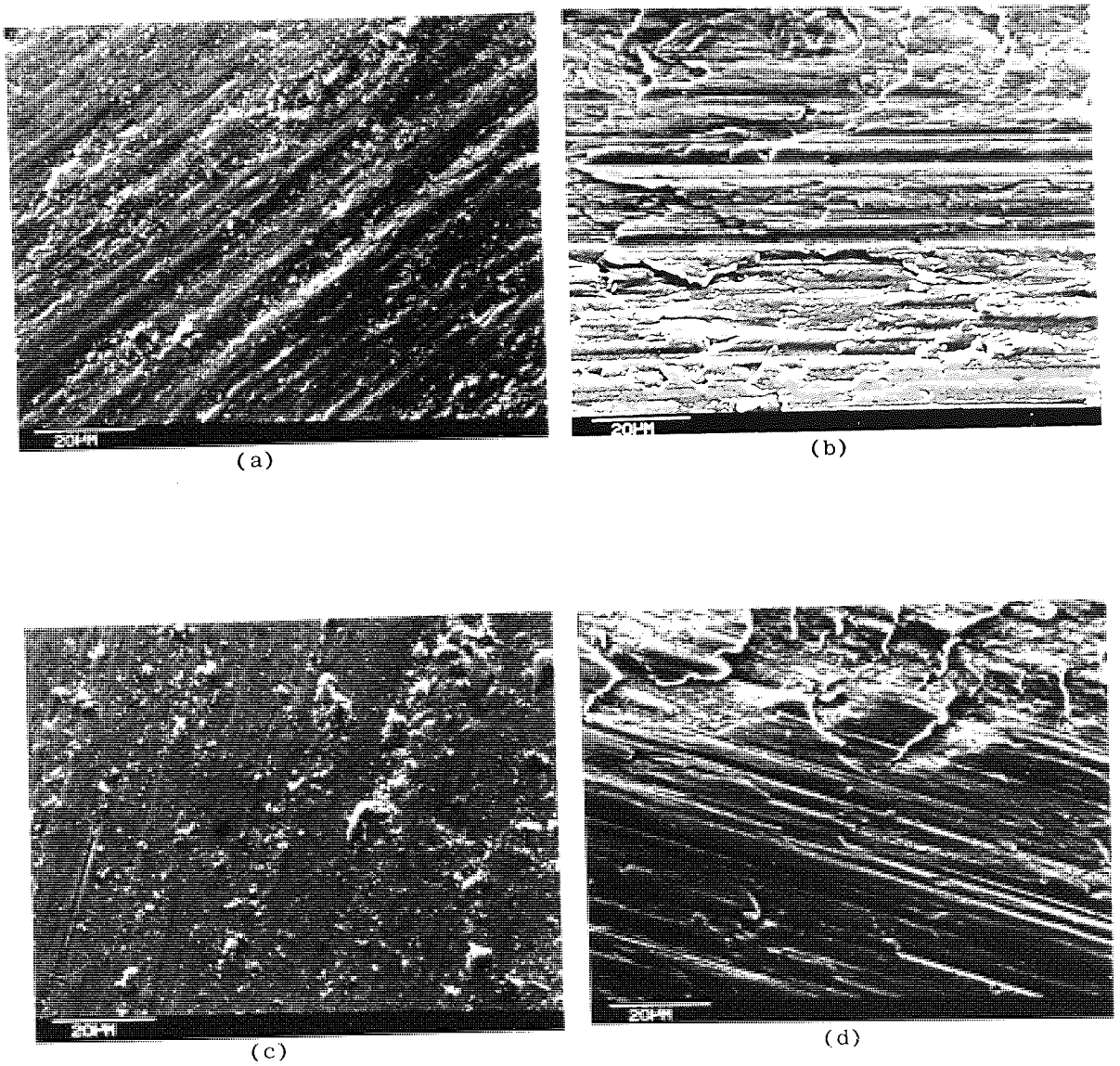

Fig. 3.40. S.E.M. photomicrographs of worn steel pin surfaces at x1000 magnification. All surfaces shown were taken from experiments conducted at a sliding speed of 2 m s^{-1} with no external heating applied to the disc.

(a) Lescalloy BG42 steel, load 19.6 N.
(b) Lescalloy BG42 steel, load 98.1 N.
(c) A.I.S.I. 440C MOD steel, load 19.6 N.
(d) A.I.S.I. 440C MOD steel, load 98.1 N.

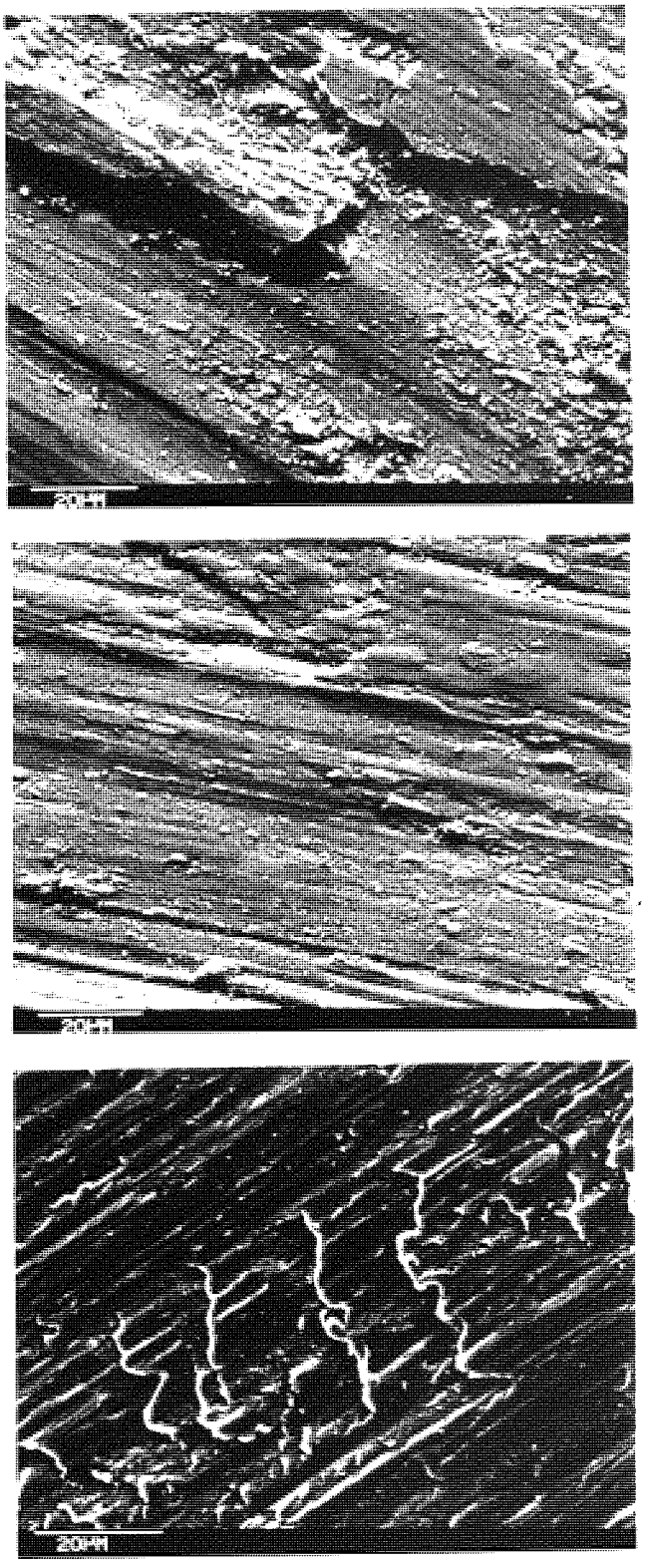

(a)

(b)

(c)

Fig. 3.41. S.E.M. photomicrographs of worn Lescalloy BG42 steel pin surfaces at x1000 magnification. All surfaces shown were taken from experiments conducted at a sliding speed of 2 m s^{-1}.

(a) Disc temperature 200 ^{o}C, load 19.6 N.
(b) Disc temperature 300 ^{o}C, load 19.6 N.
(c) Disc temperature 300 ^{o}C, load 98.1 N.

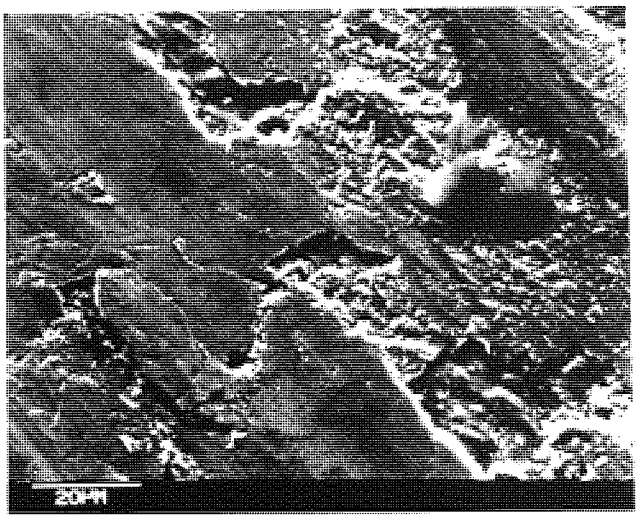

(a)

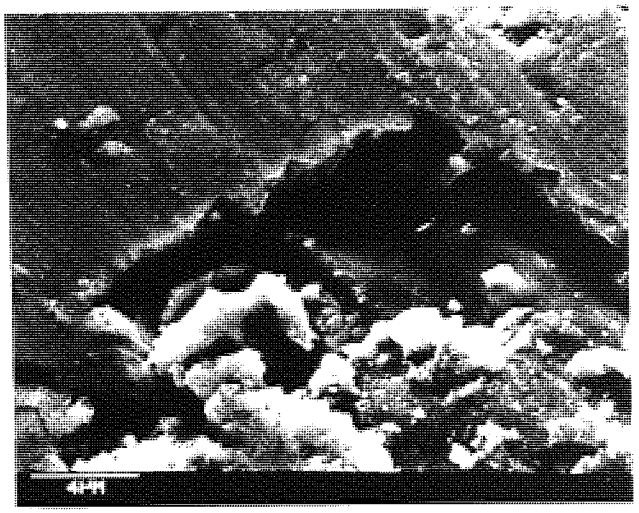

(b)

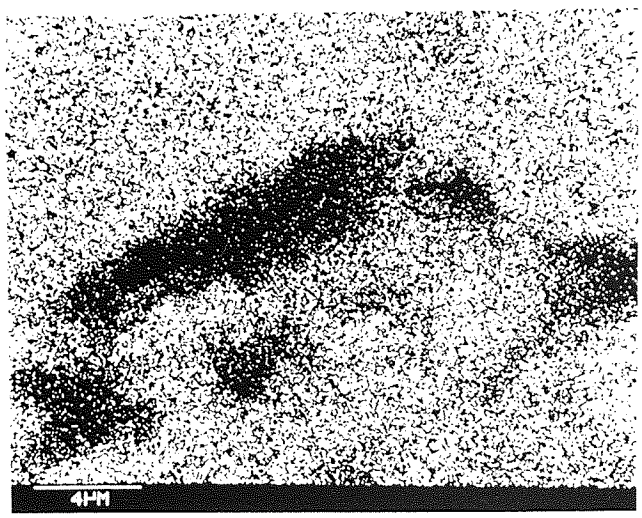

(c)

Fig. 3.42. S.E.M. photomicrographs of the worn surface of a Lescalloy BG42 steel pin. All photomicrographs shown were taken from an experiment conducted at a sliding speed of 2 $m\ s^{-1}$ with a load of 19.6 N and a disc temperature of 400 ^{o}C.

(a) Magnification x1000.
(b) Magnification x5000.
(c) Tungsten map of the area of surface shown in (b).

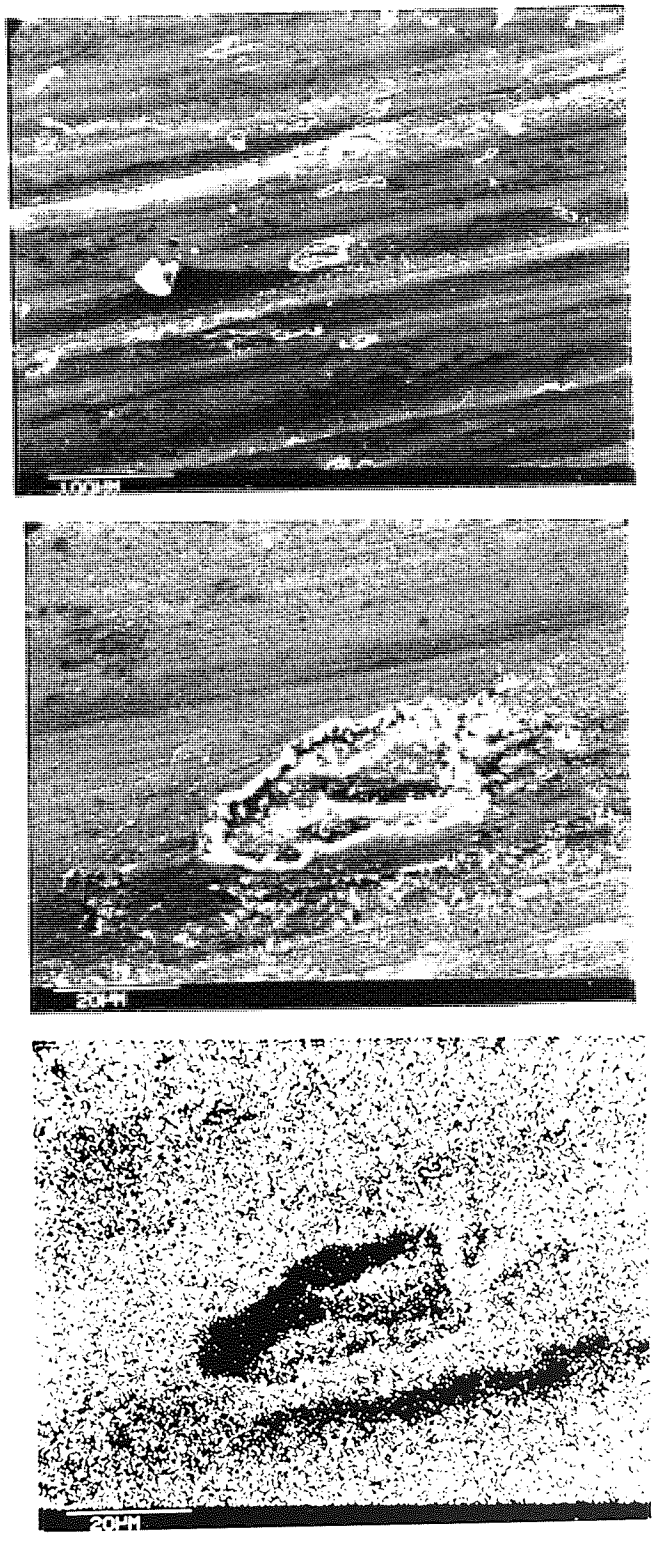

(a)

(b)

(c)

Fig. 3.43. S.E.M. photomicrographs of the worn surface of a Lescalloy BG42 steel pin. All photomicrographs shown were taken from an experiment conducted at a sliding speed of 2 $m\ s^{-1}$ with a load of 98.1 N and a disc temperature of 500 ^{o}C.

(a) Magnification x200.
(b) Magnification x1000.
(c) Tungsten map of the area of surface shown in (b).

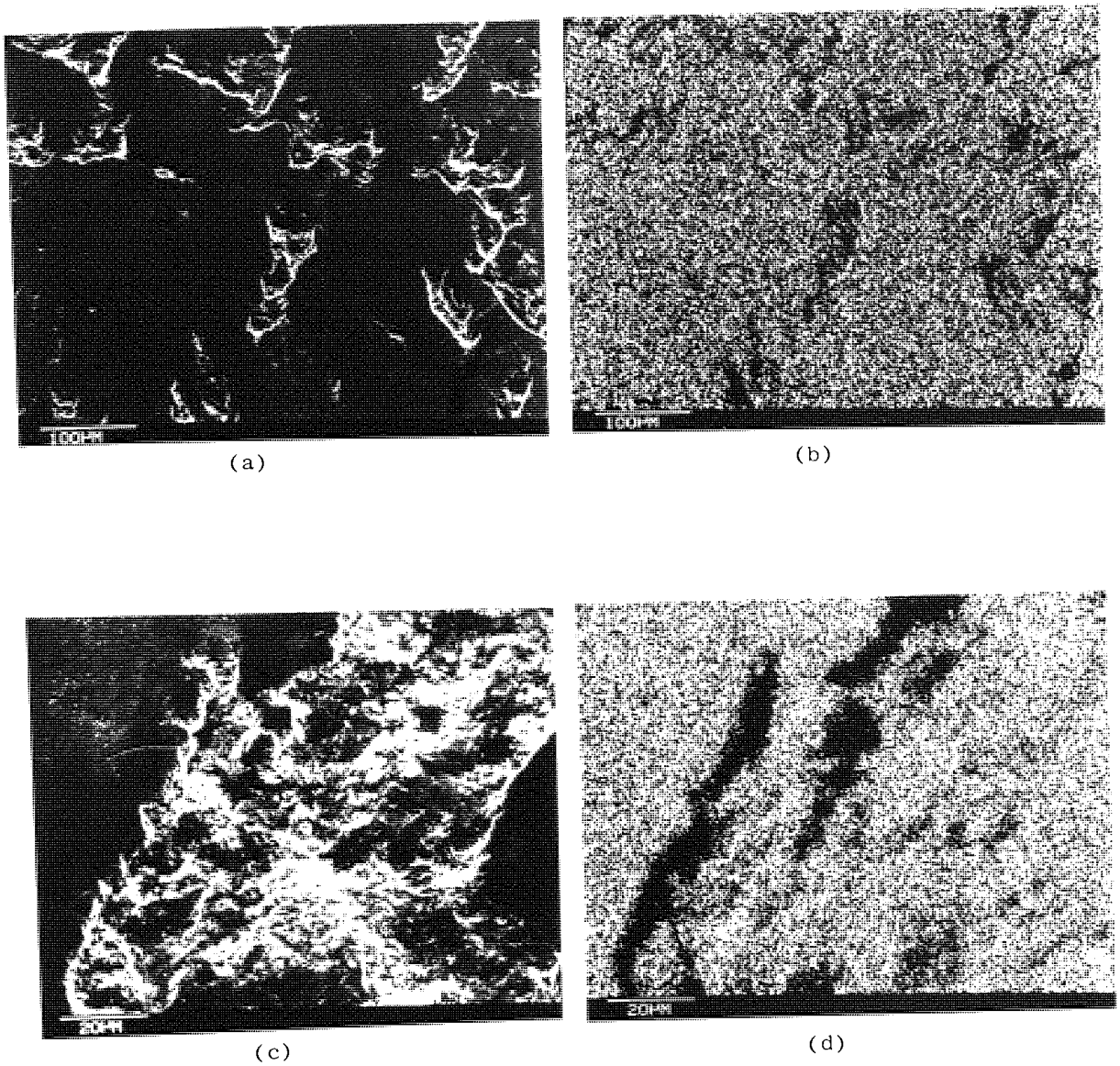

Fig. 3.44. S.E.M. photomicrographs of worn A.I.S.I. 440C MOD steel pin surfaces. All surfaces shown were taken from experiments conducted at a sliding speed of 2 m s^{-1} with a disc temperature of 500 ^{o}C.

(a) Magnification x200, load 39.2 N.
(b) Tungsten map of the area of surface shown in (a).
(c) Magnification x1000, load 98.1 N.
(d) Tungsten map of the area of surface shown in (c).

3.44(a) shows at a magnification of x200 a smooth transferred film on the surface. Figure 3.44(b) shows a tungsten elemental map of the same area of surface shown in figure 3.44(a). It can be seen that the film does not completely cover the surface. For a 98.1 N load an area of the surface where the transferred film has broke away or has not yet formed is shown in figure 3.44(c) at a magnification of x1000. Figure 3.44(d) shows a tungsten elemental map of the same area as in figure 3.44(c).

3.6 Pin Hardness Tests

Figure 3.45 shows the variation in bulk hardness of the worn surfaces of Lescalloy BG42 steel pins, as a function of temperature of the disc at which the experiment was conducted at sliding speeds of 2 m s^{-1}. The curves show the relationship at 19.6 and 98.1 N loads, figures 3.45(a) and 3.45(b) respectively. These are typical loads which show oxidational-metallic and severe wear for disc temperatures less than 400 ^{o}C as shown by X-ray data and S.E.M. analysis. Figure 3.46 shows the variation in micro-hardness versus experimental disc temperature for the same conditions. The variation in bulk hardness and micro-hardness as a function of computed surface temperature also for the same conditions are shown in figures 3.47 and 3.48 respectively. Both bulk hardness and micro-hardness values of the worn surfaces of selected A.I.S.I. 440C MOD steel pins are shown in table 3.17. Disc temperatures less than 200 ^{o}C were generated by frictional heating alone.

For the bulk hardness values the error bars are within the symbols. The depth of penetration of the diamond pyramid indentor for the micro-hardness tests was 5.0 to 7.5 μm for a hardness range of 9 x 10^{9} to 4 x 10^{9} N m^{-2} respectively. These were obtained using equation (2.20)

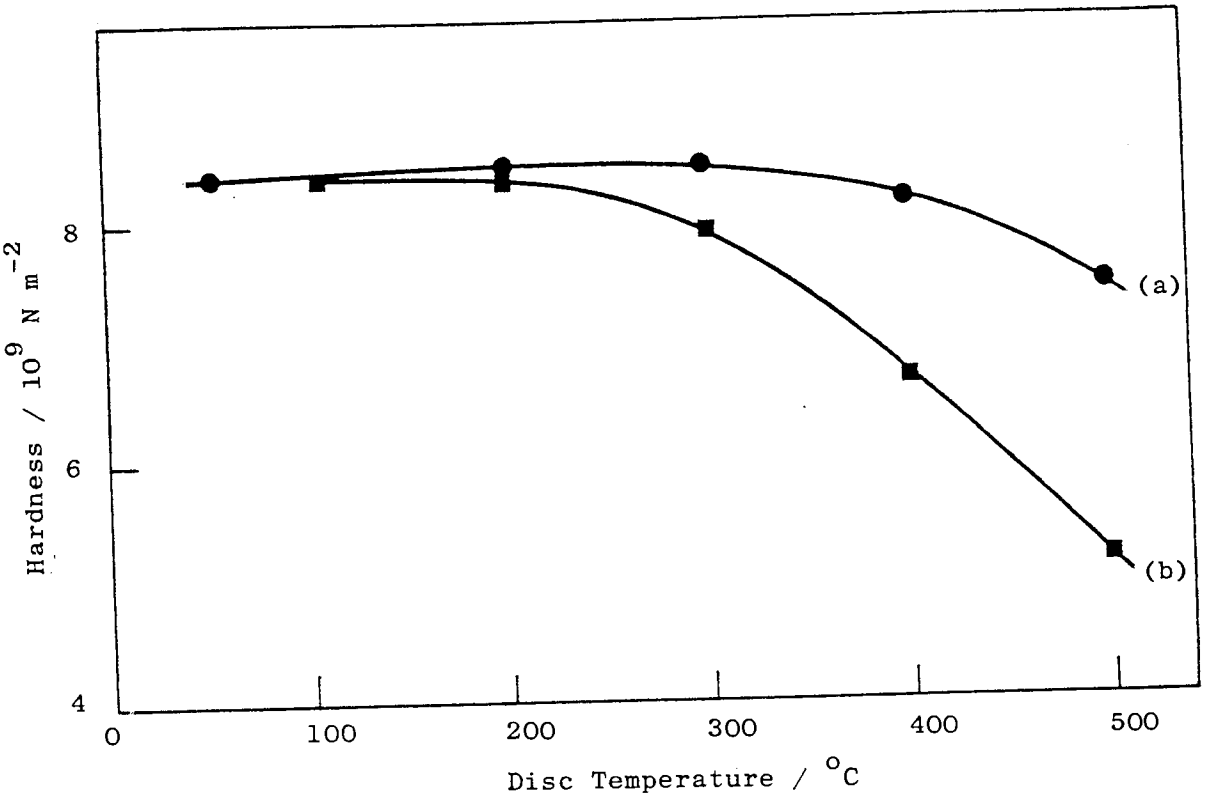

Fig. 3.45. Bulk hardness of the worn Lescalloy BG42 steel pins versus experimental disc temperature for a sliding speed of 2 m s^{-1}; (a) 19.6 N load; (b) 98.1 N load.

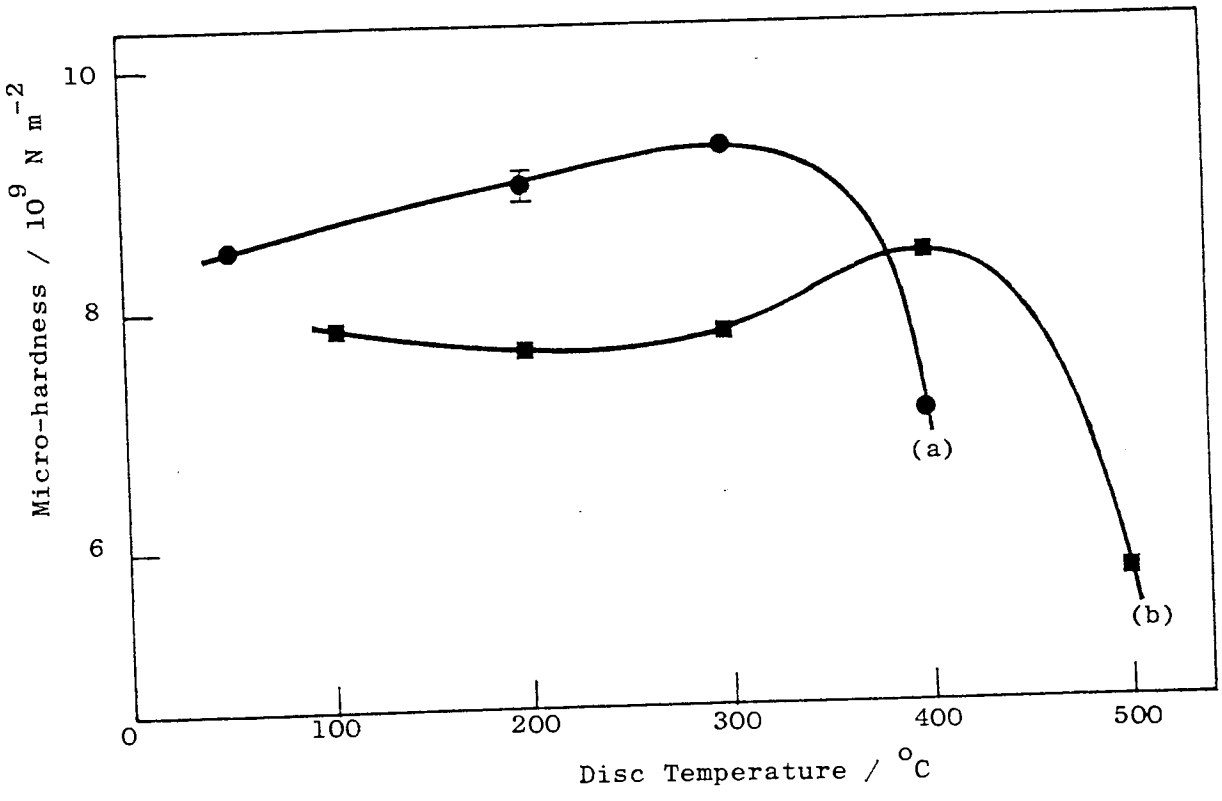

Fig. 3.46. Micro-hardness of the worn Lescalloy BG42 steel pins versus experimental disc temperature for a sliding speed of 2 m s^{-1}; (a) 19.6 N load; (b) 98.1 N load.

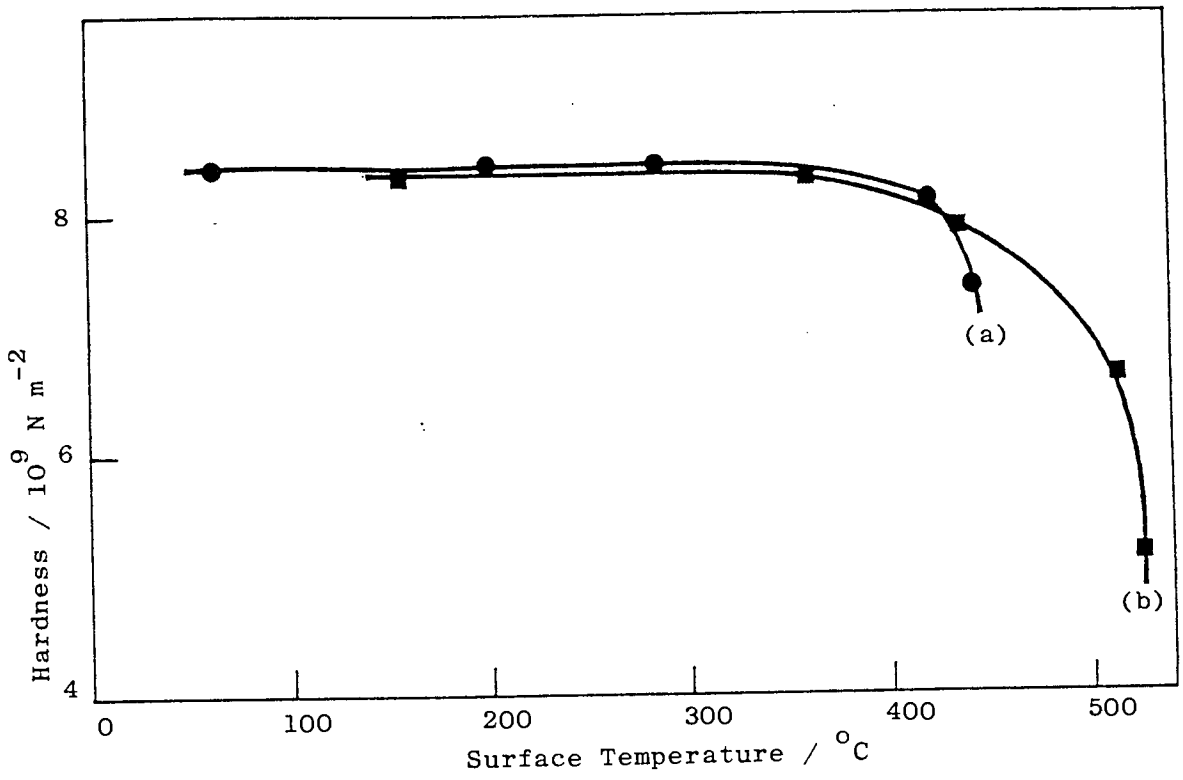

Fig. 3.47. Bulk hardness of the worn Lescalloy BG42 steel pins versus computed surface temperature for a sliding speed of 2 m s^{-1}; (a) 19.6 N load; (b) 98.1 N load.

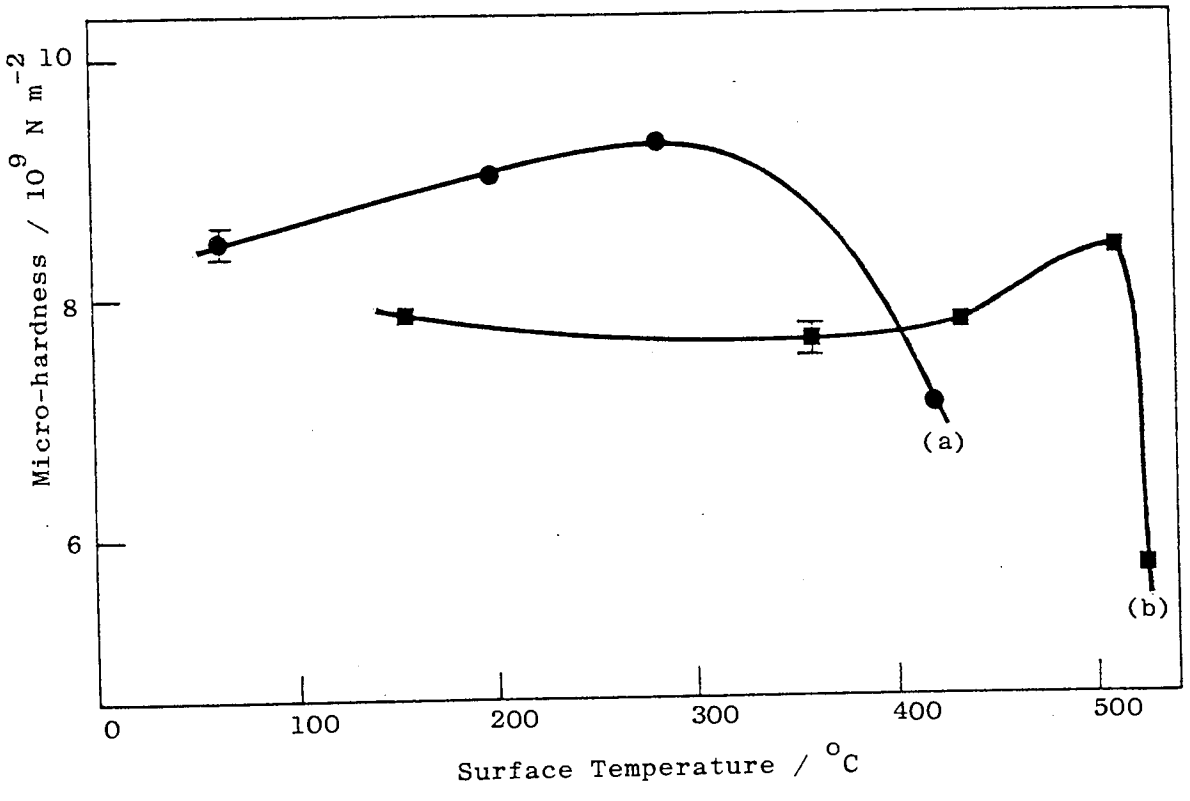

Fig. 3.48. Micro-hardness of the worn Lescalloy BG42 steel pins versus computed surface temperature for a sliding speed of 2 m s^{-1}; (a) 19.6 N load; (b) 98.1 N load.

Table 3.17. Hardness values of selected worn A.I.S.I. 440C MOD steel pins. All the experiments were carried out at a sliding speed of 2 m s^{-1}.

Load / N ± 0.9 N	Disc Temperature / °C ± 5 °C	Surface Temperature / °C ± 5%	Bulk Hardness / 10^9 N m^{-2} ± 0.05 x 10^9 N m^{-2}	Micro-hardness / 10^9 N m^{-2} ± 0.1 x 10^9 N m^{-2}
19.6	49	61	8.26	8.4
98.1	95	208	7.38	7.6
98.1	200	363	7.52	7.4
98.1	500	529	3.85	5.3

section 2.10. The depth of penetration of the diamond pyramid indentor for the bulk hardness tests was 10 times the penetration of the micro-hardness indentor.

All hardness readings were taken cold after completion of the relevant wear experiment. Figure 3.45 as one would expect, shows a decrease in hardness with increasing experimental disc temperature. The high load curve fall is much greater indicating the influence of frictional heating on the sub-surface layers immediately below the real areas of contact.

The micro-hardness curves, due to the much lower penetration depth of the indentor, are more representative of changes at the contacting surface on the steel pin. The 19.6 N load curve figure 3.46(a), shows an increase in micro-hardness up to a disc temperature of about 300 °C (surface temperature 286 °C), because oxides are present on the surface as shown by X-ray diffraction. For greater temperatures the micro-hardness falls rapidly, due to material in the form of oxides being transferred from the disc to the pin as shown by X-ray data and S.E.M.

analysis. For the high load curve figure 3.46(b), the micro-hardness increases after a disc temperature of about 300 ^{o}C (surface temperature 434 ^{o}C) with tungsten carbide WC, rhombohedral and γ-Fe_2O_3 oxides appearing on the surface as shown in table 3.12. For disc temperatures greater than about 400 ^{o}C (surface temperature 513 ^{o}C), it rapidly decreases due to material in the form of oxides being transferred from disc to pin as shown by X-ray data and S.E.M. analysis. For the A.I.S.I. 440C MOD steel pins table 3.17, the values follow the same trends but the magnitudes are lower as expected.

3.7 Oxidational Parameter Measurements

The oxide film thickness measured by ellipsometry varying with time is shown in figure 3.49, for Lescalloy BG42 and A.I.S.I. 440C MOD stainless steels over the temperature range 200 to 600 ^{o}C. For both types of steel at temperatures less than 400 ^{o}C the oxidation rate is logarithmic, figures 3.49(a) and 3.49(b). For temperatures greater than 400 ^{o}C the oxidation rate appears to be parabolic, figures 3.49(d), 3.49(e) and 3.49(f). The parabolic law is connected with the growth of a continuous oxide film, the thickening of which is controlled by migration or diffusion through the film. At low temperatures such movement through the film will be negligibly slow, but leakage of oxygen through definite discontinuities can continue. Almost any process in which the oxidation rate is slow would conform to some kind of logarithmic law.

When the oxidation rate is parabolic the oxide film thickness h_o (m) is given by equation (3.5).

$$h_o = k_p^{1/2} t^{1/2} + c \quad \ldots\ldots\ldots\ldots\ldots\ldots\ldots\ldots\ldots\ldots (3.5)$$

Where k_p is the parabolic rate constant, t the time and c is a constant. By plotting the oxide film thickness against the square

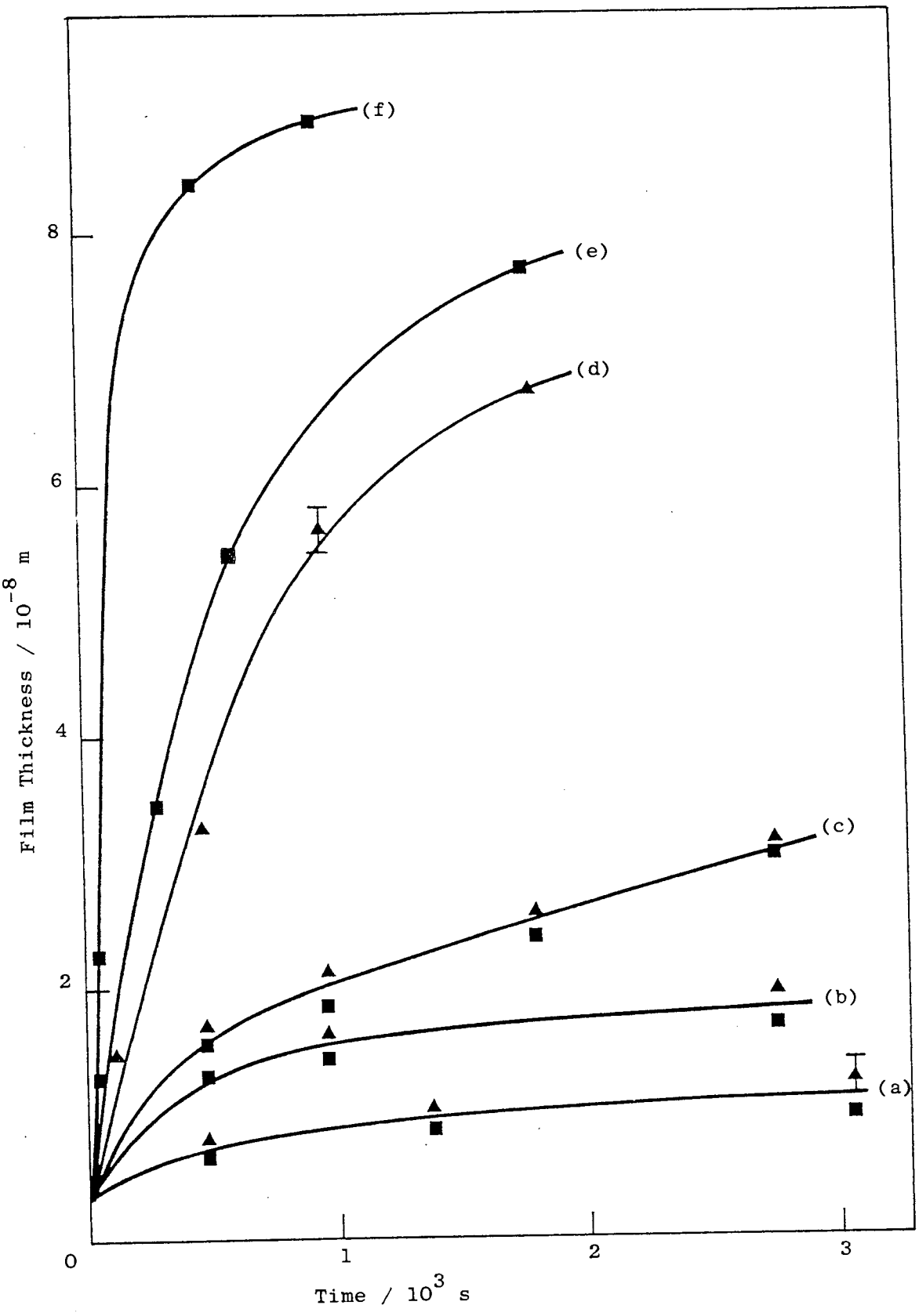

Fig. 3.49. Oxide film thickness on martensitic stainless steel as a function of time; (a) furnace temperature 200 °C; (b), (c), (d), (e) and (f) for oxidation temperatures of 300, 400, 450, 500 and 600 °C respectively. ■ - Lescalloy BG42 steel. ▲ - A.I.S.I. 440C MOD steel.

root of the time shown in figure 3.50, the parabolic rate constant was determined for oxidation temperatures of 450, 500 and 600 ^{o}C. The slope of the graph is equal to $k_p^{1/2}$. For oxidation temperatures of 450, 500 and 600 ^{o}C the parabolic rate constants k_p were found to be $(2.2 \pm 0.2) \times 10^{-18}$, $(3.4 \pm 0.5) \times 10^{-18}$ and $(9.5 \pm 2) \times 10^{-18}$ $m^2 s^{-1}$ respectively.

The parabolic rate constant k_p ($m^2 s^{-1}$) is related to the activation energy for parabolic oxidation Q_p ($J\ mol^{-1}$) by equation (3.6), Kubaschewski and Hopkins.[49]

$$k_p = A_p \exp - Q_p / R T_o \quad \ldots\ldots\ldots\ldots\ldots\ldots\ldots\ldots\ldots\ldots\ldots\ldots (3.6)$$

A_p is the Arrhenius constant, R is the gas constant and T_o is the oxidation temperature.

$$\log_{10} k_p = \log_{10} A_p - Q_p / 2.303\ R\ T_o \quad \ldots\ldots\ldots\ldots\ldots\ldots\ldots\ldots (3.7)$$

A graph was plotted of $\log_{10} k_p$ versus $1 / T_o$ figure 3.51, where the slope of the graph is equal to $- Q_p / 2.303\ R$. The slope was obtained using a statistical formula:-

$$Q_p / 2.303\ R = \frac{n (\Sigma x y) - (\Sigma x) (\Sigma y)}{n (\Sigma x^2) - (\Sigma x)^2} \quad \ldots\ldots\ldots\ldots\ldots\ldots\ldots\ldots (3.8)$$

where $y = \log_{10} k_p$ and $x = 1 / T_o$.

Hence $Q_p = (52 \pm 5) \times 10^3\ J\ mol^{-1}$.

The intercept of the graph $\log_{10} A_p$ was given by equation (3.9).

$$\log_{10} A_p = \frac{(\Sigma y) (\Sigma x^2) - (\Sigma x) (\Sigma x y)}{n (\Sigma x^2) - (\Sigma x)^2} \quad \ldots\ldots\ldots\ldots\ldots\ldots\ldots\ldots (3.9)$$

Hence $A_p = (1.0 \pm 0.4) \times 10^{-14}\ m^2 s^{-1}$.

When the oxidation rate is logarithmic the oxide film thickness h_o (m) is given by equation (3.10), Kubaschewski and Hopkins.[49]

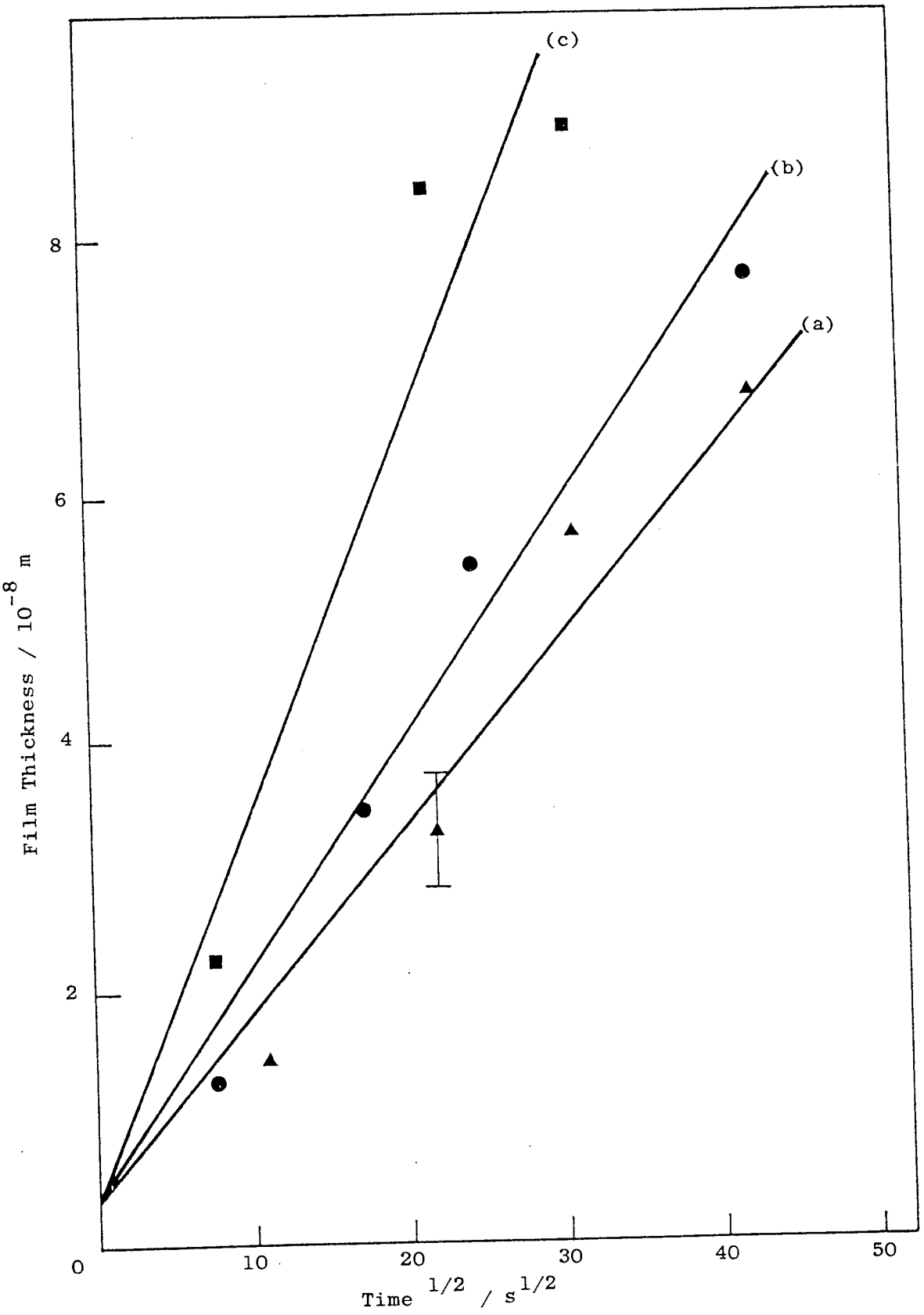

Fig. 3.50. Oxide film thickness on martensitic stainless steel as a function of time $^{1/2}$; (a) oxidation temperature 450 °C; (b) oxidation temperature 500 °C; (c) oxidation temperature 600 °C.

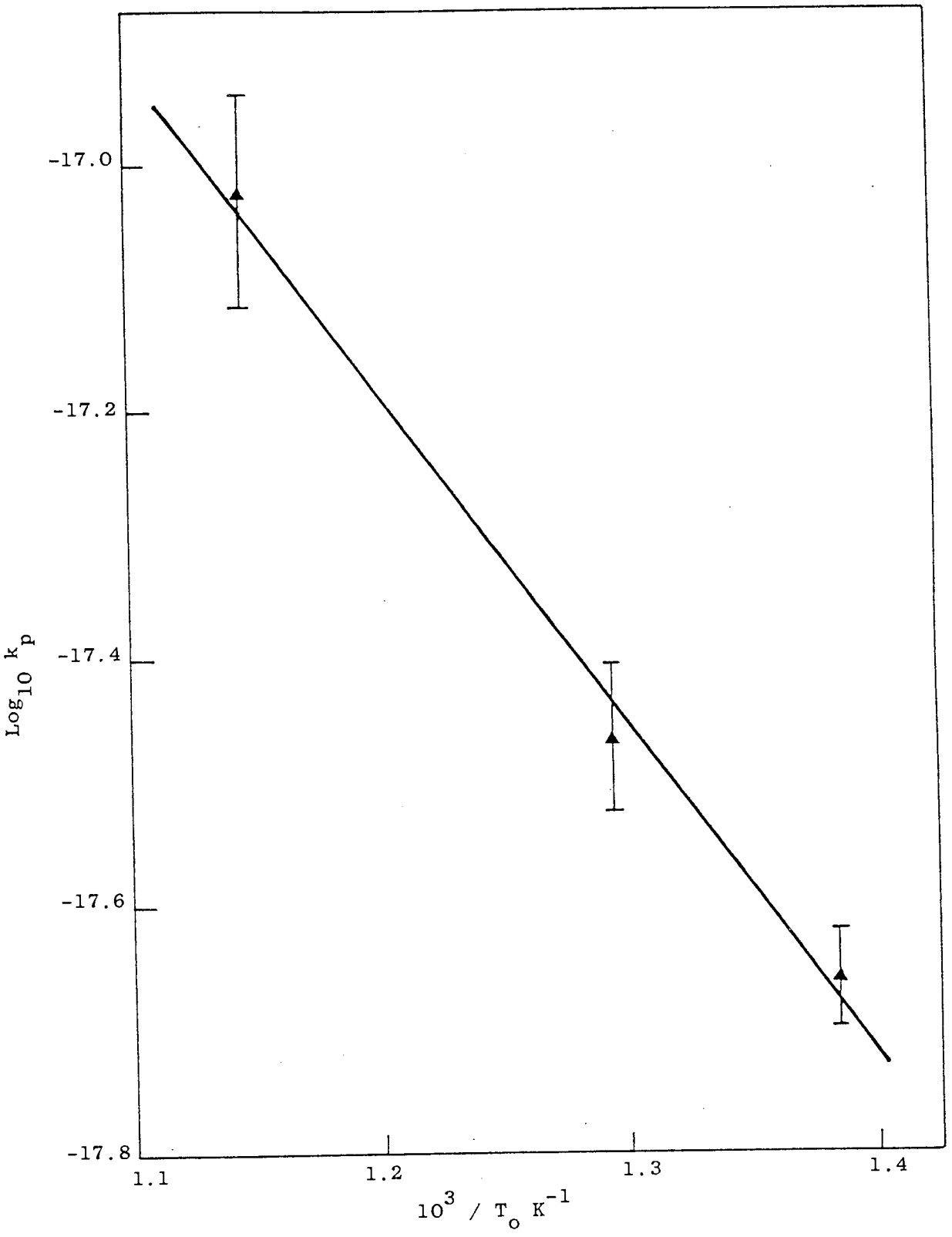

Fig. 3.51. $Log_{10}\ k_p$ as a function of inverse oxidation temperature.

$$h_o = k_e \ln (a t + b) \quad \ldots\ldots\ldots\ldots\ldots\ldots\ldots\ldots\ldots\ldots\ldots\ldots (3.10)$$

Where k_e is the rate constant, t the time and a b are unknowns. Differentiation of the above equation and inverting produces equation (3.11).

$$dt / dh_o = t / k_e + b / k_e a \quad \ldots\ldots\ldots\ldots\ldots\ldots\ldots\ldots\ldots\ldots\ldots\ldots (3.11)$$

By plotting dt / dh_o against t the rate constants k_e were determined for oxidation temperatures of 200 and 300 ^{o}C. For the Lescalloy BG42 steel, the rate constants k_e were found to be $(1.0 \pm 0.3) \times 10^{-9}$ and $(1.6 \pm 0.1) \times 10^{-9}$ m for oxidation temperatures of 200 and 300 ^{o}C respectively. The activation energy Q for logarithmic oxidation was determined using equation (3.7) and found to be $(11 \pm 9) \times 10^{3}$ J mol^{-1}.

CHAPTER 4

DISCUSSION

4.1 Identification of Wear Mechanisms

Referring initially to figures 3.3, 3.4, 3.8, 3.9, 3.10 and 3.11 for pin-on-disc experiments with no external heating, the results indicate two distinct wear mechanisms. For loads below about 40 N the pin surfaces are relatively smooth, as shown in figures 3.40(a) and 3.40(c) for Lescalloy BG42 and A.I.S.I. 440C MOD steel pins respectively and are typical of those associated with oxidational wear. The wear debris were of small particle size and non-metallic in appearance. However although these observations might indicate oxidational wear, X-ray diffraction analysis of debris and surfaces showed large amounts of metal together with the oxide as shown in tables 3.10, 3.11 and 3.14. For both types of steel pins the debris contained α-Fe(Cr), rhombohedral oxide, tungsten carbide and γ-Fe with sometimes γ-Fe_2O_3 being detected as shown in tables 3.10 and 3.14. α-Fe(Cr) indicates the original bulk steel structure, where γ-Fe indicates austenite which is of lower hardness. The rhombohedral oxide is a solid solution consisting of a mixture of α-Fe_2O_3 and Cr_2O_3, Isherwood and Quinn.[51]

The tungsten transfer identified by the energy dispersive analyser on a Lescalloy BG42 steel pin, at a 19.6 N load and a sliding speed of 2 m s^{-1} figures 3.37 and 3.38, is in the form of tungsten carbide as shown in table 3.11. Table 3.16 shows that this is also true for the A.I.S.I. 440C MOD steel pins for the same conditions. Golden and Rowe[34] showed that when WC-6% Co was slid slowly over stainless steel under a load of 14.7 N, almost the whole of the transferred carbide was strongly bonded to the stainless steel. When reciprocating traversals were made a considerable proportion of the transferred

carbide was scattered loosely on the surface. This explains why tungsten carbide is found in the wear debris as shown in tables 3.10 and 3.14.

The magnitude of the wear rate suggest that the mechanism is only partially oxidational. Considering the hardness difference of the materials (Lescalloy BG42 steel 8.29 x 10^9 N m^{-2}, A.I.S.I. 440C MOD steel 8.09 x 10^9 N m^{-2} and WC-11% Co 13.00 x 10^9 N m^{-2}) it is more probably a mixed oxidational-abrasive mechanism. The frictional temperatures generated shown in figures 3.23 and 3.24, were not high enough either to produce a completely stable oxide film and hence true oxidational mild wear with an expected wear rate of about 10^{-14} m^3 m^{-1}, or to produce degeneration of the sintered WC-11% Co. Thus the oxide formed afforded limited protection, with a consequently lower wear rate than would have been expected if it had not been present.

For loads above about 40 N the wear for both steels in all cases was typical severe wear. The debris consisted of large metallic particles which when analysed were shown to be a mixture of α-Fe(Cr), γ-Fe and tungsten carbide. No oxides were present either in the debris or on the surfaces as shown in tables 3.10, 3.12 and 3.14. The pins surface was free of tungsten as shown by the energy dispersive analyser, figures 3.37 and 3.38 and table 3.16, which confirms the X-ray analysis, table 3.12. For sliding speeds greater than 0.6 m s^{-1} the wear rate starts to increase rapidly at the high loads, this is due to the decreasing hardness of the pin substrate which is confirmed by γ-Fe becoming more predominant in the wear debris. Figures 3.4 and 3.10 show that for this type of wear the wear rate of the softer A.I.S.I. 440C MOD steel is greater for the same sliding speed. For both types of steel pins, the coefficient of friction is similar

within the limits of experimental error and decreases with increasing load as shown in figure 3.11.

The increase in wear rate with increase in sliding speed is due to temperature effects. The surface temperature increases linearly with increasing load within the limits of experimental error as shown in figures 3.23 and 3.24. The increase in frictional heating leads to surface softening and subsequent reduction in abrasion resistance as described by Kruschov,[82] together with a reduction in shear strength. The hardness of the Lescalloy BG42 martensitic stainless steel falls from 8.29×10^9 N m^{-2} at room temperature to about 6.03×10^9 N m^{-2} at 500 °C, where the hardness of the A.I.S.I. 440C MOD steel falls from 8.09×10^9 N m^{-2} to about 5.56×10^9 N m^{-2} according to Parks.[83] Dawihl and Frisch[56] reported that cemented tungsten carbide has excellent hot hardness and hot strength. The heat flow per-second along the pin at the interface between the pin and disc H_1, starts to increase more rapidly with load for sliding speeds greater than 0.6 m s^{-1} as shown in figures 3.18 and 3.19. This shows there is an increase in the number of asperities in contact beneath the pin, Rowson and Quinn,[81] which confirms the decreasing hardness of the pin substrate due to frictional heating. There is the expected increase in H_1 with increasing sliding speed. For the A.I.S.I. 440C MOD steel pins H_1 is greater as expected since it is of lower hardness. The decreasing hardness of the pin substrate for Lescalloy BG42 steel is also confirmed by figure 3.22, which shows the experimentally measured division of heat at the pin-disc interface at a sliding speed of 2 m s^{-1} increasing rapidly after a load of about 50 N. Table 3.1 shows the maximum attainable temperatures of the real area of contact for Lescalloy BG42 steel pins. From the S.E.M. photomicrographs for

both types of steel pins figures 3.40(b) and 3.40(d), the surfaces show evidence of both plastic flow of the steel and deep grooves formed by abrasive action which are typical of those associated with severe wear.

A typical wear track on the disc produced by the severe wear mechanism is shown in figure 3.29(b). This wear track was produced by a Lescalloy BG42 steel pin with a 147.1 N load at a sliding speed of 2 m s^{-1}. X-ray data displayed in table 3.15 shows that steel has been bonded to the disc indicating the possibility of some kind of adhesive wear.

The materials are not designed to run at low temperatures and the results presented in figures 3.5, 3.6, 3.7, 3.12, 3.13, 3.14, 3.15, 3.16, 3.17 and 3.27 are of more importance to this study. For disc temperatures less than 400 ^{o}C, the curves are very similar in nature to the frictional heated experiments as shown in figures 3.12 and 3.14 for Lescalloy BG42 and A.I.S.I. 440C MOD steels respectively. The 500 ^{o}C curve for both steels however shows significantly lower wear rates indicating a different mechanism. Considering tables 3.11, 3.12 and 3.14, the results indicate that for disc temperatures up to 300 ^{o}C, wear mechanisms are the same as those as in the frictionally heated experiments.

In the low load region below 40 N a mixed oxidational-abrasive wear mechanism is predominant. An S.E.M. photomicrograph is shown in figure 3.41(a), taken from an experiment using a Lescalloy BG42 steel pin conducted at a load of 19.6 N and a disc temperature of 200 ^{o}C. It shows an area of steel surface where an oxide plateau is beginning to break up to form debris. The debris consist of α-Fe(Cr), rhombohedral oxide, γ-Fe, γ-Fe_2O_3 and tungsten carbide where the surface

bears the rhombohedral oxide as shown in table 3.11. For the same conditions but at a disc temperature of 300 ^{o}C, oxide is also present on the surface as shown in figure 3.41(b). The debris consist of α-Fe(Cr), γ-Fe_2O_3, rhombohedral oxide, γ-Fe and the surface shows both oxides and tungsten carbide.

A typical wear track on the WC-11% Co disc produced by the oxidational-abrasive wear mechanism is shown in figure 3.29(a). The wear track was formed by a Lescalloy BG42 steel pin with a 19.6 N load at a disc temperature of 300 ^{o}C and a sliding speed of 2 m s^{-1}. From the profile the wear rate of the disc was found to be $(5.0 \pm 0.4) \times 10^{-14}$ m^3 m^{-1}. This shows the wear rate of the disc was small compared to the wear rate of the pin which was 20 times greater, figure 3.12. Golden and Rowe[35] concluded that for cobalt bonded tungsten carbide, both the soft matrix and the hard grains wear steadily away together during dry sliding. Miller[36] also stated that hard solids can undergo extensive wear when rubbed against metals of much lower hardness. This effect is due partly to the abrading effect of small particles at the harder material which becomes dislodged and dragged across the surface. The sights from which particles are removed may be inclusions, defects or perhaps asperities which are subject to thermal shock or fatigue type failures. Golden and Rowe[34] reported that for metals of low hardness, a greater amount of these hard abrasive particles are pushed down well into the metal. This possibly explains the absence of tungsten carbide in the wear debris, but also differences in magnitude of wear rates indicates that this is not a major factor affecting wear.

For loads greater than 40 N both the debris and surface analysis suggest a severe wear mechanism. For both types of steel the wear

rate increases with load as expected, as shown in figure 3.5 for a disc temperature of 200 ^{o}C and a sliding speed of 2 m s^{-1}. The shape of the curves are similar with the A.I.S.I. 440C MOD steel pins of lower hardness having the greater wear rate for this type of wear. An S.E.M. photomicrograph is shown in figure 3.41(c), taken from an experiment using a Lescalloy BG42 steel pin conducted at a load of 98.1 N at a disc temperature of 300 ^{o}C and a sliding speed of 2 m s^{-1}. The surface shows evidence of both plastic flow of the steel and grooves formed by the abrasive action of the much harder WC-11% Co disc. As shown in table 3.12, the debris consisted of γ-Fe, WC, α-Fe(Cr) and rhombohedral oxide with the surface showing traces of the oxide which probably formed on cooling.

At a disc temperature of 400 ^{o}C some degeneration of the WC-11% Co disc begins to occur. Table 3.11 shows that tungstic oxide WO_3 and cobalt tungsten oxide $CoWO_4$ appears on the surface of the steel pins by transfer from the disc. Figures 3.12, 3.14, 3.16 and 3.27 show a dramatic decrease in wear rate when the disc temperature exceeds 400 ^{o}C for all loads. For Lescalloy BG42 steel pins at a disc temperature of 400 ^{o}C the wear rate increases with load as expected as shown in figure 3.6. For loads less than about 30 N S.E.M. analysis figure 3.37 and X-ray data table 3.11, show there is transfer of material from the disc to the pin in the form of cobalt tungsten oxide $CoWO_4$, tungstic oxide WO_3 and tungsten carbide WC. Between loads of about 30 and 122 N no major transfer of material is occurring as shown in table 3.12, except for a little tungsten carbide WC. Table 3.13 shows that no oxides are present in the debris for loads above 122 N indicating a severe wear mechanism. S.E.M. photmicrographs are shown in figures 3.42(a), 3.42(b) and 3.42(c), taken from an experiment using

a Lescalloy BG42 pin conducted at a load of 19.6 N at a disc temperature of 400 ^{o}C and a sliding speed of 2 m s^{-1}. Figure 3.42(a) shows smooth areas which are transferred material from the disc Figure 3.42(c) shows a tungsten elemental map of the same area as in figure 3.42(b). For the same conditions but at a load of 98.1 N table 3.15 shows that steel has been found bonded to the WC-11% Co disc.

According to Hansen[46] tungsten carbide of hexangonal structure remains stable up to a temperature of 2600 ^{o}C, Orton[52] reports it remains stable up to 1760 ^{o}C and Sara[53] reports it decomposes into the face-centred cubic phase at a temperature of 2755 ^{o}C. It is not envisaged that temperatures approaching these values could be attained in these experiments. As shown in figure 1.3 WC-11% Co exists up to a temperature of about 1300 ^{o}C, Rautala and Norton.[58] From figure 1.4, Gurland[59] reports that WC-16% Co also exists up to a temperature of about 1300 ^{o}C. Because the temperatures are very high no change is likely to occur in the hexagonal tungsten carbide structure and this is confirmed by X-ray diffraction analysis, tables 3.11, 3.12, 3.13 and 3.14. Even though cobalt was not detected, according to Edwards and Lipson[60] a transformation from face-centred cubic phase to the close-packed hexagonal phase on cooling begins at a temperature of about 400 ^{o}C. Troiano and Tokich[61] reported it occurred at a temperature of 388 ^{o}C. They found that this type of reaction could not be detected in fine grained cobalt. Owen and Madoc-Jones[62] reported that at temperatures above 450 ^{o}C the face-centred cubic structure was the stable phase.

At a disc temperature of 500 ^{o}C the A.I.S.I. 440C MOD steel pins show a linear increase in wear rate with load as shown in figure 3.7(b). At all loads cobalt tungsten oxide $CoWO_4$ and tungstic oxide WO_3 give

rise to strong X-ray diffraction lines in the debris as shown in table 3.14. Webb et.al.[64] reported the oxide film formed on tungsten carbide at a temperature of 700 ^{o}C revealed only the presence of yellow tungstic oxide WO_3. They found that it oxidized according to a linear rate law due to rupture of the oxide film by the formation of CO and CO_2. Newkirk[65] reported that the onset of rapid oxidation occurred at a temperature of about 565 ^{o}C for macrocrystalline tungsten carbide. For the Lescalloy BG42 steel pins figure 3.7(a), for loads less than about 80 N the debris and surfaces are similar to those of the A.I.S.I. 440C MOD steel pins as shown in tables 3.11, 3.13 and 3.14. Above 80 N load chemical reactions occur increasing the wear rate, producing iron tungsten oxide Fe_2WO_6 and chromium tungsten oxide Cr_2WO_6 on the surface of the pins which is also found present in the wear debris, tables 3.12 and 3.13. Besides cobalt tungsten oxide $CoWO_4$, the only other cobalt oxide detected was cobaltosic oxide Co_3O_4. Young[55] reports that the cobaltosic oxide Co_3O_4 is the stable oxide at temperatures less than about 850 ^{o}C, which is in agreement with the pin surface temperatures. The cobaltic oxide Co_2O_3 is completely converted into cobaltosic oxide Co_3O_4 at temperatures above 265 ^{o}C.

For Lescalloy BG42 steel pins there is the usual decrease in the coefficient of friction with increasing load, except at disc temperatures of 400 and 500 ^{o}C as shown in figure 3.13. For both types of steel pins figures 3.25 and 3.26, the surface temperature is proportional to load within the limits of experimental error at all disc temperatures. For Lescalloy BG42 steel pins figure 3.16, the initial increase in wear rate is followed by a sharp decrease at temperatures above 300 to 350 ^{o}C depending on load. For loads less than about 40 N there is an

oxidational-abrasive wear mechanism approaching the maximum wear rate temperature, above which there is transfer of material in the form of oxides from the disc to the pin as shown in table 3.11. For loads above 40 N there is a severe wear mechanism up to the maximum wear rate temperature, above which the wear rate decreases due to a series of complex interactions, including oxide film formation on the steel surface and degeneration and transfer of material from the WC-11% Co disc to the pin as shown in table 3.12. The transition from high to low wear rate is dependent on the temperature at the real area of contact, which is more closely related to that of the pin rather than the disc. So from figure 3.27 the maximum wear rate occurs at pin surface temperatures of 310, 335, 370, 430 and 540 ^{o}C for loads of 19.6, 39.2, 58.9, 98.1 and 147.1 N respectively. Trent[38] [39] found that at a temperature of about 1300 ^{o}C there was the formation of an extremely thin fused layer between the steel chip and the cemented carbide tool surface, consisting of an alloy of tungsten carbide with the steel.

Figures 3.37 and 3.38 show that tungsten transfer to the steel pin for a 19.6 N load increases for disc and surface temperatures above about 300 ^{o}C. For a 98.1 N load there is no tungsten transfer until the disc temperature exceeds 400 ^{o}C (surface temperature 513 ^{o}C). The X-ray analysis as shown in table 3.11, suggests that the tungsten transfer for loads less than 40 N is initially in the form of tungsten carbide WC and then cobalt tungsten oxide $CoWO_4$ and tungstic oxide WO_3. For Lescalloy BG42 steel pins there are chemical reactions occurring for loads above about 80 N probably after transfer, producing iron tungsten oxide Fe_2WO_6 and chromium tungsten oxide Cr_2WO_6 as shown in table 3.12. This transfer obviously leads to the very low wear rates

of the steel measured at a disc temperature of 500 ^{o}C. S.E.M. photomicrographs are shown in figures 3.43(a), 3.43(b) and 3.43(c), taken from an experiment using a Lescalloy BG42 steel pin conducted at a load of 98.1 N at a disc temperature of 500 ^{o}C and a sliding speed of 2 m s^{-1}. Figures 3.43(a) and 3.43(b) show a smooth film as does 3.43(c), a tungsten elemental map of the same area. S.E.M. photomicrographs are shown in figures 3.44(a) and 3.44(b), taken from an experiment using a A.I.S.I. 440C MOD steel pin for the same conditions but at a load of 39.2 N. They show that the smooth transferred film does not completely cover the surface. For a 98.1 N load the S.E.M. photmicrographs are shown in figures 3.44(c) and 3.44(d). They show an area on the surface when the transferred film has broken away or has not yet formed.

Figure 3.19 shows that for A.I.S.I. 440C MOD steel pins, the heat flow per-second along the pin at the interface between the pin and disc H_1, at a disc temperature of 500 ^{o}C only increases slightly with load, where its magnitude at about 140 N load is less than at a disc temperature of 200 ^{o}C. This confirms there is a large amount of material transfer from the disc to the pin which acts like an insulating layer reducing the heat flow rate along the pin. The same effect occurs for the Lescalloy BG42 steel pins as shown in figure 3.20.

The bulk hardness values given in figures 3.45 and 3.47 are not true representations of surface hardness, because of the large depth of penetration of the indentor of 50 to 75 μm for a hardness range of 9×10^{9} to 4×10^{9} N m^{-2} respectively. However they show a decrease in pin hardness with increasing temperature for both 19.6 and 98.1 N loads for surface temperatures greater than about 360 ^{o}C as shown in figure 3.47, indicating a lowering of abrasion resistance. The

micro-hardness measurements figures 3.46 and 3.48, confirm the proposed wear mechanisms. It is surface sensitive with a depth of penetration of 5.0 to 7.5 μm for a hardness range of 9×10^9 to 4×10^9 N m^{-2} respectively. Considering the low load curve 19.6 N figures 3.46(a) and 3.48(a), the increasing amount of oxides as shown in table 3.11 present on the pin surface leading to the proposed mixed oxidational-abrasive wear mechanism, causes an increase in surface hardness up to a disc temperature of about 300 ^{o}C (surface temperature 286 ^{o}C). Transfer of disc material in the form of oxides significantly reduces the surface hardness. The fact that sub-surface hardness is also reduced at this point must not be neglected since this may also have an effect. In the case of the high load curve 98.1 N figures 3.46(b) and 3.48(b), no significant amount of oxide is present on the surface up to a disc temperature of about 400 ^{o}C, the wear being severe and metallic. The micro-hardness increases after a disc temperature of about 300 ^{o}C (surface temperature 434 ^{o}C) with γ-Fe_2O_3, rhombohedral oxide and tungsten carbide WC appearing on the steel pin surface at a disc temperature of 400 ^{o}C (surface temperature 513 ^{o}C) as shown in table 3.12. As the temperature increases the transfer of material from the disc again rapidly reduces the surface hardness. For the A.I.S.I. 440C MOD steel pins the values follow the same trends but the magnitudes are lower as expected as shown in table 3.17.

Typical wear tracks on the WC-11% Co disc, formed by A.I.S.I. 440C MOD steel pins at a disc temperature of 500 ^{o}C and loads of 39.2 and 98.1 N are shown in figures 3.30 and 3.31 respectively. For a 39.2 N load figures 3.30, the wear rate was $(2.3 \pm 0.2) \times 10^{-12}$ m^3 m^{-1} which was about 80 times greater than the wear rate of the pin. Again this confirms that the predominant wear mechanism at this temperature is

one of degeneration of the disc material leading to transfer.

The results of the angular contact bearing tests appear to confirm that the same wear mechanisms are occurring in this very different experimental configuration. For the Lescalloy BG42 steel angular contact bearings, the track wear showed a maximum at a temperature of about 260 ^{o}C as shown in figure 3.1(a). In this region assuming pure sliding, the track wear rate corresponds to $(1.3 \pm 0.3) \times 10^{-11}$ m^3 m^{-1}. Since rolling is also present the wear rate due to sliding can be greater than this value. Table 3.8 shows the wear debris consisted of tungsten carbide WC and α-Fe(Cr) before the maximum track wear temperature. From the magnitude of the wear rate and debris analysis it appears there is a severe wear mechanism operating. At a temperature of 300 and 350 ^{o}C the wear debris consisted of rhombohedral oxide, tungsten carbide WC and α-Fe(Cr), with tungstic oxide WO_3 and cobalt tungsten oxide $CoWO_4$ being first detected at a temperature of 400 ^{o}C as shown in table 3.8. This suggests that the track wear decreases due to oxide films and transfer of material from the balls. At a bearing temperature of 500 ^{o}C iron tungsten oxide Fe_2WO_6 and chromium tungsten oxide Cr_2WO_6 was also detected in the wear debris indicating chemcial reactions similar to pin-on-disc experiments. For temperatures above the maximum track wear temperature S.E.M. analysis figure 3.36, shows there is an increase in the amount of tungsten transfer to the wear track, where the transfer is initially in the form of tungsten carbide WC according to debris analysis.

For the A.I.S.I. 440C MOD steel the track wear and wear debris were similar, but with tungstic oxide WO_3 being first detected at a temperature of 350 ^{o}C as shown in table 3.9. S.E.M. photomicrographs of a worn Lescalloy BG42 and A.I.S.I. 440C MOD steel race at a temperature of 350 ^{o}C are shown in figures 3.39(b) and 3.39(d) respectively.

The surface of the Lescalloy BG42 bearing race is coated with an oxide while the 440C MOD steel race shows small areas of transferred ball material, possibly tungstic oxide WO_3.

For similar angular contact bearings made from Lescalloy BG42 martensitic stainless steel with WC-11% Co balls tested under similar conditions, Parks[44] showed there is a progressive increase in wear with increasing temperature up to a peak in the 300 to 350 ^{o}C temperature region as shown in figure 1.2. He reported firstly the material softened off as the temperature rose and there was the formation of various types of oxides which supports the present situation.

For both types of steel bearings minimum ball wear as shown in figure 3.2 was at approximately 100 ^{o}C higher than the temperature at which maximum track wear occurred. This was a temperature of about 360 ^{o}C for Lescalloy BG42 steel and a temperature of about 300 ^{o}C for A.I.S.I. 440C MOD steel bearings. Below this temperature the balls had metal transfer from the race which was identified by glancing angle X-ray diffraction which supports the severe wear mechanism.

4.2 The Oxidational-Abrasive Wear Mechanism

For the pin-on-disc experiments, oxidational-abrasive wear mainly occurred for loads below 40 N with disc and pin surface temperatures less than about 300 ^{o}C for sliding speeds greater than 0.6 m s^{-1}. The pin surfaces are relatively smooth as shown by the S.E.M. photomicrographs figures 3.40(a) and 3.40(c) and the wear debris were of small particle size and non-metallic in appearance. These conditions are typical of mild wear or oxidational wear according to Archard and Hirst.[2] X-ray diffraction analysis of debris and surfaces showed large amounts of metal together with oxide where the debris contained α-Fe(Cr), rhombohedral oxide, γ-Fe with sometimes tungsten carbide

WC and γ-Fe_2O_3 being detected as shown in tables 3.10, 3.11 and 3.14. Sometimes tungsten carbide WC was also detected on the pin surfaces as shown in table 3.11. A typical wear track on the WC-11% Co disc figure 3.29(a), showed the wear rate of the disc to be small compared to the wear rate of the pin. The magnitude of the wear rate and X-ray data suggests the oxide formed on the pin gave only limited protection. Archard and Hirst[33] using high speed tool steel, concluded that the final wear mechanism between run-in surfaces under mild wear conditions is one of abrasion by the loose oxide wear particles.

The wear rate, which is the volume removed per unit sliding distance w ($m^3\ m^{-1}$) is given by the Archard[8] wear law, equation (1.1). Using equation (1.3) values of K, the probability of producing a wear particle at any given asperity encounter were calculated and are shown in table 4.1. Disc temperatures less than 200 ^{o}C were generated by frictional

Table 4.1. The K factors produced by the oxidational-abrasive wear mechanism.

Steel Pin	Speed/m s^{-1} $\pm$ 0.05 m s^{-1}	Load / N $\pm$ 0.9 N	Temperature / ^{o}C Disc $\pm$ 5 ^{o}C	Surface $\pm$ 5%	Wear Rate/ $10^{-13}\ m^3\ m^{-1}$ $\pm$ 7%	K / 10^{-4} $\pm$ 20%
BG42	2.00	4.9	32	37	0.87	1.5
BG42	2.00	9.8	41	40	3.49	2.9
BG42	2.00	19.6	53	64	4.21	1.8
BG42	2.00	9.8	200	152	3.03	2.6
BG42	2.00	19.6	200	201	7.99	3.4
BG42	2.00	19.6	300	286	9.83	4.2
BG42	3.00	9.8	46	50	1.73	1.5
BG42	3.00	19.6	57	92	5.01	2.1
440C MOD	2.00	9.8	40	49	1.47	1.2
440C MOD	2.00	19.6	49	61	5.45	2.2
440C MOD	2.00	9.8	200	199	2.58	2.1
440C MOD	2.00	19.6	200	206	4.34	1.8

heating alone.

The oxidational wear mechanism which has gradually evolved over the past 19 years by Quinn,[15] [16] [19] [20] [22] [23] Quinn et.al.,[17] Sullivan et.al.,[84] Quinn and Sullivan[24] gives a suitable expression for the K factors found in mild wear.

$$K = d\, A_p \exp - (Q_p / R\, T_o) / U\, f^2\, h_c^{\,2}\, \rho^2 \quad \ldots\ldots\ldots\ldots\ldots\ldots (4.1)$$

A_p is the Arrhenius constant for parabolic oxidation during wear, Q_p the activation energy for parabolic oxidation, R the gas constant and d is the distance of a wearing asperity contact during which oxidation occurs at the contact temperature given by T_o. U is the linear sliding speed, f is the mass fraction of oxide which is oxygen, h_c the critical oxide film thickness and ρ the average density of the oxide. Substituting for d by equation (1.8) produces equation (4.2).

$$K = 2\, W^{1/2}\, A_p \exp - (Q_p / R\, T_o) / \pi^{1/2}\, N^{1/2}\, p^{1/2}\, U\, f^2\, h_c^{\,2}\, \rho^2 \quad \ldots (4.2)$$

Where W is the load, N the number of asperity contacts and p the bulk hardness of the softer of the two materials.

The bulk hardness values were $(8.29 \pm 0.05) \times 10^9$ N m^{-2} for Lescalloy BG42 steel and $(8.09 \pm 0.05) \times 10^9$ N m^{-2} for A.I.S.I. 440C MOD steel where R the gas constant is 8.314 J ^{o}C^{-1} mol^{-1}. For α-Fe_2O_3 the factor f = 0.3006, for Cr_2O_3 f = 0.3158, so therefore the average value was taken. From equation (2.17) the maximum effective depth of penetration of the X-rays through a rhombohedral oxide film was found to be about 40 μm. Since the pin substrate was detected at all loads and disc temperatures, the thickness of all the oxide films are very much lower. The critical oxide film thickness h_c on the asperities could not be measured experimentally. Sullivan et.al.[84] showed that h_c was practically constant for a given speed with increase

in load, but showed a slight decrease as speed was reduced. The mean values of h_c obtained were 2.2 μm at a sliding speed of 3 m s^{-1} and 1.7 μm at a sliding speed of 2 m s^{-1}. Due to the thickness of the oxide films a diffusion process is occurring at the wearing asperity contacts which indicates parabolic oxidation. The activation energy for parabolic oxidation Q_p was found to be from ellipsometry measurements $(52 \pm 5) \times 10^3$ J mol^{-1} and the Arrhenius constant $A_p = (1.0 \pm 0.4) \times 10^{-14}$ m^2 s^{-1} as shown in section 3.7. Multiplying by the square of the average density of the rhombohedral oxide film $A_p = (3 \pm 1) \times 10^{-7}$ kg^2 m^{-4} s^{-1}. The density for α-Fe_2O_3 and Cr_2O_3 was 5.24×10^3 and 5.48×10^3 kg m^{-3} respectively. Values of N and T_o obtained by Sullivan et.al.[84] using BS970 EN8 low-alloy steel were utilised since they could not be obtained experimentally. For a linear sliding speed of 3 m s^{-1} the values of N were obtained from Rowson et.al.[85] using EN31 steel. Work within the Aston tribology group suggests that these values are typical for a whole range of steels. Therefore using equation (4.2) the theoretical values of K were calculated for the unheated disc experiments and are shown in table 4.2. Equation (4.2) does not apply to the heated disc experiments because it does not take into account the out of contact oxidation.

Table 4.2 shows that the theoretical values of K are very much smaller than the experimental values. Assuming tribo-oxidation takes place, the rate of growth of the oxide film is quite different to that measured under static conditions. According to Sullivan et.al.[84] the activation energy Q_p, which depends on relative potential barrier heights will remain the same in both static and sliding cases. The Arrhenius constant A_p however, will be very different in the tribological

Table 4.2. The theoretical K values and the tribological derived A_p values for the unheated disc experiments.

Steel Pin	U / m s^{-1} $\pm$ 0.05 m s^{-1}	W / N $\pm$ 0.9 N	T_o / ^oC	N	K / 10^{-4} (Expt.) $\pm$ 20%	K	A_p / kg^2 m^{-4} s^{-1}
BG42	2.00	4.9	230	70	1.5	9.2×10^{-20}	4.6×10^{8}
BG42	2.00	9.8	320	170	2.9	1.8×10^{-16}	4.8×10^{5}
BG42	2.00	19.6	440	310	1.8	3.8×10^{-14}	1.3×10^{3}
BG42	3.00	9.8	380	100	1.5	2.0×10^{-15}	2.1×10^{4}
BG42	3.00	19.6	480	200	2.1	6.2×10^{-14}	9.9×10^{2}
440C MOD	2.00	9.8	320	170	1.2	1.8×10^{-16}	2.0×10^{5}
440C MOD	2.00	19.6	440	310	2.2	3.9×10^{-14}	1.7×10^{3}

situation since it depends on surface conditioning, voids and dislocations. The experimental K values are of the same order of magnitude for the various loads, speeds and also disc temperatures as shown in table 4.1. The theoretical K values show an increase with increasing load and speed.

Using the experimental K values and assuming the oxidational theory of mild wear applies equation (4.2), values of A_p were calculated and are shown in table 4.2. The A_p values tend to decrease with an increase in load W and with linear sliding speed U. Table 4.2 shows all the A_p values to be very much larger than the value measured under static conditions which also agrees with Sullivan et.al.[84] This is due to the greater degree of surface disruption which occurs during sliding. It seems then that for this limited range of experiments up to loads of 40 N without external heating the oxidational wear theory could describe the wear process. We have however to take account of the large differences in hardness and thus some abrasion which is also likely to occur. Again the equation cannot be applied to elevated temperatures but all the evidence suggests that the same mechanism is occurring.

4.3 The Severe Wear Mechanism

Severe wear mainly occurred for loads above 40 N and disc temperatures less than 400 ^{o}C for sliding speeds greater than 0.6 m s^{-1}. From the S.E.M. photomicrographs figures 3.40(b), 3.40(d) and 3.41(c), the pin surfaces show evidence of both plastic flow of the steel and grooves formed by the abrasive action of the much harder WC-11% Co disc. For both Lescalloy BG42 and A.I.S.I. 440C MOD steel pins the debris consisted of large metallic particles which when analysed were shown to be a mixture of α-Fe(Cr), γ-Fe and tungsten carbide WC. There were no oxides present either in the debris or on the surfaces

as shown in tables 3.10, 3.12 and 3.14. These conditions are typical of those associated with severe wear according to Archard and Hirst.[2]

On a typical wear track shown in figure 3.29(b), X-ray data shows that steel has been transferred to the disc. This is similar to Kerridge and Lancaster,[5] who investigated the severe wear of 60/40 brass on hardened steel. They found a transferred film of the softer material builds up on the hard surface. There is adhesion between the surfaces which causes part of the surface to be removed by a cold welding mechanism, Bowden and Tabor.[3] Also there is wear of the WC-11% Co disc as shown in figure 3.29(b), which is due to abrasive action. For the angular contact bearing experiments, the severe wear mechanism occurred at temperatures equal to and less than 260 and 200 ^{o}C for Lescalloy BG42 and A.I.S.I. 440C MOD steel bearings respectively. This is supported by the magnitude of the wear rates and X-ray diffraction analysis.

Using equation (1.3) for the pin-on-disc experiments values of K, the probability of producing a wear particle at any given asperity encounter were calculated and are shown in table 4.3. Disc temperatures less than 200 ^{o}C were generated by frictional heating alone.

The only established quantitative theory which may be appropriate to this wear regime is the delamination theory for metallic wear proposed by Suh,[7] [12] this gives an expression for the K factors where the wear rate is given by equation (1.4). The theory is based on the formation of dislocations and vacancies in the subsurface layers. The theory relates wear rate to the formation of subsurface cracks eventually leading to the formation of wear particles. It is broadly based on an adhesive mechanism and while adhesions of some sort is evident from plastic flow on the steel surfaces, abrasion must also take a

Table 4.3. The K factors produced by the severe wear mechanism.

Steel Pin	Speed / m s^{-1}	Load / N	Temperature / °C Disc	Surface	Wear Rate / 10^{-11} m^3 m^{-1}	K / 10^{-3}
	± 0.05 m s^{-1}	± 0.9 N	± 5 °C	± 5%	± 7%	± 10%
BG42	2.00	58.9	83	103	1.15	1.6
BG42	2.00	98.1	105	157	2.43	2.1
BG42	2.00	132.4	106	227	3.83	2.4
BG42	2.00	147.1	106	279	5.58	3.1
BG42	2.00	58.9	200	295	2.01	2.8
BG42	2.00	98.1	200	360	4.11	3.5
BG42	2.00	147.1	200	-	11.16	6.3
BG42	2.00	98.1	300	434	4.82	4.1
BG42	2.00	147.1	300	535	14.65	8.3
BG42	3.00	58.9	100	208	1.31	1.8
BG42	3.00	98.1	119	300	3.51	3.0
BG42	3.00	147.1	125	-	11.84	6.7
440C MOD	2.00	58.9	74	157	1.80	2.5
440C MOD	2.00	98.1	95	208	4.26	3.5
440C MOD	2.00	147.1	98	-	8.96	4.9
440C MOD	2.00	58.9	200	284	3.11	4.3
440C MOD	2.00	98.1	200	363	7.03	5.8
440C MOD	2.00	147.1	200	399	21.50	11.8

prominent part in the mechanism. For these reasons K values could not be obtained from the expression since not all the parameters were appropriate and could not be measured experimentally. In severe wear according to Kerridge,[86] plastic shearing led to transfer of metal from one surface to the other, subsequent transfer led to growth of the transferred layer which finally breaks up producing wear debris. The break up of the layer probably occurs once a critical accumulation of recoverable strain-energy per unit area is exceeded.

A measure of abrasive wear resistance is the amount of elastic deformation that the surface can sustain. Burwell[28] gave an expression for the elastic limit of strain, equation (1.10). The larger the elastic limit of strain the better should the surface be able to resist damage. Therefore we can say K is a function of the elastic modulus E ($N\ m^{-2}$) divided by the bulk hardness of the softer of the two materials p ($N\ m^{-2}$). The increase in T_s (^{o}C) the temperature of the surface of the pin outside the real area of contact, leads to surface softening and subsequent reduction in abrasion resistance, Kruschov.[82] Since no oxide film is present T_s is closely related to the temperature of the real area of contact between the pin and the disc. Therefore the K values can be possibly expressed by the empirical relationship equation (4.3), where T_a is the temperature of the surroundings and 1.01×10^{-5} the constant of proportionality.

$$K = 1.01 \times 10^{-5}\ E\ T_s / p\ T_a \qquad \ldots\ldots\ldots\ldots\ldots\ldots\ldots\ldots\ldots\ldots (4.3)$$

The bulk hardness values p were $(8.29 \pm 0.05) \times 10^{9}\ N\ m^{-2}$ for Lescalloy BG42 steel and $(8.09 \pm 0.05) \times 10^{9}\ N\ m^{-2}$ for A.I.S.I. 440C MOD steel, where the elastic modulus for stainless steel $E = 2.06 \times 10^{11}\ N\ m^{-2}$. T_a the temperature of the surroundings was taken as 20 ^{o}C.

Therefore using equation (4.3) the theoretical values of K were calculated and are shown in table 4.4.

Table 4.4. The theoretical K values derived for the severe wear mechanism.

Steel Pin	Surface Temperature / °C ± 5%	K / 10^{-3} (Experimental) ± 10%	K / 10^{-3} ± 6%
BG42	103	1.6	1.3
BG42	157	2.1	2.0
BG42	208	1.8	2.6
BG42	227	2.4	2.8
BG42	279	3.1	3.5
BG42	295	2.8	3.7
BG42	300	3.0	3.8
BG42	360	3.5	4.5
BG42	434	4.1	5.4
BG42	535	8.3	6.7
440C MOD	157	2.5	2.0
440C MOD	208	3.5	2.7
440C MOD	284	4.3	3.7
440C MOD	363	5.8	4.7
440C MOD	399	11.8	5.1

Table 4.4 and figure 4.1 show good agreement between the theoretical K values and experimental values for K factors less than 6.0×10^{-3}. Therefore other factors must be involved such as for example the number of asperity contacts. The sliding wear mechanisms reviewed by Childs[87] show that plastic flow depends on the ratio of the interfacial shear strength at a contact to the shear flow stress of the metal. Also contact theories, reviewed by Archard[88] show that an appropriate roughness parameter may be interpreted as the mean slope of the high spots flattened by the contact. In order to test equation (4.3) to its full extent, materials with very different E /p ratios

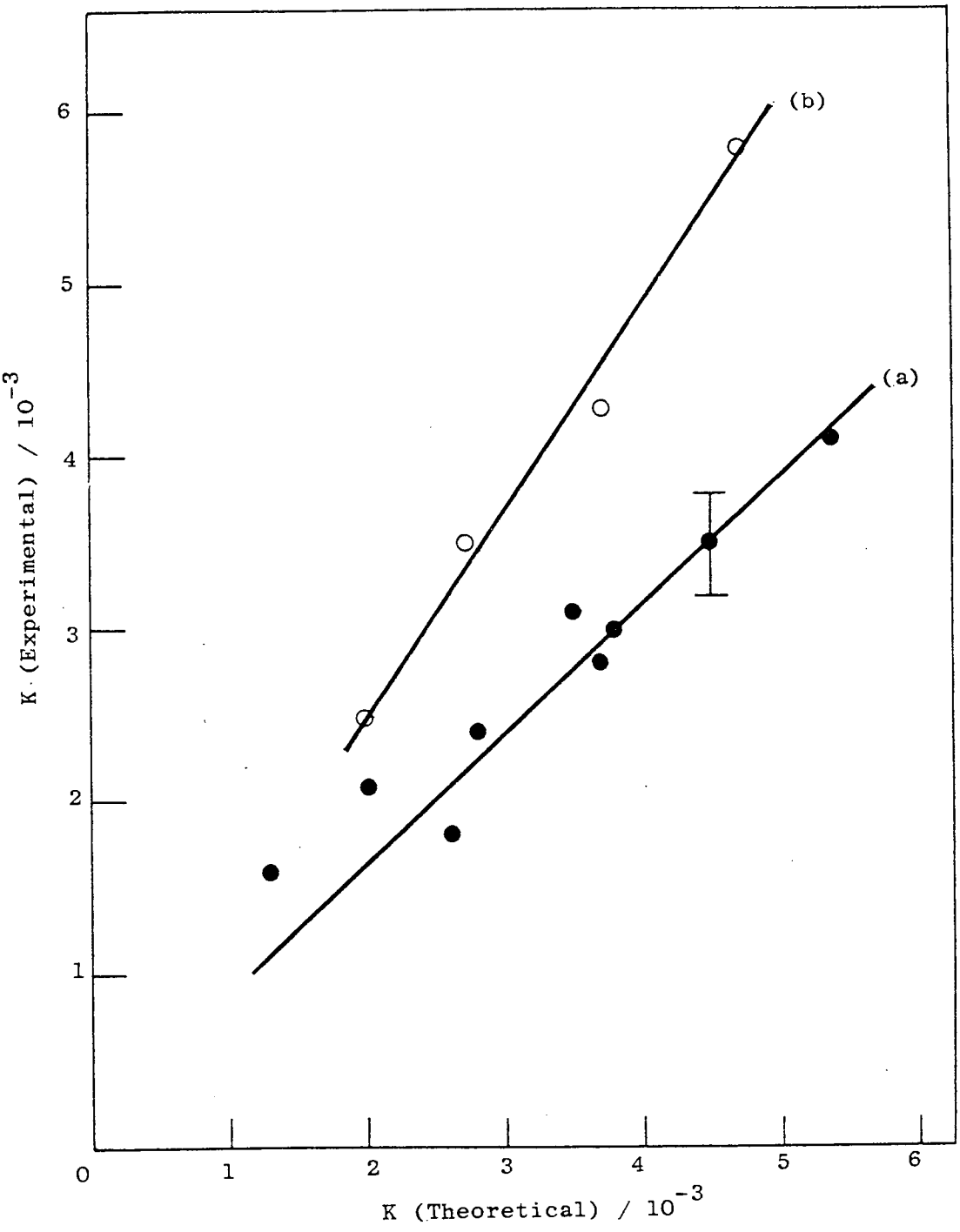

Fig. 4.1. The experimental K values versus the theoretical K values derived for the severe wear mechanism; (a) Lescalloy BG42 steel pins; (b) A.I.S.I. 440C MOD steel pins.

need to be used.

4.4 The High Temperature Wear Mechanism

For the pin-on-disc experiments, the high temperature wear mechanism occurred at all loads 19.6 to 147.1 N for disc and pin surface temperature greater than 400 ^{o}C. Some degeneration of the WC-11% Co disc begins to occur, since tungstic oxide WO_3 and cobalt tungsten oxide $CoWO_4$ appears on the surface of the pins and in the wear debris as shown in tables 3.11, 3.12, 3.13 and 3.14 decreasing the wear rate of the pin. For the Lescalloy BG42 steel pins above about 80 N load, chemical reactions occur producing iron tungsten oxide Fe_2WO_6 and chromium tungsten oxide Cr_2WO_6 on the surface of the pins which were also detected in the wear debris as shown in tables 3.12 and 3.13. The chemical reactions occurring after transfer can be represented by the following equations, where all the oxides are in their highest oxidation states.

$$Fe_2O_3 + WO_3 \longrightarrow Fe_2WO_6$$

$$Cr_2O_3 + WO_3 \longrightarrow Cr_2WO_6$$

S.E.M. photomicrographs figures 3.42, 3.43 and 3.44 show that the smooth films do not completely cover the surface. A typical wear track on the WC-11% Co disc figure 3.30, showed the wear rate of the disc to be large compared to the wear rate of the pin.

The largest amount of tungsten transfer occurred at a load of 19.6 N and a disc temperature of 500 ^{o}C according to S.E.M. analysis, figure 3.37. The surface film consisted of tungstic oxide WO_3 and cobalt tungsten oxide $CoWO_4$ as shown in table 3.11 which gave strong X-ray diffraction lines. From equation (2.17) the maximum effective depth of penetration of the X-rays was found to be about 7 μm. Since

the steel substrate was detected this suggests that the thickness of the transferred film is less. For the angular contact bearing experiments, the high temperature wear mechanism occurred at temperatures above 200 and 260 ^{o}C for A.I.S.I. 440C MOD and Lescalloy BG42 steel bearings respectively. This is supported by S.E.M. and X-ray diffraction analysis.

Again using equation (1.3) for the pin-on-disc experiments values of K, the probability of producing a wear particle at any given asperity encounter were calculated and are shown in table 4.5.

Table 4.5. The K factors produced by the high temperature wear mechanism. All the experiments were carried out at a sliding speed of 2 m s^{-1}.

Steel Pin	Load / N $\pm$ 0.9 N	Temperature / ^{o}C Disc $\pm$ 5 ^{o}C	Surface $\pm$ 5%	Wear Rate / 10^{-13} m^3 m^{-1} $\pm$ 7%	K / 10^{-5} $\pm$ 12%
BG42	19.6	400	420	1.67	7.1
BG42	19.6	500	441	0.14	0.6
BG42	39.2	500	-	0.40	0.9
BG42	58.9	500	487	0.52	0.7
BG42	98.1	500	524	5.12	4.3
BG42	147.1	500	-	7.36	4.1
440C MOD	39.2	500	517	0.29	0.6
440C MOD	58.9	500	515	1.01	1.4
440C MOD	98.1	500	529	1.10	0.9
440C MOD	147.1	500	554	2.51	1.4

This is the most complex wear mechanism of the three described since so many competing reactions are taking place. There is degeneration break down and oxidation of the tungsten carbide disc, removal and transfer of material from the disc, oxidation of the steel surfaces and

chemical reactions taking place at the steel surface. Wear by the removal of the oxide film from the surface of the pin might then be by a number of processes including fatigue or differential thermal expansion. All these factors make quantitative analysis of the wear rates or a derivation of an expression for K impossible.

CHAPTER 5

CONCLUSIONS

From the evidence gained from this investigation there are three distinct mechanisms for the wear of martensitic stainless steel against WC-11% Co with increase in load and temperature.

At low laods below 40 N with disc and pin surface temperatures up to about 300 ^{o}C for sliding speeds greater than 0.6 m s^{-1} the mechanism is oxidational-abrasive. The wear debris taken from Lescalloy BG42 and A.I.S.I. 440C MOD steel pins were of small particle size and non-metallic in appearance, where X-ray data showed large amounts of metal together with the oxide. The most predominant oxide was the rhombohedral oxide, which was present in the debris and on the relatively smooth pin surfaces with sometimes also tungsten carbide being detected. There is no evidence of true mild oxidational wear either from debris, surface analysis or from the magnitude of wear rates. Profilometry measurements indicated the wear rate of the WC-11% Co disc to be small compared to the wear rate of the steel pin.

For both types of steel pins the wear rate, which is the volume removed per unit sliding distance ranged from $(8.7 \pm 0.6) \times 10^{-14}$ to $(9.8 \pm 0.7) \times 10^{-13}$ m^3 m^{-1}. Values of K, the probability of producing a wear particle at any given asperity encounter were of the order of 10^{-4} for the various loads, speeds and disc temperatures used. From static oxidation experiments the activation energy for parabolic oxidation Q_p was found to be $(52 \pm 5) \times 10^3$ J mol^{-1} and the Arrhenius constant $A_p = (3 \pm 1) \times 10^{-7}$ kg^2 m^{-4} s^{-1}. For the unheated disc experiments, the theoretical values of K were obtained using the oxidational theory of mild wear equation (4.2), which were found to be very

much smaller than the experimental values. This could be explained in terms of tribo-oxidation, where the rate of growth of the oxide film is quite different to that measured under static conditions. Therefore the Arrhenius constant A_p will be very different in the tribological situation. The A_p values calculated show a decrease with an increase in load and with linear sliding speed. All the A_p values were very much larger than the value measured under static conditions, due to the greater degree of surface disruption which occurs during sliding. If A_p is taken to be 10^4 to 10^5 kg^2 m^{-4} s^{-1} the wear rate can possibly be obtained to within a few orders of magnitude. While this explanation is consistent with other work the magnitude of the difference in A_p values suggests that it is not a complete explanation. Also other workers have not found significant variation in A_p for tribological conditions with load, see for example Sullivan et.al.(84) It is more likely that true pure oxidational wear is not responsible, but that abrasion takes a significant part in the wear process.

At loads above 40 N and disc temperatures less than 400 ^oC for sliding speeds greater than 0.6 m s^{-1} the mechanism changes to severe wear or metallic wear. For both types of steel pins the debris consisted of large metallic particles which X-ray data showed to be a mixture of α-Fe(Cr), γ - Fe and tungsten carbide, with no oxides present either in the debris or on the surfaces. Here the rate of removal of the steel must be far greater than the rate of formation of an oxide film, thus allowing no oxidative protection. An S.E.M. study of the surfaces in this region indicated plastic flow of the steel and abrasive wear, with X-ray data showing that adhesive wear was also taking place. Surface profilometry measurements showed wear of the WC-11% Co disc was due to abrasive action. This is possibly caused by

small particles of the tungsten carbide which becomes dislodged and dragged across the surface.

For both types of steel pins the wear rate ranged from (1.15 ± 0.08) x 10^{-11} to (2.1 ± 0.1) x 10^{-10} m^3 m^{-1}, where the K values were of the order of 10^{-3} to 10^{-2} for the various loads, speeds and disc temperatures used. The theoretical K values obtained using equation (4.3), showed good agreement with the experimental values within the limits of experimental error. The equation is an over simplification and many other factors must be involved such as the number of asperity contacts, interfacial shear strength at a contact and the shear flow stress. However, the correlation is interesting and worthy of note.

At all loads 19.6 to 147.1 N with disc and pin surface temperatures greater than 400 ^{o}C a third wear mechanism appears. This is due to the degeneration of the sintered WC-11% Co and transfer of relatively soft oxide films to the surface of the steel. These transfer films of tungstic oxide WO_3 and cobalt tungsten oxide $CoWO_4$ indentified by X-ray data which gave strong X-ray diffraction lines produces an effective bearing material, thus dramatically reducing the wear rate of the steel pin. According to S.E.M. analysis the higher the load the greater the surface temperature required for material transfer, where X-ray data showed that the tungsten transfer was initially in the form of tungsten carbide. The S.E.M. photomicrographs for both types of steel pins show the smooth films do not completely cover the surface but that load bearing plateau are formed. According to X-ray data the thickness of these films are less than about 7 μm. Surface profilometry measurements in this region, showed the wear rate of the WC-11% Co disc to be large compared to the wear rate of the steel pin. This is to be expected due to the large amount of transfer.

For Lescalloy BG42 steel pins above about 80 N load chemical re-

actions occur increasing the wear rate of the pin. X-ray data showed that iron tungsten oxide Fe_2WO_6 and chromium tungsten oxide Cr_2WO_6 were present on the surface of the pins and also in the wear debris. The chemical reactions occurring after transfer can be represented by the following equations, where all the oxides are in their highest oxidation states.

$$Fe_2O_3 + WO_3 \longrightarrow Fe_2WO_6$$

$$Cr_2O_3 + WO_3 \longrightarrow Cr_2WO_6$$

For both types of steel pins the wear rate ranged from $(1.4 \pm 0.1) \times 10^{-14}$ to $(7.4 \pm 0.5) \times 10^{-13}$ $m^3\ m^{-1}$, where the K values were of the order of 10^{-5} to 10^{-4}. Due to the complex nature of the sliding process it was not possible to obtain theoretical K values. It is interesting to note that these are of the same order as the values measured for mild wear at low loads and temperatures.

Now comparing the results from the angular contact bearing simulation tests to those of the pin-on-disc experiments. In spite of the very different type of test, the first essentially rolling with some sliding the second pure sliding, the results indicate that both the severe wear and high temperature wear mechanisms are occurring.

From the magnitude of the wear rates and debris analysis, the severe wear mechanism occurred at bearing temperatures equal to and less than 260 and 200 ^{o}C for Lescalloy BG42 and A.I.S.I. 440C MOD steel bearings respectively. Like the pin-on-disc experiments adhesive wear was also occurring, where the WC-11% Co balls had metal transfer from the bearing race identified by X-ray analysis. For Lescalloy BG42 and A.I.S.I. 440C MOD steel bearings there was a reduction in the track wear for temperatures above 260 and 200 ^{o}C respectively. Here the high temperature wear mechanism was occurring according to S.E.M. analysis,

which showed an increase in the amount of tungsten transfer to the wear track. At a bearing temperature of 500 and 450 ^{o}C for Lescalloy BG42 and A.I.S.I. 440C MOD steel bearings respectively, X-ray data showed that the same chemical reactions were occurring as in the pin-on-disc experiments. It seems therefore that as long as the conditions of wear are established through examination of debris and surfaces, the simple pin-on-disc test may be useful as a screening test for material selection, without going to the considerable expense of producing angular contact bearings in these special materials.

In order to test equation (4.3) to its full extent an expression to obtain the K factors for the severe wear mechanism, materials with very different elastic modulus to hardness ratios need to be used. Since the simple pin-on-disc test may be useful as a screening test for material selection, work on many other materials would also be necessary to establish the absolute validity of this test.

APPENDIX 1

The Heat Flow along the Pin

The heat flow theory was originally developed by Coy[70] where the pin was held in a heat flow calorimeter as shown in figure 2.13. First considering the heat flow in the insulated portion of the pin, the heat flow per second leaving the section of the pin where the thermocouple measuring T_A is conducting heat away H_3 ($J\ s^{-1}$) is given by equation (a).

$$H_3 = K_s \pi R_t^2 M \left[\frac{(T_A - T_C) \cosh (M L_3) - (T_B - T_C)}{\sinh (M L_3)} \right] \quad \ldots\ldots(a)$$

$$M^2 = 2 K_i / K_s R_t^2 \ln (R_a / R_t) \quad \ldots\ldots\ldots\ldots\ldots\ldots\ldots\ldots(b)$$

In these equations K_s and K_i are the thermal conductivities of the steel pin and insulator respectively. R_a is the outer radius of the insulating medium, R_t is the radius of the pin, L_3 the distance between the thermocouples recording T_A and T_B and T_C is the thermocouple reading at the inside diameter of the copper cylinder around the pin and insulator. The heat flow along the thermocouple wire measuring T_A is $(H_2 - H_3)$, where H_2 is the heat flow per second entering the section of the pin where the thermocouple measuring T_A is conducting heat away. It is assumed that the temperature of the thermocouple wire at the outer cylindrical surface of the sindanyo is equal to T_C.

$$H_2 = \frac{C (T_A - T_C)}{(R_a - R_t)} + H_3 \quad \ldots\ldots\ldots\ldots\ldots\ldots\ldots\ldots(c)$$

C is the conductance of the thermocouple wire.

Now considering the heat flow in the exposed portion of the pin.

It is assumed that there is no temperature gradient along the radii of the pin, although heat is transferred from the cylindrical outer surface of the pin to the air. The heat flow per second along the pin at the interface between the pin and disc H_1 ($J\ s^{-1}$) and the temperature of the surface of the pin outside the real area of contact T_s (^{o}C) are given by the following expressions.

$$H_1 = \frac{K_s \pi R_t}{Z} (T_A - T_E) \sinh (L_1 / Z R_t) + H_2 \cosh (L_1 / Z R_t) \quad ..(d)$$

$$T_s = (T_A - T_E) \cosh (L_1 / Z R_t) + \frac{Z H_2}{K_S \pi R_t} \sinh (L_1 / Z R_t) + T_E \quad ....(e)$$

$$Z = \left[\frac{K_s}{2 R_t h} \right]^{1/2} \quad .....(f)$$

T_E is the temperature of air flowing past the pin well away from the boundary layer on the cylindrical surface of the pin. L_1 is the final length of pin exposed to the air between the holder and the disc and h is the heat transfer coefficient from the cylindrical exposed surface of the pin to the air. It was assumed that the air which flows past the pin has a temperature T_C.

Before H_1 and T_s can be calculated values for the heat transfer coefficient to the air must be obtained. This is an experimentally derived quantity which overcomes the necessity for analysing the complex heat flow situation, in which the surface layer of air around a solid transfers heat by conduction whilst the bulk of the air transfer heat by convection. It is found from the universal curve between Nusselt number (N_{Nu}) and Reynolds number (N_{Re}) for heating and cooling of air flowing normal to single cylinders, McAdams.[89]

$$N_{Re} = 2 R_t U / v \quad .....(g)$$

$$N_{Nu} = 2 R_t h / K_{air} \quad .....(h)$$

U is the speed at which air is flowing past the cylindrical surface of the pin, which is assumed to be equal to the linear sliding speed of the disc at the pin, v is the kinematic viscosity of air and K_{air} is the thermal conductivity of air. N_{Re} can be calculated and a value of N_{Nu} obtained from the graph, hence a value for h can be obtained.

The experimentally measured division of heat at the pin-disc interface, α(expt) and the total heat per second evolved at the pin-disc interface for no external heating H(total) (J s^{-1}) are given by the following expressions.

$$\alpha(\text{expt}) = H_1 \,/\, H(\text{total}) \quad \ldots\ldots\ldots\ldots\ldots\ldots\ldots\ldots\ldots\ldots (i)$$

$$H(\text{total}) = F\ U \quad \ldots\ldots\ldots\ldots\ldots\ldots\ldots\ldots\ldots\ldots\ldots\ldots (j)$$

H_1 is the heat flow per second along the pin at the interface between the pin and disc, U is the linear sliding speed of the disc at the pin and F the frictional force.

A computer programme was written enabling H_1, T_s, α(expt) and H(total) to be calculated. A copy of the programme in Fortran is shown in figure 1. The variable parameters were:-

U - the linear sliding speed of the disc at the pin (m s^{-1})

W - load (N)

F - frictional force (N)

T_A - temperature recorded by thermocouple at pin surface just as it emerges from pin holder (^{o}C)

T_B - temperature recorded by thermocouple situated at a distance L_3 along the cylindrical surface of the pin from the thermocouple recording T_A (^{o}C)

T_C - thermocouple reading at the inside diameter of the copper cylinder around the pin and insulator (^{o}C)

L_1 - the final length of pin exposed to the air between the holder and the disc (m).

```
DOCUMENT     HEATFLOW

      MASTER HEATFLOW
      REAL KI, KS, L1, L3, M
      DIMENSION U(30), W(30), FF(30), TA(30), TB(30),TC(30),
     2 L1(30), HTOT(30), DELTAE(30), TS(30), H1(30)
      DATA KS, KI, RA, PI/ 23.86, 0.1045, 0.00781, 3.14159/
      DATA L3, RT, C/ 0.0156, 0.00326, 0.000011174/
      M = SQRT(2 * KI/((KS * (RT**2))*ALOG(RA/RT)))
      READ(1,10) NEXP
  10  FORMAT(I0)
      DO 20 I = 1,NEXP
      READ(1,30) U(I), W(I), FF(I), TA(I), TB(I), TC(I), L1(I)
  30  FORMAT (7F0.0)
  20  CONTINUE
      WRITE (2,40)
  40  FORMAT (1H1,6HEXP NO,4X,5HSPEED,5X,4HLOAD,4X,8HFRICTION,3X,
     2 2HTA,4X,2HTB,4X,2HTC,4X,2HH1,4X,2HH2,4X,2HH3,3X,4HHTOT,
     3 5X,4HDEXP,5X,2HTS)
        I = 0
        DO 50 I = 1,NEXP
        RRE = (2.0*RT*U(I))/(1.461E-05)
        IF(RRE.LE.4.0) GO TO 41
        IF(RRE.LE.40.0) GO TO 42
        IF(RRE.LE.4000.0) GO TO 43
        IF(RRE.LE.40000.0) GO TO 44
        IF (RRE.LE.250000.0) GO TO 45
  41    RNU = 0.891*(RRE**0.33)
        GO TO 46
  42    RNU = 0.821*(RRE**0.385)
        GO TO 46
  43    RNU = 0.615*(RRE**0.466)
        GO TO 46
  44    RNU = 0.174*(RRE**0.618)
        GO TO 46
  45    RNU = 0.0239*(RRE**0.805)
  46    H = (RNU*0.02711)/(2.0*RT)
        Z = SQRT(KS/(2.0*RT*H))
        A = L1(I)/(Z*RT)
        B = TA(I) - TB(I)
        D = TB(I) - TC(I)
        E = TA(I) - TC(I)
        H3=KS*PI*(RT**2)*M*((E*COSH(M*L3))-D)/SINH(M*L3)
        H2= ((C*E)/(RA-RT))+H3
        H1(I)=(PI*RT*(KS/Z)*(E*SINH(A)))+(H2*COSH(A))
        HTOT(I)=FF(I)*U(I)
        DELTAE(I)=H1(I)/HTOT(I)
        TS(I) = (E*COSH(A))+((Z*H2/(KS*PI*RT))*SINH(A))+TC(I)
        WRITE(2,60) I,U(I),W(I),FF(I),TA(I),TB(I),TC(I),H1(I),H2,H3,
     2 HTOT(I),DELTAE(I),TS(I)
  60    FORMAT(1H ,1X,I2,6X,F6.2,3X,F6.2,4X,F6.2,2X,F6.1,1X,F5.1,1X,
     2 F5.1,1X,F5.2,1X,F5.2,1X,F5.2,1X,F6.2,2X,F5.3,3X,F6.1)
  50    CONTINUE
        STOP
        END
        FINISH
****
```

Fig. 1. The heat flow computer programme.

Values of the experimental parameters:-

K_s = thermal conductivity of the steel pin

$= 23.86\ J\ s^{-1}\ m^{-1}\ {}^{o}C^{-1}$

K_i = thermal conductivity of the insulator (sindanyo)

$= 0.1045\ J\ s^{-1}\ m^{-1}\ {}^{o}C^{-1}$

R_a = outer radius of the insulating medium

$= (7.81 \pm 0.02) \times 10^{-3}\ m$

L_3 = distance between the thermocouples recording T_A and T_B

$= (1.56 \pm 0.05) \times 10^{-2}\ m$

R_t = radius of the pin

$= (3.26 \pm 0.02) \times 10^{-3}\ m$

C = conductance of the thermocouple wire

$= 1.174 \times 10^{-5}\ J\ s^{-1}\ m\ {}^{o}C^{-1}$

K_{air} = thermal conductivity of air

$= 2.711 \times 10^{-2}\ J\ s^{-1}\ m^{-1}\ {}^{o}C^{-1}$

v = kinematic viscosity of air

$= 1.461 \times 10^{-5}\ m^{2}\ s^{-1}$.

APPENDIX 2

Determination of Film Thickness by Ellipsometry

Ellipsometry is a technique that allows the determination of the thickness of a thin film on a flat substrate. It is capable of measuring a film thickness to within $\pm$ 0.3 Å, that is a sensitivity much greater than that obtained with the method based on light interference. There is no elaborate sample preparation required and films can also be studied under liquids. More details of the application of ellipsometry for the examination and monitoring of surfaces are given by Neal.[76] [90]

The basic layout of the ellipsometer is shown in figure 2.15. Films a few Å thick on a metallic substrate can be detected by measuring the ellipticity of light after reflection. If the electric vector of the incident light is parallel or perpendicular to the plane of incidence, no changes result on reflection and these directions are used as reference positions or azimuths. But if plane polarized light makes an angle other than 0 or 90 degrees with respect to the plane of incidence, the reflected light is elliptically polarized. Elliptically polarized light is defined as two perpendicular vibrations of different amplitudes out of phase. Analysis of the elliptically polarized reflected light, gives the ratio of the axes and the orientation of the ellipse with respect to the two azimuthal directions. The ellipse depends on the angle of incidence and on the optical constants of the metal n and k.

The determination of film thickness is described by Neal and Fane,[79] where the basic equation of ellipsometry is given by equation (a).

$$r_p / r_s = \tan \Psi \exp (i \Delta) \quad \ldots\ldots\ldots\ldots\ldots\ldots\ldots\ldots\ldots\ldots (a)$$

Where r_p and r_s are the Fresnel reflection coefficients for light with

electric vectors parallel and perpendicular to the plane of incidence respectively. Ψ is the relative amplitude reduction ratio and Δ is the relative phase difference between the p and s components.

Values of Ψ and Δ are modified by the presence of a surface layer. In the early stages of film growth (i.e. up to about 10 nm) the changes in Ψ and Δ from that of a clean surface are proportional to film thickness, equations (b) and (c).

$$\Psi = \bar{\Psi} - A\ t \quad \text{.................................(b)}$$

$$\Delta = \bar{\Delta} - B\ t \quad \text{.................................(c)}$$

$\bar{\Psi}$ and $\bar{\Delta}$ relate to a clean surface and Ψ and Δ relate to a surface with a layer of thickness t superimposed. A and B are constants for a given combination of surface and film. For thicker films more exact equations need to be used.

One must first consider a film free surface, where the Fresnel reflection coefficients for light travelling from medium o to 1 are given by equations (d) and (e).

$$r_{01(p)} = \frac{n_0 \cos \phi_1 - n_1 \cos \phi_0}{n_0 \cos \phi_1 + n_1 \cos \phi_0} \quad \text{..................(d)}$$

$$r_{01(s)} = \frac{n_0 \cos \phi_0 - n_1 \cos \phi_1}{n_0 \cos \phi_0 + n_1 \cos \phi_1} \quad \text{..................(e)}$$

ϕ_0 and ϕ_1 are the angles of incidence and refraction respectively, with the non absorbing media having refractive indices n_0 and n_1. For absorbing media both n_0 and n_1 would be complex. Suffixes (p) and (s) refer to vectors parallel and perpendicular to the plane of incidence respectively. For opaque film free surfaces, n and k are related to the instrument readings Ψ and Δ through equations (a), (d) and (e), given in a form suitable for computation by Ditchburn.(91)

For a non absorbing surface film of refractive index n_1 on a

substrate of refractive index n_2, the Fresnel reflection coefficients for light incident in air or vacuum are written as:-

$$r_p = \frac{r_{o1(p)} + r_{12(p)} \exp D}{1 + r_{o1(p)} r_{12(p)} \exp D} \qquad \ldots\ldots\ldots\ldots\ldots\ldots\ldots\ldots\ldots\ldots (f)$$

with a similar expression for r_s.

$$D = 4 \pi i n_1 (\cos \phi_1) t / \lambda \qquad \ldots\ldots\ldots\ldots\ldots\ldots\ldots\ldots\ldots\ldots (g)$$

Where t is the film thickness and λ is the wavelength of light. For absorbing media a complex refractive index $N = n - ik$ replaces the refractive index n. A computer programme has been written by O'Shea[92] enabling the film thickness to be easily determined.

REFERENCES

1. BURWELL, J.T. and STRANG, C.D., On the Empirical Law of Adhesive Wear, J. Appl. Phys., Vol.23, pp.18-28, 1952.

2. ARCHARD, J.F. and HIRST, W., The Wear of Metals under Unlubricated Conditions, Proc. Roy. Soc. (London), Vol.A236, pp.397-410, 1956.

3. BOWDEN, F.P. and TABOR, D., The Friction and Lubrication of Solids, Clarendon Press, Oxford, 1954.

4. QUINN, T.F.J., The Classifications, Laws, Mechanisms and Theories of Wear, Fundamentals of Tribology, N.P.Suh and N.Saka (Eds.), MIT Press, Cambridge, Massachusetts, pp.447-492, 1980.

5. KERRIDGE, M. and LANCASTER, J.K., The Stages in a Process of Severe Metallic Wear, Proc. Roy. Soc. (London), Vol.A236, pp.250-264, 1956.

6. WELSH, N.C., The Dry Wear of Steels, Phil. Trans, Proc. Roy. Soc. (London), Vol.A257, pp.31-70, 1965.

7. SUH, N.P., An Overview of the Delamination Theory of Wear, Wear Vol.44, pp.1-16, 1977.

8. ARCHARD, J.F., Single Contacts and Multiple Encounters, J. Appl. Phys., Vol.32, pp.1420-1425, 1961.

9. ARCHARD, J.F., Contact and Rubbing of Flat surfaces, J. Appl. Phys., Vol.24, pp.981-988, 1953.

10. RABINOWICZ, E., Friction and Wear of Materials, J. Wiley and Sons, Chapter 6, 1965.

11. FINKIN, E.F., Speculations on the Theory of Adhesive Wear, Wear, Vol.18, pp.207-213, 1971.

12. SUH, N.P., The Delamination Theory of Wear, Wear, Vol.25, pp.111-124, 1973.

13. ENGEL, P.A., Impact Wear of Materials, Elsevier Scientific Pub. Co., Amsterdam, pp.15-17, 1976.

14. ARCHARD, J.F., The Wear of Metals, New Scientist, Vol.5, pp.1299-1301, 1959.

15. QUINN, T.F.J., The Role of Oxidation in the Mild Wear of Steel, Brit. J. Appl. Phys., Vol.13, pp.33-37, 1962.

16. QUINN, T.F.J., An Experimental Study of the Thermal Aspects of Sliding Contacts and Their Relation to the Unlubricated Wear of Steels, Proc. Inst. Mech. Engrs., Vol.183, Pt.3P, pp.129-137, 1968-69.

17. QUINN, T.F.J., ROWSON, D.M. and SULLIVAN, J.L., Application of the Oxidational Theory of Mild Wear to the Sliding Wear of Low Alloy Steel, Wear, Vol.65, pp.1-20, 1980.

18. TAO, F.F., A Study of Oxidation Phenomena in Corrosive Wear, ASLE Trans., Vol.12, pp.97-105, 1969.

19. QUINN, T.F.J., Oxidational Wear, Wear, Vol.18, pp.413-419, 1971.

20. QUINN, T.F.J., Dry Wear of Steel as Revealed by Electron Microscopy and X-Ray Diffraction, Proc. Inst. Mech. Engrs., Vol.182, Pt.3N, pp.201-213, 1967-68.

21. EARLES, S.W.E. and POWELL, D.G., Stability of Self-Generated Oxide Films on Unlubricated En1A Steel Surfaces, Proc. Inst. Mech. Engrs., Vol.182, Pt.3N, pp.167-174, 1967-68.

22. QUINN, T.F.J., The Effect of 'Hot-Spot' Temperatures on the Unlubricated Wear of Steel, ASLE Trans., Vol.10, pp.158-168, 1967.

23. QUINN, T.F.J., The Division of Heat and Surface Temperatures at Sliding Steel Interfaces and Their Relation to Oxidational Wear, ASLE Trans., Vol.21, pp.78-86, 1978.

24. QUINN, T.F.J. and SULLIVAN, J.L., A Review of Oxidational Wear, Proc. ASME Int. Conf. on Wear of Materials, St. Louis, pp.110-116, 1977.

25. QUINN, T.F.J. and WOOLLEY, J.L., The Unlubricated Wear of 3% Cr-½% Mo Steel, Lubrication Engineering, Vol.26, pp.312-319, 1970.

26. ARCHARD, J.F., The Temperature of Rubbing Surfaces, Wear, Vol.2, pp.438-455, 1958-59.

27. TENWICK, N. and EARLES, S.W.E., A Simplified Theory for the Oxidative Wear of Steels, Wear, Vol.18, pp.381-391, 1971.

28. BURWELL, J.T., Survey of Possible Wear Mechanisms, Wear, Vol.1, pp.119-141, 1957-58.

29. HAWORTH, R.D., Abrasive Wear of Metals, Metal Progr., Vol.55, pp.842-848, 1949.

30. OBERLE, T.L., Properties Influencing Wear of Metals, J. Metals, Vol.3, pp.438-439G, 1951.

31. SEDRIKS, A.J. and MULHEARN, T.O., Mechanics of Cutting and Rubbing in Simulated Abrasive Processes, Wear, Vol.6, pp.457-466, 1963.

32. SEDRIKS, A.J. and MULHEARN, T.O., The Effect of Work-Hardening on the Mechanics of Cutting in Simulated Abrasive Processes, Wear, Vol.7, pp.451-459, 1964.

33. ARCHARD, J.F. and HIRST, W., An Examination of a Mild Wear Process, Proc. Roy. Soc. (Lon.), Vol.A238, pp.515-528, 1957.

34. GOLDEN, J. and ROWE, G.W., Transfer of Tungsten Carbide to Soft Metals During Single-Traverse and Reciprocating Sliding, Brit. J. Appl. Phys., Vol.9, pp.120-121, 1958.

35. GOLDEN, J. and ROWE, G.W., Wear of the Hard and Soft Phases in Cobalt-bonded Tungsten Carbide, Brit. J. Appl. Phys., Vol.11, pp.517-520, 1960.

36. MILLER, D.R., Friction and Abrasion of Hard Solids at High Sliding Speeds, Proc. Roy. Soc. (London), Vol.A269, pp. 368-384, 1962.

37. BOWDEN, F.P. and PERSSON, P.A., Deformation, Heating and Melting of Solids in High-Speed Friction, Proc. Roy. Soc. (London), Vol.A260, pp.433-458, 1961.

38. TRENT, E.M., Some Factors Affecting Wear on Cemented Carbide Tools, Proc. Inst. Mech. Engrs., Vol.166, pp.64-70, 1952.

39. TRENT, E.M., Wear Processes on Cemented Carbide Tools Used in Cutting Steel, Proc. Roy. Soc. (London), Vol.A212, pp.467-470, 1952.

40. JAMES, M.R., Coated Cemented Carbide Cutting Tools, Metallurgist and Materials Technologist, Vol.9, pp.483-486, 1977.

41. TRENT, E.M., Cutting Steel and Iron With Cemented Carbide Tools, J. Iron and Steel Inst., Vol.201, pp.1001-1015, 1963.

42. SHIMURA, H. and TSUYA, Y., Effects of Atmosphere on the Wear Rate of Some Ceramics and Cermets, Proc. ASME Int. Conf. on Wear of Materials, St. Louis, pp.452-461, 1977.

43. MORDIKE, B.L., The Frictional Properties of Carbides and Borides at High Temperatures, Wear, Vol.3, pp.374-387, 1960.

44. PARKS, M.V., The Evaluation of High Temperature Ballscrew and Bearing Assemblies, Internal Research Report, Lucas Aerospace Ltd., Wolverhampton, England, 1971.

45. ALEXANDER, W.and STREET, A., Metals in the Service of Man, Penguin Ltd., England, U.S.A., Australia, 5th Ed., Ch.11 and pp.176-177, 1973.

46. HANSEN, M., Constitution of Binary Alloys, McGraw-Hill, New York, Toronto, London, 2nd Ed., p.354 and p.392, 1958.

47. BUNGARDT, V.K., KUNZE, E. and HORN, E., Untersuchungen über den Aufbau des Systems Eisen-Chrom-kohlenstoff, Arch. Eisenhüttenw., Vol.29, pp.193-203, 1958.

48. COLOMBIER, L. and HOCHMANN, J., Stainless and Heat Resisting Steels, E. Arnold Ltd., Ch.1, Ch.2, p.321, p.322, p.326 and p.357, 1967.

49. KUBASCHEWSKI, O. and HOPKINS, B.E., Oxidation of Metals and Alloys, Butterworths, London, pp.192-194, 1953.

50. STODDART, C.T.H. and HONDROS, E.D., Element Profiles Across Thin Oxide Films, Nature Physical Sci., Vol.237, pp.90-91, 1972.

51. ISHERWOOD, B.J. and QUINN, T.F.J., The Application of a Glancing Angle X-Ray Diffraction Film Technique to the Study of Low Temperature Oxidation of Iron Chromium Alloys, Brit. J. Appl. Phys., Vol.18, pp.717-725, 1967.

52. ORTON, G.W., Phase Transitions in the System Tungsten-Carbon, Trans. Met. Soc. AIME, Vol.230, pp.600-602, 1964.

53. SARA, R.V., Phase Equilibria in the System Tungsten-Carbon, J. Am. Ceram. Soc., Vol.48, pp.251-257, 1965.

54. RIECK, G.D., Tungsten and its Compounds, Pergamon Press, London, 1st Ed., p.82, 1967.

55. YOUNG, R.S., Cobalt Its Chemistry, Metallurgy and Uses, Chapman and Hall Ltd., London, pp.78-80 and pp.261-265, 1960.

56. DAWIHL, W. and FRISCH, B., Wear Properties of Tungsten Carbide and Aluminium Oxide Sintered Materials, Wear, Vol.12, pp.17-25, 1968.

57. GURLAND, J. and NORTON, J.T., Role of the Binder Phase in Cemented Tungsten Carbide-Cobalt Alloys, J. Metals, Vol.4, pp.1051-1056, 1952.

58. RAUTALA, P. and NORTON, J.T., Tungsten-Cobalt-Carbon System, Trans. AIME, Vol.194, pp.1045-1050, 1952.

59. GURLAND, J., A study of the Effect of Carbon Content on the Structure and Properties of Sintered WC-Co Alloys, Trans. AIME, Vol.200, pp.285-290, 1954.

60. EDWARDS, O.S. and LIPSON, H., An X-Ray Study of the Transformation of Cobalt, J. Inst. Metals, Vol.69, pp.177-188, 1943.

61. TROIANO, A.R. and TOKICH, J.L., The Transformation of Cobalt, Trans. AIME, Vol.175, pp.728-741, 1948.

62. OWEN, E.A. and MADOC-JONES, D., Effect of Grain Size on the Crystal Structure of Cobalt, Proc. Phys. Soc., Vol.B67, pp. 456-466, 1954.

63. WEBB, W.W., NORTON, J.T. and WAGNER, C., Oxidation of Tungsten, J. Electrochem. Soc., Vol.103, pp.107-111, 1956.

64. WEBB, W.W., NORTON, J.T. and WAGNER, C., Oxidation Studies in Metal-Carbon Systems, J. Electrochem Soc., Vol.103, pp.112-117, 1956.

65. NEWKIRK, A.E., The Oxidation of Tungsten Carbide, J. Am. Chem. Soc., Vol.77, pp.4521-4522, 1955.

66. GULBRANSEN, E.A. and ANDREW, K.F., The Kinetics of the Oxidation of Cobalt, J. Electrochem. Soc., Vol.98, pp.241-251, 1951.

67. TIMOSHENKO, S.P. and GOODIER, J.N., Theory of Elasticity, McGraw-Hill, New York, London, 3rd Ed., pp. 409-414, 1970.

68. LEVIT, G.A., Calculations of Recirculating Ball Screw and Nut Transmissions, Machines and Tooling, Vol.34, pp.9-16, 1963.

69. DUNCKLEY, P.M., The Effect of Elevated Temperature and Speed Upon the Wear of Mild Steel, Ph.D. Thesis, Aston University, Birmingham, 1977.

70. COY, R.C., An Investigation of the Mechanisms of the Unlubricated Wear of EN26 Steel Using Several Physical Techniques, M.Sc. Thesis, Aston University, Birmingham, 1971.

71. PEISER, H.S., ROOKSBY, H.P. and WILSON, A.J.C., X-Ray Diffraction by Polycrystalline Materials, Chapman and Hall Ltd.,London, pp.660-662, 1960.

72. HENRY, N.F.M., LIPSON, H. and WOOSTER, W.A., The Interpretation of X-Ray Diffraction photographs, Macmillan and Co. Ltd., 2nd Ed., p.31, 1961.

73. CULLITY, B.D., Elements of X-Ray Diffraction, Addison-Wesley Co., London, pp.269-272, 1959.

74. SOUTHWORTH, H.N., Introduction to Modern Microscopy, Wykeham Publications Ltd., London, pp.27-29, 1975.

75. ANDERSEN, C.A., Electron Probe Microanalysis of Thin Layers and Small Particles with Emphasis on Light Element Determinations, The Electron Microprobe, T.D. Mckinley, K.F.J.Heinrich and D.B.Wittry (Eds.), J. Wiley and Sons, New York, London, Sydney, pp.58-74, 1966.

76. NEAL, W.E.J., Application of Ellipsometry to Surface Films and Film Growth, Surface Technology, Vol.6, pp.81-110, 1977.

77. LATHAM, R.V. and BRAH, A.S., The Influence of Surface Oxidation on the Electron Tunnelling Mechanism of Microparticle Charge Reversal During a Bouncing Impact on a Charged Conductor, J. Phys. D: Appl. Phys., Vol.10, pp.151-167, 1977.

78. FANE, R.W., NEAL, W.E.J. and LATHAM, R.V., Ellipsometric Observations of an Electron-Bombarded Stainless Steel Surface, J. Appl. Phys., Vol.44, pp.740-743, 1973.

79. NEAL, W.E.J. and FANE, R.W., Ellipsometry and its Applications to Surface Examination, J. Phy. Sci. Instruments, Vol.6, pp.409-416, 1973.

80. HILL, R.M. and WEAVER, C., The Optical Properties of Chrome, Trans. Faraday Soc., Vol.54, pp.1140-1146, 1958.

81. ROWSON, D.M. and QUINN, T.F.J., Frictional Heating and the Oxidational Theory of Wear, J. Phys. D: Appl. Phys., Vol.13, pp.209-219, 1980.

82. KRUSCHOV, M.M., Principles of Abrasive Wear, Wear, Vol.28, pp.69-88, 1974.

83. PARKS, M.V., High Temperature Hardness Characteristics of Materials, Internal Research Report, Lucas Aerospace Ltd., Wolverhampton, England, 1971.

84. SULLIVAN, J.L. QUINN, T.F.J. and ROWSON, D.M., Developments in the Oxidational Theory of Mild Wear, Tribology Int., Vol.13, pp.153-158, 1980.

85. ROWSON, D.M., QUINN, T.F.J. and SULLIVAN, J.L., Private Communication, Aston University, Birmingham, 1980.

86. KERRIDGE, M., Metal Transfer and the Wear Process, Proc. Phys. Soc., Vol.B68, pp.400-407, 1955.

87. CHILDS, T.H.C., The Sliding Wear Mechanisms of Metals, Mainly Steels, Tribology Int., Vol.13, pp.285-293, 1980.

88. ARCHARD, J.F., Surface Topography and Tribology, Tribology Int., Vol.7, pp.213-220, 1974.

89. MCADAMS, W.H., Heat Transmission, McGraw-Hill, New York, 3rd Ed., p.259, 1954.

90. NEAL, W.E.J., Surface Optical Spectroscopy, Physics in Technology, Vol.8, pp.238-243, 1977.

91. DITCHBURN, R.W., Some New Formulas For Determining the Optical Constants From Measurements on Reflected Light, J. Op. Soc. Am., Vol.45, pp.743-748, 1955.

92. O'SHEA, K.R., The Variation of Optical and Electrical Properties Due to Annealing of Thin Vapour-Quenched Aluminium Films, Ph.D. Thesis, Aston University, Birmingham, 1971.

Eur. J. Phys. 2 (1981) 69–74. Printed in Northern Ireland

An ellipsometer for student experiments

W E J Neal and S J Petraitis

Physics Department, University of Aston in Birmingham, Birmingham B4 7ET, England

Received 5 February 1981, in final form 11 May 1981

Wear, 75 (1982) 87 - 103

THE WEAR OF MARTENSITIC STAINLESS STEEL AGAINST TUNGSTEN CARBIDE AT TEMPERATURES UP TO 500 °C*

J. L. SULLIVAN and S. J. PETRAITIS

University of Aston in Birmingham, Gosta Green, Birmingham B4 7ET (Gt. Britain)

(Received May 28, 1981)